



Cranfield University

School of Industrial and Manufacturing Science

PhD

Neil J. Woodward

**POOL OSCILLATIONS AND CAST VARIATIONS -
PENETRATION CONTROL FOR ORBITAL TIG WELDING
OF AUSTENITIC STAINLESS STEEL TUBING**

Supervisor: Dr. Ian M. Richardson

March 1997

Abstract

Pool oscillations in tungsten inert gas welding pools have been used in a closed-loop control system for orbital welding of ultra high purity tubing, determining a target level of penetration by altering the welding current in real-time. The technique is ideally suited to this application since it does not contravene the cleanliness requirements for the inner bore and can be implemented outside the small orbital heads that are commonly used. The results presented in this thesis show how clear pool oscillation signals in extremely small molten pools can be monitored by optimising the welding conditions and signal processing of the arc voltage signal. As an indicator of the likely variation in cast behaviour present particularly in austenitic stainless steels, a 'time-to-penetrate' characterisation was made of the materials, using the time of the transition from the Mode 1 to the Mode 3 oscillation behaviour as the measured variable. By applying the test across a range of welding currents, significant insight was obtained into the cast and associated penetration behaviour. Late transitions indicated casts that exhibited significantly different responses to the more usually applied welding procedures, especially at the lower levels of welding current (highlighting their potentially more problematic penetration behaviour). It was shown that the established theoretical models were difficult to apply with certainty to moving weld pools, and consequently a fuzzy logic model was used in the control strategy. The closed-loop system comprised a user-interface PC, a control rack and commercial welding power source - control signals were applied every 2 to 3 Hz. Mode 3 pool oscillations were found to offer a more than satisfactory sensitivity to the inner bead width created for the various casts of 1.65 mm wall thickness materials studied.

This thesis is dedicated to my parents, Mary and Jack Woodward, who have always given the most positive support throughout my education and life.

Acknowledgements

I would like to thank Matt Goodall and Pat Hopper at Isotek Electronics for their work on the user-interface PC and control rack, and Jesper Mogenson (formerly of Migatronic) for his work with the serial communications and the BDH 320 power source. Julian Tapp (now at TWI) engaged in many lively discussions about the work and its application to ultra-high purity tubing. Dr Kawal Chawla is particularly acknowledged for his work on 'C' programming the majority of the software that was used for the research work. John Nixon also gave the necessary assistance with analogue electronic circuitry design. Professor John Norrish (now at the University of Wollongong, Australia) provided the initial inspiration back in 1993, and Dr. Ian Richardson followed with invaluable questions and further support.

I would also like to thank all the people involved with the Welding Group (present and previous) for their good humour, knowledge and assistance.

Marian Loveday has always been totally supportive throughout this research work and particularly enjoyed some of my descriptions of weld pool oscillations.

Contents

	<i>Page Nº.</i>
<u>ABSTRACT</u>	I
<u>ACKNOWLEDGEMENTS</u>	II
<u>CONTENTS</u>	III
List of appended tables	IX
List of appended figures	X
<u>SYMBOLS AND ABBREVIATIONS</u>	XVI
1. <u>INTRODUCTION</u>	1
2. <u>LITERATURE SURVEY</u>	5
2.1 <u>Background</u>	5
2.2 <u>Principal oscillation methods</u>	7
2.2.1 Free response: arc light intensity and voltage	7
2.2.2 Resonant or forced response	8
2.2.3 Summary	9
2.3 <u>Theoretical mathematical modelling of natural frequency</u>	10
2.3.1 Fully penetrated molten pools	11
2.3.2 Partially penetrated molten pools	13
2.3.3 Summary	14
2.4 <u>Observed oscillation behaviour</u>	16
2.4.1 Amplitude	16
2.4.2 Damping	17
2.4.3 Partial, full and mixed-mode responses	17
2.4.4 Material dynamic response	18

Contents

2.5	<u>Effects of welding parameters and operating conditions on pool and oscillation behaviour</u>	20
2.5.1	Shielding gas	20
2.5.2	Welding current (pulsed and sinusoidal application)	22
2.5.3	Travel speed	24
2.5.4	Tungsten geometry	25
2.5.5	Arc length	26
2.5.6	Joint preparation	27
2.5.7	Orbital position and gravity	28
2.5.8	Surface tension, γ	29
2.5.9	Summary	32
2.6	<u>Other factors influencing the application of pool oscillations</u>	33
2.6.1	Cast-to-cast behaviour	33
2.6.2	Pulsed (-TIG) current welding	35
2.6.3	Arc pressure distribution and magnitude	37
2.6.4	Power source characteristics and signal processing	38
2.6.5	Fast Fourier Transform	39
2.7	<u>Control methods</u>	40
2.7.1	Conventional control methods	40
2.7.2	Fuzzy logic in welding process control	42
2.8	<u>Concluding remarks</u>	45
<hr/>		
3.	<u>EQUIPMENT AND MATERIALS</u>	46
3.1	<u>Equipment</u>	46
3.1.1	Equipment description	46
	<i>AMI 207 and AMI heads</i>	46
	<i>Experimental orbital system</i>	48
	<i>Pool oscillation measurement and software</i>	49
3.1.2	Measurement techniques	52
	<i>Arc voltage</i>	52
	<i>Welding current</i>	52
	<i>Resultant bead profile</i>	52
	<i>Inner bead surface roughness</i>	53

Contents

3.1.3	Standard experimental procedures	53
	<i>Material preparation</i>	53
	<i>Joint preparation</i>	54
	<i>Electrode setting, cleaning and integrity</i>	54
	<i>Pre- and post purging</i>	54
	<i>Orbital welding procedure</i>	54
3.1.4	Calibration of the closed-loop system	56
	<i>System operation</i>	56
	<i>User-interface & logging PC performance</i>	57
	<i>Serial communications protocol reliability</i>	58
	<i>Closed-loop system</i>	59
3.2	<u>Materials</u>	60
3.2.1	Tube and pipe material description	60
3.2.2	Tube and pipe material composition	60
<hr/>		
4.	<u>EXPERIMENTAL PROGRAMME</u>	61
4.1	<u>Experimental design</u>	61
4.2	<u>Fundamental oscillation experimentation</u>	62
4.2.1	Filtration of arc voltage signal	62
4.2.2	Arc voltage response to current on copper block	63
4.2.3	Arc voltage signal processing	64
4.2.4	Basic welding parameters	65
	<i>Stationary spot welding and signal quality</i>	65
	<i>Orbital welding and penetration</i>	66
	<i>Travel speed, pulse current level,</i>	
	<i>inner bead surface roughness and outer bead appearance</i>	66
	<i>Travel speed and signal quality</i>	67
4.3	<u>Effect of cast-to-cast variation on oscillation behaviour</u>	68
4.3.1	Stationary pool and time-to-penetrate studies	68
	<i>Part 1 - Small diameter tubing</i>	68
	<i>Part 2 - Medium diameter pipe</i>	70
4.3.2	Cast-to-cast variations in moving weld pools	71
4.4	<u>Real-time logging and reliability of frequency response</u>	73
4.4.1	Configuration of real-time logging	73
4.4.2	Reliability and smoothing of response	75

Contents

4.5	<u>Application of fuzzy logic to pool oscillations and penetration behaviour</u>	77
4.5.1	Single-input/single-output model	77
4.5.2	Operating performance	81
	<i>Open- and closed-loop trials</i>	81
	<i>Step change recovery</i>	82
<hr/>		
5.	<u>EXPERIMENTAL RESULTS</u>	83
5.1	<u>Introduction</u>	83
5.2	<u>Fundamental oscillation experimentation</u>	83
5.2.1	Filtration of arc voltage signal	83
5.2.2	Arc voltage response to pulsed current on copper block	84
5.2.3	Arc voltage signal processing	85
5.2.4	Basic welding parameters	87
	<i>Stationary spot welding and signal quality</i>	87
	<i>Orbital welding and penetration</i>	89
	<i>Travel speed, pulse current level and surface roughness</i>	90
	<i>Travel speed and signal quality</i>	91
5.2.5	Fundamental oscillation experimentation summary	92
5.3	<u>Effect of cast-to-cast on oscillation behaviour</u>	93
5.3.1	Stationary pool and time-to-penetrate studies	93
	<i>Part 1 - Small diameter tubing</i>	93
	<i>Part 2 - Medium diameter pipe</i>	95
5.3.2	Cast-to-cast variations in moving weld pools	97
5.3.3	Effect of cast-to-cast and surface tension on oscillation behaviour summary	99
5.4	<u>Real-time logging and reliability of frequency response</u>	101
5.4.1	Configuration of real-time logging	101
5.4.2	Reliability and smoothing of response	102
5.5	<u>Application of fuzzy logic to pool oscillations and penetration behaviour</u>	105
5.5.1	Single-input/single-output model	105
5.5.2	Operating performance	105
	<i>Open- and closed-loop trials</i>	106
	<i>Step change recovery</i>	109
5.5.3	Application of control strategy summary	110

6.	<u>DISCUSSION</u>	112
6.1	<u>Introduction</u>	112
6.1.1	Sources of error	112
6.2	<u>Observations and theory</u>	114
6.2.1	Basic welding parameters - experimental observations	114
	<i>Quality and reliability of the pool oscillation signal</i>	114
	<i>Pool frequency and penetration - Mode 1 to 3 transition</i>	116
	<i>Pool frequency and penetration - weld bead formation</i>	118
	<i>Pool frequency and orbital position</i>	119
	<i>Evidence of mixed-mode behaviour</i>	120
6.2.2	Theoretical predictions and practical measurements	
	(Pool size and frequency)	122
	<i>Mode 3 - basic work - stationary pools</i>	122
	<i>Mode 3 - stationary pool and time-to-penetrate studies</i>	123
	<i>Mode 1 - stationary pools</i>	124
6.2.3	Summary	125
6.3	<u>Cast effect on pool oscillations</u>	126
6.3.1	Surface tension and penetration/frequency behaviour	126
	<i>Cast-to-cast work - 1.65 mm WT material - stationary pools</i>	127
	<i>Cast-to-cast work - 1.65 mm WT material - moving pools</i>	128
	<i>Cast-to-cast work - 3.91 mm WT material - stationary pools</i>	129
6.3.2	'Time-to-penetrate' studies	130
	<i>1.65 mm WT material</i>	130
	<i>3.91 mm WT material</i>	131
6.3.3	Summary	132
6.4	<u>Application to orbital welding</u>	134
6.4.1	Sensitivity of pool frequency to operating variables	134
	<i>Constant parameter work</i>	134
	<i>Control work</i>	136
6.4.2	Reliability for monitoring/control of penetration	138
	<i>Reliability and smoothing</i>	138
	<i>Application of the fuzzy model</i>	139
	<i>Performance of control system and full penetration welds</i>	140
6.4.3	Summary	142

Contents

6.5	<u>Overall discussion summary</u>	143
6.5.1	Theoretical modelling of pool behaviour	143
6.5.2	Application of pool frequency to cast behaviour and penetration control	144

7.	<u>CONCLUSIONS</u>	145
-----------	---------------------------	------------

	<u>IMPLICATIONS OF THE RESEARCH</u>	147
--	--	------------

	<u>SUGGESTIONS FOR FUTURE WORK</u>	148
--	---	------------

	<u>REFERENCES</u>	149
--	--------------------------	------------

	<u>APPENDED TABLES AND FIGURES</u>	159
--	---	------------

Contents

LIST OF APPENDED TABLES

- from the Literature survey (§2) -

Table 1	Surface tension and cast, Keene (1985)	159
----------------	---	------------

- from Equipment and materials (§3) -

Table 2	Equipment list	160
Table 3	Real-time performance of oscillation software	161
Table 4	Tube and pipe material description	162
Table 5	Tube and pipe material certificate chemical composition (as supplied)	163

- from the Experimental programme (§4) -

Table 6	Initial pool oscillation welding parameters	164
Table 7	AMI 207 V/I characteristic static arc parameters	164
Table 8	Pulsed current on copper static arc parameters	164
Table 9	Typical partial and full penetration pool oscillation welding parameters used for the optimisation of the arc voltage signal response	165
Table 10	Stationary spot welding parameters - peak current and time study	165
Table 11	Standard welding parameters - variation in penetration and orbital position	165
Table 12	Travel speed and peak current magnitude effect on inner bead profile	166
Table 13	Base current and penetration effect on outer bead appearance	166
Table 14	Welding parameters - travel speed variation and signal quality	166
Table 15	Time-to-penetrate and surface tension study parameters (Part 1)	167
Table 16	Time-to-penetrate and surface tension study parameters (Part 2)	167
Table 17	Standard pulsed TIG welding procedure	168
Table 18	Straight d.c. welding procedures	168
Table 19	Pool oscillation procedures	168
Table 20	Pool oscillation procedure - PARTIAL and FULL penetration conditions (2 conditions, 1 pass)	169

Contents

Table 21	Pool oscillation procedure - PARTIAL and FULL penetration conditions (2 conditions, 1 pass)	169
Table 22	Fuzzy logic model parameters	170
Table 23	Open-loop oscillation procedure and monitoring parameters - full and over-penetration conditions	171
Table 24	Closed-loop oscillation procedure - full penetration conditions - target frequency 80 Hz	172
Table 25	Fuzzy logic control parameters for 120 Hz target frequency	173

- from the Experimental results (§5) -

Table 26	Stationary spot welding - effect of pulse magnitude and duration	174
Table 27	Surface tension predictions from membrane and Yoo's model for electro-polished ('EP'), low sulphur ('LS Kobe'), Cast 1 and 2 materials	175
Table 28	Cast-to-cast variation - effect of standard, straight d.c., and oscillation procedures on bead width and frequency - low sulphur LS ('LS Kobe') and high sulphur HS ('Cast 1') casts	176

- from the Discussion (§6) -

Table 29	Lower pool surface and Mode 1 to 3 transition - example results (20 Amps set current)	177
Table 30	Orbital position and Mode 3 frequency response ('cast-to-cast' work)	177
Table 31	Cast behaviour and stationary pool sizes	177
Table 32	Time-to-penetrate (1.65 mm wall thickness)	178
Table 33	Sensitivity of pool frequency to inner bead width, and frequency to base current (1.65 mm WT material)	178
Table 34	Sensitivity of pool frequency to inner bead width and base current (cast-to-cast comparison)	178
Table 35	Delay in frequency response with change in base current (Step change in $I_b = 12.5$ Amps for 1.65 mm WT)	179
Table 36	Delay in frequency response with change in base current (Step change in $I_b = 20.0$ Amps for 3.18 mm WT)	179
Table 37	Real-time frequency response of 1.65 mm WT tubing - average and standard deviation	179
Table 38	Sensitivity of fuzzy logic model to pool frequency	180

LIST OF APPENDED FIGURES

- from the Literature survey (§2) -

Figure 1	Generalised frequency behaviour	181
Figure 2	Modified current pulsing - Nakata (1994)	182
Figure 3	Pulsed current designation	182
Figure 4	Symmetric & sloshing oscillation modes - Yoo (1993)	183
Figure 5	Error in predicted frequency with surface tension variation	184
Figure 6	Partial and full penetration conditions - Xiao (1993)	185
Figure 7	Effect of welding speed - Hardt (1985)	186
Figure 8	Tungsten geometry	186
Figure 9	Orbital welding control variables - Krüger (1994)	187
Figure 10	Effect of workpiece position - Shirali and Mills (1993)	188
Figure 11	Surface tension / temperature behaviour	189
Figure 12	Effect of cast variation - Hinata (1994)	189
Figure 13	Reported effect of rate of rise of current on arc pressure - Barabokhin (1976)	190
Figure 14	Weld pool frequency control system - Madigan (1986)	190
Figure 15	Synchronized pulsing and pool oscillations - Andersen (1993)	191
Figure 16	Fuzzy logic strategy	191

- from Equipment and materials (§2) -

Figure 17	Arc Machines 207 power source and AMI head in laboratory	192
Figure 18	AMI 9-1500 orbital head	192
Figure 19	Exploded view - 9-1500 head	193
Figure 20	Isotek VME-Bus control rack (19") and Migatronix BDH320 Commander power source	193
Figure 21	Schematic of control system set-up	194
Figure 22	Layout of signal processing hardware	195
Figure 23	Tri-Tool facing machine for butt joint preparation	196
Figure 24	Closed-loop operating sequence schematic	197
Figure 25	Control of orbital welding (event cycle)	198
Figure 26	Calibration of power source using serial communications (via a stand-alone PC)	199

Contents

Figure 27	Calibration of control of power source using user-interface PC - automatic 'hot-key' command and control rack	200
Figure 28	Transient current signal - forced output ± 5 Amps - ideal system response for closed-loop control	201
Figure 29	Transient current signal - forced output ± 5 Amps - typical system response for closed-loop control	202

- from the Experimental programme (§4) -

Figure 30	Graphical presentation of input and output membership functions, example input and resulting lambda cuts for resultant crisp output (target frequency of 80 Hz)	203
Figure 31	Input/Output curve for fuzzy logic model	204

- from the Experimental results (§5) -

Figure 32	Arc voltage trace from passive R-C filtration	205
Figure 33	V/I Characteristic for AMI 207 TIG arc on solid copper bar	206
Figure 34	Arc voltage response to shielding gas - copper anode	207
Figure 35	Effect of tungsten degradation on arc voltage signal - response to current pulse	208
Figure 36	Power source pulsing characteristics - copper anode (AMI 207 and BDH 320)	209
Figure 37	Transient arc voltage response - partial and full penetration SS316L 38.1 mm diameter 1.65 mm WT	210
Figure 38	Signal processing the arc voltage - optimisation of the fully penetrated response	211
Figure 39	Signal processing the arc voltage - optimisation of the partially penetrated response	212
Figure 40	Typical output frequency after analogue signal processing and A/D conversion (Fast Fourier Transform analysis)	213
Figure 41	Typical pool frequency response vs. average pool size - stationary spot welding	214
Figure 42	Effect of pulse magnitude on pool oscillation - stationary pool - 2 mm WT SS316L	215
Figure 43	FFT spectra for two stationary pools - predominantly Mode 3 and a mixed-mode response	216
Figure 44	Basic welding parameters - effect of welding current upon pool frequency 04:30 position (I)	217

Contents

Figure 45	Basic welding parameters - effect of welding current upon pool frequency 04:30 position (II)	218
Figure 46	Frequency response for 4 orbital positions SS316L 38.1 mm diameter 1.65 mm WT	219
Figure 47	Penetration profiles from the effect of penetration upon frequency (1) - Base Current 10.0 to 17.5 Amps	220
Figure 48	Penetration profiles from the effect of penetration upon frequency (2) - Base Current 20.0 to 27.5 Amps	221
Figure 49	Effect of orbital position - full penetration weld on SS316L 35 mm diameter 2 mm wall thickness material	222
Figure 50	Surface roughness of inner beads - speed & current pulse trials	223
Figure 51	Effect of penetration upon outer bead appearance	224
Figure 52	Effect of welding speed upon quality of arc voltage signal	225
Figure 53	Stationary weld pool - electro-polished ('EP') material	226
Figure 54	Stationary weld pool - 'Cast 1' material	227
Figure 55	Stationary weld pool - 3D time (pulse number) & base current versus frequency plot (SS316L 35 mm diameter 2 mm WT)	228
Figure 56	Surface tension and frequency plots from membrane and Yoo's model for electro-polished ('EP'), low sulphur ('LS Kobe'), Cast 1 and 2 materials	229
Figure 57	Cast-to-cast variations - spot weld test and time-to-penetrate ('280410' and 'MS097' casts)	230
Figure 58	Cast-to-cast variations - spot weld test and time-to-penetrate ('2" Pipe 2' and '2" Pipe 4' casts)	231
Figure 59	Observed pool frequency and surface tension prediction from stationary spot test	232
Figure 60	Cast-to-cast variation - effect of welding current on pool frequency and inner bead width (low sulphur LS 'LS Kobe' and high sulphur HS 'Cast 1' casts)	233
Figure 61	Cast-to-cast variation - effect of welding current on pool frequency and outer bead width (low sulphur LS 'LS Kobe' and high sulphur HS 'Cast 1' casts)	234
Figure 62	Cast-to-cast variation - effect of heat input upon inner bead width (low sulphur LS 'LS Kobe' and high sulphur HS 'Cast 1' casts)	235
Figure 63	Frequency response for 4 orbital positions - low sulphur LS 'LS Kobe' and high sulphur HS 'Cast 1' casts	236
Figure 64	Signal conditioned arc voltage response - partially penetrated condition in LS ('LS Kobe') material	237

Contents

Figure 65	Signal conditioned arc voltage response - partially penetrated condition in <i>HS</i> ('Cast 1') material	238
Figure 66	Arc voltage response - fully penetrated condition in <i>LS</i> ('LS Kobe') material	239
Figure 67	Arc voltage response - fully penetrated condition in <i>HS</i> ('Cast 1') material	240
Figure 68	Real-time frequency response - PARTIAL to FULL penetration - 'Cast 1' and 'Cast 2'	241
Figure 69	Real-time frequency response - FULL to PARTIAL penetration - 'Cast 1' and 'Cast 2'	242
Figure 70	Partial & full penetration response - bead on tube - 4 segments (partial, full, partial, full penetration conditions) ('1.5" Thick' material)	243
Figure 71	Partial & full penetration response - SQUARE BUTT JOINT - 4 orbital segments - pool frequency & current plot, bead widths & pool frequency plot ('1.5" Thick' material)	244
Figure 72	Inner and outer beads of square butt joint in '1.5" Thick' material for partial and full penetration response	245
Figure 73	Open-loop control output - full penetration leading to over-penetration weld on electro-polished material	246
Figure 74	Closed-loop behaviour - direct fuzzy interference - 'Cast 2' material - 80 Hz target frequency - TEST I	247
Figure 75	Closed-loop behaviour - direct fuzzy interference - 'Cast 2' material - 80 Hz target frequency - TEST II	248
Figure 76	Closed-loop behaviour - direct fuzzy interference - 'Cast 2' material - 80 Hz target frequency - TEST III	249
Figure 77	Inner beads of 'Cast 2' and Electro-polished material using closed-loop control	250
Figure 78	Closed-loop behaviour - direct fuzzy interference - 'LS Kobe' material - 80 Hz target frequency	251
Figure 79	Closed-loop behaviour - direct fuzzy interference - 'Cast 2' material - modified parameters - 120 Hz target frequency	252
Figure 80	Inner beads of 'LS Kobe' material (closed-loop control with set target frequency) and 'Cast 2' material with imposed base current step changes	253
Figure 81	Closed-loop behaviour - direct fuzzy interference - 'Cast 2' material - 80 Hz target frequency - 8 Amp step increase	254
Figure 82	Closed-loop behaviour - direct fuzzy interference - 'Cast 2' material - 80 Hz target frequency - 6 Amp step increase	255

Contents

Figure 83	Closed-loop behaviour - direct fuzzy interference - 'Cast 2' material - 80 Hz target frequency - 4 Amp step increase	256
Figure 84	Closed-loop behaviour - direct fuzzy interference - 'Cast 2' material - 80 Hz target frequency - 2 Amp step increase	257
 <i>- from the Discussion (§6) -</i>		
Figure 85	Proposed mixed-mode behaviour	258
Figure 86	Stationary pools (basic work) - comparison between experimentally observed data and Xiao (1992) for Mode 3	258
Figure 87	'Time-to-penetrate' behaviour - 'Cast 1' (HS) and 'LS Kobe' (LS) materials	259

SYMBOLS AND ABBREVIATIONS

	[usual units quoted in brackets]	
a	weld pool surface radius	[mm]
a _{eq}	pool radius - equivalent	[mm]
a _t	pool radius - top	[mm]
a _b	pool radius - bottom	[mm]
A/D	analogue-to-digital	
AVC	arc voltage control	
D	weld pool depth	[mm]
E	electric field strength	[V/mm]
f _p	pulsing frequency of current [(t _p + t _b) ⁻¹ for square wave pulsing]	[Hz]
f _d	frequency response (most dominant in oscillatory period - correlating with the highest normalised output from the Fast Fourier Transform after hardware and software signal processing)	[Hz]
f _{M1}	Mode 1 frequency (partial penetration)	[Hz]
f _{M2}	Mode 2 frequency (partial penetration)	[Hz]
f _{M3}	Mode 3 frequency (full penetration)	[Hz]
FFT	Fast Fourier Transform	
FSD	full scale deflection	
GTA	Gas Tungsten Arc	
H	material thickness	[mm]
H ₂	Hydrogen	
HS	high sulphur	
I	welding current, average or constant	[Amps]
IBW	inner bead width	[mm]
I _b	base current	[Amps]
I _p	peak current	[Amps]
L	weld pool length	[mm]
L _{col}	plasma column length	[mm]
L _{arc}	arc length	[mm]
LS	low sulphur	
MIG/MAG	Metal Inert Gas / Metal Active Gas	
MMA	Manual Metal Arc	
OBW	outer bead width	[mm]
p	side-wall slope (top pool width or length / bottom pool width or length)	
P _{arc}	pressure exerted by the arc on the pool surface	[N/m ² or Pa]
PG	purge gas (flow rate)	[l/min]
PID	Proportional Integral Derivative	
PLL	Phase Locked Loop	
PS	power source	

Symbols and abbreviations

R_s	average surface roughness (inner bead)	$[\mu\text{m}]$
R_{max}	maximum surface roughness (inner bead)	$[\mu\text{m}]$
R_q	statistical derivation of root mean square of surface roughness (weighting to predominant features of surface)	$[\mu\text{m}]$
S	welding travel speed	$[\text{mm}/\text{min}]$
SG	shielding gas	$[\text{l}/\text{min}]$
SS	stainless steel	
t	time	$[\text{s}]$
t_b	base current duration	$[\text{s}]$
t_d	damping duration	$[\text{s}]$
t_{max}	critical occurrence of melt-through (γ -test)	$[\text{mm}]$
t_p	peak current duration	$[\text{s}]$
T	temperature	$[\text{°C}]$
TIG	Tungsten Inert Gas	
V	arc voltage, average	$[\text{V}]$
V_s	potential difference across the anode fall region	$[\text{V}]$
V_{amp}	voltage amplitude of oscillatory response	$[\text{V}]$
V_c	potential difference across the cathode fall region	$[\text{V}]$
V_{col}	potential difference across the plasma column	$[\text{V}]$
W	weld pool width <i>or</i> diameter ($= 2a$) for circular pools	$[\text{mm}]$
WT	wall thickness	$[\text{mm}]$
α	thermal diffusivity	$[\text{mm}^2/\text{s}]$
γ	surface tension	$[\text{N}/\text{m}]$
γ_{iron}	surface tension for specific material (iron for example)	$[\text{N}/\text{m}]$
π	Pi constant	
ρ_s	density of solid material	$[\text{kg}/\text{m}^3]$
ρ_l	density of liquid material	$[\text{kg}/\text{m}^3]$
τ	time constant	
ω_n	natural frequency	$[\text{rad}/\text{s}]$

Symbols and abbreviations

Fuzzy Logic labels

The following fuzzy logic labels were used to define the state of penetration (using the weld pool frequency):

OP	over-penetrated
SO	slightly over-penetrated
FP	fully penetrated
PP	partially penetrated
SP	slightly penetrated

Corresponding output labels were defined in a similar manner, to classify the appropriate change in the base welding current variable:

-LG	negative large change (delta base current)
-SM	negative small change (delta base current)
ZE	zero change
+SM	positive small change
+LG	positive large change

SECTION 1.

INTRODUCTION

1. INTRODUCTION

Fusion welding processes are used as effective joining methods for many iron-based, nickel-copper, aluminium and titanium materials. One of the most common joints to be made is an orbital or circumferential weld between two pipes or tubes, since piping and tubing is used in multitudinous industries, including:

- electronic and medical (for high purity gas supply),
- aerospace and space (for fuel piping and ducting),
- dairy, petrochemical, and power generation (process plant),
- oil and gas (as transportation lines).

There are many types of joint (square butt, V- and J-prep, narrow gap) and different welding processes have been suited to the various applications. Most orbital joints involve the same complexities however, in addition to the more usual problems of fit-up, root gap, thickness variations, and so on. These include:

- variable heat build-up and dissipation around the joint, and
- the effect of gravity upon the behaviour and shape of the molten weld pool.

The above factors are also dependent upon the tube or pipe joint geometry itself, the thermal properties of the material, as well as the welding parameters actually used.

In order to account for the above complexities, automatic welding systems are employed that modify welding parameters during the completion of the joint - travel speed, welding current or voltage, weave parameters, wire-addition rate, etc. Each application has its own particular requirements, in terms of the material, alloy and treatment used, its strength, damage tolerance, corrosion resistance, creep resistance, thermal properties and so on. For high quality joints, the TIG (Tungsten Inert Gas) or GTAW (Gas Tungsten Arc Welding Process) is predominantly used where an arc is struck between a non-consumable tungsten electrode and the work-piece, usually using argon or helium shielding gas, although other gas additions are occasionally used. The high quality results produced by the TIG process are favoured by the aerospace and electronic industries where the control of the bead profile can be a stringent requirement.

Introduction

The common grades of austenitic stainless steels are used for tubing applications in many of the above industries (AISI 304, 304L, 316, 316L), since they offer a reasonable compromise between cost, weight, strength, corrosion resistance and weldability. Unfortunately although they are relatively straightforward to weld, they suffer from 'cast-to-cast variations'. A TIG welding procedure that has been derived for one batch of SS316L for example, can produce a significantly different bead profile on a different batch despite the fact that they can both still be classified as '316L'. Wider, shallower beads have been observed with certain casts, and deeper, narrower beads with others. Many causes of this phenomenon have been debated and a review of the current thinking is related in the literature survey (§2.6.1).

It is generally believed that certain minor constituents present at the surface of the molten pool play a major role in the predominant flow behaviour. Improved manufacturing techniques have resulted in the production of 'cleaner' austenitic stainless steels, with reduced levels of minor elements. Consequently, these steels could present significant weldability problems. Variation in the bead profiles generated is critically important for orbital welding of pipe and tube, since:

- lack of penetration can result from wide, shallow beads which may then go undetected since the back-face is rarely accessible in small diameter tubing (unless a non-destructive technique is applied),
- any lack of penetration can be wholly detrimental to the strength and structural integrity of the joint - the unfused interface can act as a crack-starter under tensile and bending loads and can also act as a reservoir to trap moisture and contamination in the case of ultra-high purity tubing.

Currently the only common form of sensing offered by many proprietary automatic orbital systems is arc voltage control, where the arc length is adjusted around the joint to maintain a constant arc voltage and heat input. Many industries have identified that the next most important step for application development relates to the need for intelligent process control (see Nomura, 1994, and Ushio, 1994).

Various basic methods with differing control mechanisms have been used for *penetration* control of the TIG process over the years:

Introduction

- **top-face sensing**, the observed geometry of the upper surface profile has been used to predict the bead depth (Wu, 1996, or Kovacevic, 1996 for example) by CCD camera etc., tracer elements detected at the upper surface that were deposited on the under side have been used to identify formation of the inner bead,
- **back-face sensing**, where the penetration width was directly observed with optical or infra-red instrumentation, or inferred by the use of temperature measurement,
- **through-the-arc sensing** where characteristics of the arc voltage are used to identify the state of the weld pool - Bicknell (1994) observed the voltage drop as the pool surface rose and fell as the transition from the partial to the full penetration state was made in 1G conditions.

A comprehensive review of sensor systems for top-face penetration control was made by Anderson (1995). In recent years, significant research has been undertaken into the use of pool oscillations as a method of penetration control. By observing the natural frequency of the pool the size and penetration condition of the pool can be inferred. The natural frequency can be monitored in the arc voltage as it is a function of the arc length, which oscillates with the top surface of the pool after a short excitation force, usually applied via the welding current.

This thesis focuses upon the application of this technique to different casts of relatively small-bore austenitic stainless steel tubing (38.1 mm outer diameter with 1.65 mm wall thickness), as often used by the electronics industry. The pool oscillation method is ideally suited for the penetration control of ultra-high purity small-bore tubing since:

- it does not necessitate intrusion into the back-face thereby compromising the high cleanliness requirements,
- it can be implemented without the use of an external sensing element which would be difficult to manoeuvre in a relatively small and size restricted orbital head.

'Time-to-penetrate' studies were also applied using pool oscillations as a measure of the level and state of penetration, to study the differing penetration behaviour of the various batches of material used (the studies were also extended to include some thicker material casts).

Introduction

All the tables and figures referred to in the text can be found at the back of the thesis (see 'Appended tables and figures'). The literature survey (§2) reviews theoretical pool oscillation behaviour, pool oscillation research to date and also provides a comprehensive review of other factors which affect the application of pool oscillations. A description of all the equipment and materials used for the research work can be found in section 3, together with calibration details of the *closed-loop system* that was employed. Experimental work (§4) was generally divided into studies of the basic pool oscillation mechanism, cast-to-cast effects in thin and thick materials (1.65 and 3.91 mm wall thickness respectively), and real-time work using pool oscillations to control the penetration in the smaller tubing.

Theoretical models of pool behaviour were found not to offer a reliable prediction of pool geometry from the observed pool frequency. Consequently, fuzzy logic was used to provide a framework for the penetration control mechanism, providing an interface between the monitored pool frequency and the necessary changes in welding parameters. A review of other published welding applications of fuzzy logic is included at the end of the literature survey.

Discussion of the research work presented is divided into three fundamental areas: correlation of the practical observations with the published theory, the effect of cast upon the pool geometry and the associated oscillation signals, and the application of the pool oscillation frequency to penetration control of orbital welding. The thesis ends with the conclusions from the research work.

SECTION 2.

LITERATURE SURVEY

2.1 Background

2.2 Principal oscillation methods

2.2.1 Free response: arc light intensity and voltage

2.2.2 Resonant or forced response

2.2.3 Summary

2.3 Theoretical mathematical modelling of natural frequency

2.3.1 Fully penetrated molten pools

2.3.2 Partially penetrated molten pools

2.3.3 Summary

2.4 Observed Oscillation Behaviour

2.4.1 Amplitude

2.4.2 Damping

2.4.3 Partial, full and mixed-mode responses

2.4.4 Material dynamic response

2.5 Effects of welding parameters and operating conditions on pool and oscillation behaviour

2.5.1 Shielding gas

2.5.2 Welding current (pulsed and sinusoidal application)

2.5.3 Travel speed

2.5.4 Tungsten geometry

2.5.5 Arc length

-
- 2.5.6** Joint preparation
 - 2.5.7** Orbital position and gravity
 - 2.5.8** Surface tension, γ
 - 2.5.9** Summary

2.6 Other factors influencing the application of pool oscillations

- 2.6.1** Cast-to-cast behaviour
- 2.6.2** Pulsed (-TIG) current welding
- 2.6.3** Arc pressure distribution and magnitude
- 2.6.4** Power source characteristics and signal processing
- 2.6.5** Fast fourier transform

2.7 Control methods

- 2.7.1** Conventional control methods
- 2.7.2** Fuzzy logic in welding process control

2.8 Concluding remarks

2. LITERATURE SURVEY

2.1 Background

The natural phenomenon of weld pool oscillations was first identified in the literature by Kotecki (1972) relating the observed natural frequency of a TIG weld pool to its size, mass, and surface tension, γ , by using high speed filming. Following this initial study many researchers have used the dynamic aspect of a molten pool's behaviour as a monitoring and control method of weld pool size and hence penetration. The vertical motion of the pool affects the arc length accordingly and since both arc voltage and arc light intensity are directly related to the arc length, both measurable parameters can be used as sensing elements. Many authors in the past have concentrated upon using the arc voltage, presumably for its ease of measurement. In general, the arc light intensity measurement has received less attention, although it has recently been directly compared with voltage for the relative differences in signal amplitude, damping and robustness (Yoo, 1993).

The motion of the pool can be categorised into one of several dominant vibration modes and it has been established that the frequencies exhibited by elliptical, partially penetrated weld pools are significantly higher than those of fully penetrated weld pools. This is in accordance with what might be intuitively expected upon examination - see Figure 1.

The generalised frequency behaviour illustrated indicates what can be sensed by monitoring the arc voltage or arc light intensity. Exact theoretical vibration modes, including the categorisation of 'slosh' modes have been detailed by authors such as Maruo (1993). Departures from ideal behaviour by actual weld pools have been observed and reported by Xiao (1993) and Yoo (1993).

Both free and forced vibrations of the pool have been used to sense the natural frequency. The most common method is to induce free vibration by the use of a short duration peak welding current pulse imposed upon a base current to impart a short impulse force via the arc upon the pool surface. Some authors have used a sinusoidal welding current applied to a stationary pool and detected the amplified response at resonance to infer the instantaneous pool size from the input frequency (Wang, 1993). Lillquist (1987) used the welding current, or the shielding gas flow rate as input variables with the use of a short frequency sweep (a variation in

Literature survey

frequency over the frequency range of interest) to detect amplification at the resonant frequency.

The application of the pool oscillation technique using arc voltage sensing offers several advantages, as already described. Unfortunately, problems and complexities encountered during previous research have so far hampered its application for welding control purposes. The main problems can be summarised as:

- the existence of Mode 2 (the slosh mode) in some fully penetrated pools (see Figure 1),
- relating the mathematical theoretical predictions of weld pool frequency to actual observed values, which is complicated by the departure of actual weld pools from theoretically ideal shapes,
- the decreased travel speed and short arc lengths necessitated compared with usual practice,
- and the quality of the sensing signal in relaying the oscillatory behaviour.

Although the most attention has been paid to the incidence and potential use for TIG welding both den Ouden (1993) and Nakata (1994) have found benefits for MIG. den Ouden found that the stability of the short-circuiting (dip transfer) MIG process was dependent upon the oscillation frequency of the pool and that only when the transfer frequency was equal to the natural frequency of the pool was the optimum process stability achieved. By using the natural frequency of the fully penetrated pool Nakata optimised grain refinement of the weld metal when current pulsing. The derived procedure involved pulsing at ≈ 90 Hz, to maintain arc stability, with the more dominant pulsing between high and low current pulses at the lower natural frequency of 30 Hz - see Figure 2. Optimisation was attributed to both the alloy developed as well as the stirring inside the molten pool caused by the pulsing.

Some work has also been performed on the incidence of pool oscillations in laser welding. Postacioglu (1991) provided theoretical mathematical modelling for pool frequencies during keyhole welding, and some correlation was provided by Semak (1995) from practical observations of pool amplitude and frequency for an austenitic stainless steel (SS304). Work performed on laser welds to date has not employed the use of pool oscillations as a method of monitoring or controlling keyhole size.

2.2 Principal oscillation methods

Two principal oscillation methods have been applied by previous researchers. Firstly a free response resulting from an imparted energy pulse has been studied. Usually the pulse has been applied via the welding current when travelling at a constant welding speed. Secondly, a forced response has been employed by applying a sinusoidal forcing input invoking an amplified response of the pool at the resonant frequency. This has been previously applied to a stationary 'spot' weld with subsequent travel occurring at a lower current to form a continuous joint.

2.2.1 Free response: arc light intensity and voltage

Both the arc light intensity and voltage can reflect the change in arc length. The arc itself can be subdivided into three regions exhibiting markedly different physical properties: the cathode fall zone, the plasma column and the anode fall zone. Whilst the cathode and anode fall zones have relatively constant potential for a given set of physical welding conditions (electrode type, geometry, shielding gas etc.), the potential of the plasma column itself is heavily dependent upon the arc length. The relationship between the total arc voltage and arc length is almost linear (Lancaster, 1984), and greatly influenced by the shielding gas employed (see §2.5.1). A change in arc length resulting from surface movement of the weld pool is directly reflected in both the magnitudes of the *arc light intensity* and the *arc voltage*. Pool oscillations have been monitored by measuring the associated variations light amplitude (as emitted by the welding arc - usually sensed by using a fibre-optic located locally to the arc) and the arc voltage (sensed by connecting leads to the electrode and work-piece).

A 'free response' of the pool can be generated by imposing a short impulse of energy upon the pool surface. This can be achieved by either pulsing the welding current or the shielding gas flow rate. A short impulse of relatively high current imposes a greater force upon the surface of the pool (see §2.6.3 for more detail), so that the molten pool vibrates at its natural frequency for a short period once the force is removed.

Researchers into the phenomenon of pool oscillations have often used a basic excitation pulse as shown in Figure 3 (Xiao, 1993 and Yoo, 1993, Suga, 1996), whereas others have modified the approach to optimise the response. Connelly (1986) used a high frequency - 1 to 15 kHz - pulsed current at both base and peak levels, as well as an intermediate level of current between base and peak before the free response was monitored. Smoother and more regular waveforms were reported via the arc voltage.

Literature survey

The imposition of the short current pulse upon a more conventional pulsed TIG programme has also been investigated (Aendenroomer, 1994). Modifications to the applied arc force direction by Wang (1988) improved the performance of this technique, by magnetically re-directing the arc back towards the geometric centre of the weld-pool for the instant that the peak current pulse was applied.

Peak current durations of 3 to 10 milliseconds are typically used with base current durations between 0.3 and 0.5 seconds. Authors using the straightforward pulsed approach often use a peak current which is 100 Amps higher than the base current.

The use of shielding gases which generate comparatively high electric field strengths are preferred (helium or argon with hydrogen, typically 5 to 10%, as opposed to pure argon), since the signal amplitude waveforms resulting from the excitation are relatively small.

Recently it has been claimed that the arc light intensity is a more robust signal than the arc voltage revealing clear oscillations at higher travel speeds, with a greater signal-to-noise ratio (Barborak, 1994, Yoo, 1994, and Deam, 1989).

Andersen (1993) presented one optimised approach by employing a Phase Locked Loop (PLL) to excite the pool in phase with the oscillations resulting in a comparative decrease of the required current pulse peak level (I_p).

2.2.2 Resonant or forced response

The use of a sinusoidal current waveform overcomes two problems: the deterioration of the oscillation signal with time through damping, and forcing the response of the pool to be comparatively regular because of the form of the input current. Input current is varied between base, I_b , and peak, I_p , sinusoidally at the frequency of the desired weld pool size. Once the weld pool reaches the appropriate size, amplification of the vertical displacement will occur at the pool's resonant frequency. The amplitude of the voltage signal can be monitored and used as a trigger to cease application of the welding current, apply a lower current and move to the next location forming an overlapping series of spots.

Wang (1993) used the approach to effect closed-loop control on carbon and stainless steel plate (1-2 mm thick) with high welding speeds (140 - 180 mm/min), although a wide bead was generated by the stationary arcs used. Work on an aluminium alloy with a.c. has also been published where

Literature survey

electrode cleaning is performed during the electrode positive (DCEP) moving arc period.

Mixed-mode responses which have been observed in freely oscillating pools can be minimised using the forced input. Mode 2 behaviour and mixed-mode response (two frequencies occurring at the same time) have been observed in fully penetrated pools when using a free response to singular impulse. Neither of these observations were reported in Wang's work. It could be that forcing the weld pool behaviour results in a more regular, pure modal response. Additionally, it is highly pertinent that the forced approach often utilises a stationary arc.

Stationary arc welding is more easily facilitated on thicker materials and also usually results in a wider bead than from continuous travel. A continuous travel application was used by Lillquist (1987) who modulated either the welding current or the shielding gas flow rate (through a conventional TIG torch) and detected the amplified response of the signal amplitude at the resonant frequency via the arc light intensity.

2.2.3 Summary

Both the free and forced response of the weld pool have been employed as means of using the oscillation of the pool to control the penetration. Forced responses, where the pool is usually excited by a single frequency by the welding current or shielding gas have generally been used on thicker materials or where the control system has become quite specific. The free response of the pool has frequently been used since it can be employed using pulsed procedures that are close to those used in industrial practice, with relatively standard equipment.

Hybrid approaches have also been adopted - Andersen's (1993) Phase Locked Loop generated free responses at regular intervals resulting in a constant oscillation of the pool. Aendenroomer (1996) used a pulsed-TIG procedure with excitation pulses at the start of the peak and base current periods to generate and control a full and partial penetration response respectively.

2.3 Theoretical mathematical modelling of natural frequency

Previously derived theoretical models have inevitably idealised the welding situation. In reality, there are *many* potential variants to be considered:

- the geometry of the weld pool (elliptical upper and lower surfaces, tapered pool sides, teardrop or eccentricity effect from travelling pools, etc.),
- misalignment, root gap, thickness tolerances, etc.,
- the variation of surface tension with temperature and surface activity of minor elements (see §2.5.8),
- the geometry of the excitation force with respect to the geometric centre of the pool, and
- the variation of density with temperature.

In addition, if varying heat dissipation characteristics are experienced, a more complex weld pool geometry from irregular heat flow situations can occur. In order to assess the behaviour of the molten pool basic assumptions have been made. Most authors have assumed the following:

- surface tension (γ) is a constant,
- density (ρ_l) is a constant, and
- the weld pool shape is geometrically regular.

For example, Maruo (1993) has accounted for elliptically shaped weld pools and provided a model for a comprehensive parameter range, although no account has been made for the different profile between upper and lower surfaces. Whereas Yoo (1993) accounted for the difference by including an additional modelling parameter - the side-wall slope, p - as well as modelling elliptical pools.

The simplistic models presented in Figure 1 as Modes 1, 2, and 3 do occur in practice in the partial and fully penetrated conditions respectively. The generation of Modes 1 and 3 responses can be relatively straightforward with a considered selection of pulsing parameters (see Xiao, 1992 for example). However, departures from this behaviour have been frequently observed and the main additional cases to be taken into account are:

- the occasional existence of a Mode 1 or 2 response in fully penetrated pools, with the derivation of a further 'transitional mode' (see (e) in Figure 4), and
- the resulting alteration of the response with increasing travel speed or current as the pool shape becomes more eccentric.

Most weld joint control requirements are for the completion of fully penetrated joints. The modelling of the partially penetrated responses is nevertheless important in order to assess the degree of alteration of the welding parameters required to achieve the full penetration state.

Yoo (1993) classified the response categories as shown in side-profile in Figure 4. The transition mode of a Mode 1 response in a pool with a lower free surface is shown in diagram (e), and the slosh modes in diagrams (b) and (d). Elliptical pools are modelled by the inclusion of parameters W (Weld Pool Width) and L (Weld Pool Length) [not shown in the diagram].

2.3.1 Fully penetrated molten pools

A membrane model has been presented by many authors. Kotecki's original derivation, based upon the vibration of a plane stretched circular membrane, as illustrated schematically by (a) in Figure 4 (top and bottom surfaces having equal radius) has been little altered in form in subsequent years (Kotecki, 1972) - see Equation 1.

$$f_{M3} = \frac{0.54}{a} \sqrt{\frac{\gamma}{\rho_l H}} \quad \text{Eq. [1]}$$

Here,

f_{M3} is the predicted frequency for a Mode 3 oscillation (Hz),
 a is the general pool radius (m),
 γ is the acting surface tension (N/m),
 ρ_l is the density of the liquid material (kg/m³), and
 H is the material thickness (m).

An effectively identical relationship formed the basis for Hardt's work at the Massachusetts Institute of Technology with several co-workers (see Zacksenhouse, 1983, for example). A further refinement based on an equivalent pool diameter was presented by Xiao (1992) (from a classical hydrodynamics derivation). An equivalent diameter was adopted to compensate for lower and upper surface size differences - see Equation 2.

$$a_{eq}^2 = \frac{1}{3} (a_t^2 + a_t a_b + a_b^2) \quad \text{Eq. [2]}$$

Subscript eq denotes an equivalent pool radius, with t and b for pool radius - top and bottom surfaces - respectively.

Results published by all authors show reasonable correlation, particularly for larger pool sizes with vertical walls. Kotecki compared a measurement of the frequency and instantaneous stationary pool size to derive experimental values of surface tension for Al, Cu, Ni, Fe, Ti materials. Although the estimates were the correct order of magnitude, some scatter was evident.

Surface tension values for austenitic stainless steels have been observed to be subject to a significant degree of variation and this has a corresponding effect upon the frequency prediction. Assuming a value of surface tension without any direct measurement of the material cast used could result in a considerable degree of error in the expected frequency response. Example values are plotted to illustrate this point in Figure 5 (see also §2.5.8 and §2.6.1 for further detail on the implications of surface tension variation).

Maruo (1993) presented a theoretical relation for elliptical pools ($W/L \neq 1$), enabling predictions for any pool shape. Correlation with physical pool behaviour was not performed. The basis was identical to that adopted by Xiao and predicts Mode 3 frequencies for the case of the plane circular pool (see Equation 1). Yoo (1993) accounts for the side-wall slope of the fully penetrated pool, and identifies it as 'p' (top pool surface width or length/bottom pool surface width or length).

For the full penetration Mode 3 oscillation, Yoo developed a second-order mass-spring-damper system and derived the frequency relation from an energy method - see Equation 3.

$$f_{M3} = \frac{1}{2 \pi} \sqrt{ \frac{8 \gamma p}{\rho_l H} \cdot \left(\frac{1}{L^2} + \frac{1}{W^2} \right) \cdot (1 + p^4) } \quad \text{Eq [3]}$$

Here:

p is the side-wall slope parameter,
L is the weld pool length (m), and
W is the weld pool width (m).

If a side-wall slope of unity is assumed and the pool is circular, Yoo's relation for pool frequency is some 17% lower than the membrane model. In addition to the frequency model, the degree of damping was also modelled by accounting for the effects of travel speed and molten metal viscosity. It was observed by video that the Mode 3 symmetrical oscillation behaviour was only evident for side-wall slope, $p = 0.5$ and above ie. that even with a relatively small lower free surface higher frequency modes were exhibited at the pool surface. Eccentricity of the pool by increasing travel speed etc. was found to decrease the expected frequency response.

2.3.2 Partially penetrated molten pools

Xiao (1992) derived partial penetration models, simplifying them with assumptions. She assumed that realistic pools have a pool depth/pool diameter ratio of greater than 0.2 ie. that they are generally not shallow and wide, and that the effect of the gravitational force can be neglected:

$$f_{M1} = \frac{5.84}{W^{3/2}} \sqrt{\frac{\gamma}{\rho_l}} \quad \text{Eq. [4]}$$

Here f_{M1} is the predicted frequency for a Mode 1 oscillation (note the units used in Equations 1 and 3).

$$f_{M2} = \frac{3.37}{W^{3/2}} \sqrt{\frac{\gamma}{\rho_l}} \quad \text{Eq. [5]}$$

Here f_{M2} is the predicted frequency for a Mode 2 oscillation (the slosh mode).

For practical weld pool sizes, the error involved in making the assumptions is small. Comparisons of Mode 1 behaviour for austenitic stainless steel (SS304) and ferritic steel (Fe 360) showed a close correlation with theory. The theoretical relation derived by Yoo for partially penetrated pools was dependent upon an additional empirical parameter: n , described as a parameter chosen to be compatible with the penetration condition (an amplitude descriptor). This further complicates a theoretical prediction of pool frequency from the given physical parameters.

2.3.3 Summary

Theoretical treatments of the pool oscillation model have been made by several authors, and recent work by Xiao (1992) confirms the validity of Maruo and Hirata's work (1993). Further, more detailed modal studies were carried out by Yoo (1993) deriving transitional and mixed-mode predictions, however these models involved the use of an extra parameter derived empirically from the amplitude of the oscillation. An explicit model was only presented for the full penetration case (diagram a. in Figure 4) - see Equation 3.

The potential use of the pool oscillation frequency might thus be summarised as follows:

- if the acting surface tension, liquid density and material thickness are known, and the pool oscillation frequency measured (either via the arc light intensity or the arc voltage) an estimate of either the pool diameter can be made for the case of a fully penetrated pool, or the pool depth for the case of a partially penetrated pool.

This is presuming that the modal behaviour of the oscillating pool is known at the time of frequency measurement, which is a reasonable assumption since the frequency responses for the fundamental modes are quite well separated - see Figure 1.

However, the acting surface tension for some commonly used materials for orbital welding is not a material constant. It changes significantly with the bulk material temperature, and since the pool surface under a TIG arc has a temperature gradient the surface tension alters accordingly. The overall surface temperature of the pool can also be affected by the magnitude of the mean welding current applied. Minor elements present in austenitic grades of stainless steel are also thought to cause extreme variability in penetration behaviour under identical welding conditions because of their effect upon the acting surface tension (see also §2.5.8 and §2.6.1).

Without an accurate knowledge of the surface tension behaviour, the pool width/depth cannot be derived from the oscillation frequency measurement according to the equations presented above.

Literature survey

A method of applying pool oscillations has to be derived that is either not dependent upon a prior knowledge of surface tension, since this is likely to be erroneous for the case of the welding arc, or can account for the variations in surface tension that are likely to be encountered. Aendenrooier (1994) applied an approach based upon establishing a full penetration condition (Mode 3) during a peak pulse of current, and a partial penetration response (Mode 1) during the base current pulse. A 'binary' type of control of the peak pulse current was applied by assuming under-penetration with two Mode 1 responses (ie. to the base and peak current pulses) and over-penetration with two Mode 3 responses. This method did not depend upon the surface tension and relied only upon the modal differences between the responses to the peak and base current responses.

2.4 Observed oscillation behaviour

This section will review the dynamic behaviour of the weld pool with reference to the oscillation modes in general terms, and subsequently the effect of specific material properties.

2.4.1 Amplitude

The amplitude of the motion can be derived either via the arc voltage, arc light intensity or by direct observation. Kotecki (1972) observed that surface motion in the fully penetrated pool was not only vertical but also rotational. It has been observed that during the high current pulse there is an initial surface wave in fully penetrated pools (Ecer, 1981). However, this discussion will be confined to the vertical motion associated with the bulk movement of the pool that generally occurs during the base current (I_b) pulse.

Xiao (1992) directly observed a smaller amplitude in Mode 2 pools than for Mode 1, with Mode 3 larger than either. Although the arc voltage reflects the oscillation by altering with the arc length, the amplitude that might be derived from a simplistic assumption that the small change in arc length (δL_{ac}) results in a direct change in the arc voltage (δV) (see Equation 6 in §2.5.5) for a given electric field strength, E , under-estimates the actual pool amplitude. The arc voltage appears to yield an assessment of the 'average' arc length rather than the axial vertical electrode tip to pool surface distance. These measurements are confirmed by the results published by Xiao (1992) and Andersen (1993). Correspondingly, this particularly affects the voltage amplitude (V_{amp}) for the partial penetration cases.

Studies of arc voltage and arc length by other authors do not generally include the case of the vibrating, or oscillating, weld pool - only comparatively static pool surfaces are considered.

The amplitude of any oscillatory behaviour is heavily dependent upon the arc force used to generate it and correspondingly affected by all the variables which affect the arc force and its distribution: shielding gas, current magnitude, and rate of rise, electrode diameter, vertex angle and truncation etc. (see also §2.6.3). Since the surface tension of the pool specifically acts to maintain equilibrium under the action of the arc force the magnitude of the pool amplitude is also dependent on γ , as well as the bulk material properties. Lin (1987) found that an optimum maximum amplitude resulted from using a peak pulse time (t_p) of 5 milliseconds for the parameters used. This is a typical value from researchers using the single-

pulse approach. Richardson (1989) observed an increasing signal amplitude with increasing pulse current (I_p), and a decreasing signal amplitude with increasing arc voltage (from a corresponding increase in arc length) when using Inconel 718 material.

It should be pointed out that using a conventional pulsed TIG program with an argon shielding gas does not tend to produce weld pools with significant oscillation amplitudes.

2.4.2 Damping

Oscillations damp out due to a loss of energy in stationary pools at a rate dependent upon the viscosity of the molten material, and moving pools also constantly contribute unmelted material to the pool and subsequently solidify, adding to the energy dissipation. Accordingly, damping exhibited in moving pools is higher than for stationary ones, and increasing travel speed inevitably causes higher damping.

At relatively high travel speeds for this type of work both Yoo (1993) and Barborak (1994) record the identification of oscillations in the arc light signal, with only noise in the arc voltage. Typical full penetration pool oscillations for a SS304 of 3 mm thickness might take around 400 milliseconds to damp out for a 'slow' travel speed of 60-90 mm/min, whereas higher travel speeds result in a typical damping duration of less than 200 milliseconds as recorded by arc light (Barborak, 1994). The quality of signal processing, both at the analogue and digital stages directly affects observations that have been made. The characteristics of the power source combined with the filtration strategies and mathematical processing can also have detrimental effects on the resulting signal.

2.4.3 Partial, full and mixed-mode responses

The transition from a partially penetrated weld pool to a fully penetrated weld pool can be traced through the dominant frequency response. As already highlighted, the lower frequency response associated with Mode 3 oscillation only begins to occur once the lower free surface is fairly well established. It has been estimated that only once the lower surface width is greater than half the upper surface width is Mode 3 dominant (Xiao, 1992).

Mixed-mode signals can occur in two ways :

- the initial occurrence of a partial penetration response (Mode 1 or 2) with a transition to a full penetration response (Mode 3) identified in the free response application, attributed to the delay between the peak current pulse application and the consequential thermal response in melting through the thickness and/or,
- the simultaneous combination of modal responses usually occurring in a fully penetrated pool with a Mode 1 surface wave imposed on the vertical motion of the fully penetrated response, ie. (e) of Figure 4.

Averaging of the time period is obviously inadequate and inaccurate in resolving mixed-mode signals. Spectral analysis using a Fast Fourier Transform would not necessarily resolve the difference between the above two conditions - although it would assess the strength of the modes in terms of amplitude. Time-based Fast Fourier Transform approaches can be used to resolve frequencies that develop or change with time.

It has been stated that the existence of mixed-mode signals complicate the potential application of pool oscillations. If the lower frequency mode can be detected using a proficient spectral analysis method then the presence or absence of the full penetration condition can be deduced ie. a 'true' low frequency response can only be present if full penetration has occurred and a lower free surface has been formed.

Detecting partially penetrated responses is more difficult to achieve due to the associated decreased amplitude and increased damping characteristics. For the free response case whilst Xiao (1992) fully reports these signals (see Figure 6), recent work published by Bicknell (1994) found difficulty in extracting a partially penetrated response from comparatively thin 0.9 and 1.6 mm thick austenitic stainless steel (SS304).

2.4.4 Material dynamic response

The pool oscillation approach to penetration control has been applied to several materials: copper, ferritic steel (Fe 360), austenitic stainless steels (SS304, SS316), High Strength Low Alloy (HSLA) steels, Inconel 718 and aluminium. Many researchers have used SS304 or SS316, since these grades are extremely common in practical process pipework applications. The influence of surface tension and density upon the frequency has been

given earlier in §2.3. The thermal conductivity, specific heat and thermal diffusivity of the material also affect the actual pool size for a given parameter set.

Successful investigation of the free and forced approaches has been undertaken upon mild and stainless steels. Connelly (1986) used various excitation pulses to regulate the response of comparatively thick High Strength Low Alloy steels. Wang (1993) used the forced response upon aluminium with a variable polarity power source. Oscillations were monitored during the electrode negative phase, prior to a short positive cleaning phase.

2.5 Effects of welding parameters and operating conditions on pool and oscillation behaviour

2.5.1 Shielding gas

The characteristics of the shielding gas which are especially important when considering the motion of the pool are:

- the generated average electric field strength, E , which governs the sensitivity of the arc voltage to the arc length,
- the magnitude of the excess arc pressure exerted on the pool surface for a given current amplitude as this is the usual excitation mechanism, and
- the influence of the physical properties of the gas used upon the resulting pool size and shape.

It is also important that the gas does not cause problems relating to the mechanical properties and microstructure of the weld metal.

Researchers have used the following gases: helium, argon, and argon with hydrogen additions. In general, helium is used for its higher electric field strength and resulting sensitivity, argon for the increased arc pressure generated, and argon with hydrogen additions for a combination of the two. Use of helium or hydrogen additions to argon can offer benefits in terms of reasonable arc initiation, due to the contribution of the ionization potential of argon to the start-up characteristics, and higher welding speeds or decreased currents due to a higher heat input from the helium/hydrogen.

Cleaner beads of austenitic stainless steels can be produced by using argon with hydrogen additions since the hydrogen acts partially to reduce oxygen present in the local welding environment, and it is for this reason that it can be a preferred shielding and backing gas for ultra-high purity applications (Tsuraha, 1990). The reduction of oxygen in the molten pool surface when hydrogen was present in the argon shielding gas was proposed by Wen (1986) when measuring the surface tension of an austenitic stainless steel, SS304 (also see §2.5.8). The reducing effect of hydrogen upon the oxygen (and hence the surface tension since oxygen is known to be a surface active element) also has implications for the penetration behaviour of austenitic stainless steel welds in particular (also see §2.6.1). Hooijmans (1995) observed the effect of hydrogen upon the electric field

strength and expressed the rate of increase in voltage as 0.3V./vol. %H₂ (for an arc length of 3 mm). Higher melting efficiencies were obtained with increasing hydrogen additions (15% melting efficiency for pure argon, and 40% for argon with 15% hydrogen reported) which were attributed to the higher thermal conductivity of hydrogen.

The electric field strength of a Gas Tungsten Arc is typically 0.8 V/mm in argon, and 1.8 V/mm in helium. Zijp (1994) showed that an increase in the electric field strength by mixing argon and helium only occurred for 75% helium and above. A similar result was presented by Glickstein (1982) who also presented a marked decrease in the electric field strength of the helium arc with a small concentration of aluminium vapour. The possible presence of aluminium in the weld pool and subsequent vapourisation under the welding arc was also suggested at the time as a contribution to cast-to-cast problems for austenitic stainless steels.

Helium has been used by most researchers concerned with the free response of the pool (Xiao, 1992, Madigan, 1986 etc.). Forced response of the pool has enabled the use of argon, despite the resulting lower sensitivity, since amplification of the response results in a larger voltage amplitude (Wang, 1993). Slight differences in frequency response have been noted by investigators when using helium compared with argon, although these could be attributed to the effect of the shielding gas upon the shape and size of the weld pool.

In contradiction with some previous authors, Tam (1989) thought that the flatter power spectral density response of the pool oscillation signal from using argon as opposed to helium meant that the use of argon would be preferential. This might be expected from the larger force imparted using argon for the same welding parameters generating a larger amplitude and more pronounced frequency response, despite the associated reduction in electric field strength.

Mixing argon, helium and hydrogen, to optimise the pool oscillation conditions has not been reported (for example BOC Helishield H4 nominally contains 85% Ar, 11% He, and 4% H₂). If the arc force characteristics of argon with hydrogen, and the electric field strength of helium could be realised, a more ideal oscillatory response might be observed. The use of small additions to a bulk argon shielding gas using a TIG torch with double gas flow have also been investigated to help reduce cast to cast variations in stainless steels - an addition of 1% SO₂ was found to increase D/W for AISI 316L (Luijendijk, 1995).

Compatibility between shielding gas and material used is also a primary concern. The use of hydrogen in particular has been reported to cause porosity in thick section nickel, and nickel alloys above a level of 5% (Monel and Inconel etc.), and cause cracking in some carbon and alloy steels. Multi-pass welds with hydrogen additions have not been recommended for austenitic stainless steels (Lucas, 1992). Hooijmans (1995) found a level of 15% hydrogen in argon produced porosity in stainless steel AISI 321.

2.5.2 Welding current (pulsed and sinusoidal application)

Given that the welding current is used as the main control parameter for the TIG process, it would be anticipated that many combinations of the phenomenon of pool oscillations and the welding current have been researched. To date, the simple 'square wave' peak current pulse has been employed in free response applications, and a sinusoidally varying current for forced responses. The influence of the current is immediate since it is used as the excitation mechanism for the pool. It affects the magnitude of the arc force imparted to the surface and the resulting dynamic behaviour of the pool and also acts as the control variable governing heat input and hence bead shape during welding.

For the free response applications, typically a short duration high current pulse of the order of 2 to 5 milliseconds, 100 Amps above the base current optimises the response (Lin, 1987, Xiao, 1992 etc.). Significantly longer durations of the peak time (t_p) do not affect the magnitude of the frequency response unless the effect upon overall heat input becomes significant. The bulk free response of the pool at its natural frequency is quite robust - Lin (1987) observed little change in the dominant pool frequency, f_d , for a peak time of 1 to 10 ms, although a long peak pulse time can complicate the immediate reaction somewhat. If the pool is caused to move away from the arc by the first impulse and still under the influence of the higher force from the *peak* current, a free oscillation (under the lower force exerted by the *base* current) that would then more readily occur might be suppressed. Lower levels of peak current tend to result in a notably smaller response amplitude, V_{amp} , which would be expected from the dependence of the arc force magnitude upon the square of the current (see Richardson, 1989, for example). The exact effects of the current pulse parameters used are also heavily dependent upon the shielding gas, which determines the arc force imparted and the electric field strength.

The usual pulsed current form applied to generate pool oscillations is a short peak current pulse followed by a long background pulse - see **Figure 3**. An inversion of this approach has been suggested (ie. a short t_b and long t_p) although it is difficult to see a practical application that would generate a sufficient current amplitude ($I_p - I_b$), and would also be subject to repression of pool oscillation during the application of the peak current as described above.

More complex excitation and current waveforms were employed by Connelly (1986) who super-imposed milli- and micro-pulsing current levels (ie. current pulses with milli- and microsecond durations) upon a conventional pulsed TIG wave shape with an additional intermediate current level between peak and base. More stable voltage waveforms were reportedly observed as a result.

Maintaining a constant base current whilst altering local heat dissipation rates or material geometry yields an according change in frequency response, as illustrated by Xiao (1993) in **Figure 6**.

The step change in thickness clearly causes a corresponding frequency response with the transition from partial to full penetration, and back to partial penetration conditions. This type of distinct change in thickness is rarely encountered in practice, and smaller thickness changes or more complex heat build-up conditions result in a much less distinct difference in the frequency response.

Sinusoidal current pulsing results in the need for a much smaller current amplitude in comparison with the free response - Wang (1993) used an amplitude of only 40 Amps for 1 to 3 mm thick steel, even with argon as the shielding gas.

In work studying the incidence and causes of cracking in weld run-outs, Barnett (1992) reported differing pool aspect ratios (L/W) generated by the current level ranging from $L/W = 1.0$ (50 Amps) to $L/W = 1.5$ (150 Amps) for a continuous welding speed of 165 mm/min. Aspect ratios directly affect the associated oscillation frequency - as modelled theoretically by Maruo and Hirata (1993).

In general, previous research has not employed particularly high currents, although Connelly (1986) noted that inconsistent responses were generated when welding High Strength Low Alloy (HSLA) steels with currents above 350 Amps (pulse amplitude 100 Amps), which were attributed to the large, wide pools generated.

2.5.3 Travel speed

Researchers utilising a straightforward free response method have used relatively low travel speeds to obtain signals of optimised quality, typically:

Madigan (1986)	38 mm/min,
Deam (1989)	45 mm/min,
Connelly (1986)	50 to 100 mm/min,
Tam (1989)	94 to 127 mm/min.

A low travel speed can mean that Mode 2 (slosh) rather than Mode 1 behaviour is exhibited in partially penetrated pools (Xiao, 1993), whereas a high travel speed results in a higher solidification rate and hence damping of the oscillatory response. Significantly higher travel speeds can result in the position of the arc root being ahead of the geometric centre of the molten pool, thus delivering an asymmetric excitation force to the pool which in turn favours a slosh response in a fully or partially penetrated pool. Rapid electromagnetic deflection of the arc towards the centre of the pool at the moment of peak current enabled Wang (1988) to achieve a relatively high speed - up to 200 mm/min.

Richardson (1989) observed a rapid deterioration of the quality of the pool oscillation signal when welding above 38 mm/min with Inconel 718.

The arc light intensity has been reported as revealing the oscillation behaviour of the pool at higher speeds than the voltage. Yoo (1993) reported that at 150 mm/min the voltage signal had deteriorated badly whilst the arc light still contained some regular waveform. Similar results are presented by Barborak (1994). This has been attributed to the arc light signal being comparably more sensitive to changes in the length of the plasma column.

Eccentricity of the pool shape caused by higher travel speeds has been observed to decrease the frequency response (Yoo, 1993). Hardt (1985) in a control system based on monitoring the back-bead width by an optical sensor accounted for the effect of welding speed on pool shape - as shown in Figure 7.

Rapid stationary spot welding of thin stainless sheet (1 mm) using a forced response enabled Wang (1993) to achieve an effective welding speed of 140 to 180 mm/min. Conventionally, however, this type of welding is often slower in comparison with continuous motion because of the degree of overlapping required for thicker joints.

2.5.4 Tungsten geometry

Although the TIG welding process might at first have appeared to be a relatively straightforward process, in practice this has not proved to be the case. The advent of automated equipment effectively eliminated changes that might have been made by a manual welder in response to joint or material variations. Tungsten geometry has been found to have a significant effect upon beads produced using the TIG process. Studies of the effects of tungsten geometry can effectively be divided into two areas: first, those which concentrate upon the physical measurement of the magnitude and distribution of the arc force generated, usually upon a copper block, and second, those which measure the degree of penetration of either thin or thick plates (most often quantified as D/W).

Recent work by Yasuda (1989) and Hiraoka draw similar conclusions with respect to the maximum arc pressure generated. For a given current both found that the excess arc pressure (P_{arc}) increased with increasing electrode diameter. Hiraoka (1986) showed that the effect was more marked for vertex angles of 45 to 90°, and the higher currents of 200 to 300 Amps. Increasing the truncation diameter - the flat on the electrode tip - was found to decrease P_{arc} - also see §2.6.3 - (see Figure 8).

Vertex angle has always been reported to have a significant effect upon maximum arc pressure and penetration. Hiraoka reports a significant peak in the arc pressure at a vertex angle of 45°, double that at 15 and 90° for arc lengths of 2 to 8 mm for a 200 Amp argon arc. Early work on the effect upon penetration was later categorised according to whether it had been performed upon thin sheet, as a full penetration weld, or upon relatively thick plate, as a partial penetration weld, due to the comparatively different heat flow conditions.

Both Key (1980) and Shirali (1993) have reported increasing penetration for increasing vertex angle (15 to 90°) - with argon as the shielding gas. Key's work with helium and hydrogen additions demonstrated that the previous observation with respect to penetration does not necessarily hold true for 'thick' material (12.7 mm) - less sensitivity to vertex angle was apparent with other helium/argon and argon/hydrogen mixtures. Stability of the arc also becomes a governing factor for selecting vertex angle, and for this reason the sharper angles were preferred - 30° to 60° (Key, 1980).

2.5.5 Arc length

The influence of the arc length upon the arc voltage (V) can be appreciated from the fundamental relations expressed by Quigley (1977) as:

$$V = V_a + V_{col} + V_c \quad \text{Eq. [6]}$$

Here:

V_a is the potential difference across the anode fall region,
 V_{col} is the potential difference across the plasma column, and
 V_c is the potential difference across the cathode fall region.

$$E = \frac{V_{col}}{L_{col}} \quad \text{Eq. [7]}$$

Here:

E is the electric field strength, and
 L_{col} is the length of the plasma column.

Gas tungsten arcs in argon typically have 0.5 to 1.0 V/mm average electric field strength, E. Given that the anode and cathode potential drops (V_a and V_c respectively) are relatively constant for given physical parameters, the change in arc length caused by the oscillation of the pool surface results in a corresponding change in the voltage across the plasma column (V_{col}) and hence the total measured voltage (V). The geometric centre of the pool is directly affected when vibrating in Modes 1 or 3, and although the Mode 2 response (slosh) is less direct in its influence over the average arc length, voltage oscillations have been recorded successfully.

Helium exhibits a higher average electric field strength than argon (Lancaster, 1984) and consequently the measured arc voltage drop is more sensitive to changes in arc length caused by an oscillating pool. Many authors have used helium as the shielding gas for this reason.

Xiao (1992) used arc lengths in the range of 1 to 5 mm, and observed that for a peak current (I_p) of 300 Amps, oscillations were not detectable above 3 mm in argon and 5 mm in helium. The arc length was found to affect the critical peak current duration (t_{pc}) defined as the threshold time between the generation of Modes 1 or 2. Increasing the arc length, for a constant critical peak duration, was found to favour the generation of Mode 2.

It was suggested by Andersen (1993) that the dynamic behaviour of the pool does not affect the 'effective' arc length as might be inferred from the relations of Equations 6 and 7. The oscillation amplitude of the pool does not cause the expected change in magnitude of arc voltage, since it is proposed that the potential of the plasma column is not necessarily directly proportional to the tungsten to pool surface distance on the central vertical axis. This is corroborated by comparing the amplitude directly observed by Xiao (1992) stationary and travelling pools with what might be expected in the presence of the helium arc used and its associated electric field strength. This means that the use of the voltage is not necessarily as sensitive as a simplistic application of Equations 6 and 7 might suggest.

In an assessment of the sensitivity of the detection of oscillatory behaviour with an increase in arc length, Sorensen (1989) observed that oscillations could be detected up to the point of arc instability. Richardson (1989) observed drastic reductions in the signal amplitude with an increasing arc length. However, in general, much of the research reviewed above adopts the use of comparatively short arc lengths of the order of 1 to 3 mm, which are typically used in TIG welding practice.

2.5.6 Preparation

The effect of the material surface condition has been found to affect pool geometry results for a given set of welding parameters. For standard pulsed TIG conditions Boughton (1973) found that different pulse durations were required to achieve full penetration on austenitic stainless steel depending upon whether wire-brushing or machining was used as a preparation. A shorter peak pulse duration was required to effect full penetration for the machined surface.

Campbell (1993) attributed increases in penetration for a precipitation hardenable austenitic stainless steel to the method of preparation. Wire-brushing the surface, when compared with machining, was found to increase the surface roughness and also the thickness of the oxide layer for the material tested. Differences in fusion shape characteristics were attributed to the effect of the available oxygen in the pool melt upon the convective flow within the pool caused by the surface tension/temperature gradient changes (see also §2.5.8 and §2.6.1). It was acknowledged that comparative tests upon SS304L and SS316L did not reveal as significant penetration changes and the particular alloy (JBK-75) tested was believed to be more sensitive to the effects of oxygen.

2.5.7 Orbital position and gravity

Orbital joints involve two main additional complexities:

- variable heat accumulation around the welding circumference dependent upon welding parameters, diameter, thickness, joint geometry, and thermal properties of the material ie. the heat input and the heat dissipation rate, and
- the effect of the changing direction of the gravitational force upon the molten pool and its shape during cooling.

In order to develop consistent orbital beads, Kulik (1993) reports the use of many methods: activating fluxes in the shielding gas, pressure and composition of the shielding gas, electrode displacement for stepped joints, and current modulation. A general schematic of the various potential controls implemented during a typical orbital cycle is well illustrated by Krüger (1994) - see Figure 9.

Orbital pipe welding procedures invariably involve decreasing the current during the pass and Lee (1991) theoretically quantified the temperature profile for straight d.c. welding parameters and a typical pipe joint using the finite element method. Small diameter, thick joints tend to present the greatest challenge and the model was verified by comparison with earlier published results. For static parameters (constant voltage and current) both peak and mean temperatures were found to increase during the pass for subsequent locations around the circumference. Lho (1992) conducted a similar study using a three-dimensional difference method, but extended the experimental work to achieve a target top and bottom bead width by applying a theoretically predicted current for a given welding speed and material parameters with consistent results. Both studies, however, used aluminium as the test material, which has not been reported to be as subject to cast variations as stainless steel.

To compensate for the effects of gravity upon the molten metal and the resulting bead shape around an orbital joint, Cornu (1988) reported the use of a varying pressure backing gas - a positive pressure in the 11 to 1 o'clock positions and even a negative pressure (less than atmospheric) for the 6 o'clock, to support and then draw in the bead respectively. In general theoretical modelling of TIG weld pools has focused on the downhand position and the effect of gravity upon the pool shape has not been fully reported.

Deam's (1989) report on the MELODY sensor based on arc light noted sagging and undercut in the 6 and 12 o'clock positions on 4 mm to 6 mm wall thickness 50 mm outer diameter stainless steel (SS316) pipe from an autogenous single-pass run. Controlling the current to yield a frequency that was too low could have caused the over-penetration problems.

Differences in penetration resulting from workpiece positional changes observed by Shirali (1993) found that when welding with pure argon shielding gas, penetration was the highest for downhand (0°), lowest overhead (180°), and intermediate at the 45° and 90° positions. See Figure 10 for Shirali's schematic illustration of the changing positions and relative force directions.

2.5.8 Surface tension, γ

The theoretical frequency response of the weld pool is directly proportional to the square root of the acting surface tension of the weld pool (see Equations 1, 3, 4 and 5 in §2.3) and before a review of factors affecting surface tension is made, it is important to note that surface tension values for steels vary significantly with temperature and the derivation of a single value for the case of welding pool surface under the presence of a free burning TIG arc might be too simplistic.

Experimental evaluations of surface tension, even when solely considering the welding situation, have not always fully accounted for this. The temperature gradient across welding pool surfaces results in a significant variation in surface tension ie. a surface tension/temperature gradient (dy/dT) is present. Flow in the molten pool caused by the surface tension/temperature gradient is known as Marangoni flow, and is shown as one of the forces (M) acting in the pool in Figure 10. Although the influence of Marangoni flow upon the pool geometry has been widely debated for numerous years, recently many authors have mathematically modelled the influence of all the forces acting in the pool on the molten flow and found Marangoni flow to be a significant driving force (for example, the influence of sulphur upon the surface tension/temperature gradient and resultant pool geometry in laser welds was illustrated by Pitscheneder (1996)).

Physical measurements of surface tension for liquid metals are prone to a degree of error and uncertainty. Iida (1994) stated that an inaccuracy for metals of up to 10% may be likely, and that the temperature coefficient of surface tension (dy/dT) may differ by up to some 50% from measured values.

Pure iron at its melting point of 1535°C has a reported surface tension ranging from 1500 to 1800 dyne/cm (mN/m) and the effect of introducing sulphur or oxygen, and carbon or phosphorous to a lesser extent, is to reduce the surface tension value for a given temperature (Matsunawa, 1982). By plotting quoted γ_{iron} values against year of publication, Iida (1994) demonstrated a convergence over the last ten years towards 1.9 N/m in the vicinity of the melting point.

Elements that are surface-active affect the surface tension directly, and it has been proposed that their influence is less marked with increasing temperature due to the associated increased volatilization (Heiple and Roper, 1982). This is the fundamental mechanism often cited as the cause of cast-to-cast variability in stainless steels (see §2.6.1) and thus operating values of surface tension vary significantly. The effect of the surface tension forces upon the overall flow regime in the weld pool has been modelled theoretically (for example see Matsunawa, 1987, and Zacharia, 1995). Typical operating parameters employed in the model demonstrated the importance of the surface tension/temperature gradient in TIG weld pools and its primary effect upon the dominant flow regime in the molten pool, the resultant pool geometry and the penetration behaviour. Zacharia's model focused upon the behaviour in thin material, 1.5 mm thick AISI 304 SS.

Surface tension observations from Keene (1985) are given in Table 1. Experimental values of surface tension derived using the levitated drop technique are subject to potential error from the quality of the gaseous environmental atmosphere (usually an argon/helium mix) and the influence of impurities can be significant. Unless surface tension testing is employed, only an accurate knowledge of cast behaviour and temperature could enable a reasonable approximation of γ for iron based materials. Theoretical predictions of the pool oscillation frequency, for given pool sizes are thus potentially subject to this degree of uncertainty.

Takeuchi (1992) employed an experimental evaluation (the melt/burn through method) of surface tension, based on a tapered weld specimen where:

$$\gamma = \frac{13.6 / V}{t_{\text{max}} \sqrt{T_s}} \quad \text{Eq. [8]}$$

Here,

I is welding current,

t_{\max} is the critical thickness for occurrence of melt-through, and

S is the welding speed.

Evaluation of the surface tension was made using a 200 Amp TIG arc, at 3 mm arc length, with argon shielding gas at 10 l/min. Surface tension dependence upon temperature was reproduced by varying welding current and speed to obtain a variation of the heat input.

Results of the form expected (shown above by Keene, and further described in §2.6.1) were found for the austenitic stainless steel (SS304) with sulphur and bismuth additions. However, the surface tension values were notably lower than values published using the levitated or sessile drop techniques. Although Takeuchi measured welding heat input, as opposed to temperature, for a SS304 steel with 0.001% sulphur, γ decreased from 1.20 down to 1.00 N/m with increasing heat input. For a similar cast of the same steel containing 0.030% sulphur, γ increased from 0.85 to 1.00 N/m over the same heat input range. Results with additions of bismuth were of the same form, although still notably lower than those from other sources. Takeuchi correlated this behaviour with Marangoni flow by assuming that the pool temperature was nearly proportional to the heat input. It would appear from this that the overall surface tension value derived using this method would be significantly different from that when measured in isolation by the more usual means ie. as reported by Keene in Table 1.

Data published by Wen and Lundin (1986) for a SS304 under simulated arc conditions - a plasma arc at 20 Amps - with the drop weight method supports the above. In pure Argon, γ was measured at 1.17 N/m, and with Argon + 10% Hydrogen 1.28 N/m. The addition of hydrogen to argon affects many variables associated with the welding arc: the reducing nature could have reduced the oxygen on the pool surface, and since oxygen is also known to be surface active, a corresponding change in γ would be a likely result. Nevertheless these values are much lower than those quoted above by Keene (see Table 1) and supported by other authors.

Both the results from Takeuchi (1992) and Wen and Lundin (1986) suggest that it would be inappropriate to measure surface tension in isolation at a constant surface temperature and apply the measured result to the material cast response under a welding arc.

Kotecki (1972) derived surface tension values from observed oscillating pools using the membrane model (already discussed) for the fully penetrated condition and reported γ_{iron} to be 1.51 to 1.58 N/m. Again this is slightly lower than previously published values. The steel used did contain some minor elements, and these could have contributed to the derived lower value.

By re-arranging Equation 4, a value of surface tension can be predicted from Mode 1 pool oscillations if the frequency of oscillation (f_{M1}), pool width and liquid density are known or can be measured. Xiao (1994) measured Mode 1 oscillations via the arc voltage and pool temperature using an infra-red pyrometer to predict the surface tension/temperature behaviour (under both argon and helium welding arcs) of a technically pure iron with an extrapolated result of 1.9 N/m at its melting point. This result, however, is in agreement with surface tension measurements made by the more traditional methods.

Theoretical predictions of the pool oscillation frequencies for austenitic stainless steels are thus prone to a reasonably significant degree of uncertainty, due to both the value of the surface tension used and whether it is appropriate to *welding conditions*. The possibility of the welding arc reducing the effect of some of the surface active elements, thereby affecting the surface tension of that particular cast of a material at the temperature chosen, cannot be discounted either.

The consequences of cast-to-cast variations and the associated surface tension variability are outlined further in §2.6.1.

2.5.9 Summary

This section reviewed the effects of the primary welding parameters and operating conditions upon both the general weld pool and also the specific pool oscillation behaviour. This was of primary importance since all these factors can affect the pool geometry and hence the frequency. Some of the parameters are fundamental to the application of the pool oscillation technique, in particular the shielding gas, welding current, travel speed and surface tension.

2.6 Other factors influencing the application of pool oscillations

2.6.1 Cast-to-cast behaviour

Problems with so called cast-to-cast behaviour of austenitic stainless steels have been highlighted in the literature since 1967 and a brief review of the current understanding of the problem is made here. This is considered to be important since the fluid flow regime and resulting pool geometry from applied weld procedures impacts upon the use of the weld pool oscillations as a way of controlling the penetration. Many causes and observed effects of cast-to-cast variation have been proposed: anode spot behaviour, welding current, power density, Lorentz forces, viscosity of the molten metal etc. Recent articles consistently highlight the Marangoni-convection model as being a governing force in cast-to-cast variations. The surface tension/temperature gradient (dy/dT) is thought to play a dominant role in relatively low current, autogenous GTA welds. For casts containing particularly low levels of surface active impurities the usual flow regime is reversed and fluid flows towards the edge of the pool (rather than downwards) resulting in wide, shallow beads, with a significant lack of penetration. Increasing the welding current can sometimes result in an increased flow towards the edge of the pool, and not the desired increase in penetration. (Marangoni models are reported widely elsewhere, in pure mathematical literature for example.)

Heiple and Roper (1982) were the first proponents of this explanation for the behavioural differences, and Figure 11 summarises the observed surface tension/temperature relationship for iron with impurities such as sulphur and to a lesser extent, oxygen. Their convection model was subsequently supported by results from laser and electron beam welds - questioning many previous and some subsequent propositions, from other researchers, based on characteristics that are unique to the gas tungsten arc (Heiple et al., 1983).

It is believed that the surface active elements migrate towards the weld pool boundary and decrease the acting surface tension, although their influence decreases as the temperature is increased. The effect upon the surface tension is marked, but more importantly the surface tension/temperature gradient (dy/dT) changes sign for the steel. The corresponding variation of surface tension on the pool surface results in a reversal of flow on the surface and subsequently in the pool. Detailed recent assessments made by Pollard (1988) and Mills (1993) confirm this model of behaviour. Since Lorentz, aerodynamic drag and buoyancy forces also act on the pool, a simplistic generalisation of the possible heat and

fluid flow conditions is unwise. Other minor elements present (Mg, Ca, Ce) can combine with the surface active elements and lessen their effect ie. stable calcium sulphides can be formed which have not been reported to affect pool behaviour significantly unlike the soluble sulphur level.

Observations by Takeuchi (1992) validate the Marangoni model: surface active bismuth (added to SS304 to aid machinability) had a significant effect upon the bead shapes generated by a 100 to 200 Amp TIG arc, both stationary and travelling (40 ppm Bi caused a 30% reduction in γ). Surface tension and bead shape behaviour was exactly as would be predicted from Heiple's results with sulphur (as Figure 11).

The characteristics of poor weldability are classified by Lambert (1991) as typically: long response times during start-up, comparatively stable arcs and flat weld surfaces without weld pool ripple markings. Good weldability was found in casts which had rough weld surfaces, less stable arcs and good start-up penetration. However, Lambert proposes that the bead differences are caused by a broader anode spot, with an associated lower current density which results from the arc being attracted to particles with low work functions. It is thought that these particles are at the pool edges, thus broadening the arc and the resulting convective flow.

The resulting flat surfaces from low sulphur casts have been taken advantage of by ultra-high purity tubing manufacturers. Minimisation of the inner bead surface roughness is a desirable objective, in order to minimise potential sites of particulate accumulation compromising the cleanliness 'chain'. Surface roughness values (R_{max}) quoted show lower values for Vacuum Oxygen Decarburised (VOD) and Vacuum Arc Remelted (VAR) stainless steels as opposed to a conventional melt SS316L. This is attributed to the tighter control over the minor elements (eg. $S < 0.002\%$) [see 'Excel Clean and Clean Dry Gold EP Pipe' from Kobe Steel sales literature].

Hinata (1994) reports clearly different behaviour between casts of austenitic stainless steel (SS304) with differing sulphur contents (0.001 and 0.008%), and additionally clearly illustrated the problems encountered when joining the two casts together (see Figure 12).

Although it has not been specifically reported, the observed stability of the arcs associated with casts with low minor element constituents ($S < 40$ ppm, or 0.004%) and the associated less turbulent radially outward flow, might be expected to produce voltage oscillations which are comparatively clear.

Despite some of the contradictory models proposed for the cause of cast-to-cast variations, the resulting effects are similar and the steps to combat them are quite common to a number of authors: slower travel speeds, shorter arc lengths, the use of argon with hydrogen, or helium as a shielding gas. Specifying limits for the minor element composition is also often recommended, although recently the use of surface-active pastes to force the weld pool to adopt a desirable flow pattern has been researched by the Paton Institute and the US Navy Joining Centre. Hinata (1993) effectively performed this task with promising results by using a flux-cored wire as an alternative addition to solid wire, where the sulphur content of the wire was known to be relatively high (0.009%).

It should be noted that a simple control over the soluble sulphur content, for example, to aid weldability is not automatically practicable since it is primarily present due to the addition of scrap in the manufacturing process (unless it is remelted), and often used to aid machinability although it can also decrease corrosion resistance and ductility.

Wareing (1989) applied a stationary weld pool test and a 'time-to-penetrate' parameter to characterise the weldability of various austenitic stainless steel casts with respect to cast-to-cast variations. He observed that the 'viscous' casts exhibited a comparatively long time-to-penetrate, as might be expected. Small thickness variations were found to produce effects that were similar to cast variations. Using a 5% hydrogen addition to the argon shielding gas, or a higher welding current minimised the differences between the material casts.

2.6.2 Pulsed (-TIG) current welding

The advantages of the use of pulsed current in TIG welding have been evident and reported for at least the last twenty years. Initially, the following was envisaged - the use of the primary pulse with zero travel speed to obtain the desired penetration characteristics, and moving only during a background pulse, as solidification occurs. As further process advantages arose, the use of pulsed TIG weld programs became more accepted as common practice. A higher degree of control over the resulting bead can be obtained, and the overall heat input can be decreased, generating less distortion than steady direct current. Pulsed TIG programs are used in various ways now: zero travel on the primary pulse, different welding speeds between the primary and background pulses, and also continuous travel. Particularly thick orbital joints can be completed by current limited sets using a zero travel speed with the high current pulse. Orbital welding of high quality tubing particularly benefits from the added

positional control, and minimised heat build-up. Cornu (1988) also reports that a greater tolerance to root gap is provided by current pulsing, since pool depression experienced at the high welding current serves to spread the pool.

Different researchers have sought to make the application of pulsed TIG parameters more straightforward in various ways. Early work by Boughton (1973) based an approach upon a constant thermal efficiency ($I_p \cdot t_p = \text{constant}$) obtainable with short duration high currents, predicting peak current level and duration from material thickness and the thermal diffusivity (α). Similar work at Cranfield by Turner (1985) found that optimum conditions resulted from high peak current (I_p), short duration peak pulse time (t_p), low base current (I_b), longer duration base pulse time (t_b). A high rate of heat input was applied during the pulse period allowing dissipation during the comparatively longer base period. Becker (1978) related the peak current (I_p) to the travel speed divided by the fraction of time at peak current [$T_s \cdot (t_b + t_p)/t_p$]. The overall aim of the research was consistent - to reduce the heat input and to increase predictability.

The physical effects caused by pulsing the current are applicable to the generation of pool oscillations - predominantly the cyclical heat input, and the variance in the arc pressure on the pool surface.

During the debate about weld pool fluid motion, and the resulting penetration behaviour, Ecer (1981) studied the weld pool surface motion to ascertain stirring of the pool by pulsation of the welding current. In terms of the pool surface two pre-dominant flows were observed:

- firstly, a radial wave travelling outwards towards the pool edge and then reflected back, occurring during the peak current pulse, and
- secondly, the up and down oscillatory behaviour, that has since been well documented.

The radial surface wave motion reached a maximum during the first 10 ms after the peak current pulse (I_p) was applied and subsequently the vertical oscillatory motion dominated during the application of the base current (I_b). Mixed-mode responses have been observed by Yoo (1994) and Xiao (1992), and the occurrence of this radial flow might contribute to an initial mixed oscillation response. The thermal effect of the peak current pulse must also be accounted for ie. a delay between the initial peak of the heat input and the consequent melting of the material and establishment of the

full penetration condition.

Maruo (1985) linked the occurrence of humping caused by pulsed current parameters to the dynamic response of the molten pool ie. the natural frequency. Accordingly, humping was observed at the critical frequency from a minimum of current amplitude since the pool was resonating. To avoid this kind of problem, current pulses used to create pool oscillations for penetration monitoring must be applied after the pool motion has ceased. A model of the frequency response was presented (see §2.3.1) which demonstrated good correlation with the results.

Utilising high frequency pulsed current arcs has been proposed as advantageous by some authors. Increased penetration whilst maintaining a relatively constant top surface bead width for increasing pulse frequency was reported by Saedi (1988), who attributed the increase to more vigorous electromagnetic stirring (maximum frequency employed of 3 kHz). Omar's (1979) results however reported little or no increase in bead depth when pulsing between 2 and 20 kHz and saw no advantage in high frequency pulsing. Utilising image processing and infra-red photography, Zhao (1988), analysed straight d.c and high frequency pulsed argon arcs and found a constriction of the arc from the radial distribution of the temperature at 16.3 kHz. Concentration of the arc with rapid rise has also been recently reported by Hirata (1994) - see also next section, §2.6.3.

2.6.3 Arc pressure distribution and magnitude

Use of the arc pressure, and the optimisation of its effect, is central to most research concerning the use of pool oscillations. A great deal of research has also been focused upon minimising the unfavourable effects resulting from the generation of an excessive arc force.

The change in momentum of the plasma jet and the electromagnetic 'pinch' effect both contribute to the force upon the molten pool surface which is normal in distribution (Lancaster, 1984). Its magnitude is proportional to the square of the welding current, (Allum, 1981, and Richardson, 1991). Barabokhin (1976) found that the magnitude of the excess gas dynamic pressure was also dependent upon the rate of current rise, (di/dt) . Rises of 1 to 5 kA/sec were found to produce significantly higher pressures than for a steady discharge (for a 100 Amp arc $P_{ac} = 375$ Pa for a 5 kA/sec rise, compared with 125 Pa for a stationary discharge). Typically the current was 'pulsed' from 20 to 125 Amps. The higher pressure was attributed to a temporary increase in the flux density and acceleration of the plasma stream. Hiraoka (1986) measured and reported steady-state arc pressure,

but recognised the short peak of arc pressure after initiation. Barabokhin's results are illustrated in Figure 13.

This is supported by Maruo's observations of the humping bead caused by pulsed current since at a given critical frequency the square wave causes a smaller current amplitude to result in humping, whereas sinusoidal and triangular waveforms support larger current amplitudes (since their current rise times are lower) (Maruo, 1985, and also see §2.6.2).

Some debate has surrounded this because an increased current density increases the self-induced magnetic field around the arc, and hence its 'stiffness'. Glickstein (1982) observed only an increased arc diameter, and not current density using a Dimetrics High Frequency Pulsed Welder and rejected the concept, although the current rise time was not reported for comparison.

Some of the physical characteristics of the TIG arc can be partially dependent upon the electrode itself: diameter, tip geometry - surface quality, angle, truncation. It is reported that increasing the electrode angle decreases the maximum force experienced at the anode (Lancaster, 1984). In addition to this, Yasuda (1989) reported that for a current of 150 Amps, increasing the electrode diameter from 1.6 mm to 3.2 mm increased the arc force, whereas for currents of 120 to 150 Amps truncating the electrode, ie. flattening the tip, decreased the arc force by around 20%.

Increasing the arc length also decreases the excess arc pressure (Richardson, 1991). Savage (1979) reported an almost linear decrease in the arc force with increase in arc length. In comparison with an argon arc, a highly significant decrease in the force imparted by a helium arc for the same welding current is reported by Lancaster (1984) and Norrish (1992).

2.6.4 Power source characteristics and signal processing

Welding power sources have been based upon different electrical, and electronic principles. Power control has been achieved by means of:

- tapped transformers, saturable reactors, auxiliary inductors and thyristors, and
- series regulators, primary and secondary inverters.

For GTA welding constant current, static V/A characteristics are generally required, and although this has been provided proficiently in a number of

ways, closer inspection of the delivered current characteristic shows that although the mean value is usually accurate, the transient is rarely a 'dead value' and rise-times vary. Primary and secondary inverter designs which are now industry standard, mostly operate at frequencies that are of the order of 20 to 100 kiloHertz (with rapid rise-times) which are consequently well spatially separated from typical molten pool frequencies. Low pass filtration is relatively easy to implement with sharp knee-bend filter design such as Chebyshev and Butterworth providing excellent attenuation of the unwanted high frequency signals.

Earlier power sources with characteristic frequencies in the area of interest ie. 0 to 500 Hz, are more troublesome for pool oscillation applications, and the use of band-pass filters has been necessitated (Madigan, 1986).

2.6.5 Fast Fourier Transform

Converting data from a time-series to a frequency domain can be efficiently performed using a Fourier transform, based on the use of the Fourier series representing any waveform by a summation of sine and cosine series. Many digital applications benefit from the reduced number of calculations, compared with previous conventional methods, associated with performing a Fast Fourier Transform (FFT) to obtain the spectral information.

The concept is ideally applicable to continuous data-logging of electronic signals. The analogue to digital (A/D) conversion at a specified sample rate together with the number of points used in the FFT determines the resolution of the output frequency spectrum ($\text{Resolution} = \text{Sample Rate} / N^{\circ} \text{ of Points}$). The tolerance of the FFT to noise is far better than direct zero-crossing or period determination techniques involving synchronous averaging for example and provides more information on whether there are multiple dominant frequencies present. As for all data logging applications aliasing can be experienced if too low a sample rate is used. Research into pool oscillations should use sample rates of 5 kHz and upwards to ensure adequate information is obtained about the high frequency small weld pools (see Xiao, 1992 for typical pool oscillation frequencies).

Yoo (1993) used a minimal 128 point FFT after data logging. A real-time application was prevented by the limitations of the processor available. Xiao (1992) used 1024 points with a 1 kHz sample rate, whilst Madigan and Renwick (1986) and other earlier authors relied upon direct measurement of the period and subsequent averaging to reject spurious results. Bishop (1993) provides a short review of the derivation and application of the Fourier series.

A hardware FFT in the form of a plug-in card was used by Bicknell (1994) although it was limited in speed and unable to be implemented in real-time. A frequency resolution of 2 Hz was reported.

2.7 Control methods

2.7.1 Conventional control methods

In order to account for the effects of unexpected changes in process variables, such as heat dissipation or material thickness, a closed-loop control system must be employed. Nearly all commercially available welding power sources are open-loop in this respect and no measurement of the actual state of the weld is made. Feedback is usually employed to ensure the accurate delivery of the welding parameters themselves: current, and arc voltage via the arc length (AVC, Arc Voltage Control, where torch height is automatically adjusted to maintain a constant arc voltage which can be used to account for ovality in pipe-welding for example). Many control variables are of potential interest for automated welding applications: seam-tracking, bead width, surface profile, penetration, keyhole size in plasma welding, stand-off (MIG) or arc length (TIG).

Several different output variables have been previously employed in order to control the bead profile in the TIG process:

- inner and outer bead widths, measured directly by optical means,
- fusion area, measured by infra-red imaging,
- thermal response from thermocouples etc.

For TIG it is usual to use the welding current rather than the travel speed as the primary input variable, either in terms of its pulsed profile or magnitude.

Traditional control strategies have adopted PID (Proportional Integral Derivative) control methods, although more recently the use of adaptive control methods has also been employed. Wu (1996) used a rule-based PID controller to modify PID coefficient values that made the control action. The error and error variation rate were used for the rule evaluation. Recent work in welding research has also turned to artificial neural networks and fuzzy logic control. Kovacevic (1996) used neural networks in conjunction with a top-face sensing (high shutter speed camera) and control system.

The primary aim of all the techniques is the same: to provide an effective control of the selected output variable in a stable manner, whilst process dynamics may alter unpredictably.

Linear welding situations (butt welding sheet or plate or seam welding tube) usually concern seam-tracking and penetration control with the heat dissipation characteristics remaining relatively constant. Rotary and orbital welding tends to invoke more complex heat dissipation characteristics either through the local geometry near the circumferential joint (tee or bend) or build-up creating a 'pre-heat'. Thick tubes of relatively small diameter pose the greatest problem in terms of heat build-up, although the exact behaviour will also be determined by the thermal properties of the material.

Suzuki (1991) compared conventional proportional-integral (PI) performance with two adaptive strategies: Self-Tuning Control (STC), and Model Referenced Adaptive Control (MRAC). From a heat balance it was shown that although a first order system could be used to describe the response of the weld pool to the heat input, the time constant (τ) and system gain were also dependent upon pool radius, material thickness and temperature gradient. The effect of heat build-up was demonstrated by the open-loop response to different step inputs of welding current with differing gains and time constants from different step magnitudes. Both the adaptive controllers were shown to be superior to the PI controller in closed-loop square wave tests: over-shoot by the PI response was evident, despite prior extensive tuning of the control variables.

For the travelling arc pool oscillation researchers, the proportional-integral (PI), and proportional-integral-derivative (PID) controllers have been used in the majority of cases. Madigan's (1986) control strategy was effective when faced with variable heat-sinking conditions - see Figure 14. Madigan used the feedforward gain to provide an initial base current level appropriate to the degree of penetration desired.

Wang (1993) used the small decrease in amplitude after resonance in the stationary arc application as the control signal to decrease the welding current and initiate travel to the next spot.

Feedback control was employed by Aendenrooier (1994) using a pulsed TIG approach, with additional short duration pulses to generate pool oscillations. The desired full penetration level was determined by the occurrence of Mode 1 and 3 oscillations in the base and peak pulse times respectively, whilst under- and over-penetration was sensed by dual Mode 1 or 3 responses.

Satisfactory orbital welds were made in 60 mm diameter, 3 mm wall thickness structural steel (Fe 360) for a range of welding speeds (48 to 84 mm/min). Heat build-up in the pipe was accounted for and the pulse current altered accordingly, although bead geometry was not reported.

Andersen (1993) used a Phase Locked Loop (PLL) to control weld bead size via oscillation of the pool at its natural frequency - excitation of the weld pool was timed to coincide in-phase with the oscillation of the pool. Consequently oscillation frequency could be inferred from the power supply excitation pulses. Both conventional current pulsing and sinusoidal current profiles were tested, although the short duration peak current approach was reported to offer improved performance. Figure 15 shows the voltage response derived from the arc light intensity from a synchronized current pulse.

Note: The arc light signal is the oscillatory signal at the TOP and the welding current the square wave pulsed signal at the BOTTOM of Figure 15.

2.7.2 Fuzzy logic in welding process control

In fuzzy logic, the truth of any statement is a matter of degree.

None of the control methods described above adequately characterise the specific situation of the non-linear response of the weld pool frequency in relation to the penetration condition. As has been shown by many authors, oscillations can occur in either the partial (Mode 1) or the fully penetrated condition (Mode 3) and the transition between the two modes is not necessarily explicit. It has been suggested that Mode 1 behaviour can occur in weld pools with a lower free surface and that Mode 3 behaviour will only begin to become evident after the approximation of $a_b/a_t > 0.5$ is true ie. after a threshold lower pool surface size has been reached. Accounting for the transition between the two dominant modes in the control methodology is therefore fundamentally important.

'Fuzzy Logic' introduced by Zadeh (1965) has been employed in many control situations where such ambiguities exist. It provides a crisp output value from a set of input conditions, where the relation between the input and output is either too mathematically complex for a real-time application or where there is no adequate explicit model. Membership functions are used to categorise the input and output parameters into 'fuzzy sets' and these membership functions relate a 'degree of truth' for a specific crisp

input or output, ie. how true the input or output is in relation to that fuzzy set. Fuzzy sets can be overlapping, accounting for the multiplicity evident in some control situations, for example a weld pool may be described as being mostly partially penetrated and only slightly fully penetrated, which would correspond to the definition of a partially penetrated fuzzy set and a fully penetrated fuzzy set.

A set of rules are used to relate the fuzzy input to the fuzzy output, even if there are multiple input/outputs. Complex membership functions can be used to describe input/outputs and the rules are written for the desired operating conditions, according to intuitive judgement or criteria based on known physical behaviour. In the most straightforward instance rules consist of a series of if-then statements. The basic strategy is outlined below in Figure 16, however for a more thorough examination of fuzzy principles, refer to 'Fuzzy Thinking' by Kosko (1994) or 'Fuzzy Set Theory and its Applications' by Zimmerman (1991). The figure shows the case for a single input/output strategy, but is equally applicable to multiple input/outputs.

Fuzzy models, like the one illustrated, can also be incorporated into more conventional PID techniques. The input and outputs shown would be discrete values, as for conventional control applications with the fuzzy interference model as the intermediate step.

A comprehensive review of the use of sensors and control systems in arc welding is provided by Nomura (1994) who evaluated the use of fuzzy logic in the following welding control strategies:

- seam tracking - tracing the position of the welding torch mounted on the robot arm,
- power source control of CO₂ short arc welding (MAG) - with the aim of minimising spatter, and
- positional sensing of a MIG torch in a groove using a mechanically rotated welding arc.

Rehfeldt (1993) used fuzzy logic to detect and classify behaviour differences in the arc voltage of the short arc metal active gas (MAG) welding process, revealing process disturbances such as mill-scale and the presence of paint and oil. Fuzzy logic enabled the characterisation of each disturbance although each cause was not linear in its effect.

Neural networks and fuzzy logic have been combined for some welding control applications - Kaneko (1995) estimated weld pool depth from the surface profile of a metal inert gas (MIG) weld and controlled penetration depth despite disturbances such as irregular groove width. A neural network was used to replace the 'complex mathematical modelling that would be needed to compute the pool depth from heat input and metal flow information available. Fuzzy interference was used as the control method ie. fuzzy logic was used to provide the relationships between the input and the output parameters. Early work on the same system was published by Yamane (1993) which described the derivation and performance of the fuzzy control system. Fuzzy logic has also been implemented in production power source control units for improved arc starting by compensating for variations in torch angle and wire stick-out (Sandford, 1994).

Since the implementation of fuzzy logic does not require an explicit mathematical solution, most of the formal stability criteria cannot be applied to a control system based on fuzzy logic. Additionally, most fuzzy control systems are non-linear and occasionally time-variant. The direct method of Liapunov has been proposed (Motorola, 1992) as the most appropriate way of assessing stability. A number of 'good practice' guidelines have also been produced:

- the use of too few membership functions will result in a lethargic response and may fail to provide the output from a small input change,
- if more control is required in a particular region of interest or sensitivity, the membership function density should be increased.

Motorola (1992) produced overlap indices, where a qualitative assessment of the degree of overlap of the membership functions was made, relating the ability of the control system to cope with ambiguity and the smoothness of the operation to two overlap indices (overlap ratio and overlap robustness).

Fuzzy logic is potentially an ideal tool for modelling a non-linear response for a real-time application, enabling a more rapid development of an appropriate control strategy. Its use with the control of penetration via pool oscillations is also pertinent since the transition between partial and full penetration modes (Modes 1 and 3 distinctly in the most straightforward case) is not readily available unless the pool width is already known ie. $a_b/a_t > 0.5$ (as discussed previously). Material cast and surface tension

variation also prevents the theoretical models being used directly in a control strategy.

2.8 Concluding remarks

From a review of the published literature available to date, the following main points may be extracted that are of central interest to the work presented in this thesis:

- the use of weld pool oscillations via the arc voltage as a non-intrusive through-the-arc sensing technique in relation to tube/pipe welding has not been adequately described as a potential method of monitoring or controlling the penetration behaviour,
- the dependence of the frequency response of pool oscillations on the surface tension behaviour of the material and the known associated variations encountered when welding austenitic stainless steels and their penetration behaviour in particular, has not been described,
- a way of modelling, and accounting for the difference between, partial and full penetration responses into real-time monitoring and control has not been presented - control strategies employed so far have not fully accounted for the transition between Mode 1 and Mode 3 behaviour.

SECTION 3.

EQUIPMENT AND MATERIALS

3.1 Equipment

- 3.1.1 Equipment description
 - AMI 207 and AMI heads*
 - Experimental orbital system*
 - Pool oscillation measurement and software*
- 3.1.2 Measurement techniques
 - Arc voltage*
 - Welding current*
 - Resultant bead profile*
 - Inner bead surface roughness*
- 3.1.3 Standard experimental procedures
 - Material preparation*
 - Joint preparation*
 - Electrode setting, cleaning and integrity*
 - Pre- and post purging*
 - Orbital welding procedure*
- 3.1.4 Calibration of the closed-loop system
 - System operation*
 - User-interface & logging PC performance*
 - Serial communications protocol reliability*
 - Closed-loop system*

3.2 Materials

- 3.2.1 Tube and pipe material description
 - 3.2.2 Tube and pipe material composition
-

3. EQUIPMENT AND MATERIALS

The primary equipment used for the experimental work is shown in Figures 17 to 23 at the back of the thesis, and described below in detail in section 3.1.1. A summary table detailing the equipment is also given in Table 2.

3.1 Equipment

Table 2 gives an overview of the equipment used during the experimental programme.

3.1.1 Equipment description

Orbital welding the tubing was essentially facilitated with two basic equipment configurations:

1. the commercially available Arc Machines AMI 207 with orbital head, either the AMI 9-1500 or the AMI 9-4500, or
2. the experimental orbital system, comprising user-interface PC, Isotek control rack and Migatron BDH320 triple power source and orbital head (as for 1.).

In general terms, the AMI207 was used for initial experimental work, observing pool oscillations in an open-loop fashion with various pre-determined experimental parameters. The experimental orbital system (2. above) was developed and used to effect closed-loop control of penetration, by controlling the level of the base welding current, using a fuzzy logic model based on pool oscillation signals detected in the arc voltage.

AMI 207 and AMI heads

The AMI 207 with an appropriate welding head constitutes a complete autogenous orbital welding system. Control over all the parameters necessary to complete an autogenous orbital TIG weld is provided by the AMI207. It is shown in the laboratory with an orbital head for 1.5" tubing (the 9-1500) in Figure 17.

An operating current limit of 150 Amps provides a more than adequate working envelope for the majority of tube welding applications.

Equipment and materials

It allows set programming of pre- and post-purge times, initial current delays, pulse welding parameters (peak and base current to 0.1 Amp resolution, peak and base times to 0.01 second resolution, and also peak and base welding speeds to 0.01 RPM - for 'stepped' or 'overlap' welding), different segments, slope-down time, and welding direction. Arc ignition is automatically applied by a high frequency start. The power module contained within the AMI207 is a 66 kHz inverter.

The Arc Machines controller was used for the initial work, although it could not be used for the closed-loop control work since it could not be adaptively controlled. Once the *WELD START* command was given the parameters were applied as pre-programmed.

The two heads used were the AMI 9-1500 (limited to a maximum of 25.4 mm diameter tubing), and the AMI 9-4500 (for 101.6 mm tube or pipe diameter maximum). The 9-1500 head has a maximum operating speed of 10 RPM, and the 9-4500 4 RPM. A close-up of the 9-1500 head with 25.4 mm tubing is given in Figure 18. Both heads are closed chambers and completely fill with shielding gas during welding. Purge gas for the inner bore of the tube/pipe must be supplied and controlled separately.

The orbital welding heads were limited to autogenous TIG with a single rotational axis of motion. Both $\phi 1.6$ mm and $\phi 2.4$ mm electrodes could be used in both heads. Arc length was fixed by a single grub screw in the rotor. The rotor was driven by a servo motor with tachometer, with a direct gear drive for the 9-1500 head and a gear and chain drive for the 9-4500 head. The degree of concentricity between the tube or pipe was dependent upon the quality of the clamping jaws used on either side of the weld joint.

An exploded view of the component parts of the 9-1500 head is given in Figure 19. In operation, supply of current to the electrode is made through the water-cooled 'crescent contactor' shown in the bottom right of the picture. The geared rotor (shown in the middle of the top half of the picture), carrying the tungsten electrode, is in permanent contact with the contactor whilst it rotates and thus the gear assembly is also at the same polarity as the electrode when welding. A d.c. servo motor with tachometer provides a controlled speed of rotation via the gearing shown.

Experimental orbital system

The experimental orbital system was developed under a Brite-EuRAM project (Adaptable Modular Orbital Systems, BE-5114-92), funded by the European Commission. It comprised a user-interface PC, an Isotek control rack and Migatron power source. This system has also been used for plasma keyhole welding of large diameter and thickness duplex stainless steel pipes, micro-plasma welding of small diameter and thickness titanium and aerospace alloy tubes, and MIG welding large diameter carbon steel pipeline, with various other orbital welding heads.

The *user-interface PC* provided a dual function. It acted as a data input point for all the welding parameters to be stored and applied, and provided control during the process for modification of parameters in real-time by the operator. The software used on the PC ran on the OS/2 operating system and used DB2/2 for OS/2 for parameter storage. The software was developed by Isotek Ltd for the Brite project for a windows-type application.

Data logging software used to detect and measure pool oscillations was also migrated onto the user-interface PC for the final closed-loop control system. The software ran on a DOS session under OS/2 at the same time as the welding control software. An Amplicon PC30D analogue-to-digital converter was installed in the user-interface PC to log the voltage and current transient signals. The A/D card was connected to signal conditioning hardware via a 50-way ribbon cable. The software used to detect and process the pool oscillation signals was originally developed by Medcen Ltd and modified by the author to include the fuzzy logic model.

The *Isotek control rack* performed all the primary control tasks - gas flows, communications with the power source and user-interface PC, and amplified d.c. servo signals for the head rotation via the d.c. servo motor on the AMI heads. It was developed and built by Isotek. Figure 20 shows the rack and the Migatron BDH320 power source in the laboratory. The operation of the rack was controlled by a VME-bus based processor running AMX real-time software. The software running on the VME-bus was also written by Isotek for the Brite project.

The control rack performed the control of the welding process itself by instructing the power source using serial communications and controlling gas valves (also using serial communications) and motion axes accordingly. Serial communications were also used to link the user-interface PC with the control rack. Start/stop and alterations ('Hot-key' commands) to the

motion or welding parameters were received by the control rack from the user-interface PC.

The BDH320 triple *Migatronic power source* (for MMA, TIG and MIG welding) is a standard commercially available inverter power source which operates at 100 kHz. The EPROMs contained within the power source were developed by Migatronic for the Brite project, facilitating serial communications at a 9.6k baud rate. The protocol used for the control of the BDH320 was written to allow a rapid and flexible control of the power source - all the process and parameter functions could be set via the communications link. It also enabled a degree of integrity by providing information on its own status of operation (welding, operating arc voltage and welding current etc.).

This equipment inherently possessed a *great* deal of flexibility. All the usual welding parameters associated with pulsed TIG could be controlled, with the additional advantage that they could be modified or adaptively controlled during welding for penetration control. The main limitations on the control of the welding parameters for this research work were:

- the welding current was defined with a resolution of ± 1 Amp,
- the pulsing frequency was defined with a resolution of ± 1 Hz.

A schematic of the integrated experimental control system is given in Figure 21. The serial communication connections between the user-interface PC (1.) and control rack (3.) and power source (5.) are shown as 2. and 4. respectively. Control of the rotation and gas flow to the orbital head was routed through the orbital head umbilical (6.) which also carried the power cables from the BDH320 (shown as 5.). Voltage connections were made at the orbital head (10.), and a current probe around the electrode lead in the umbilical (11.) provided the necessary sensing elements for the penetration control. Analogue signal processing was performed in a separate unit, shown as 12. - prior to digital conversion in the user-interface PC.

Full details of the pool oscillation software versions used and hardware are contained in the following sections.

Pool oscillation measurement and software

Pool oscillation measurements that were used for experimental results were measured using the following configurations:

Equipment and materials

- 486 DX33 with the Migatronic signal conditioning board and additional analogue circuitry to aid FFT processing, Amplicon PC30D analogue-to-digital card, and ArcWatch software (logging the full voltage and current transients), pool frequency calculations were then performed using an FFT utility or converting the data file to ASCII and using a purpose written Fortran program to extract the pool frequencies using an FFT routine,
- *the above hardware* with Brite LOG software (written by Dr. Kawal Chawla of Medcen Ltd.), performing the FFT routine in real-time and plotting the transient voltage signal and logging the derived frequency history,
- Pentium P90 with *the above signal conditioning* running graphical Brite LOG software with optimised computational speed for real-time monitoring or AMOS1 MON for control operation - including the fuzzy logic model (developed by the author).

ArcWatch software, from Medcen Ltd., provides a standardised interface to control and analyze transient recording of arc voltage, welding current and wire-feed speed signals, via 'windows' of specific sizes that can be separated by intervals if desired. The input sensing signals are passed through a signal conditioning module and converted into digital signals (via the Amplicon PC30D A/D card) which are stored in a memory buffer and saved to hard or floppy disk. Storing transient data in memory limits the amount of the data that can be logged (48 kilobytes of binary data can be stored). Basic data analysis tasks can be rapidly performed on the welding data (means, averages, standard deviations etc.). The transient acquisition parameters can all be configured for each sampling run (sample rate, the number of channels, window size - number of data points in each window, window interval - in seconds, etc.).

The standard ArcWatch signal conditioning unit did not offer sufficient sensitivity or filtering for the pool oscillation signals - initially only large amplitude signals could be easily detected. At this time the filtration was based on a passive R-C filter ($R = 10 \text{ k}\Omega$, $C = 0.01 \mu\text{F}$), which has since been substantially upgraded.

Clear pool oscillation signals were obtained by using the Migatronic signal conditioning unit (originally designed to report parameters to a commercial robot interface) which had active filtering and capacitive decoupling (a

Equipment and materials

10 kHz low-pass Butterworth filter, 4th order, 6-pole) in conjunction with the ArcWatch unit. This signal conditioning also offered a comparatively high sensitivity with a 0 to 20 Volts input (arc voltage) yielding a -5 to +5 Volt output.

John Nixon, from the Marine Technology Group, designed a small analogue card that was placed between the Migatron signal conditioning board and the analogue-to-digital card to further optimise and refine the pool oscillation signals, by subtracting the mean and amplifying the frequency component of the signal. Component values (R & C) were selected to optimise the arc voltage signal into two separate channels - one for low frequency (less than 150 Hz) oscillations, and one for high (greater than 150 Hz). The reasons for this separation are discussed later. The details of this circuit are shown in Figure 22.

Arc voltage and welding current signals were logged on channels 1 and 2 (as per usual practice). Modified arc voltage signals were logged on channels 3 and 4.

The component values used were:

R = 10 k Ω & C = 1 μ F (Channel 3 - > 150 Hz optimum response),
R = 30 k Ω & C = 1 μ F (Channel 4 - < 150 Hz optimum response).

The standard ArcWatch software was converted by Dr. Chawla (of Medcen Ltd.) into a real-time routine, here referred to as Brite LOG (graphical) and AMOS1 MON (text based for speed) that did not store all the transient data. A single window of data was analyzed at a time and only the *results* logged and plotted before allowing a further window to be processed in the same way. Specifically, the average voltage and welding current were reported in addition to the most dominant pool oscillation frequency, derived from an FFT of the processed voltage signals. A post-trigger delay was included to avoid including the voltage response during the current pulse in the data to be analysed ie. transient data prior to the oscillation of the pool. The FFT size could also be set to optimise the sampling of the oscillation signal.

Additional mathematical treatment of the voltage signals to further optimise partial penetration (Mode 1) signals in particular, and inclusion of the fuzzy logic model was performed by the author - this was included into both the Brite LOG and AMOS1 MON 'C' code and compiled.

Equipment and materials

The details of the derivation of the optimised signal conditioning hardware and software smoothing rules can be found in the experimental programme (§4.2.1, 4.2.3, 4.4.1 and 4.4.2).

Figure 22 shows the layout of the various signal conditioning boards used in relation to the analogue-to-digital card and PC.

3.1.2 Measurement techniques

Arc voltage

The arc voltage was measured at the orbital head for maximum sensitivity, and to avoid voltage drops across the welding power cables. Connections were made to the earth bonding strap on the outer of the head, and to the negative electrode via a wire installed inside the head attached to the rotor contactor. Attachment of the leads was always made after the high frequency start - since the high frequency start could destroy components on the signal conditioning board if left connected. The voltage cables were connected to the signal conditioning board directly.

Attaching the leads inside the welding power source behind the high frequency injection unit (to facilitate leaving the voltage leads permanently connected) was tried, however the loss in sensitivity of the voltage signal was too great.

Calibration of the arc voltage was made using a reference signal generating source.

Welding current

The welding current was sensed with 0 to 350 Amps Hall effect probe (supplied by Migatronik used in conjunction with their signal conditioning board), on the negative cable. The signal conditioning unit was supplied calibrated for the 0 to 350 Amp probe and subsequent logged signals were in good agreement with the set current values on both the AMI 207 and BDH 320 power sources. The AMI 207 was calibrated using a reference resistance load bank by Arc Machines, Derby.

Resultant bead profile

Orbital bead profiles generated during the experimental programme were measured visually using a vernier calibrated rule (stated accuracy of ± 0.05 mm - visual measurement accuracy of ± 0.1 mm estimated). For

continuous welds 20 measurements of outer and inner bead width were made at regular intervals around the full circumference after sawing the tube into two equal pieces longitudinally. The average outer bead width, average inner bead width, and also the standard deviations of the measurements are presented in the results section. Stationary spot welds were measured by measuring the upper and lower diameters in 4 places (0°, 45° 90°, 135° as viewed from above) and taking the average.

Penetration profiles have been used only as an illustrative tool for assessment of the state of penetration. The magnitude and variance of the bead widths have been taken as the primary measurement variables. The penetration profiles shown were obtained by sawing the orbital welds into two pieces longitudinally and polishing each half using graded grit paper with water followed by polishing on a diamond wheel and etch using Marble's reagent (50 ml HCl, 10g CuSO₄, 50 ml H₂O).

Inner Bead Surface Roughness

Quality of the inner bead of the weld is an important consideration for high purity and ultra-high purity applications. An assessment criterion that has been used to determine the disturbance of the bore profile is inner bead surface roughness. Some measurements were made during this work by Rank Taylor Hobson using a profilometer and 0.8 μm cut-off (which was determined to be appropriate by Rank Taylor Hobson given the curvature of the specimens).

Both R_a and R_q indices are used as indicators of the bead profile. R_a is the average surface roughness, whereas R_q accounts for the difference between the maximum and minimum values recorded in the measurement.

3.1.3 Standard experimental procedures

Material preparation

As standard practice all outer surfaces were abraded with grit paper and degreased with acetone. Surfaces that were contaminated by wrapping tape etc. were finished first. Inner tube/pipe surfaces were only degreased with acetone since the focus of the penetration control work was for ultra-high purity applications with electro-polished bores.

Joint preparation

Square butt joints were machined using the Tri-tool facing machine, shown in Figure 23. A standard electric drill provides powered rotation of the facing tool that provides the desired square butt joint preparation in the tube after indexing in a small amount upon each revolution of the tool around the tube.

Electrode setting, cleaning and integrity

Arc lengths were set by clamping one side of the tube/pipe or copper cylinder in the head. The electrode was installed in the 12 o'clock position with a feeler gauge between the tube/pipe and electrode tip. Occasional deterioration of the electrode by oxidation was removed using a grit paper rub and acetone rinse after removal from the head. Maintenance of the standard electrode geometry was necessary for the integrity of the voltage signal. Not more than 10 welds were made without re-grinding the electrode to the required geometry.

Pre- and post purging

Standard pre- and post purge times of 60 seconds were used for cleanliness and minimised oxidation of the bead. The internal purge gas used was always Argon supplied direct from a cylinder with regulator and a 0 to 20 litres flowmeter (Ar/CO₂). Plastic end-caps were used to maintain a reasonable atmosphere inside the pipe/tube whilst welding (a typical white end-cap is partly shown on the left of Figure 18). Pre- and post purge times were used for the both the shield and purge gas flows.

Orbital welding procedure

A typical standard 'open-loop' orbital welding procedure consisted of the following events:

- a.* programming the AMI 207 or the User-Interface PC with the desired welding parameters (for the different segments),
- b.* setting the desired transient logging parameters (window size, sample rate etc.) on the data logging PC - either the Elonex 486 or the User-Interface PC itself for the later work,
- c.* installing the tube to be welded into the orbital head after preparation, closing the rear clamping cheek of the head,
- d.* rotating the electrode and rotor to the 12 o'clock position and checking the arc length with a feeler gauge,

Equipment and materials

- e.* closing the orbital head, and connecting inner purge end-caps,
- f.* starting the pre-purge,
- g.* waiting for the high frequency arc initiation,
- h.* connection of the voltage leads,
- i.* prompting the ArcWatch PC if necessary to save and log more data, until the weld ends,
- j.* awaiting post-purge before removal of the tube/pipe.

A typical standard 'closed-loop' orbital welding procedure consisted of the following events:

- a.* programming the User-Interface PC with the desired *starting* welding parameters (single segment only), and the starting the AMOS1 MON fuzzy interference engine software running under a DOS session,
- b.* installing the tube to be welded into the orbital head after preparation, closing the rear clamping cheek of the head,
- c.* rotating the electrode and rotor to the 12 o'clock position and checking the arc length with a feeler gauge,
- d.* closing the orbital head, and connecting inner purge end-caps,
- e.* starting the pre-purge,
- f.* waiting for the high frequency arc initiation,
- g.* connection of the voltage leads,
- h.* awaiting post-purge before removal of the tube/pipe.

Note: these procedures were based on optimised logging and fuzzy logic model parameters that were previously determined.

The closed-loop system provided a method of regulating the degree of penetration without the need to determine the desired welding current level and segment duration to maintain an even bead profile.

3.1.4 Calibration of the closed-loop system

System operation

In order to close the control loop, the real-time monitoring software was run on the user-interface computer and Isotek control rack using the following strategy.

1. Control software (Isotek software running on OS/2 using DB2/2 as a database) was used to prepare the weld procedure, including the start and stop characteristics and the welding duration, using short current pulses to generate pool oscillations. A base current was selected that was *likely* to deliver the required degree of penetration (as an initial set-point). The control software was used to start the automatic orbital weld.
2. The real-time monitoring software (also running on the control computer as a DOS session) detected the current pulses at the appropriate times and logged the arc voltage response. A flag file was then used to indicate that a data output had been created by the monitoring software (the weld pool frequency and the desired change in base current).
3. The control software used a small OS/2 utility programme ('delta-reader' - provided by Isotek) to check for the existence of the flag file. Upon detecting the existence of the flag file, the data output file was opened and read.
4. The value of change that had been written as data output by the real-time monitoring software was then applied by the control software as a 'hot-key' to the base current ie. an automatic change to the base current to effect control of the penetration state of the weld pool.

This method had the advantage of creating an *add-on* control function for weld pool oscillation penetration control without disrupting the existing software functioning as an interface and control for orbital welding. It had the disadvantage of using an analogue to digital card (Amplicon PC30D) that was not supported by OS/2 so that the software could be compiled for DOS only and did not benefit from the advantages of multi-tasking and task prioritisation that OS/2 then offered.

It was found that the high frequency start used to initiate the welding arc triggered the software prior to the pulses used to generate the pool oscillations. For this reason, the first control output from the first pulse was not applied. The offset limits in the user-interface software were used to limit the level of base current applied by the AMOS1 MON software.

A schematic of the overall closed-loop operating sequence is provided in Figure 24. The actual welding cycle is illustrated in Figure 25, showing the sequence of events that must occur for the penetration control to be effected *between* the excitation pulses. The events contained within the whole *orbital welding cycle* are also shown in the box in the same figure (top right hand side).

User-interface & logging PC performance

The operating performance of the user-interface PC was characterised by observing the number of windows that could be analysed in 60 seconds for different sample rates and window sizes. The graphics program 'Brite LOG' was run as a DOS session only, and the text program 'AMOS1 MON' was run as a DOS session only, as a DOS session when running OS/2, and as a DOS session when running OS/2 with the user-interface software running. In this way the maximum operating speed of the system could be determined by establishing the maximum number of pulses that could be processed for an appropriate logging time (in comparison with the duration of the pool oscillation signal after the current pulse).

Table 3 shows the performance of the control PC under the various conditions tested:

1. as a graphics program running stand-alone under DOS,
2. as the basic text program without graphics DOS,
3. as the text program running on a virtual RAMDRIVE under OS/2, and
4. as 3. with the user-interface welding software operating.

The results from the different sample rates and window sizes are given in the table. Overall performance was assessed by measuring the number of windows that were logged in one minute, without any triggering mechanism ie. no current pulse. In addition to the derived maximum operating frequency data, further data columns are given that reflect the computation time taken, where the computation time is taken to be the difference between one minute and the time taken to collect the data for the number of windows processed in that minute (at the associated sample rate and window size).

Equipment and materials

It can be seen that for a given sample rate and window size, the greatest performance was given by the DOS text session (the 'C' program was compiled for DOS - the OS/2 driver for the A/D card had not been supplied thus preventing compilation for OS/2). A slight loss in performance was experienced when running under OS/2, but this was partially recovered, as shown, by using a virtual RAMDRIVE. A further slight loss in performance when running the user-interface software was also apparent. This can be attributed to the multi-tasking nature of OS/2 and that some time was then being taken up by the serial communications needed for the user-interface software.

It is interesting to note that for each vertical data set the computation time increased with the number of windows processed, and that the smallest computation time was experienced when the largest window size (1024 points) and the smallest sampling rate (8 kHz) were used. This might suggest that the optimal performance was obtained when the computer was logging as opposed to calculating. However, the compromise between gathering enough data to perform an accurate and adequate frequency analysis and obtaining a reasonable operating performance (pulses per second) was made.

Window sizes of 512 points with 10 to 16 kHz sampling rates were subsequently used resulting in a possible pulsing frequency of 3 to 4 Hz (as shown by the highlighted figures in Table 3) as working point solutions.

Serial communications protocol reliability

Many problems were experienced during the development of the serial communications protocol by Migatronix. In order to calibrate the use of the serial communications as a control tool, the power source was driven by a stand-alone PC (the 486 DX33), and the welding current was monitored on the Pentium P90. The monitoring parameters were:

Sample rate:	16 kHz,
Window size:	512 points,
Post trigger delay:	40 points, and
FFT size:	400 points.

The TIG arc was run on a solid copper anode. The welding current was changed by +5 or -5 Amps every 5th pulse (with the current pulsing at 2 Hz).

Validation of the serial communication protocol used to drive the power source can be made by examining the logged current points in Figure 26. Changes in current demand to the power source were responded to with consistent regularity - this is illustrated by the fact that although the average welding current points for each window are plotted, they are wholly consistent at each level of base current demanded and at the changes of demand.

Closed-loop system

The overall system performance was tested by forcing the output automatically ie. +5 Amps change to the base current for 10 current pulses followed by -5 Amps for 10 current pulses. The delivered welding current was monitored both on the user-interface PC and a separate PC running ArcWatch software. The performance of the system is shown in Figure 27. The average welding current on a solid copper anode was logged as before, although it can be seen that the actual application of each change in the welding current command issued was not 100% reliable. It can be seen that the overall trend was fully maintained ie. no commands were lost, although some commands were either not issued at the right time or not responded to in sufficient time before the following current pulse. In the example shown, only four signals had been 'queued' out of the application of 195. These instances are clearly circled in the figure.

By logging the exact transient current response, this behaviour was verified. The *ideal* system response is shown in Figure 28. The change of welding current occurred prior to the application of the next current pulse. Queuing of the signal is illustrated in Figure 29 where two commands are seen to have been applied in one instance ie. a single -10 Amps rather than two -5 Amps following each other in sequence. Isotek provided a verification of the time of issue between the control rack software receiving the change in welding current command at the control rack (from the user-interface PC) and the issue of the change in welding current command to the power source. The delay was shown to be minimal, only 10 or 20 ms at most. The 'queuing' was therefore attributed to the prioritisation of tasks by the software operating within the power source controller (monitoring welding operations, pulsing the welding current, changing the welding current according to incoming signals on the serial communications port etc.) and the decreased amount of time available to respond in comparison with the previous test work (see sub-section above).

3.2 Materials

3.2.1 Tube and pipe material description

The austenitic stainless steel tube and pipe materials used for the experimental programme are detailed in Table 4. For the bulk of the work, 1.5" diameter, 16SWG material (38.1 mm diameter, 1.65 mm wall thickness) was used since this is a typical size for ultra high purity applications.

Larger wall thickness materials were also used to extend the scope of some of the aspects of the studies, and in particular to demonstrate radically different cast behaviour.

Note: '1.5" Thick' is so-called since the wall thickness is high for the diameter (0.125" or 3.18 mm), in comparison to the more typically used 16SWG.

For the 'welded' certified types shown, the pipes have been formed from sheet, rolled and seam welded.

3.2.2 Tube and pipe material composition

The declared chemical composition from the suppliers of the tube and pipe materials used in the experimental programme are shown in Table 5.

It is perhaps noteworthy that the material casts with the lower sulphur contents ('LS Kobe' and '1.5" Thick' at $S = 0.001\%$) are from Japan where the trend to produce 'cleaner' steels is becoming more evident. This trend might provide a greater challenge for welding these materials, since the lower sulphur materials are often associated with a difficult to weld characteristic.

SECTION 4.

EXPERIMENTAL PROGRAMME

4.1 Experimental design

4.2 Fundamental oscillation experimentation

4.2.1 Filtration of arc voltage signal

4.2.2 Arc voltage response to current on copper block

4.2.3 Arc voltage signal processing

4.2.4 Basic welding parameters

Stationary spot welding and signal quality

Orbital welding and penetration

Travel speed, pulse current level,

inner bead surface roughness and outer bead appearance

Travel speed and signal quality

4.3 Effect of cast-to-cast variation on oscillation behaviour

4.3.1 Stationary pool and time-to-penetrate studies

Part 1 - Small diameter tubing

Part 2 - Medium diameter pipe

4.3.2 Cast-to-cast variations in moving weld pools

4.4 Real-time logging and reliability of frequency response

4.4.1 Configuration of real-time logging

4.4.2 Reliability and smoothing of response

4.5 Application of fuzzy logic to pool oscillations and penetration behaviour

4.5.1 Single-input/single-output model

4.5.2 Operating performance

Open- and closed-loop trials

Step change recovery

,

. . .

,

4. EXPERIMENTAL PROGRAMME

4.1 Experimental design

The form of the experimentation carried out for this thesis varied depending upon the primary objective of the work: given the nature of the weld pool, with respect to the effects of the many operating variables already reviewed, much of the work presented was based upon isolating the effects produced when changing a single variable, or comparing a single variable effect upon cast differences, for example. Some of the work even eliminated the weld pool itself and utilised a TIG arc and a copper block to assess some of the more absolute arc voltage effects.

The main focus of the experimental work centred around establishing sound, robust operating parameters, investigating the effects of disturbances upon the derived signals, and furthering the practical application of pool oscillations to tube welding. With this in mind, casts of material were used with an anticipated spread in behavioural response ie. casts with minor constituent variations that were suspected to cause observable performance differences. Additionally, since one of the experimental objectives was to assess the sensitivity of the pool oscillations employed to the degree of penetration, often conditions were selected that highlighted the spread of states of penetration, from significantly under-penetrated to over-penetrated for example.

In the following sections progression from experimentation with initial fundamental oscillation work, basic welding parameters, through to signal processing work is presented providing operating parameters and *initial* output results. More detailed experimentation is then described progressing the work to the effects of cast-to-cast variations on stationary and moving weld pools, *real-time* operation and consequent fuzzy logic modelling for closed-loop control of the degree of penetration, with the goal of maintaining the full penetration condition.

Refer to the Symbols and abbreviations section (at the start of the thesis) for an explanation of the abbreviations used for the procedural parameters, and also the equipment and materials tables (Tables 2, 3 and 4, in the Appendix).

4.2 Fundamental oscillation experimentation

In order to generate, identify and measure weld pool oscillations, a number of short separate experimental procedures were carried out to optimise the response, investigate alternative methods, and configure equipment.

Initial experimentation adopted procedures as used by the reviewed literature for generating a 'free response' in the weld pool for constant travel speed welding: shielding gases generating comparatively high electric field strengths, argon/hydrogen and helium, etc., current pulsing parameters of short duration peak current level 100 Amps above base current level, and, pulsing frequencies of 2 to 4 Hz, for example.

In these first experiments, analysis of pool frequencies was performed by a Fast Fourier Transform routine applied in the ArcWatch™ software with limits for the data set manually at the start and end of the oscillation signal.

4.2.1 Filtration of arc voltage signal

Central experimental aim: *to obtain clear pool oscillation signals in the arc voltage as reviewed in the literature, using contemporary inverter power sources.*

Using the standard ArcWatch™ configuration (with the signal conditioning based on passive R-C filtration - see Section 3 for the values), the parameters shown in Table 6 were used in order to generate pool oscillations for an initial trial.

From the results it was clear that a passive low-pass R-C filter ($R = 10\text{ k}\Omega$, $C = 0.01\text{ }\mu\text{F}$) was inadequate to filter all the noise from the inverting power source, to reveal the relatively small amplitude pool oscillation signals. A Migatron signal conditioning board was then used (Butterworth 4th Order, 6-Pole, 10 kHz low-pass active filter) with a Phillips digital oscilloscope to monitor the output from the signal conditioning board. The results confirmed the suitability of this initial experimental configuration and welding procedure. After observing typical pool oscillation frequencies, the sample rate used for subsequent monitoring of the arc voltage signal was selected to be several orders of magnitude higher than the highest expected pool frequency to avoid the effects of aliasing when sampling at too low a sample rate and provide a reasonable resolution of the waveform generated.

Experimental programme

Typically sample rates of 4 to 5 kHz per channel were subsequently adopted (yielding 10 data points per period for an observed pool frequency of 500 Hz for example).

4.2.2 Arc voltage response to current on copper block

Central experimental aim: to observe the 'absolute' arc voltage characteristic upon solid copper eliminating the molten pool.

In order to establish the basic relationship between the arc voltage and the welding current for both argon and argon with a hydrogen addition, a short experimental trial with the AMI 207 power source was carried out. The arc length was varied for the argon with hydrogen shielding gas to obtain information about the absolute effect of arc length upon arc voltage (this could be subsequently used as a comparison with the arc voltage amplitude caused by the change in arc length from an oscillating weld pool).

A static TIG arc was struck on a solid copper anode with constant welding current. The arc voltage was logged with ArcWatch and the Migatronic signal conditioning board, logging 2 channels @ 8 kHz for 8 seconds during a 12 second welding run. Table 7 shows the ranges of values of constant current (I) and arc length (L_{arc}) that were used.

The copper anode was water cooled between each weld run to maintain a constant initial anode temperature.

The characteristic response of the arc voltage to a pulsed current input on a copper block was then logged in order establish the difference between the arc effects from the shielding gas and pulsed current on a static/solid anode, and the effects of any oscillatory behaviour of the surface of a molten weld pool. The pulsed current duration and magnitude is typical of that used to generate pool oscillations. The experimental parameters used are given in Table 8.

In addition, the effects of the quality of the tungsten electrode were assessed - a particularly damaged electrode (with a balled tip) was used and found to have a significant effect on the arc voltage signal. Subsequent experimental work adopted tungstens that maintained the basic ground geometry without damage or deterioration. In practice, no more than ten weld runs were made before regrinding to re-establish the chosen geometry.

Experimental programme

The difference between the two power sources used (the American Arc Machines AMI207 and the Danish Migatronic BDH320) was also determined with the above welding parameters - 2 channels were logged @ 20 kHz, to monitor in detail the transient profile of the actual delivered current pulse.

4.2.3 Arc voltage signal processing

Central experimental aim: *to attempt to process the arc voltage signal in such a way so as to improve its sensitivity to pool oscillations.*

In order to optimise the small amplitude arc voltage signals from partially penetrated welding pools in relatively thin material (1.65 mm nominal wall thickness), an additional analogue signal processing circuit was added to amplify the oscillatory signal and separate it from the base voltage level. The location and detail of this circuit is described at the end of §3.1.1.

The difference between partial and full penetration signals in thin material is notable. For lower welding currents, the small amplitude oscillation response can be short in duration and super-imposed upon the arc voltage response from the current pulse itself. The work performed in section 4.2.2 above illustrated the static voltage signal that could be expected from the use of the large amplitude short duration current pulse (I_p).

The aim of using additional analogue signal processing circuitry was to provide a resultant signal with as close to a zero mean as possible, in order to aid subsequent FFT processing. A small circuit was designed to provide amplification of the incoming signal and remove the 'd.c.' component. A single circuit could not be found that could optimise both partial and full penetration signals (the characteristic initial base voltage response from the lower welding currents was of a similar frequency response to the full penetration oscillatory signals).

Consequently, two circuits were used: one to maximise the response of small amplitude high frequency partial penetration signals present in the 1.65 mm WT SS316L material ($R = 10\text{ k}\Omega$ & $C = 1\text{ }\mu\text{F}$, as shown in Figure 22), and the other to maximise the response of large amplitude, lower frequency full penetration signals ($R = 30\text{ k}\Omega$ & $C = 1\text{ }\mu\text{F}$), with a cut-off between the two at approximately 150 Hz (a frequency level established by earlier experimentation).

Table 9 shows the welding parameters used to optimise the signals and the values of base welding current (I_b) that were used to vary the response from a partial to a full penetration response. The resulting clarity of the pool oscillation signals meant that the maximum response from a Fast Fourier Transform analysis could be used reliably to determine the dominant oscillatory frequency present in the weld pool.

4.2.4 Basic welding parameters

Central experimental aim(s): *to observe the effects upon the pool oscillation signal of some of the more fundamental welding parameters - by observing behaviour in stationary pools, in moving pools with varying levels of penetration and travel speed, and assessing the effect of typical pool oscillation procedures upon the inner bead surface roughness generated.*

Stationary spot welding and signal quality

In order to assess the effect of pulse magnitude and duration upon the quality of the pool oscillation signal, trials were made using the two power sources available (the AMI 207 and the BDH 320) and a range of peak current (I_p) and peak pulse time (t_p) values in stationary pools - Table 10 shows the experimental parameters used.

The signals were logged using ArcWatch with the Migatron signal conditioning unit @ 4 kHz (4 channels) in order to have a full picture of the oscillation signal during the short welding procedure, which comprised a 15 Amp constant current for 4 seconds to stabilise the pool, followed by a 30 Amp base current with corresponding peak current pulse for 10 seconds.

The resolution of the AMI207 pulse times is limited to ± 0.01 seconds. Experiments with the AMI207 adopted the use of 10 and 20 millisecond peak current pulses (t_p) accordingly for both Argon with 5% H_2 and 10% H_2 shielding gases. Comparative experiments were also performed with the BDH320, although 5 and 15 millisecond pulses were also investigated for the Argon with 10% H_2 to provide additional data.

Orbital welding and penetration

In order to assess the fundamental effect of penetration upon the measured pool frequency the base current was used as a control variable. Eight levels of base current were examined to investigate the resulting effect on the pool frequency. All the welds were made as full orbital passes (bead on tube) and the arc voltage and welding current signals were monitored at the 01:30, 04:30, 07:30 and 10:30 positions, to allow a reasonable delay after starting at the 12:00 position for the voltage connections to be made, and a short delay in between the ArcWatch logging runs.

In an attempt to maintain a relatively constant bead geometry around the orbital joint the base current was decreased in each subsequent segment (4 equal segments to construct one orbital pass) to account for the heat build-up, according to the following basic formula:

$$\begin{aligned} 2^{\text{nd}} \text{ quarter welding current} &= 0.975 \times 1^{\text{st}} \text{ quarter welding current,} \\ 3^{\text{rd}} \text{ quarter welding current} &= 0.975 \times 2^{\text{nd}} \text{ quarter welding current,} \\ &\text{and so on.} \end{aligned}$$

Table 11 details the welding parameters and the different values of base current (I_b) that were used.

Straight d.c. welds were also made without the peak current pulse i.e. at constant current, to assess the effect of the peak current pulse upon the penetration profile.

Both the transient arc voltage and welding current were logged @ 10 kHz (4.8 seconds of data) using ArcWatch and the Migatronic signal conditioning board. The frequency was calculated as an average of 9 windows at each position and both the average and standard deviation of the overall frequency response at each position or base current level were calculated.

Travel speed, pulse current level, inner bead surface roughness and outer bead appearance

It was apparent from the studies of basic welding parameters that the current pulse used to generate the oscillation of the pool caused an apparent change in the inner bead profile - especially in comparison with straight d.c. procedures for example. It was thought that the main causes of the profile were the welding speed, affecting the number of pulses per unit length, and the level of peak current affecting the oscillation amplitude.

Experimental programme

In order to assess the quality of the inner bead profile, welding trials were made with various travel speeds and two levels of peak current. The surface roughness profiles of the inner beads were then measured by Rank Taylor Hobson.

Welding parameters were as per Table 11, with travel speed and peak current variations as per Table 12. The variation in base current level was used to maintain a correlative degree of penetration for the variation in welding speed employed.

The effect of pool oscillations upon the outer surface appearance was also examined, as an additional correlation for the pool frequency measurements and as a measure of the effect upon the bead profile. The nominal wall thickness (WT) was machined down to 2.5 mm for the purposes of this study to facilitate autogenous full penetration welding using the AMI207 (preliminary trials had demonstrated the need for this since the AMI207 is limited to 150 Amps) - see Table 13 for the experimental parameters and the variation in base welding current (I_b).

Travel speed and signal quality

It has been reported in the literature that the arc voltage signal in particular deteriorates at high travel speeds. The following welding trials were used to assess the effect of the travel speed upon the quality of the oscillation signal. In order to account for the decrease in heat input with the higher travel speeds the base current was increased to maintain a similar degree of penetration. Table 14 details the various welding current (I_b) and speed (S) combinations used (shown as 1., 2., 3., and 4.).

Experimental programme

4.3 Effect of cast-to-cast variation on oscillation behaviour

4.3.1 Stationary pool and time-to-penetrate studies

Central experimental aim(s): *to observe the effect of cast-to-cast variation on pool oscillation signals in stationary pools, to determine whether the pool oscillation frequency/time characteristic offers a valuable insight into penetration behaviour and/or cast weldability.*

Part 1 - Small diameter tubing

In order to investigate the effect of the variation of cast and the possibility of using weld pool oscillations as a static test to characterise the material behaviour, a series of stationary spot welds were made on several different casts of tubing. Stationary welds were made in order to keep the upper pool surface as close to plane circular as possible. The welding current level selected ensured sufficient time for the pool size to grow under the influence of arc heating so that a progression from the partially penetrated to the fully penetrated state could be monitored. The specific aims of this part of the experimental programme were:

- to assess whether the *average acting* surface tension under the welding arc, γ , varied for each material cast by using the observed pool oscillation frequency and theory (relating frequency, pool size and material density) to offer a theoretical prediction,
- to see if any aspect of the stationary pool oscillation and penetration behaviour could be used to predict material behaviour either in terms of penetration behaviour under a moving arc, and hence more elongated weld pool, or as an initial characterisation assessment of the cast 'weldability'.

Four casts of 1.65 mm wall thickness material were used (this was the nominal wall thickness as supplied by the manufacturers). The Sandvik material of 2.0 mm (WT) was also used to extend the range of welding currents that could be applied. A short 2.5 second application of non-pulsed current at 15 Amps was used *prior* to pulsing to stabilise the arc, and to allow the voltage connections to be made (after the high frequency arc initiation). The pulsed current was then applied for 10.0 seconds.

Experimental programme

Experimental parameters are given in Table 15 which details the range of base welding current (I_b) for the 1.65 mm material and the extended range applied to the 2.0 mm material.

Prediction of the *average acting* surface tension from the observed oscillation behaviour adopted the following equations and assumptions:

- the use of the Xiao/Kotecki membrane model for Mode 3, full penetration oscillation - see Equation 1 - for plane circular pools with straight vertical side-walls,
- the use of the Yoo model for Mode 3, full penetration oscillation - see Equation 3 - for plane circular pools with straight vertical side-walls, ie. $p = 1.0$,
- the assumption that the material density is the same, $\rho = 7800 \text{ kg/m}^3$, for each material cast, and that the density does not alter significantly with the temperatures generated (estimated $\Delta\rho$ to be 2% maximum),
- the material thicknesses were as certified by the suppliers - as noted, it has been reported in the literature that material thickness can significantly affect the time-to-penetrate and that there can be variation in material *as supplied* (see note below),
- the assumption that the pool did not increase in size significantly after the last current pulse used to measure the *lowest* pool frequency.

Measurement of the upper and lower pool surface diameters was made in 4 places by a vernier calibrated microscope. The lowest dominant pool frequency (f_d) evident in the fully penetrated condition (ie. $f_d = f_{M3}$) prior to arc extinction was used in the calculations for the prediction of the surface tension.

Note: although the supplier's certification (A269) allows a potential thickness variation of $\pm 10\%$ from nominal, experimental measurements of wall thickness at various locations on the casts investigated did not determine any significant deviation from the stated nominal thickness.

Experimental programme

Welding was made in a constant 12 o'clock position with the tube in the 5G orientation. Extraction of the pool frequencies from the binary data created by ArcWatch™ was performed by converting the entire binary file to ASCII, and using a Fortran program to perform a Fast Fourier Transform on the arc voltage data after the application of the 125 Amp current pulse.

Part 2 - Medium diameter pipe

In order to investigate the possibility of using pool oscillations as an indication of weldability or time-to-penetrate further, the same procedures were applied to thicker materials. Two casts of material were used that were known to be extremely difficult to weld and compared with casts that were comparatively straightforward. Software was used that provided an output of the pool frequency in real-time (Brite LOG software) for a visual indication of pool behaviour. The standard derived test applied was repeated 3 times for each material cast.

The aims and assumptions for this part of the experimental programme are identical to **Part 1 - Small diameter tubing**, although it was thought that the greater thickness of material would allow a greater resolution of both the repeatability of the experimentation and the differences in behaviour between the 'difficult' and 'easy' to weld casts.

A short 4 second application of non-pulsed current at 15 Amps was used prior to pulsing to stabilise the arc, and to allow voltage connections to be made. The pulsed current was then applied for 30.0 seconds - the standard test parameters applied to all the material casts in this part of the study are detailed in **Table 16**.

The signals (arc voltage, welding current and the two signal processed arc voltage channels) were logged @ 16 kHz, with 1024 points per window, a trigger current of 120 Amps, an 80 point post trigger delay with 900 points used for the FFT. Moving average of ten point periods were also used for data smoothing of the transient voltage signals.

4.3.2 Cast-to-cast variations in moving weld pools

Central experimental aim(s): *to observe the effect of cast-to-cast variation on pool oscillation signals in moving pools, to determine whether there is any correlation between pool oscillations observed in stationary and moving pools for different material casts.*

The effects of cast variations on penetration behaviour are well known (see §2.6.1 for detail) and two casts of material were chosen that were known to exhibit different resultant bead geometries from the same welding procedures, despite both being SS316L certified. In particular one material was comparatively low in sulphur level ('LS Kobe' had only 0.001% S.), whilst the previously used 'Cast 1' was relatively high (0.011% S.).

The experimental programme was devised to assess the behavioural differences between the two casts: a standard pulsed TIG programme, straight d.c. welds with Ar 10% H₂, and pulsing with Ar 10% H₂ to generate pool oscillations. Bead appearance, average and standard deviation of the outer and inner bead widths (as measured from 20 locations around the 120 mm circumference), and the mean arc voltage level were recorded for the welding runs. The frequency responses for the oscillation runs were logged using ArcWatch software and Migatron signal conditioning logging at 20 kHz (4 channels). All welds were made bead-on-tube.

Parameters for the standard pulsed TIG, the straight d.c., and the pool oscillation procedures are given in Tables 17, 18 and 19 respectively.

The specific aims of this part of the experimental work were:

- to observe and measure any significant cast differences of two relatively thin-wall (1.65 mm) 316L steels with respect to observed penetration behaviour for standard pulsed, straight d.c. and oscillation generating welding procedures,
- to see if the predominant fluid flow regimes in the molten pools of the two casts were reflected in the clarity of the oscillatory response, since it has been observed that the radially outward surface flow of low sulphur steels is significantly less turbulent than the radially inward flow of high sulphur steels,

Experimental programme

- to determine whether the oscillatory behaviour (dominant pool frequency) in response to the current pulsing applied revealed the cast differences in accordance with the pool size/shape,
- to investigate the possibility of using the oscillations generated in the molten pool to control the weld bead produced, despite the potential existence of cast variations.

In order to account for heat build-up around the orbital joint, the current was altered per quarter segment to maintain a relatively consistent level of penetration as detailed previously (in §4.2.4 - a factor of 0.975 was applied to the following orbital segments). For the standard pulsed TIG procedure, the peak current (I_p) was altered, since this formed the dominant heat input parameter. For the straight d.c. and pool oscillation procedures the base current (I_b) was altered as previously described.

Note: for the sake of comparison and brevity, in the results section and corresponding figures 'Cast 1' is also referred to as 'HS' ie. high sulphur, and 'LS Kobe' as 'LS' ie. low sulphur, since this was thought to be the main difference in chemical composition and possible cause of differences in behaviour for the same welding parameters (see Keene, 1985, for example).

4.4 Real-Time logging and reliability of frequency response

4.4.1 Configuration of real-time logging

Central experimental aim: *to monitor the real-time pool frequency responses to all the peak current pulses applied.*

Software was provided to allow the calculation of the pool oscillation frequency in real-time (by Dr Kawal Chawla, of Medcen Ltd) - the software referred to in this thesis as 'Brite LOG'. The following basic operational sequence was devised:

- a. Trigger of data logging by the current pulse (typical 125 Amps for 5 to 10 ms) used to generate pool oscillations.

4 channels logged:

arc voltage	(Ch 1),
welding current	(Ch 2),
processed voltage 1 (> 150 Hz optimum)	(Ch 3),
processed voltage 2 (< 150 Hz optimum)	(Ch 4).

- b. Data logging at specified sample rate and window size, after post trigger delay elapsed (set by the number of points).
- c. Calculation of the dominant frequency response (f_d) from the FFT software processing of data according to the number of data points in the FFT (remainder zero-padded), subtraction of means and smoothing.
- d. Screen plot of processed transient data (not stored), screen plot and store of frequency history, average arc voltage and welding current for each window stored.
- e. Dead-time before recurrence of event a. or the end of the sequence.

Program utilities were also provided for: oscilloscope mode, post-weld analysis of frequency, arc voltage and welding current data, file storage and recall, weld procedure storage and recall. The compromise between

Experimental programme

obtaining sufficient transient data for analysis and allowing enough time for all necessary calculations prior to the application of the next current pulse was then experimentally determined.

Typically, the following parameters represented a workable real-time solution on the 486 DX 33 MHz:

Sample rate:	8 to 16 kHz (ie. 2 to 4 kHz per channel),
Window size:	512 Points,
Post trigger delay:	40 Points,
FFT size:	400 Points.

The number of points in the FFT software was 2048 ie. 400 points were used from the transient data, zero-padded, and a 2048 point FFT used for calculation to obtain a reasonable frequency resolution. The above parameters resulted in the ability to fully track and log all the transient voltage responses when current pulsing at 2 to 3 Hz ie. there was sufficient time for the processor to log all channels for the specified duration, perform the FFT calculations after some mathematical treatment of the signal, display and store the outputs, prior to the occurrence of the next current pulse and data set. Comparisons between window sizes and sample rates were performed to determine the maximum speed of operation with maximum data gathering. A Pentium P90 computer was also compared with the 486 DX33 for speed. The P90 was used as the user-interface computer for the Isotek control system. (See §3.1.1 for the calibration work performed.)

To test the response of the software and validate the ability of the software to monitor and analyse partial penetration signals in real-time, orbital welds were made on several casts of SS316L ϕ 1.5" 16SWG, splitting each single orbital pass into two segments (partial [1.] and full [2.] penetration conditions respectively). The corresponding welding parameters are given in Table 20. The reverse of the procedure was also applied, so that full penetration conditions were followed by partial penetration conditions.

4.4.2 Reliability and smoothing of response

Central experimental aim: *to optimise the performance of the real-time pool oscillation frequency signal and smooth out erroneous or chaotic disturbances that might destabilise the intended control strategy.*

The reliability of the frequency response is crucial to the use of pool oscillations as a potential control technique. It is inherently dependent upon the stability of the arc voltage signal, which in turn is subject to a number of factors, including the surface quality of material to be welded, impurities entering the arc either via the shielding gas flow or from the welding environment, behaviour of the anode spot, significant deterioration of the electrode surface due to oxidation or over-heating, and rapid changes in weld preparation such as material thickness, root gap, or fit-up.

In addition to the potential noise disturbances, the derived system had to be able to adequately cope with both partial and fully penetrated responses, since partial penetration responses in comparatively thin materials are quite small in magnitude and damp out quickly.

Initially only the 'raw' response data was logged for various pool sizes. However, it became apparent that additional software rules and filtration were required for stability for control purposes. Various strategies were employed to optimise the real-time response and stabilise the operating performance, and the following list summarises the derived approach after much experimentation.

A section of 'C' code, written the author, was included into the Brite LOG software to mathematically treat the pool oscillation signals to further improve the reliability of using the FFT to detect the dominant pool oscillation frequency. The Brite LOG software was also modified in the following ways.

- Frequencies of > 500 Hz and < 30 Hz were rejected, since they were known to be too high and low for likely pool responses.
- Signals logged on channel 3 were split into two sequential halves for the logging duration, the second half discarded, and the first half repeated for the data window, to maximise arc voltage data containing the relatively short duration partial penetration response.

Experimental programme

- Means of the data for channel 3 were subtracted in one-quarter FFT size blocks from the channel 3 data, and one-half FFT size blocks from channel 4 data to ensure the data was as close to zero-mean as possible before FFT processing.
- Transient data was passed through a moving average routine of 10 point period to smooth unwanted high frequency noise transients.
- A response with a difference of > 30 Hz in comparison with the previous window was rejected for control purposes.

The assumption behind the above 'rules' was that the weld pool produced by the TIG welding current invokes a relatively slow response, and that output response changes should only be used as a basis for control if the short-term trend is consistent and reliable.

To investigate the stability of the response after applying the new 'rules', experimentation was carried out that divided a single orbital pass into 4 segments, with different penetration conditions in each (partial [1.], full [2.], partial [3.] and full [4.] conditions) on relatively thick material (SS316L $\phi 1.5"$ 0.125" nominal WT) to highlight the range of the frequency response. The main variable was the base current, I_b - all the experimental parameters are given in Table 21.

These welding parameters were also applied to a standard square butt joint (prepared on the Tri-Tool facing machine) that was manually tack-welded.

4.5 Application of fuzzy logic to pool oscillations and penetration behaviour

4.5.1 Single-input/single-output model

Central experimental aim: to develop and apply a fuzzy logic model in real-time to control the level of penetration via the base current, accounting for the difference between partial and full penetration conditions.

As described previously, the weld pool oscillation frequency was used as a measurement variable to assess the state of penetration of the weld pool. Base current (I_b) was used to alter the heat input in order to change the level of penetration and observe the effect on weld pool frequency, in an open-loop, pre-programmed fashion.

In order to develop a closed-loop control of the process the desired input variable (weld pool frequency) had to be linked to the output variable (the heat input of the process determining the level of penetration, in this case 'delta base current' as a small change to the process heat input). Several complexities are involved in the application of a control strategy using weld pool oscillations for austenitic stainless steel tubes:

- the frequency response for the predominant oscillation modes (Modes 1 and 3) can be significantly altered by the cast behaviour, despite being certified SS316L or SS304L, and unless an accurate knowledge of the surface tension/temperature behaviour is known, a frequency prediction cannot be made accurately according to the basic theory (Equations 1, 3, 4 and 5),
- theoretical modelling can be subject to several degrees of error concerning the effects of variation of surface tension behaviour in particular, and the actual pool geometry that is often over-simplified for theoretical models, and
- the transition from Mode 1 (partially penetrated oscillation mode) to Mode 3 (fully penetrated oscillation mode) for a given material cast and thickness results in a non-linear response between the pool frequency and the state of penetration.

Experimental programme

A control strategy had to be developed that linked a *single-input* to a *single-output*, and accounted for the above considerations. The use of fuzzy logic met the above conditions and offered the ability to model the state of penetration via the weld pool frequency using an intuitive framework:

1	Over-penetrated	(OP),
2	Slightly over-penetrated	(SO),
3	Fully penetrated	(FP),
4	Partially penetrated	(PP),
5	Slightly penetrated	(SP).

The above classifications represent the *input membership functions* used (representing the state of penetration). *Output membership functions* for the output variable were then classified in a similar manner (for the delta base current ie. the change in the base current variable, directly affecting the process heat input):

1	-ve LARGE DELTA CURRENT	(-LG),
2	-ve SMALL DELTA CURRENT	(-SM),
3	ZERO CHANGE	(ZE),
4	+ve SMALL DELTA CURRENT	(+ SM),
5	+ve LARGE DELTA CURRENT	(+ LG).

The advantages of using a fuzzy logic model to relate the weld pool frequency to a desired output signal (a change in the base current, I_b) were:

- the quantification of the input and output variables, and the relationship between them, could be made in a fuzzy way that was not dependent upon modelling the behaviour based on physical properties and potentially computationally intensive calculations and the inherent various degrees of error,
- a higher degree of sensitivity could be employed in the area of interest (ie. where the pool is fully penetrated and can become over-penetrated with a change in frequency response),
- a lower degree of sensitivity could be used in the transition area between Mode 1 and Mode 3 frequencies (since a pool in 16SWG material might drop from 250 or 300 Hz to 90 or 100 Hz for a small change in conditions),

- a single model could be used to account for the system behaviour, despite the presence of two predominant oscillation modes.

An initial model relating the weld pool frequency to the delta base current output was constructed using Microsoft Excel 5.

The model essentially involved defining the input and output membership functions, using triangular and trapezoidal function shapes, quantifying the membership of an example input (fuzzification), evaluating the rules relating the input and output membership functions, and deriving the corresponding crisp output (defuzzification) delta base current using the centroid (or centre of gravity, COG) method.

Table 22 provides a summary of the fuzzy logic model, detailing the input and output membership function labels, and the values that were used to define the functions.

Note: the construction of the fuzzy logic model adopted certain 'ground rules' that are important and have been described by many other authors (Motorola, 1992, and Kosko, 1994, for example), namely that the number of membership functions in each set is often odd (balanced about a central target, or zero output) and that each function in either the input/output set should overlap to a certain degree to avoid Boolean operation.

Figure 30 provides a graphical representation of the membership functions and an example pool frequency input and corresponding output from the fuzzy logic model.

Since a single-input, single-output model was used the relation between the input and output membership functions was direct. For the example illustrated, a crisp input frequency of 90 Hz corresponds to a 0.75 degree of membership of the 'FP' fully penetrated set and a 0.22 degree of membership of the 'PP' set. This would correspond to a 'fuzzy' description of:

'the pool frequency of 90 Hz represents a weld pool that is mostly in the fully penetrated condition and partly in the partially penetrated condition'.

Experimental programme

This results in a 0.75 degree of membership in the 'ZE' zero change and a 0.22 degree of membership of the '+SM' positive small change (delta current) output sets, corresponding to the following 'fuzzy' control decision:

'the welding current should be left mostly unchanged but slightly increased with a small positive change'.

The degrees of membership in the output membership function sets were used to provide 'lambda cuts' relating the degree of truth of each set. This formed the basis for the crisp output calculated from the centre of gravity of the resulting sets, in this case +0.52 Amps (calculated from an integration of the applicable lambda-cut output membership functions in 0.1 Amp intervals). Different methods of 'defuzzification' could have been used, however the centre of gravity method was known to give the smoothest output, although computationally it was not the fastest method.

A measured pool frequency of 80 Hz would result in a 1.00 degree of membership in the 'FP' fully penetrated set only and a corresponding 1.00 degree of membership of the 'ZE' zero change set (to the welding current), with centre of gravity of 0.0 Amps (the c. of g. of the trapezoid 'ZE' defined by the output membership coefficients given in Table 22).

By running the model for all the example inputs (using Microsoft Excel), an input/output characterisation can be made of the fuzzy logic model - this is shown graphically in Figure 31.

Conversion of the model to a 'C' routine was then performed for inclusion into the real-time monitoring software, consisting of many variable arrays, IF-THEN statements, and a 'minimum/maximum' comparator for the membership functions and degree of truth 'lambda-cut' operators.

4.5.2 Operating performance

Central experimental aim(s): *to include the fuzzy logic model into the real-time monitoring software and to interface with the Isotek user-interface software to control the base current whilst welding, and hence close the loop, and further to make some assessment of the stability of the control strategy with disturbance step inputs.*

Open- and closed-loop trials

The open-loop behaviour of the control rules and fuzzy model was analysed using a full penetration condition on the electro-polished $\phi 1.5''$ material ('EP'). The condition was chosen to result in a degree of over-penetration at the end of the weld ie. the welding current would usually be reduced to account for the heat build up. The previous smoothing routine used for the weld pool frequency (changes of greater than 30 Hz were 'ignored') was transferred to the control routine. Pool frequencies were reported as measured - it was expected that some 'noise' would thus be present in subsequent pool frequency measurements.

All the experimental parameters are reported in Table 23.

Closed-loop trials with the system were then made. An initial pool frequency of 80 Hz was selected as the target. This frequency was selected as being a relatively stable full penetration signal that was established after the transition to Mode 3. The experimental parameters that were used are detailed below. Three trials were made with these parameters (designated Test I, II and III for the 'Cast 2' material).

The power source base current level could only be set in ± 1 Amp increments. Unfortunately this meant that the equipment configuration could not be used to effect a fine degree of control on the pool frequency. For this reason subsequent work focused upon the stability of the control model and the application of the model to different material casts. In order to obtain a greater number of control decisions within the same orbital weld circumference the pulsing frequency was increased to 3 Hz to obtain a better response time despite the ± 1 Amp resolution limit.

To test the ability of the model to cope with different casts of material, the fuzzy logic model - target centred about 80 Hz pool oscillation frequency - was also applied to both the low sulphur material ('LS Kobe') for three tests

Experimental programme

(I, II and III) and also a square butt joint using electro-polished material ('EP'). Experimental parameters were used as for Table 24 for both these material casts.

During initial preparatory and optimisation work with the closed-loop system and the 80 Hz target frequency it was noted that when an excitation pulse time of 5 ms was used, a stable pool frequency response of 120 Hz was generated. This had caused some problems in the early work - the 5 ms pulse (t_p) generated both 80 and 120 Hz frequencies with stability in both conditions with the control strategy consequently cycling between the two. In order to demonstrate the stability of the control strategy using another full penetration target frequency, the fuzzy logic control variables were altered to target 120 Hz as the goal and the excitation pulse of 5 ms was used. Experimental parameters were used as previously (ie. see Table 24) above, except that the fuzzy logic control parameters were centred about 120 Hz, as detailed in Table 25.

Three tests were performed on 'Cast 2' material with 120 Hz target pool frequency, designated Tests I, II and III.

Step change recovery

The stability of the control system was also tested with a step change in the welding current in the 6 o'clock position implemented by the user-interface control software ie. the orbital pass was divided into two segments (45 seconds each), and a difference of +8, +6, +4 or +2 Amps was implemented in the second segment for each case. All other experimental parameters were as shown in Table 24 except the initial base current set-point which was selected to be 27 Amps to give a full penetration weld in this position with a desired initial target frequency response of 80 Hz.

SECTION 5.

EXPERIMENTAL RESULTS

5.1 Introduction

5.2 Fundamental oscillation experimentation

5.2.1 Filtration of the arc voltage signal

5.2.2 Arc voltage response to current on copper block

5.2.3 Arc voltage signal processing

5.2.4 Basic welding parameters

Stationary spot welding and signal quality

Orbital welding and penetration

Travel speed, pulse current level,

inner bead surface roughness and outer bead appearance

Travel speed and signal quality

5.2.5 Fundamental oscillation experimentation summary

5.3 Effect of cast-to-cast variation on oscillation behaviour

5.3.1 Stationary pool and time-to-penetrate studies

Part 1 - Small diameter tubing

Part 2 - Medium diameter pipe

5.3.2 Cast-to-cast variations in moving weld pools

5.3.3 Effect of cast-to-cast and surface tension on oscillation behaviour summary

5.4 Real-time logging and reliability of frequency response

5.4.1 Configuration of real-time logging

5.4.2 Reliability and smoothing of response

5.5 Application of fuzzy logic to pool oscillations and penetration behaviour

5.5.1 Single-input/single-output model

5.5.2 Operating performance

Open- and closed-loop trials

Step change recovery

5.5.3 Application of control strategy summary

5. EXPERIMENTAL RESULTS

5.1 Introduction

In this section results are presented from the experimental work described in §4, referring to the appended figures and tables. All the sections correspond with the sections as presented in the Experimental programme (section 4), beginning with the fundamental oscillation experimentation and ending with the closed-loop control work.

5.2 Fundamental oscillation experimentation

5.2.1 Filtration of the arc voltage signal

Adequate filtration of the arc voltage signals from the inverter power sources was necessary in order to reveal the pool oscillation signals clearly. Figure 32 shows an oscillation signal present in the transient arc voltage signal after a short current pulse that generated a fully penetrated oscillation in the molten pool present under the arc. In the first stages of experimentation, passive R-C (resistive and capacitive - $R = 10 \text{ k}\Omega$, $C = 0.01 \mu\text{F}$) filters were used that did not filter the characteristic of the power source adequately. The pool oscillation signal was still visible although obscured by the unfiltered 'noise' of the high frequency inverter power source. The high frequency (66 and 100 kHz for the AMI 207 and BDH 320 respectively) switching characteristic was not adequately filtered by standard passive filtration.

With the use of active filters, such as the 4th order 6-Pole low-pass Butterworth (10 kHz cut-off), the high frequency inverting characteristics of the power sources were filtered out completely and only the lower frequency effects of the molten pool motion (in this case oscillatory after the excitation pulse) were observed in the arc voltage trace. Later figures show the comparatively 'clean' signals.

(Figure 34 shows the response on copper and Figure 37 shows partial and full penetration signals in 1.65 mm wall thickness stainless steel - even the small amplitude partial penetration oscillation signal that damps out over approximately 40 milliseconds can be clearly seen in the logged arc voltage signal.)

Experimental results

5.2.2 Arc voltage response to current on copper block

Note: Argon with a 10% hydrogen addition was subsequently found to be an optimum shielding gas for extracting extremely small partially penetrated signals. For this reason the 'static' arc voltage on copper and power source characteristic work adopted both argon and argon with a 10% hydrogen addition.

The 'static' response of the arc voltage to welding current for the AMI 207 is shown in Figure 33. Different arc lengths were used for argon with a 10% hydrogen addition to obtain a comparison between the voltage amplitude generated by absolute arc length changes and those made by the oscillation of the pool itself (this is discussed later). It is shown that there is a significant increase in the overall arc voltage when comparing argon at 1.5 mm arc length with argon with a 10% hydrogen addition. A significant arc voltage increase is observed for a relatively small increase in arc length for the argon with 10% hydrogen addition shielding gas.

Given that the voltages across the anode and cathode fall regions (V_a and V_c) can be assumed to have been relatively constant (see §2.5.5), it is observed that the electric field strength of the arc containing the 10% hydrogen addition was much higher than the argon arc ie. if a free burning argon arc were extended by 1 mm in length, it would be expected that the arc voltage would increase by 0.8 V. (see §2.5.1), comparatively the argon with 10% hydrogen arc increased by up to 3.8 Volts for the lower values of welding current (increases of only 1.0 Volt were observed for higher values of welding current).

In order to distinguish between the 'static' response of the arc voltage upon a solid copper anode and pool oscillation signals present in molten material, a welding current pulse was used that was typical of pool oscillation procedures (25 Amp base current with a 125 Amp pulse for 10 ms). Figure 34 illustrates the typical responses for argon, and argon with 1.5% and 10% hydrogen additions.

Since a characteristic recovery of the arc voltage to a relatively stable steady state condition after the high amplitude short duration current pulse was observed for the welding currents applied, it was expected that this characteristic would also be present in the molten pool oscillation signals. It was important to eliminate this potentially erroneous response in the interpretation of the time-domain signal and the pool oscillation frequency determination since it was evident with a solid anode.

Experimental results

Disturbance of the static signal was also observed when using a tungsten with notable degradation of the point geometry (ie. with a balled point after excessive usage without regrinding) - this is shown in Figure 35. All experimentation involving the generation of pool oscillation signals adopted the use of tungstens with good point geometry.

The typical welding current pulse used of 100 Amp amplitude for 10 ms on copper is shown in Figure 36 for both the AMI 207 and the BDH 320 power sources. Although both power sources appeared to deliver the base and peak current levels accurately, there was a slight lag of the operation of the BDH 320 behind the AMI 207. Given that both power sources are based on high frequency inverter modules the difference was attributed to the response of the specific control electronics employed or the software regulating the pulse (some manufacturing companies prefer to deliver a 'softer' welding arc, or to avoid the possibility of overshoot that can be implicit when using extremely rapid response times).

5.2.3 Arc voltage signal processing

Previous work by pool oscillation researchers has adopted the use of relatively thick materials. Thicker materials offer a higher signal amplitude since the bulk movement under the action of current pulsing is greater. In order to investigate the use of pool oscillations on typical orbital tubing for ultra high purity applications, thicknesses of 16 SWG (nominally 1.65 mm) were used. *Partially* penetrated signals in these thicknesses were consequently of relatively small amplitude (as would be expected from a partially penetrated pool of, say, 1 mm depth).

Figure 37 shows a comparison of the corresponding arc voltage signals from a partially penetrated welding pool ($I_b = 12.5$ Amps) and a fully penetrated pool ($I_b = 27.5$ Amps). The long duration, large amplitude signals from the fully penetrated pool were comparatively straightforward to process from the time to the frequency domain (either using basic time/period measurements and averaging or using Fast Fourier Transform utilities). However, the short duration, small amplitude signals from the partially penetrated pool were more difficult to analyse in a reliable fashion.

In order to enhance the clarity of the electrical signals measured a small analogue signal processing circuit was used to:

- amplify the low frequency (below 500 Hz) pool oscillation signals, and

Experimental results

- subtract the mean offset to produce a resultant signal with as close to a zero-mean as possible.

The circuit was placed between the output of the signal conditioning board and the input of the analogue-to-digital conversion board (see Figure 22). This electrical 'pre-processing' of the signals did not impinge upon the processing time available for the later real-time application and reduced some of the mathematical treatment necessary.

Unfortunately, the slow response imposed upon the partially penetrated signal (the characteristic response of the arc voltage at that welding current level as previously illustrated in Figure 34, and highlighted in bold text in §5.2.2) was of a similar frequency response to the fully penetrated weld pool frequency signals ie. the time period for the *recovery* of the arc voltage after the application of the peak current pulse when welding with low currents was comparable to the time period of the fully penetrated oscillation signals *themselves*.

For this reason, the *same* analogue signal processing circuit could not be used to optimise the processing of both the fully and partially penetrated signals adequately for the typical material thicknesses studied. Figure 38 shows the resulting signal after optimising the signal processing circuitry for the fully penetrated response. Some noise was inevitably introduced as a result of amplification. It should be noted that for maximum sensitivity the Migatron signal conditioning board was configured to output -5 Volts for an input voltage of 0 Volts, and +5 Volts for an input voltage of 20 Volts. The lower signal shown, after analogue processing, has a close-to-zero mean.

Figure 39 shows the resulting signal after optimising the signal processing circuitry for the partially penetrated response. It can be seen that a high degree of amplification was used to make the subsequent analysis of the signal easier and more reliable. Despite the small size of the molten pool at this level of welding current, the figure clearly shows the pool oscillation information that is present in the arc voltage signal.

In subsequent work four data channels were logged simultaneously, as highlighted in §4.4.1, ie.

arc voltage	(1),
welding current	(2),
processed voltage 1 (> 150 Hz optimum)	(3),
processed voltage 2 (< 150 Hz optimum)	(4).

Experimental results

(A resistor in the analogue signal processing circuit was used to set the cut-off and attenuation of the frequency response of the processed signal - as described in §3.1.1.)

Note that the fully penetrated signal illustrated took 180 ms to damp out, whilst the partially penetrated signal took only 30 ms.

A typical normalised output frequency spectrum (a Fast Fourier Transform, where an output of 1.00 indicates the strongest response both in terms of frequency and amplitude) is shown in Figure 40 for a fully penetrated signal, at 92 Hz. The dominance of the fully penetrated oscillation signal present over any other elements such as noise, or smaller super-imposed mixed-mode responses is clearly reflected by the FFT spectrum shown.

The FFT shown was derived from the oscillatory part of the optimised signal only and does not include the voltage response to the current pulse, or the more static voltage response after the oscillation has damped out.

5.2.4 Basic welding parameters

Stationary spot welding and signal quality

Table 26 presents a subjective description of the resulting oscillatory part of the arc voltage signal, the dominant pool frequency (at the end of the weld immediately prior to the extinction of the welding arc) as determined by a Fast Fourier Transform utility, and the typical damping time of pool oscillations in stationary spot welds made on 2.0 mm wall thickness material. Both argon with 5% and 10% hydrogen additions shielding gases were used. Some comparison was also made for the two power sources used throughout the study (AMI 207 and BDH 320). It can be seen from the table that:

- a peak current (I_p) of 75 Amps generally produced only small amplitude (but quite stable) signals for the power source, shielding gas and pulse durations (t_p) investigated,
- for a given peak current level, a decreasing frequency was generally observed by either increasing the hydrogen addition to the shielding gas or increasing the pulse duration (which would be expected since an increase in either factor increases the effective heat input to the pool since the pulsed current parameters were maintained as constants),

Experimental results

- some difference was observed between the pool frequencies calculated for the pools generated by the AMI 207 and those generated by the BDH 320 for the same set currents - the pools that were generated by the BDH 320 exhibited marginally lower pool frequencies in general,
- longer damping times were generally apparent when using a higher hydrogen addition, or by using a higher peak current amplitude (t_p).

A variation in pool size was obtained during the investigation since the heat input was not kept constant. The increases in peak current level (I_p) and peak current duration (t_p) increased the heat input directly (by increasing the average welding current applied) and the increase in hydrogen addition from 5 to 10% increased the heat input by increasing the overall arc voltage dropped. A comparison between the average pool diameters of the spot welds made and the pool frequencies observed is plotted in the bar-line combination chart, Figure 41 (plotted for argon with 10% hydrogen shielding gas and the BDH 320 power source).

It is quite apparent that the highest dominant pool frequencies were generally exhibited by the smallest pools and the lowest dominant frequencies by the largest.

The effect of the increase in amplitude of the peak current is clearly illustrated by Figure 42. Although clear full penetration oscillation signals were produced by a 75 Amp peak pulse (5 ms in duration), the longer, higher amplitude waveforms were generated by the larger peak currents (I_p).

The use of 15 and 20 ms pulse durations tended towards producing mixed-mode waveforms, where both full and partial penetration modes were occasionally exhibited simultaneously. The Fast Fourier Transform of the time-domain signals revealed the strength of the higher frequency response, since it reflects the frequency and amplitude. Figure 43 illustrates a clear single mode response (at the top of the figure, for a 10 ms 150 Amp pulse) and also the occurrence of a mixed-mode oscillation (at the bottom of the figure, for a 15 ms 150 Amp pulse).

Orbital welding and penetration

The state of penetration of travelling welds produced as bead-on-tube on SS316L $\phi 1.5"$ 16SWG tubing was quite clearly revealed in the frequency of the pool oscillations measured. For these welds the arc voltage was logged at the time of welding and analysed ('off-line') for the frequency response afterwards. The higher frequency, Mode 1 response, was exhibited by welds made with a low welding current (I_b). As the welding current was increased, the frequency dropped, and once the inner bead width approached a similar magnitude to the outer bead width a low frequency, Mode 3 response, was exhibited. This is illustrated in Figure 44.

At each welding current, the high consistency of the measured frequency responses is shown by the small standard deviations measured from the responses to the nine pulses that were logged. A higher standard deviation was observed for the lower welding currents ($I_b = 10$ and 12.5 Amps in particular) as might be expected from the signals from the partially penetrated pools, since the signals were comparatively short in duration, small in amplitude and high in average frequency.

By plotting the outer and inner bead widths against the pool frequency, it can be seen that a high frequency Mode 1 response was present in pools that had an established lower bead width ie. pools that had a *degree* of full penetration (see Figure 45). The transition of the dominance of the comparatively higher frequency Mode 1 response to the lower frequency Mode 3 response was observed where the inner bead width approached the outer bead width (at approximately 3.0 to 3.5 mm). It can be seen from the chart that the outer bead width changed little with the range of welding current applied, no more than 1.5 mm, whilst the level of penetration ranged from zero to an inner bead width that was equal to the outer bead width.

Note: The small change in the outer bead width measurement for the range of penetration conditions observed illustrates the limitations of top-face sensing systems based upon that measurement alone. Pool oscillation signals monitored at the top-face however are shown to be sensitive to the state of penetration.

The magnitude and trend of the measured dominant pool frequency, with respect to the welding current (I_b) and hence level of penetration, shown in Figures 44 and 45 (for the 04:30 position only) were relatively unchanged

Experimental results

for the other orbital positions. Figure 46 shows the average pool frequency recorded over nine pulses for the 01:30, 07:30 and 10:30 positions in addition to the 04:30 position already presented, and although there is some scatter evident, the figure illustrates the relatively constant correlation between the pool frequency and the state of penetration for all the orbital positions for this material thickness and diameter.

Figures 47 and 48 show the typical penetration profiles for base currents of 10.0, 12.5, 15.0 and 17.5 Amps, and 20.0, 22.5, 25.0 and 27.5 Amps respectively. Either a state of no penetration or a 'wine glass' profile (at the top of the bead) existing in a full penetration weld is clearly evident for base currents (I_b) of 10.0 to 17.5 Amps, where a Mode 1 frequency response was predominantly observed. Some curvature of both of the side-walls is still evident for a base current of 20.0 Amps although less marked than the previous profiles. Welds made with 25.0 and 27.5 Amp base currents have quite vertical side-walls.

Welds made on slightly thicker material (2.0 mm as opposed to 16SWG nominal thickness) were also observed to display relatively consistent responses with respect to orbital position. Figure 49 illustrates the dominant pool frequency response *per window* (where each window contains the pool oscillation response to a single current pulse) for four different orbital positions at one level of base current. It is quite notable that the two lower orbital positions (04:30 and 07:30), where the pool would more naturally sag towards the electrode under the influence of gravity, exhibited generally higher frequencies (59 to 60 Hz) than the downhand positions (10:30 and 01:30) positions (55 to 56 Hz) for this material thickness.

Travel speed, pulse current level, inner bead surface roughness and outer bead appearance

The quality of the inner bead profile for ultra-high purity applications can be partly assessed by the average surface roughness of the inner bead. The surface roughnesses of the inner beads of these trials are plotted in Figure 50, showing the significant increase in surface roughness (as indicated by both R_a and R_q , for both 100 Amp and 125 Amp peak current levels) as the travel speed was decreased. This might be expected since the current pulses applied were packed more closely into the same unit length of weld with decreasing travel speed. The level of peak welding current also appears to reduce the magnitude of surface roughness for the lower welding speeds. The experimental parameters of 90 mm/min travel speed, with a 125 Amp pulse for 10 ms, that were used in the majority of

Experimental results

the work presented, appeared to offer a reasonable minimisation of the surface roughness of the inner bore with acceptable values for practical usage. Typical values of surface roughness from non-pulsed welds with optimised parameters can be as low as $1.0\ \mu\text{m}$ (R_a - Tapp, 1996).

Ripples on the outer surface of the weld formed upon cooling and solidification reflect the pool frequency present in the oscillating weld (this is how the pool frequency and the case of the oscillating pool was first identified in the literature in 1972). Figure 51 shows the outer bead appearance and the surface ripples present between the large fronts formed by the peak current pulse. Different levels of welding current generated different levels of penetration, and the corresponding pool frequencies in the oscillating pools affected the cooling and solidification patterns on the outer surface accordingly.

The pointers ('O') on each outer surface mark the large fronts caused by the single, high amplitude peak in the welding current used to generate the free oscillation in the molten pools. Accordingly, the ripples present in the profile of the lower welding current (28 Amp) damp out after each front more rapidly than the ripples shown in the profile of the weld made with the higher welding current (44 Amps in particular).

Each strong wavefront marked ('O') occurred every 0.5 second, since the pool oscillation excitation pulse current was applied at 2 Hz. A correlation between the pool ripples, as shown for the three levels of welding current indicated, and the oscillation frequency measured in the arc voltage existed:

- $I_b = 44$ Amps (bottom figure) - 10 peaks counted in half the distance between the wavefronts, ie. 9 cycles in approximately 0.25 seconds or 36 per second (36 Hz) compared to a 41 Hz oscillation in the corresponding arc voltage signal.

Travel speed and signal quality

Figure 52 shows the signal quality from welding at relatively high travel speeds. Although some clear traces of the full penetration oscillation signal were still present at the high welding speed (220 mm/min), as shown in the bottom trace, many of the responses were quite badly deteriorated, as shown in the middle trace. The comparatively regular, consistent responses obtained at the lower welding speeds are shown in the top trace of the figure.

Experimental results

5.2.5 Fundamental oscillation experimentation summary

The most important results obtained from the fundamental experimentation work showed that:

- it was necessary to use an active filtration circuit to combat the 'noise' inherent in the arc voltage signal from high frequency inverter power sources,
- some characteristics of the arc voltage response to the excitation pulse used in the welding current were inherent in the 'static' response (on solid copper),
- additional signal processing circuitry was found to be beneficial (used before the analogue-to-digital conversion) to maximise the sensitivity to small amplitude signals generated by partially penetrated molten pools and minimise subsequent time-consuming mathematical treatments before conversion to the frequency domain (ie. the effect on the FFT),
- a strong correlation existed between stationary pool size and observed oscillation frequency, with the clearest oscillation signals produced by a pulse approximately 100 Amps above the base welding current and 10 ms in duration,
- the state of penetration of moving weld pools was revealed by the pool oscillation frequency, with a drop in modal behaviour (from Mode 1 to Mode 3) as the inner bead width approached the magnitude of the outer bead width for the material and thickness studied, with quite regular and consistent responses evident around the weld for the *orbital* welds made,
- the chosen procedure parameters generated inner weld profiles that were acceptable for ultra-high purity applications,
- pool oscillation markings observed on the outer surface of the welds corresponded reasonably with frequency,
- travel speeds had to be limited to obtain an optimum level of signal quality.

5.3 Effect of cast-to-cast variation on oscillation behaviour

5.3.1 Stationary pool and time-to-penetrate studies

Part 1 - Small diameter tubing

Figures 53 and 54 illustrate the progressive frequency responses of the electro-polished 'EP' and 'Cast 1' $\phi 1.5$ " 16SWG tubing during a stationary spot weld. Each point represents the *dominant* frequency response to each sequential current pulse providing a picture of the development of each spot weld made in time. The effect of increasing the base welding current (I_b) on the frequency response is clearly shown - increasing the welding current resulted in a decrease in the dominant frequency at the end of the weld, and also decreased the 'time to penetrate' if this can be characterised by the *first* transition of the dominant pool frequency from the Mode 1 to the Mode 3 oscillation modes. This held for all the austenitic stainless steel casts tested (electro-polished 'EP', low sulphur 'LS Kobe', 'Cast 1', and 'Cast 2') - the actual frequency values from the end of the welds are presented in Table 27.

As a full picture of the development of the pool frequency in a stationary pool in 2.0 mm (nominal wall thickness) stainless steel (the '35 mill.' material), the three-dimensional surface chart shown in Figure 55 illustrates:

- the progression of the dominant pool frequency with time (shown by the pulse number) for the wide range of specific base welding currents applied ($I_b = 15.0$ to 35.0 Amps),
- the correlation between the frequency/time progression and the base welding current applied.

The 3-D plot is given for the 2.0 mm wall thickness material only since it provided more data (from the greater range of currents applied) so that a full picture of the developments in the pool could be constructed.

It is shown that at the lowest base welding currents the dominant frequency response did not switch between Modes 1 and 3, although the transition was made for the thinner materials at the same current shown in Figures 53 and 54. An increased base current generally decreased all the frequency responses over time, from the start of the formation of the spot weld, which was presumably only partially penetrated, to the end of the weld (fully penetrated) before the arc was extinguished and the pool solidified. Although the decrease in frequency was observed with an

Experimental results

increase in welding current and time, at 20 Amps (I_b) the dominant mode of oscillation appeared to switch to Mode 3 earlier than might be expected from the overall pattern established. It would seem that there was a transitional area where Mode 1 and Mode 3 oscillations could be equally well established. This is also shown in Figures 53 and 54 for 'EP' and 'Cast 1' material casts where for both 22.5 and 25.0 Amp base welding currents (and 20.0 Amps for the 'EP' cast) a higher frequency Mode 1 or mixed-mode behaviour was observed to dominate after Mode 3 signals had been observed.

Table 27 shows the pool sizes measured, the dominant frequency measured at the end of the weld immediately prior to arc extinction, and theoretical calculations of the acting surface tension (using the assumptions listed §4.3.1 of the Experimental programme). Both the classical membrane model (given as Equation 1 in the Literature survey, using an equivalent pool diameter calculated from Equation 2) and also Yoo's model (Equation 3) are used. Figure 56 shows a graphical presentation of the frequency and surface tension data presented in the table (data derived from the membrane and Yoo's model is shown in the top and the bottom charts respectively). A value of surface tension was not calculated for the 'LS Kobe' cast for a welding current of 15.0 Amps since the Mode 3 oscillation mode was not observed as the dominant pool frequency. A value could have been calculated using Equation 4, although a comparison with Yoo could not have been made since Yoo's partial penetration model requires a further empirically derived parameter.

Figure 56 shows that:

- the theoretically derived surface tension data from both models for all the material casts investigated does not suggest that a constant value of surface tension could be implied for each material cast,

ie. surface tension appears to depend upon the welding current used for the spot weld test, which might simplistically highlight a surface tension/temperature relationship that is sensitive to the range of welding currents applied,
- the surface tension predictions for each material cast and welding current are significantly different from each model, with Yoo's model yielding notably higher values,

Experimental results

- the range of surface tension values (maximum - minimum) predicted by each model for each material cast is reasonably equatable.

A consistent pattern between a theoretical prediction of the surface tension for either model and the welding current applied does not immediately emerge ie. there is an apparent variation between the material casts. It is perhaps notable that the values of surface tension predicted from the membrane model for the highest welding current applied, 25.0 Amps, have a smaller range (1.47, 1.54, 1.47 and 1.61 N/m for the 'EP, LS Kobe, Casts 1 and 2' materials respectively) ie. there is a smaller difference between them. This is also true of Yoo's model (2.12, 2.21, 2.13, and 2.32 N/m). The predictions for surface tension based on the lower welding currents vary more greatly. The differences in cast behaviour would appear to be more accentuated at the lower welding currents.

Part 2 - Medium diameter pipe

Further investigations into thicker material (pipe size '40 Schedule', typically 3.91 mm wall thickness) illustrated the range of responses to a stationary weld test. The repeatability of the behaviour of the spot welds made was demonstrated by the close profiles of the frequency/time traces for each material cast tested. Figure 57 shows the behaviour of two casts that were known to be difficult to weld. Both of these casts had a relatively low sulphur content - many literature references cite 0.007% S. as a threshold limit between cast behaviour patterns and these two casts contained 0.003% S. and 0.004% S. for '280410' and 'MS097' respectively - although many other factors and other constituents can also affect the behaviour. Neither cast exhibited any degree of a *full* penetration condition after the 30 second test at 40 Amps.

Note: The software used for this experimentation was triggered by the arc ignition, so the 4 seconds at 15 Amps as well as the 30 seconds at 40 Amps is included in the data shown in the figures.

Both casts appeared to reach a relatively stable response under the 40 Amps welding arc with little change in the frequency response after 15 to 20 seconds of the test. Although the frequency behaviour was slightly chaotic at the start of the weld, a close correlation was formed for each test (denoted 'A', 'B' and 'C') for both material casts towards the end of the time period. In total contrast with this behaviour, Figure 58 shows the characteristics of two material casts, of the same thickness designation,

Experimental results

that were known to be relatively straightforward to weld with reasonable penetration characteristics. Both casts made the transition from a Mode 1 to a Mode 3 oscillation at approximately the same time (at around 15 seconds into the test) for each test ('A', 'B', and 'C'), and followed quite similar frequency responses thereafter.

By using Equation 4 for the partial penetration response and the pool diameters measured (in addition to the Mode 3 calculations), theoretical surface tension values derived from all the tests are shown in Figure 59. Each material test yielded quite consistent values of surface tension (for tests 'A', 'B' and 'C'), however there was a highly significant difference between the values predicted from the Mode 1 model (for the '280410' and 'MS097' material casts) and those predicted from the Mode 3 model (for the '2" Pipe 2', and '2" Pipe 4' material casts).

It is assumed that the dominant oscillation mode was Mode 1 for the surface tension values calculated from Equation 4 for the '280410' and 'MS097' casts that did not penetrate. It is possible that Mode 2 (the 'slosh' mode) occurred, however this would make the surface tension estimates quite unrealistically high (by a factor of 3.0). The possibility of the excitation of Mode 2 in stationary pools (in the downhand position) under the action of short peak pulse times (t_p) has also been noted by other authors as being remote.

If the Marangoni model of surface tension behaviour is assumed to be correct, it would be expected that the values of the *average acting* surface tension predicted for the casts with low surface activity (the casts with a low sulphur constituent, '280410' and 'MS097') would be comparatively high. Casts with low surface activity, associated with a difficult to weld characteristic, have often been noted to have relatively smooth bead surface appearances. This has also been linked with the proposed dominant flow regime at the surface of the pool - from the centre of the pool outwards towards the sides. Higher surface activity is proposed to be able to create a 'reversed' dominant fluid flow regime from the outer edge of the pool towards the centre, hence creating turbulence as the flow converges at the centre, and moves downwards. It was noted that casts 'MS097' and '280410' had extremely smooth surface profiles, consistent with the proposed dominant flow regime. The '2" Pipe 2' and '2" Pipe 4' beads had comparatively rough appearances.

However, the comparative theoretical values of surface tension ('280410' and 'MS097' *versus* '2" Pipe 2' and '2" Pipe 4') computed using Mode 1 from the models do not correspond with what might have been expected

Experimental results

from a Marangoni model, since the computed estimates for γ_{280410} and γ_{MS097} were so low.

5.3.2 Cast-to-cast variations in moving weld pools

Note: For the sake of comparison, in the figures 'Cast 1' is also referred to as 'HS' (high sulphur) and 'LS Kobe' as 'LS' (low sulphur) since this was thought to be the main difference in chemical composition and possible cause for differences in behaviour with the same welding parameters.

Table 28 details the average and standard deviations of the outer and inner bead widths, the heat input derived from the applied current and arc voltage, and the pool frequency responses where appropriate from the experimental programme for cast-to-cast variations in moving weld pools. The results from the standard pulsed procedure used, and the straight d.c. runs are detailed for comparative purposes although they are not presented graphically.

Figure 60 shows the wide variation of inner bead widths measured for the range of currents applied for the two material casts (0.5 to 4.9 mm for the 'LS' cast, denoting the 'LS Kobe' material, and 2.2 to 4.1 mm for the 'HS', the 'Cast 1' material). The outer bead widths for both material casts were comparatively constant for the range of base currents applied - this is shown graphically in Figure 61 (3.2 to 4.8 mm, and 3.2 to 4.0 mm for the 'LS' and 'HS' casts respectively).

The pool frequencies and bead widths presented in these figures reflect measurements made for *all* the orbital positions for the single-pass welds made ie. the average of 20 measurements.

A relatively low base current ($I_b = 15.0$ Amps) generated a low degree of full penetration in the 'LS' material, although the average outer bead width was similar in magnitude to the 'HS' material (both 3.2 mm, with a single standard deviation of 0.1 and 0.2 mm for the 'LS' and 'HS' materials respectively). Despite the similar average outer bead width, the higher dominant pool oscillation frequency for the 'LS' cast revealed the comparatively low degree of full penetration. As the inner bead width increased with the increased base current the pool frequency dropped correspondingly. It is interesting to note that both material casts made the transition from a Mode 1 to a Mode 3 dominant oscillation mode at the same level of base current - between 20.0 and 22.5 Amps. This corresponds with previous experimental work investigating the effects of

Experimental results

penetration and orbital position presented in §4.2.4, and illustrated in the chart of the results - Figure 46.

The comparative penetration characteristics of both material casts are reflected in the pool frequency profiles:

- the relatively smaller inner and outer bead widths of the 'HS' cast associated with the larger base currents applied ($I_b = 22.5, 25.0$ and 27.5 Amps) generated slightly higher dominant pool frequencies, as might be expected if pool geometry was the major determinant (as opposed to the acting surface tension),
- the larger inner and outer bead widths of the 'LS' cast associated with the same base currents generated slightly lower dominant pool frequencies.

It is worth noting that there is quite a direct correlation between the heat inputs measured and the average inner bead widths generated for both material casts (see Figure 62). The difference between the heat input values for the two casts was generated by the different average arc voltages, since the same power source was used for both materials. The increased penetration of the 'LS' cast at the higher base currents is shown to be associated with an increase in the 'measured' heat input. The heat input calculation was based on a nominal 100% arc efficiency and is used only for comparative rather than absolute purposes.

The detailed frequency responses of the two casts investigated with respect to the four major orbital positions are illustrated in Figure 63, for the 04:30, 07:30, 10:30 and 01:30 positions. It should be noted that each point represents an average of the responses to nine excitation pulses around that position. The consistency of the frequency response measured for each material cast at each orbital position is shown for each level of base current. This is also demonstrated by the comparatively low standard deviations of frequency plotted in Figures 60 and 61.

Transient voltage responses for both material casts for partially penetrated conditions (this is taken here to mean a Mode 1 response, despite the quite small inner bead width formed at this level of current) for five consecutive current pulses are shown in Figures 64 and 65. For the sake of clarity the arc voltages shown are the ones logged after the analogue signal processing ie. channel (3) as detailed in §5.2.3, after amplification of the relatively low amplitude oscillation signals.

Figures 66 and 67 show the fully penetrated responses. Here the arc voltages are shown as logged directly from the signal conditioning unit (without the additional analogue signal processing). The 'LS Kobe' cast traces show distinctly higher voltage responses than the 'Cast 1' material, for the fully penetrated condition immediately after the excitation pulse. This effect is reflected by the average values presented in Table 28 and the overall effect on the average heat input discussed above and illustrated in Figure 62. Despite the material cast differences, the consistency of all the pool oscillation responses to each pulse applied is shown to be very well maintained.

No evidence is particularly offered from these traces with respect to the effect of dominant fluid flow differences on the *stability* of the arc voltage signal ie. it might be expected that any radially outward flow exhibited in pools with a lower surface activity would produce comparatively clear voltage signals with less noise, due to the possible absence of turbulence at the pool surface. However, a degree of noise appears on both the voltage traces for the 'LS' material as well as for the 'HS' cast. Indeed, it might be observed that the 'LS Kobe' voltage signals possess more noise interference than those illustrated from the 'Cast 1' material.

5.3.3 Effect of cast-to-cast and surface tension on oscillation behaviour summary

From the results obtained from the experimentation concerning cast-to-cast and the possible role of surface tension (or at least the theoretical modelling of the surface tension behaviour using the mathematical models presented in the literature), it can be summarised that:

- by calculating the pool frequency response (as derived from the arc voltage) from the excitation pulses used in a typical pool oscillation welding current profile, in a stationary spot weld test, a characterisation can be quite easily made of the 'time-to-penetrate' behaviour of austenitic stainless steel casts,
- materials that are readily 'weldable' (from a cast-to-cast variation point of view) exhibit pool frequency profiles accordingly ie. a transition from a typically partially penetrated frequency value (Mode 1) to a fully penetrated frequency value (Mode 3) is made during the stationary weld test,
- material casts that are less readily 'weldable' also exhibit typically characteristic pool frequency profiles ie. the transition between oscillation modes is not made,

Experimental results

- theoretical models of pool oscillation behaviour do not necessarily comply with what might be expected from the observed cast behaviour and the associated surface tension behaviour if a Marangoni model is assumed,
- differences that could be associated with cast-to-cast behaviour in moving weld pools are also reflected accordingly by the pool frequency response, although geometric pool width differences in the material casts studied could have been caused by a difference in the level of arc voltage that was observed in the arc signals, particularly after the excitation pulse,
- it might be possible to control the state and/or degree of penetration by using the pool frequency as a control variable.

5.4 Real-time logging and reliability of frequency response

5.4.1 Configuration of real-time logging

In this section the 'partial' penetration condition is taken to describe a weld pool (and associated weld bead) with a dominant frequency that is indicative of a Mode 1 oscillation response. The welding currents used in this experimentation for the 'partial' penetration condition generated beads that had comparatively small inner beads. The figures presented indicate typical 'partially penetrated' frequencies around 400 Hz as generated by a base current of 15 Amps for $\phi 1.5''$ 16SWG - compare this with the chart shown in Figure 45, the penetration profile shown in Figure 47, and it is clearly demonstrated that this is a low level of penetration that would not be accepted in practice.

Plots from the *real-time* logging of the frequency response of single-pass welds for 'Cast 1' and 'Cast 2' materials are shown in Figure 68. These figures were derived after some optimisation work was performed to determine a reasonable working point solution of the logging variables set for the hardware and software used, to provide a sufficient resolution of the frequency without compromising the speed of operation. (If too much time had been spent gathering data, or analysing a great number of data points, a low pulsing frequency would have then been necessitated). To illustrate the real-time response, both welds were split into two halves of partial and full penetration conditions by varying the base welding current (I_b) used in the welding procedure ie. an open-loop trial.

It can be seen that there is some variance in the pool frequency measured during the low base current periods for both material casts shown in Figure 68. This would be expected from the relatively small pool size established at this level of welding current and travel speed. Subsequently, the variance in the pool frequency measurement is considerably diminished for the full penetration conditions for both material casts. As illustrated, a slight decrease in the welding current was used in the second part of each 'half' of the orbital pass - this was applied in an attempt to account for the effect of heat build-up around the orbital weld and maintain a relatively constant degree of penetration.

Occasional instability is illustrated for the 'Cast 1' material in the partial penetration condition (a singular drop from 400 to 182 Hz at pulse number 20), although this was not observed for the 'Cast 2' material in this test. This type of occurrence led to the development of a smoothing rule, since it was felt that the singularity of the response was not at all typical and

Experimental results

probably due to excessive noise in the arc voltage signal or an occasional irregular pool shape.

Both traces show the lag of the pool oscillation frequency signal behind the large step change in welding current. The effect on the typical pool penetration profiles of this level of change (some 12.5 Amps) has already been illustrated (in Figures 47 and 48). The 'Cast 1' material took 12 pulses, or 6.0 seconds, to change from the established, relatively stable Mode 1 frequency to the lower Mode 3 frequency (pulse 80 yielded 400 Hz response at 15 Amps, and pulse 91 yielded 82 Hz at 27.5 Amps). Comparatively, 'Cast 2' took only 8 pulses, or 4.0 seconds (pulse 80 to pulse 87) for a similar transition.

Figure 69 shows similar traces for the reverse application of welding current - shifting from full to partial penetration conditions for 'Cast 1' and 'Cast 2'. Again, an initial lag was logged for the establishment of the full penetration condition, although in this case it was from the start of the weld rather than from an already established weld pool. The absolute lag times cannot be compared with those illustrated in Figure 68 since an indeterminate delay occurred due to the manual connection of the arc voltage leads after the high frequency (HF) arc initiation. In comparison with the transitions illustrated in Figure 68, the transition from the Mode 3 to the Mode 1 responses was extremely fast - 4 pulses, or 2.0 seconds, for both the 'Cast 1' and 'Cast 2' materials.

A singularity was again observed in the partially penetrated section of the real-time frequency log of the 'Cast 1' material.

It can be seen from both Figures 68 and 69 that despite the use of a 2048 point Fast Fourier Transform and an effective sampling rate of 4 kHz per channel (resulting in a frequency resolution from the output of the FFT of 2 Hz), certain frequencies appear to be 'preferred' (this work was performed before any smoothing or additional filtration rules were used). The initial Mode 1 response from the 'Cast 2' chart in Figure 68 might imply that there are only four preferred oscillation frequencies spaced approximately 20 Hz apart, although the actual data from the log file revealed that there was an operating frequency resolution of 2 Hz.

5.4.2 Reliability and smoothing of response

The real-time frequency (and associated welding current) plot resulting from the application of the software smoothing and filtering rules described in §4.4.2 of the experimental programme is shown in Figure 70 for a bead-on-

Experimental results

tube weld. It can be seen that the previously observed singularities in the 'partially penetrated' frequency response were effectively removed. Since the material used for this study was thicker ('1.5" Thick' with a wall thickness of 0.125" or 3.18 mm) the time lags observed behind the changes in welding current, that were applied to generate both the Mode 1 and 3 frequency responses, were significantly larger than those previously observed with the 16SWG (or 1.65 mm) material.

Time Lag 1 - pulse 25 to pulse 37 (13 pulses or 6.5 seconds)
- typical Mode 1 partial penetration response to 32.0 Amp base current (I_b) to typical full penetration Mode 3 response to 52.5 Amps

Time Lag 2 - pulse 60 to 66 (7 pulses or 3.5 seconds) -
typical Mode 3 to Mode 1

Time Lag 3 - pulse 97 to 107 (11 pulses or 5.5 seconds) -
Mode 1 to Mode 3

The average pool frequency during the first application of 32.5 Amps (I_b) - lower welding current used - was 285 Hz. After the delayed response to the higher welding current the average pool frequency was 56 Hz (pulses 37 to 60), and during the second low welding current period the average frequency was 256 Hz (pulses 66 to 96). This was lower than the frequency observed during the first low current period due to the heat build-up, and associated higher level of penetration, around the tube during the orbital pass. The average pool frequency response during the final full penetration period (pulses 107 to 132), after the delay in dropping to the low frequency Mode 3 response, was 63 Hz.

Further comparative work on a typical square butt joint (machined preparation by the Tri-Tool facing machine) is shown in Figure 71, relating the pool frequency to the applied welding current and the outer and inner bead width profile. The inner and outer surfaces of the orbital joint made are shown in Figure 72.

Again, although there are significant time lags, particularly when establishing the full penetration 'Mode 3' responses after the partial response to the lower base welding current level, the validation of the frequency profile (and the filtering strategies employed) in relating the occurrence of the state of full penetration is clearly shown by the inside surface profile. The small period of full penetration (relating to pulse numbers 31 to 55 during the first 52.5 Amp period) is shown on the right

Experimental results

hand side of the top photograph in Figure 72. There was a large time lag observed from the partial to the full penetration condition due to the thickness of the tube (0.125" or 3.18 mm) and the first period of heating - pulse 31 to pulse 55 ie. 12.5 seconds. After two periods at 32.0 Amps and a single period at 52.5 Amps, the second time lag from partial to full penetration was much decreased - from pulse 102 to pulse 113, this time only 6.0 seconds. The significant heat build-up around the tube also caused the second period of 'full' penetration to exhibit a much lower frequency (typically 52 Hz, in comparison with the previous 68 Hz), which is clearly shown by the over-penetration and pool sag on the left hand side of Figure 72.

The 16 kHz sampling rate used during this study resulted in a output frequency resolution of 2 Hz (4 channels logged and a 4 kHz per channel actual sampling rate with the use of a 2048 point Fast Fourier Transform).

The complexities of heat build-up when welding this thickness of material in a single autogenous orbital pass at this diameter are great and this is illustrated by the differing responses to the low and high constant base current periods employed. Both the relatively stable partial penetration periods were subject to more variation than the previously observed responses in the 16SWG or 1.65 mm wall thickness material.

As previously observed, the transition from the full to the partial penetration condition was comparatively rapid (pulse 66 to 71), only 6 pulses or 3.0 seconds.

5.5 Application of fuzzy logic to pool oscillations and penetration behaviour

5.5.1 Single-input/single-output model

For a typical fully penetrated weld pool frequency of 80 Hz, a fuzzy logic model was constructed that:

- centred around the target fully penetrated frequency of 80 Hz,
- was relatively sensitive to changes in frequency around the fully penetrated condition (since it was known from the earlier experimentation that increases in pool frequency resulted in a degree of weld pool sag),
- accounted for the unpredictable change in frequency response by being relatively insensitive to the change in modal behaviour (Mode 1 to Mode 3) ie. by employing a 'non-linear' response in this area.

The fuzzy classification of the various states of penetration ('OP' over-penetrated, 'SO' slightly over-penetrated, 'FP' fully penetrated, 'PP' partially penetrated, and 'SP' slightly penetrated) is shown at the top of Figure 30. The coefficients used to generate the chart are detailed in Table 22. (The derivation of the fuzzy logic model has already been presented in §4.5.1.)

The fuzzy model provided a 'delta base current' output from the dominant pool frequency, f_d , as determined by the AMOS MON1 (text based) software after the analogue signal processing, and further mathematical treatment. The derived output was written to a data file, read by the 'delta-reader' software and applied as a 'hot-key' command whilst welding ie. *closing the loop*.

5.5.2 Operating performance

The calibration and observed operating performance of the system was described in detail in §3.1.4. It is noted that not all the requests for a change in the welding current level were responded to at the appropriate time (there was an occasional delay - thought to be caused by commands being queued).

Open- and closed-loop trials

A simulation of the control system output was provided by the *open-loop* oscillation procedure described at the start of §4.5.2, with the whole integrated system operating but with the link between the oscillation software and the user-interface software disabled. The corresponding control signal, represented as a 'delta current output' (in Amps) and the pool frequency are shown in Figure 73. A constant current weld (25 Amps for the whole 90 seconds) provided a weld that inevitably became over-penetrated with heat build-up towards the end of the weld.

As already described (see §3.1.1) the resolution of the current provided by the Migatronic BDH 320 was only integer numbers of amperes. Thus the plot shown in the figure shows the acceptance of the frequency range of 80 to 98 Hz without a desired change in the control signal. However, once the frequency fell significantly below the desired target frequency, with over-penetration resulting from heat build-up, the oscillation control software was triggered into issuing several -1 Amp commands. *(These are shown in the lower chart in Figure 73.)*

Erratic changes in the pool frequency, with a magnitude of greater than 30 Hz, were discounted as described in §4.4.2 - only the relatively consistent frequency signals were responded to with desired control signals. *(This is also shown in the lower chart in Figure 73.)*

Pool frequency and welding current traces are shown for the *closed-loop* Tests I, II and III on the 'Cast 2' material in Figures 74, 75 and 76. The inner bead surfaces of the 'Cast 2' tests and an electro-polished joint ('EP' material) are shown at the top and bottom of Figure 77 respectively.

It should be stated at this point that during the control system trials the Migatronic signal conditioning board became quite damaged by high frequency strikes initiated by the Migatronic BDH 320 during the weld cycle (when it sensed that the welding current was a low value - this also occasionally happened on a software controlled slope-down). Some components were repaired during the trials, and it is estimated that some 50% of the amplitude of the signal was lost. It is presumed that this was the reason that the frequency profiles of some of the welds during the later work detailed in this section were not as consistently smooth as previously monitored - working from an attenuated signal would result in a slightly more chaotic response as the influence of noise would become greater when the signals were subsequently amplified by the additional analogue circuitry (ie. the boards shown as 5. and 6. in Figure 22).

Experimental results

The 'smoothing' strategy was also applied to the output of the control signal here, rather than the actual pool frequency. Changes greater than 30 Hz were not smoothed out of the frequency data shown, but were ignored by the control system software ie. the frequency changes appear more erratic than the previously smoothed frequency profile illustrated in Figure 71.

Figure 74 shows the rapid adjustment of the initial set point of the base current from 22 to 24 Amps (generated by 117 and 115 Hz responses at the start of the weld) during pulse 5 and 6. A subsequent consistent target frequency response of around 80 Hz was then established (typically frequencies of 86, 84 and 82 Hz were logged). Singularities were ignored by the control strategy. The main subsequent control events during this weld are summarised below.

- Two consistently high frequency responses at pulses 57 and 58 (152 and 123 Hz) resulted in a single +2 Amp control signal being applied. Subsequent pool frequencies were again re-established in the range of 80, 78, and 76 Hz.
- Two low frequencies at pulses 143 and 144 (48 seconds into the weld) resulted in a single -1 Amp signal. Shortly after (at pulse 147) another -1 Amp was issued in response to a further two low pool frequencies. This was perhaps a small overshoot since shortly afterwards a single +2 Amp was issued at pulse 162 in response to two higher pool frequencies (156 and 150 Hz).
- Stability was then maintained until pulse 218 (pool frequency 72 Hz) when another -1 Amp signal was issued.
- Further -1 Amp signals were issued at pulse 227 and 231, resulting in the maintenance of typical full penetration frequencies of 76 and 78 Hz until the end of the weld.

The inner bead width was maintained between 3.9 mm (*minimum* value) and 4.7 mm (*maximum* value) for the whole orbital weld. As shown by the second chart in Figure 74 the bead width profile was very consistent (less than 1 mm between the minimum and maximum values).

Comparative charts for Tests II and III on the same material are shown in Figures 75 and 76.

Experimental results

Test II generated a relatively uneventful control cycle. The initial set base current, I_b , of 22 Amps was initially modified and then re-established at 22 Amps during the first few pulses. A stable desired frequency response was then obtained until pulses 19 and 21 - a +1 Amp and a -1 Amp control signal effectively cancelled each other out since they were in immediate succession. Two +1 Amp control signals at pulses 92 and 98 resulted in the maintenance of a relatively steady frequency response until pulse 240, near the end of the weld (a -1 Amp control signal was issued at as the frequency dropped to 72 Hz). An inner bead width of between 3.4 mm (*minimum* value) and 4.2 mm (*maximum* value) was maintained for this weld.

Test III initially over-shot the target due to several high frequency responses at the start of the weld - frequencies of 111 to 125 Hz generated a total control signal of +7 Amps during pulses 5 to 9. Various small modifications of the base current were made between pulses 32 and 56. As the pool frequency dropped to a consistently low response, the base current was then reduced by five consecutive -1 Amps steps to 22 Amps (pulse 59 to 63). Despite the overshoot at the beginning an inner bead width of between 3.5 mm (*minimum* value) and 5.1 mm (*maximum* value) was generated for the orbital weld.

The average welding currents applied by the closed-loop system on the full orbital welds on the 'Cast 2' material with a target frequency of 80 Hz were:

Test I	25.38 Amps,
Test II	23.48 Amps,
Test III	24.66 Amps.

(The average welding current presented here is quoted to two decimal places since it was taken from data from over 200 pulses).

This gave a range of 1.87 Amps between the tests (maximum average current applied - minimum average current applied). There was some variation between the responses to the same starting conditions because of the resolution of the power source (± 1 Amp only) and the sensitivity of the fuzzy system itself. Current changes were only triggered by threshold frequency changes around the target frequency.

A square butt joint made using the closed-loop system on electro-polished material ('EP') is illustrated in the lower photograph of Figure 77. A state of full penetration was maintained around the full orbital joint, as shown,

Experimental results

and the corresponding inner bead width was measured between 3.2 and 4.2 mm.

Charts showing the pool frequency, the welding current applied, and the inner bead widths generated by Test I on the 'LS Kobe' material are shown in Figure 78. A full penetration state was maintained for the complete joint and the resulting inner bead width was measured between 3.4 and 4.3 mm. The associated average welding currents applied to all three tests on the 'LS Kobe' material were:

Test I	23.08 Amps,
Test II	24.03 Amps,
Test III	24.18 Amps.

The overall applied average welding current was quite consistent across the tests, although as shown in Figure 78 there was a small amount of variance of the applied base current during the orbital weld. (A photograph of the inner bead of Test I is given later in the top part of Figure 80.)

Typical results from the application of the 5 ms excitation pulse, generating a 120 Hz full penetration weld in the 'Cast 2' material are shown in Figure 79 (Test I). The inner bead width was maintained between 2.7 and 3.4 mm. Control over the 120 Hz penetration condition appeared relatively stable - the average welding currents applied for the three tests were:

Test I	19.71 Amps,
Test II	19.92 Amps,
Test III	18.96 Amps.

It can be seen that the range of average applied welding current for the three tests is comparable to that observed for the 80 Hz target frequency on the 'LS Kobe' material and considerably less than those applied to the 'Cast 2' material, although the overall applied current is much reduced due to the higher set target frequency.

Step change recovery

The photograph in the lower part of Figure 80 illustrates the inner bead profiles generated by the software imposed +8, +6, +4 and +2 Amp step changes and the corresponding response of the closed-loop system in attempting to re-establish a stable full penetration condition after the step change. The results from the step change recovery experimentation are illustrated graphically in Figures 81 to 84 inclusive (welding current, pool

frequency and the associated inner bead widths).

The +8 Amp step change proved too great for the stability of the control system and a relatively chaotic frequency response was monitored after the step change. As illustrated, no change was issued by the closed-loop system prior to the step change since the target frequency was consistently monitored. After the +8 Amp step, the frequency response did not stabilise. Consequently the control strategy did not issue enough negative welding current demands to recover the desired full penetration state.

Recovery from the +6 Amp step was triggered after 4.3 seconds (or 6.5 mm of weld) and a further 11 pulses (3.7 seconds) were needed to restore the target frequency to 80 Hz. The imposed +4 Amp step change resulted in a relatively slow recovery since the heat build-up was less than the larger step changes - it took 17 pulses (5.7 seconds) for the pool frequency to drop to 72 Hz where the -1 Amp command was issued. In this instance the control strategy might be observed to be over-damped due to the sensitivity of both the fuzzy logic model and the resolution of the power source at frequencies close to the target frequency. Further current reductions were then made as the 'threshold' low frequency was encountered. The +2 Amp step change resulted in a small drop in the pool frequency that was ignored.

5.5.3 Application of control strategy summary

The performance of the system was not necessarily ideal for a number of reasons:

- the sensitivity of the fuzzy logic model round the full penetration condition and the resolution of the welding power source (± 1 Amp only) resulted in a relatively inexact control of the target frequency ie. there was a tolerance band around the target frequency that did not trigger set-point changes,
- some queuing of desired demand signals was observed in the power source response.

However, it has been shown by the experimentation concerning the application of the closed-loop control system incorporating the derived fuzzy logic model that:

Experimental results

- the system employed (user-interface PC, control rack, and power source) was quite capable of meeting the demands of closed-loop operation of the application of 2 to 3 Hz excitation pulse frequency, although occasional welding current demands were 'queued',
- full penetration welds could be made using the system on different casts of $\phi 1.5"$ 16SWG SS316L material - with a reasonable level of inner bead width maintained around the complete orbital weld, with no loss in performance observed on a standard square butt joint preparation,
- some recovery by the system was demonstrated to step changes in the welding current.

SECTION 6.

DISCUSSION

6.1 Introduction

6.1.1 Sources of error

6.2 Observations and theory

6.2.1 Basic welding parameters - experimental observations

Quality and reliability of the pool oscillation signal

Pool frequency and penetration - Mode 1 to 3 transition

Pool frequency and penetration - weld bead formation

Pool frequency and orbital position

Evidence of mixed-mode behaviour

6.2.2 Theoretical predictions and practical measurements

(Pool size and frequency)

Mode 3 - basic work - stationary pools

Mode 3 - stationary pool and time-to-penetrate studies

Mode 1 - stationary pools

6.2.3 Summary

6.3 Cast effect on pool oscillations

6.3.1 Surface tension and penetration/frequency behaviour

Cast-to-cast work - 1.65 mm WT material - stationary pools

Cast-to-cast work - 1.65 mm WT material - moving pools

Cast-to-cast work - 3.91 mm WT material - stationary pools

6.3.2 'Time-to-penetrate' studies

1.65 mm WT material

3.91 mm WT material

6.3.3 Summary

6.4 Application to orbital welding

6.4.1 Sensitivity of pool frequency to operating variables

Constant parameter work

Control work

6.4.2 Reliability for monitoring/control of penetration

Reliability and smoothing

Application of the fuzzy model

Performance of control system and full penetration welds

6.4.3 Summary

6.5 Overall discussion summary

6.5.1 Theoretical modelling of pool behaviour

6.5.2 Application of pool frequency to cast behaviour and penetration control

6. DISCUSSION

6.1 Introduction

Initially the discussion focuses upon the correlation of the experimental observations made with established pool oscillation theory, considering in particular the pool frequency, the formation of the lower free surface and Mode 1 and 3 oscillation responses. The effect of material 'cast' is then examined, firstly with respect to the frequency behaviour of the materials studied. Theoretical predictions of the average acting surface tension according to pool oscillation models are then assessed, followed by the use of the 'time-to-penetrate' studies. Finally, the use of pool oscillations as a method of penetration control, particularly for orbital welding of ultra-high purity tubing is discussed (using the system derived).

A brief discussion of potential sources of error follows, before a detailed assessment is made of this research.

(An assessment of the practical relevance of the work is presented in the 'Implications of research' section, after the 'Conclusions').

Note: as highlighted in §4.3.2, for the sake of brevity, 'Cast 1' is also referred to as 'HS' ie. high sulphur, and 'LS Kobe' as 'LS' ie. low sulphur, since this was thought to be the main difference in chemical composition and possible cause of differences in behaviour for the same welding parameters.

6.1.1 Sources of error

Estimates of surface tension using pool oscillations and the membrane model (Equation 2.1) were potentially the most prone to error given the dependence upon the square of both the frequency and the bead geometry measurements. Measurement of the pool frequency using the Fast Fourier Transform was generally accurate to 1 or 2 Hz, depending upon the sample rate used (a measurement made using a 16 kHz sample rate, of 4 channels, with a 2048 point FFT would have been accurate to 2 Hz). Upper and lower bead widths were measured with a vernier calibrated rule, with an estimated accuracy of 0.1 mm - with greater confidence generated by the average bead width measurements from 20 locations around a typical 38.1 mm diameter tube.

Theoretical predictions of frequency and surface tension are also subject to the accuracy of the mathematical model representing the molten pool - elliptical pools, pools with non-vertical side-walls, pools that have a teardrop shape (in moving welds) etc. are all more difficult to treat accurately with the established models. The unknown surface tension/temperature behaviour associated with cast-to-cast variations also introduces a further source of error for theoretical predictions.

All the materials used in the study were as supplied by the manufacturer. Machined square butt preparations were made using a Tri-tool facing machine (see Figure 23) - this is conventional practice for UHP welding the material thicknesses studied. A difference in the wall thickness could have been present between material batches due to the production process. It is also possible that a material thickness variation existed as a function of orbital position ie. a lack of concentricity. For a typical Mode 3 oscillation of 2 mm pool radius, a $\pm 0.16 \text{ mm}^1$ variation in the thickness ('H' or 'WT') could result in a variation in the observed frequency of $\pm 5 \%$, (constant surface tension, γ , and density, ρ), and a variation in estimating the surface tension of $\pm 10\%$ (constant frequency, f_{M3} and density, ρ). Wareing (1989) noted that material thickness variations can have a significant effect on cast and penetration behaviour.

Overall measurement error and material geometry variations (including a 2% error in liquid density, ρ_l) could combine to result in the following *worst case* error for a typical pool of 2 mm radius in 16SWG material:

error in theoretical frequency estimation $\pm 8\%$, and
error in theoretical surface tension estimation $\pm 20\%$.

It should be noted that some of this level of error, inherent in theoretical predictions, might be reduced by increasing the size of the pools involved, by minimising the percentage error of the bead geometry measurement and achieving more ideal pool shapes. Machining joints to the required thickness would also reduce the error, although this is more usually applied to larger thickness joints (ie. not usual practice for the material sizes used in this study). Experimental measurements of wall thickness did not detect any significant deviation from the nominal value (the majority of material used for this thesis was cold drawn seamless tube).

¹ The stated tolerance is $\pm 10\%$ on material thickness for material supplied to the A269 specification.

6.2 Observations and theory

In this section the results obtained from the experimentation performed are discussed with respect to what might be expected from established theoretical models, and fundamental aspects of the behaviour are considered - for example, the effect of variation of basic welding parameters upon penetration and pool oscillation behaviour.

6.2.1 Basic welding parameters - experimental observations

Quality and reliability of the pool oscillation signal

Using the analogue signal processing circuit prior to the analogue-to-digital conversion, to maximise the gain and provide a signal with a close to zero mean value, the sensitivity of the monitoring equipment to Mode 1 signals in particular was greatly improved. This is graphically illustrated by **Figure 39**. Mode 1 oscillation signals were detected and processed with a high degree of repeatability in extremely small moving molten pools - the pool illustrated at the top of **Figure 47** was no deeper than half the material thickness (only 0.8 mm in depth). The use of argon with a 10% hydrogen addition to maximise the electric field strength and hence the sensitivity to corresponding small changes in arc length (see **Figure 33**) was also instrumental in providing this degree of sensitivity to *extremely* small pools. This is largely absent in other published work. Other work has primarily focused upon full penetration signals only in the 'thin' materials.

The *repeatability* of the Mode 1 signals was also highlighted during the cast-to-cast work. **Figures 64** and **65** illustrate five typical responses that damp out over the 36 milliseconds (approximately) following the end of the excitation pulse. The consistency of the pool oscillation waveform response is clearly shown. Real-time responses shown in **Figures 69** and **70** illustrate the reliability of processing the Mode 1 signals - a base current of 15 Amps generated responses that were consistently around 400 Hz (the responses to some 80 pulses are shown for each half of each orbital weld on the 1.65 mm WT material).

However, the clarity, amplitude and duration of the pool oscillation responses were observed to be quite sensitive to *some* of the operating parameters. Earlier published work is in accordance with this, particularly with regard to peak current level, I_p , and travel speed, S (see Lin, 1987, Xiao, 1992, etc.). **Figure 42** illustrates the need for a high magnitude excitation pulse (I_p) to produce a signal with a large amplitude and long damping time, and **Figure 52** illustrates the detrimental effect of increasing

the welding speed upon the quality and repeatability of the response.

The work described in this thesis adopted welding parameters that were typical of other pool oscillation researchers ie. the use of relatively short arc lengths (1.3 mm typical), a high electric field strength shielding gas (argon with 5 and 10% hydrogen additions), and only moderate welding speeds (90 mm/min typical). The use of arc voltage as the sensing method evidently still has these practical limitations.

It was noted that there was some slight variation in the responses in the stationary welding pools studied when applying the two power sources (the American AMI 207 and the Danish BDH 320) - see the 'stationary spot welding and signal quality' results described in §5.2.4. The frequency responses to the AMI 207 were all higher than those to the BDH 320, some 11% higher on average for all the comparative stationary welds (Table 26). Upon first examination, this would not appear to be readily accounted for by the application of the basic welding parameters alone, since the welding current and voltage monitored using the ArcWatch™ equipment revealed that the AMI 207 delivered a marginally lower average welding current (the monitored arc voltage was also lower). On average the heat input (as calculated by the voltage and current product) delivered by the AMI 207 was 3.6% lower - this figure is based on all the data. It was confirmed that the time of application of the welding current was the same for both power sources, since the number of pulses (delivered after the short application of constant current) present in the transient data files was the same. Comparative transient profiles of the welding current pulses delivered by both power sources are given in Figure 36.

The average outer bead widths were almost identical for pools established by the two power sources (*a//* peak current and time pulses, I_p & t_p):

$$\begin{aligned} \text{OBW}_{\text{AMI 207}} / \text{OBW}_{\text{BDH 320}} &= 0.99 \text{ (Argon with 5\% Hydrogen), and} \\ \text{OBW}_{\text{AMI 207}} / \text{OBW}_{\text{BDH 320}} &= 0.96 \text{ (Argon with 10\% Hydrogen).} \end{aligned}$$

However the average inner bead widths generated were considerably different:

$$\begin{aligned} \text{IBW}_{\text{AMI 207}} / \text{IBW}_{\text{BDH 320}} &= 0.89 \text{ (Argon with 5\% Hydrogen), and} \\ \text{IBW}_{\text{AMI 207}} / \text{IBW}_{\text{BDH 320}} &= 0.87 \text{ (Argon with 10\% Hydrogen).} \end{aligned}$$

It would appear then that the marginal difference in welding current (and the associated heat input) between the AMI 207 and the BDH 320 caused a corresponding change in the pool profile which would account for the

variation in pool frequency behaviour. (The 3.6% heat input difference caused on average a 12% difference in the inner bead width.)

The literature review highlighted the reported effect of current rise time upon the arc force generated (§2.6.3), and it might be observed that there is a slight difference between the monitored slew rates of the AMI 207 and the BDH 320 (with the BDH 320 lagging the AMI 207 by 1 ms at the peak of the current pulse - as shown in Figure 36). However, other researchers have reported a variation in *frequency* with a variation in arc force which was not apparent here (Lin, 1987, for example).

Reliable Mode 1 pool oscillation signals are optimised by analogue pre-processing of the signal and the use of argon with 10% hydrogen. Pool frequency signals detected in stationary pools illustrate the sensitivity to pool geometry, created by slight differences in delivered welding parameters from different power sources.

Pool frequency and penetration - Mode 1 to 3 transition

Results from the basic experimental work described in §4.2.4 'Orbital welding and penetration' and detailed in §5.2.4, illustrate the transition of a dominant frequency response (f_d) with increasing penetration that is indicative of a Mode 1 to a Mode 3 oscillation. This type of transition accords with the observations of other authors.

Bead width measurements revealed that a lower free surface had been formed *before* the frequency dropped ie. that a Mode 1 response was observed in molten pools where a lower free surface was thought to be present at the time of the application of the excitation pulse - see Figures 44 and 45. This response was also observed by Xiao (1992), in her doctoral thesis, and others. It might be considered that the use of the high current peak pulse (125 Amps for 10 milliseconds, pulsing at 2 Hz typically) has a significant contributory effect upon the heat input to the weld, despite its short duration, and therefore the formation of the lower free surface. The peak pulse itself, with its comparatively higher thermal efficiency, is often used to penetrate in pulsed procedures. Typically, the increase in power from the additional pulse is only 3 to 4% (from logged current and voltage data). This particular consideration has not been detailed by previous researchers.

The work on cast-to-cast variations (§5.3.2) employed identical procedures (using the same welding speed and shielding gas etc.) on two material casts that used both non-pulsed and pulsed current profiles. The numerical results from this experimentation are presented in Table 29 and graphically in Figure 60. It is clearly shown from the table that at 20.0 Amps (nominal set current) a lower surface had been formed for both material casts using the non-pulsed procedure, although the bead widths generated were *considerably* narrower than when using the pulsed procedure.

Although the heat inputs were reasonably comparable for the welds described, the peak pulse employed obviously had a significant effect upon the average outer bead width formed and an apparent effect upon the average inner bead width, despite the slightly lower heat input for the pulsed runs (presumably due to a slight difference in the monitored arc voltage). This partly illustrates why pulsed procedures are preferred in practice due to their ability to penetrate.

Since the lower free surface was present for the non-pulsed procedure runs, it can be reasonably assumed that the lower free surface was also present before *each application* of the peak pulse during the application of the pulsed procedures, and that the inner bead width was at least comparable in size to that established during the steady-state non-pulsed procedures. This indicates that, as might be expected, the transition from the Mode 1 to the Mode 3 frequency response cannot be *directly* associated with the transition from the partial to full penetration state and that this transition cannot be used as a sole measure of the penetration condition.

Furthermore, Xiao (1992) asserted that $a_t/a_b > 0.5$ for Mode 3 oscillations to occur. In this instance, if the lower free surface formed during pulsing (immediately prior to the application of the peak pulse) is presumed to be at least as large as that formed during the non-pulsed runs then a_t/a_b was much greater than 0.5 and Mode 1 oscillations were still observed (in contradiction with Xiao's observations).

The transition from Mode 1 to Mode 3 showed a high reliability, as indicated by Figures 46 and 63, occurring at the same level of base welding current (between 20.0 and 22.5 Amps) for the four monitored orbital positions for all the work with 1.65 mm material thickness.

For the SS316L 1.65 mm WT materials studied, the Mode 1 to 3 transition was not made until the lower free surface was significantly greater than that observed by other authors ($a_b \approx a_j$). The transition was observed between the same levels of base current for all the orbital positions.

It is thought that this observed difference in transition behaviour is accounted for by the material thickness studied - Xiao (1992) used comparatively thick materials (4 and 10 mm typically).

(It is also thought that the occurrence of the Mode 1 to 3 transition between 20.0 and 22.5 Amps for all the moving weld pools in the 1.65 mm WT materials was somewhat coincidental given the variation in the cast behaviour that was observed both in the pool geometry and associated frequency response. A discussion of cast-to-cast effects follows in §6.3.)

Pool frequency and penetration - weld bead formation

In general, decreasing Mode 1 and 3 frequencies were observed for increasing pool sizes, as might be expected from basic theory - see Equations 1 and 4, and Figure 41 for stationary pool results (1G), and Figures 45, and 60 for moving pool results (5G). This might simplistically indicate that the observed dominant pool frequency response (f_d) could be used as a measure of the *degree of penetration*.

Indeed, the results from the orbital welds made under the 'basic welding parameters' (§4.2.4) and the 'cast-to-cast variations in moving weld pools' (§4.3.2) experimentation show the general overall decrease in average frequency response with a corresponding increasing average inner bead width. It is noted, however, that the Mode 1 frequency response was more *sensitive* to the changes in the inner bead width, once it had been formed, than the Mode 3 response. This is to be expected since the pool width (both top and bottom surfaces) increased at a reasonably linear rate with the base current (see Figure 45 for example). If the other variables are assumed to be approximately constant, from theory, f_{M3} is inversely proportional to the pool radius (a), whereas f_{M1} is inversely proportional to $a^{1.5}$.

This fundamental trend was observed across the range of austenitic stainless steel material casts studied in both stationary and moving weld pools, although the specific pool frequency/size response observed varied with material cast. A quite comprehensive picture of the relationship between frequency and penetration, as a function of both the base current, I_b , and time (pulse N°.) in a stationary pool is given in Figure 55.

In accordance with pool oscillation theory, Mode 1 pool oscillations (f_{M1}) were observed to be more sensitive to the pool width than Mode 3 (f_{M3}).

Pool frequency and orbital position

Much of the *orbital* welding work carried out for this thesis was based on a nominal material thickness of 1.65 mm that is commonly used in ultra-high purity welding applications, usually referred to as 16 SWG. The variation in frequency response around the orbital welds made in this material thickness, was quite minimal - as shown by Figures 46 and 63. The average frequency responses at each level of base current (I_b) were extremely close for the four orbital positions logged, the 04:30, 07:30, 10:30 and 01:30 positions respectively, and the transitions between Mode 1 and 3 responses were all made between the same two levels of welding current (20.0 and 22.5 Amps set current) - for the 'basic welding parameters' and 'cast-to-cast variations in moving weld pools' work (results described in §5.2.4 and §5.3.2).

Full penetration pool frequencies at different orbital positions are given in Table 30 for the two material casts studied in the 'cast-to-cast' work (described in §4.3.2) - illustrated graphically in Figure 63. Aendenrooier (1996) asserted that the effect of gravity can be between 5% and 10% upon the Mode 3 frequency response when comparing the 1G and 4G positions for a weld bead of approximately 5 mm width. This was derived from pool oscillation theory presented by Maruo and Hirata (1993), since their model included the gravitational term. Aendenrooier did not observe a significant effect on the magnitude of the frequency, only that it was more difficult to observe reliable responses when the pool was sagging towards the electrode when welding downward with a constant electrode to workpiece distance. Although the frequency data observed for this thesis illustrates a notable variance in the average frequency response between the orbital positions at each level of base welding current, the trend was not consistent and cannot be attributed to the effect of the variation of the direction of the gravitational force upon the molten pool

alone. It is quite possible that the effect of the variation of the direction of the gravitational force upon the molten pool and its effect upon the *actual shape* of the molten pool itself contributed to the observed frequency variations.

(The data presented in Table 30 is an average of the response to nine pulses at each position.)

Controlling the pool size to a constant target frequency was also performed by Madigan (1986), although Aendenrooier eliminated the need for this by establishing a partial/full penetration characteristic for base and peak periods respectively. Aendenrooier applied this approach to pipe welds (60 mm in diameter).

Work on the real-time frequency response, illustrated typically by Figures 68 and 69, did not reveal significant frequency variations with orbital position ('Cast 1' and 'Cast 2' materials), as each partial/full period covers half the clock positions (12 to 6 o'clock, and 6 to 12 o'clock return).

Significant differences in pool frequency with orbital position were generally not observed - a target penetration level could be selected with a constant frequency response for the 1.65 mm WT material.

Evidence of mixed-mode behaviour

Other researchers have recommended parameters that avoid the generation of the slosh mode, Mode 2 (shown in Figures 1 and 4). In the work presented in this thesis, Mode 2 frequency responses were generally not thought to be observed. Evidence of mixed-mode responses however was noticed during the initial stationary pool work, (results described in §5.2.4) particularly for high and relatively long peak current pulses. The example shown in Figure 43 illustrates a 'mixed-mode' response where there is a clear secondary frequency present at 185 Hz, despite the presence of the low frequency dominant mode, $f_d = 61$ Hz (BDH 320 power source, argon with 10% hydrogen shielding gas). The average pool size for this stationary spot weld was 5.7 mm. If a γ/ρ ratio of 1.71×10^{-4} is assumed (since the surface tension is not known, this value gives the closest approximation to the well established Mode 3 behaviour), the basic theory presented in Equations 1, 4 and 5 yields the following frequency estimates:

$$\begin{aligned}f_{M3} &= 61 \text{ Hz (chosen to set the } \gamma/\rho \text{ ratio),} \\f_{M2} &= 102 \text{ Hz, and } f_{M1} = 177 \text{ Hz.}\end{aligned}$$

Material: '35 mill.', with a 2.0 mm nominal wall thickness.
(See Tables 4 and 5 for material designation and composition.)

It seems likely then that the secondary, less dominant response is Mode 1 (only 8 Hz difference from that indicated by the Fast Fourier Transform) rather than Mode 2. This corresponds with behaviour reported by Yoo (1993), and illustrated in Figure 4 from the literature survey, as diagram e) symmetric mode transition penetration, and illustrated in detail in Figure 85.

Figures 53 and 54 also illustrate 'unexpected' shifts in the dominant frequency during stationary pool development. It is shown that, even long after the establishment of the first low frequency, full penetration Mode 3 response, a high frequency response occasionally becomes dominant. Again, if a γ/ρ ratio is assumed, the Mode 1 estimate is typically only 15 Hz different from the average experimental values (calculated for 25.0 Amps, 'Cast 1' material - pool size data given in Table 27), whereas Mode 2 is 90 Hz different. The switch between dominant modes is partially a function of using the Fast Fourier Transform to determine the frequency - a normalised '1.00' is reported for the frequency response which is the strongest in terms of frequency and amplitude and this is used to determine f_d . If only Mode 3 responses were being sought, a routine that looked for the *lowest* frequency with a comparative normalised signal strength of above 0.7, for example, would reveal the presence of the lower free surface.

It is evident that Mode 1 & Mode 3 oscillations can be generated at the same time, in accordance with Yoo's model (1993).

6.2.2 Theoretical predictions and practical measurements (pool size and frequency)

It was not the aim of this thesis to use the established and published mathematical relations as a means of controlling the penetration condition. It was felt that they did not offer accurate enough estimates, especially given unpredictable cast variations (ie. unknown surface tension and unknown surface tension/temperature gradient behaviour, dy/dT), and the unpredictable observed 'non-linear' transition behaviour between oscillation modes. However, to offer some validation of the experimental observations and to form a basis for comparison of the work presented here with established theory (in particular Xiao, 1992, similar to Maruo and Hirata's work, 1993, and Yoo's alternative approach, 1993) the experimental results are discussed below.

Xiao's equivalent diameter (Equation 2) is used when comparing her model with experimental results, although Yoo's model provides an additional side-wall slope parameter 'p' to account for the difference in size between top and bottom surfaces, and accounts for the elliptical effect by using both pool width 'W' and length 'L' in the energy model.

Mode 3 - basic work - stationary pools

The results of the work described in §5.2.4 contained a *constant* base current level with a wide variation of peak pulses (ranging from 75 Amps for 5 ms to 150 Amps for 20 ms) resulting in a considerable spread of frequency responses (59 Hz to 104 Hz). The constant base current used in this part of the study, can be shown to contribute the majority of the heat input to the stationary pools. The *acting surface tension* can therefore be assumed to be approximately constant. This is further discussed in the next section, and in detail in §6.3.1. The linear fit of the experimental data with theoretical prediction is $y = 1.006x$, with $R^2 = 0.80$ (assuming γ and ρ). A graphical comparison between the experimentally observed frequencies at the end of the spot weld and the theoretically predicted values is given in Figure 86 (Mode 3 theoretical predictions calculated from Equation 1).

It is clearly shown that a good correlation existed with Xiao's model. Comparative data for Yoo's model (Equation 3) is not presented. Yoo's model provides estimates of pool frequency that are consistently low - average frequency of all experimental data: 78.7 Hz, Xiao's theoretical Mode 3 model average: 78.9 Hz, Yoo's theoretical Mode 3 model average: 73.8 Hz. Presumably the performance of the predictions of Yoo's model is

slightly better than expected for plane circular pools because it accounts for the side-wall slope ('p') and the difference between the length and width of the pool ('W' and 'L').

Mode 3 - stationary pool and time-to-penetrate studies

In contrast to the basic work investigating the effect of the peak pulse upon the oscillatory response, the stationary pool and 'time-to-penetrate' work employed a small *range* of base currents on the thinner materials studied: 15 to 25 Amps for the 'EP', 'LS Kobe', 'Cast 1', and 'Cast 2' materials. It is not necessarily implicit, however, that the temperature on the surface of the pool is directly related to the average welding current (varied here by different values of I_b).

After a great deal of work theoretically modelling and experimentally validating the heat and fluid flows within stationary and non-stationary weld pools, Zacharia (1995) found that the weld pool peak temperature increased with welding current, although there was no direct correlation. (Previous related work, by the same author, was published in 1993.) For this reason it is difficult to assume that the acting surface tension was relatively constant when using different base currents and hence comparative work with established theory is also potentially subject to a degree of error.

A variation in the surface temperature would cause a corresponding variation in the acting surface tension across experimental runs for the same material cast, since surface tension is directly affected by temperature. The variation in surface tension would then affect the frequency response accordingly.

This is partly the reason why established theory was not used as the control mechanism, or model, to relate the observed pool frequency with the level of penetration - the effect of surface tension is discussed further in §6.3.1.

Xiao's work (1994) concerning measurements of surface tension for pure iron under a welding arc, using pool oscillations (Mode 1) observed a temperature range of 65°C (pool surface temperature 1845 to 1910°C) for a welding current range of 45 Amps under an argon arc, generating a predicted associated surface tension range of 0.2 N/m (1.05 to 1.25 N./m). The results described in §5.3.1 on 1.65 mm material employed a current range of 10 Amps ($I_b = 15$ to 25 Amps). If the frequency data presented in Table 27 is compared with a theoretically derived frequency based on the

membrane model, using a constant surface tension and density (1.9 N/m and 7800 kg/m³ respectively), a linear fit of $y = 0.993x$ is obtained, with $R^2 = 0.87$, again illustrating a good degree of correlation. A more detailed correlation was not performed or presented because of the known potential variation in surface tension.

(A surface tension value of 1.9 N/m is adopted to verify the form of the pool oscillation response - this figure is associated with pure iron at its melting point. Figures for acting surface tension values in austenitic stainless steels in pools with variable welding current and minor element constituent variation are generally unavailable.)

Validation of experimentally observed Mode 3 stationary pool frequencies is offered by correlation with basic theory.

Mode 1 - Stationary pools

It is presumed that the mode of oscillation of the '280410' and 'MS097' casts (3.91 mm nominal wall thickness) during the 'stationary pool and time-to-penetrate studies - part 2 - medium diameter pipe' was that of Mode 1. Mode 2 oscillations are particularly difficult to generate in stationary pools unless a long time pulse is employed (t_p), or the arc is shifted from the geometric centre of the molten pool resulting in an asymmetric application of the excitation force upon the pool surface (as in the case of the moving pool at high travel speeds). The results of §5.3.1 would suggest that Mode 1 behaviour was indeed predominant, although the derived surface tension predictions appeared low (since the pool frequency measurements were accordingly low) for casts that were thought to exhibit comparatively low surface activity (resulting in the extremely smooth bead profiles observed). Mode 2 estimates of pool frequency were also unrealistically low.

During the work on 1.65 mm wall thickness, several welding runs exhibited a high frequency response towards the end of the weld (shown in Figures 53 and 54) that was suspected to be Mode 1 (this has already been partially discussed in 'evidence of mixed-mode behaviour', in §6.2.1). The correlation between predicted and theoretical frequency values for Mode 1 (using the model presented in Equation 4) using a constant value of surface tension was high and comparative Mode 2 predictions were excessively low.

6.2.3 Summary

A validation of the more fundamental frequency data presented in this thesis (from stationary pools) has been offered with regard to the observed experimental values and those predicted by established theoretical models. The specific case of austenitic stainless steels and their variable surface tension behaviour means that the validation can only be performed in terms which are not wholly specific, since the acting surface tension is not known, and varies between material cast and with surface temperature. It is also known from the literature that the surface tension behaviour under a welding arc is specifically complex and cannot necessarily be inferred from independent surface tension testing (levitated drop techniques etc.). The theoretical prediction of the pool frequency is dependent upon the square root of the value of acting surface tension.

Despite the presence of the unknown variables, particularly with regard to the acting surface tension, the frequency data established offers considerable insight into the progression of the state of penetration of the pool.

Oscillation modes have been clearly identified around the full orbital welds made, and the transition from Mode 1 to Mode 3 was explicit and constant with the orbital positions observed, although it did not provide a sole indicator of the difference between partial and full penetration.

Some evidence was also found of mixed-mode behaviour in stationary pools which was identified as Mode 1 and Mode 3 in co-existence (as identified as a transitional mode by Yoo, 1993).

6.3 Cast effect on pool oscillations

This section of the discussion considers the predictions of surface tension (from the stationary pool tests) which are made to offer an insight into the possible variations in acting surface tension. Theoretical pool oscillation models were used. Effects of cast variation upon moving weld pools, and the 'time-to-penetrate' studies utilising pool oscillations, which were used as a characterisation of material behaviour, are then considered.

6.3.1 Surface tension and penetration/frequency behaviour

Although the work described in this thesis did not seek to rely upon the application of the established theoretical models as presented in the literature, they were used as a basis to compare the *form* of the behaviour of the casts of the materials studied.

Many authors have identified the importance of the role of surface tension and its fundamental importance in determining the predominant fluid flow in relatively low current austenitic stainless steel weld pools. Although a great deal of work has been performed modelling the welding parameters, simulating the welding process, generating predicted bead profiles etc., only minimal work has been published with regard to the *acting surface tension* in the presence of a welding arc. The surface tension also has a fundamental role in the prediction of the pool frequency if the established theoretical models are considered.

The established models can be used to provide an estimate of the acting surface tension - the pool frequency can be monitored after excitation through the arc voltage, the bead geometry can be measured after arc extinction (upper, lower and thickness dimensions). Although the molten pool density is also temperature dependent, there is inherently more error in the experimental measurement of the pool frequency and bead geometry. The errors are then compounded since the prediction is a function of the square of the frequency, and the square of the pool radius (the *cube* of the pool radius if Modes 1 or 2 are used for the prediction). These errors can be minimised by using large welding pools and high pool frequencies (Xiao, 1994, used 8 mm thick material, a Mode 1 oscillation and pool widths of 5 to 8 mm and estimated an overall error of 7%).

Predictions from the models described (Xiao, 1992, and Yoo, 1993) are thus subject to these degrees of error. The difference between Yoo's and the membrane model is, however, even more amplified if it is used to estimate surface tension (γ): for a plane circular pool with straight side-

walls, the surface tension value would be some 44% greater than that predicted by the membrane model (established by Kotecki, 1972, and by Maruo and Hirata, 1993 and Xiao, 1992).

Cast-to-cast work - 1.65 mm WT material - stationary pools

Predictions of surface tension from the membrane and Yoo's model (Equations 1 and 3) for $\phi 1.5''$ SS316L 16SWG materials ('EP', 'LS Kobe', 'Cast 1' and 'Cast 2') are given in Table 27 and Figure 56. The data point for 'LS Kobe' at 15.0 Amps set current was not plotted since a Mode 3 oscillation was not observed.

All the values derived from the membrane model are within reasonable limits: it is well established that at its melting point $\gamma_{\text{iron}} = 1.9 \text{ N/m}$, and this decreases with an increase in temperature (Xiao, 1994 observed values down to 1.0 N/m at 1910°C under a *welding arc*). Comparatively, the values derived from Yoo's model are unrealistically high. This is only to be expected when there is a 17% difference for the *frequency estimation* for plane circular pools, and the surface tension is a function of the *square* of the frequency. The following discussion is therefore confined to predictions made by the membrane model which is well established for relatively plane circular pools with vertical side-walls, and correlates with the experimental work ie. the 1G stationary spot welds that were fully penetrated.

If it is assumed that the peak surface temperature is a function of the welding current, and that the peak surface temperature increases with the level of welding current (in accordance with Zacharia, 1995), then the acting surface tension values predicted by the membrane model generally decrease with temperature for each material cast. This might be expected if the material casts were generally classifiable as having 'low surface activity' (see Figure 11).

However, the flow behaviour in the 'LS Kobe' cast especially at $I_b = 15.0$ and 17.5 Amps seems to have resulted in the formation of beads with comparatively wide upper surfaces and narrow lower surfaces and produced an apparently slightly different surface tension/current profile (see Table 31 for the pool widths). As the welding current was increased the difference became less marked. This behaviour is compared with the case of the moving weld pool in the next part ('1.65 mm WT material - moving pools').

A prediction of the likely cause of the flow mechanism from the stationary pool observations alone is difficult from the limited experimental data and

sources of error involved in the surface tension calculations. Surface tension predictions for the 'LS Kobe' material are potentially subject to a further degree of error: the plane circular Mode 3 model has been used to provide an estimate of acting surface tension and whilst the other material casts stay within reasonable bounds for this model, maintaining quite vertical side-walls (p), the 'LS Kobe' material had a quite different pool geometry ($p = 0.53$ and 0.74 for $I_b = 15.0$ and 17.5 Amps).

It is difficult to explain the apparently different behaviour in the low sulphur material at low welding currents from the 'static' stationary pool observations (ie. lowest pool frequency, f_d) and associated surface tension calculations alone. However, the 'time-to-penetrate' studies offered more information - this is discussed in §6.3.2.

Cast-to-cast work - 1.65 mm WT material - moving pools

The predominant flow mechanism in the 'LS Kobe' material cast pool could have been *surface tension driven flow* (ie. the Marangoni model) at the lower welding currents. This type of flow regime is associated with surface flows that travel outwards towards the edge of the pool, rather than downwards (see §2.5.8). This type of behaviour was apparent both in the stationary pools (described above) and in the moving pools for the lower welding currents (in particular, $I_b = 15.0$ and 17.5 Amps) around the full orbital weld. For the moving pools, the observed outer bead widths for the low welding currents were *similar* for both casts (on average, 3.2 to 3.4 mm, with minimal standard deviation), however the inner bead widths generated in the 'LS Kobe' material (denoted 'LS') were again significantly lower than for the 'Cast 1' ('HS') - see Table 28 and Figures 60 and 61.

It appears that the dominance of the fluid flow regime in the 'LS Kobe' material both within the stationary and the moving weld pools changed as the welding current was increased. Some indication of the penetration characteristic of the 'LS Kobe' material might have been gleaned from the acting surface tension values and bead geometry derived from the stationary pool work. More detail on the form of the penetration behaviour was revealed by the time-to-penetrate behaviour (see §6.3.2).

Observations of the behaviour of the 'LS Kobe' cast in both stationary and moving pools could then lead to the conclusion that *surface tension driven flow* dominated at the lower welding currents that was then either reversed or overcome by the higher welding currents.

If the stationary and moving pool measurements and predictions are examined collectively, some evidence is offered for radially outward flow at the lower welding currents in the low sulphur material - which could have been surface tension driven, supporting the Marangoni model.

The pool geometries which were measured for the low and high sulphur materials (as shown by Figure 60) caused associated changes in the pool frequency responses. The differences in observed pool geometry (across the range of applied base currents) between the two casts could have been caused by the difference in heat input profiles - as shown in Figure 62. However, the measured pool frequency profiles offer at least a comparative indication of the pool geometry, and the difference in cast behaviour.

Cast-to-cast work - 3.91 mm WT material - stationary pools

Figure 59 illustrates the theoretically derived surface tension values for the '280410' and 'MS097' material casts that did not penetrate, using the Mode 1 model (Equation 4), and for the '2" Pipe 2' and '2" Pipe 4' material casts using the membrane model, Mode 3 (Equation 1). As highlighted in the results section, §5.3.1 Part 2 - Medium diameter pipe, the surface tension values computed from the Mode 1 model seem comparatively low.

Since the sulphur levels were notably low for both materials (0.003 and 0.004%), the resulting outer bead appearances smooth, and the pools relatively wide and shallow, it might have been anticipated that there would be little surface activity and an outward fluid flow driven by surface tension, where a comparatively high value acted at the centre, with lower values operating at the cooler pool extremities. This type of behaviour has been well documented by other authors observing cast behaviour directly (Lambert, 1991, etc.) and others providing mathematical models, correlating fluid flow forces acting on and within the pool (Zacharia, 1993). This would lead to an expected value of acting surface tension that should have been comparatively high (possibly tending towards 1.9 N/m) despite the possibility of a surface tension/temperature gradient, dy/dT - however, this was not the case using the Mode 1 model (acting average surface tension estimates: $\gamma_{280410} = 1.05$ N/m, and $\gamma_{MS097} = 1.06$ N/m).

It is thought that the discrepancy can be accounted for by a number of possibilities - either the associated measurement errors in predicting surface tension from the pool oscillation models (*particularly* when using Mode 1

oscillations), or the accuracy of the model itself in representing the pool oscillation and surface tension behaviour in a shallow pool. Alternatively the acting surface tension was quite different from that which might be expected from the literature ie. for Marangoni flow and casts that have been identified as difficult to weld.

The Mode 1 pool oscillation model does not offer estimations of average acting surface tension that match expected values for the thicker material casts studied which are known to be difficult to weld and exhibit distinct radially outward flow.

6.3.2 'Time-to-penetrate' studies

1.65 mm WT material

The penetration characteristics of the four material casts studied were further revealed by the *first* transition of the pool frequency from Mode 1 to Mode 3, although it is likely that a lower pool surface was present before the transition between the oscillation modes was made ie. in this sense the transition observed is not a true 'time-to-penetrate'. Charts showing the detailed behaviour of the 'EP' and 'Cast 1' materials for different base currents are given in Figures 53 and 54.

Table 32 reveals in particular the marked difference between the behaviour of the stationary pool of the 'LS Kobe' cast and the other material casts, particularly at the lower levels of base welding current. Twenty pulses were applied in the 10.0 second duration pulsed test. The transition from Mode 1 to Mode 3 was not made at 15.0 Amps (I_b) and the transition at 17.5 Amps was significantly later (at 8.0 seconds into the test) than the other casts (at 3.0 s. for 'EP' and 'Cast 1', and 4.5 s. for 'Cast 2').

Wareing (1989) noted that the difference between cast behaviour for viscous and fluid casts - difficult and easy to penetrate respectively - as characterised by the 'time-to-penetrate' was minimised with an increase in the welding current. Using the pool oscillation frequency as a measure of the penetration offers a fine resolution of the penetration condition. The results illustrated above also show the decreased difference in behaviour at the higher welding currents, in accordance with Wareing's observations.

The resolution of the timing is subject to the pulsing frequency ie. 2 Hz pulses obviously enable identification of the first transition only to the nearest $\frac{1}{2}$ second. A limit on the pulse frequency is naturally imposed by

the pool oscillation response itself - applying a peak current pulse prior to the decay of the response from the previous pulse would result in an undesired amplification or decay of the oscillatory response.

The penetration behaviour of the 'LS Kobe' material for moving weld pools has already been discussed - at the lower levels of welding current, the penetration is comparatively low. The 'time-to-penetrate' characteristic as given by the time from the start of the test to the *first* transition between Mode 1 and Mode 3 evidently yields an insight into the penetration behaviour of the material cast. Figure 87 illustrates the comparative time-to-penetrate profiles for the 'Cast 1' (HS) and 'LS Kobe' (LS) materials used in the moving weld pool study. It is perhaps notable that the difference in behaviour is associated with the Japanese, low sulphur cast.

The 'time-to-penetrate' characteristic, as indicated by the transition from the Mode 1 to 3 pool oscillation response, provides further detail of the penetration behaviour. Particular differences exhibited by the lower sulphur material are clearly highlighted by the later transition times in the stationary tests.

The 'time-to-penetrate' study *again* highlights the characteristic behaviour of the 'LS Kobe' material. It is possible that the dissimilar heat input profiles might have caused the comparative differences in penetration behaviour in the moving weld pools. However, given the observed differences in the surface tension predictions at lower welding currents, and the associated later transitions identified in the 'time-to-penetrate' profiles it can only be concluded that there is a significant difference in the cast behaviour that has an associated effect on the pool oscillations.

3.91 mm WT material

Frequency/time traces are given in Figures 57 and 58 for the difficult-to-weld and easy-to-weld casts respectively of 3.91 mm (nominal wall thickness - standard pipe schedule 40). Casts '280410' and 'MS097' did not penetrate during the 30 second run of pulsed current. The higher sulphur material casts, '2" Pipe 2' and '2" Pipe 4', made the transitions between Mode 1 and Mode 3 frequency consistently for the three tests applied, both at around 15.0 seconds into the test. It was known that these casts were relatively easy to weld autogenously.

Discussion

Data was not presented which illustrated the effect of increasing the welding current on casts '280410' and 'MS097' - penetration was not obtained in a stationary test with 60 Amps for 60 seconds. In fact, weld procedures which obtained a satisfactory joint in these material casts at this thickness proved to be intractable.

The pool oscillation frequency/time characteristic yields a rapid material comparison - in this case verifying the extremely difficult behaviour of two austenitic stainless steel casts, since the transition (a characteristic frequency 'drop') between the Mode 1 and the Mode 3 response was not made. The reliability of the technique for both the easy and difficult to weld materials is illustrated by the extremely close correlation of the pool frequency results obtained from tests 'A', 'B' and 'C' for each material cast.

Comparative differences between the cast behaviour of 3.91 mm WT material are clearly indicated by their 'time-to-penetrate' characteristics (as indicated by the transition from Mode 1 to 3 response).

6.3.3 Summary

The surface tension figures alone are perhaps difficult to interpret with confidence or associate with expected flow behaviour - however, the resultant bead geometry and 'time-to-penetrate' pool oscillation profiles from relatively standard stationary pool tests appear to reveal significant aspects of penetration behaviour. The behaviour also appears correlative with moving weld pools. Some evidence is found for Marangoni flow, in the 'LS Kobe' material at the lower levels of welding current applied, with comparatively wider outer beads and narrower inner beads. The dominance of this flow was not observed with the higher levels of welding current.

(It was noted however, that the experimental results indicated a difference in the applied heat inputs for the moving weld pools which could have been a contributing factor to this difference in behaviour.)

Frequency data offered by stationary pool (involving both a theoretical calculation of the surface tension, based on the Mode 3 model, and the 'time-to-penetrate' profile) and moving weld pool runs offers quite an insight into the penetration behaviour of a material cast.

Work on the thicker materials which was expected to illustrate more clearly the surface tension/pool frequency behaviour did not necessarily vindicate the association of a comparatively high *acting surface tension* (from the **Mode 1** model) with a 'difficult-to-weld' or a dominant flow regime that was radially outward (surface tension predictions were surprisingly low). Materials which were known to have a 'difficult-to-weld' characteristic were however quite easily identified by the pool frequency/time trace, from a short stationary 'time-to-penetrate' test.

Note: Pool oscillation models do not make any assessment of the dominant flow regime in the pool, and offer at best only an estimate of the average acting surface tension. More information with regard to pool behaviour is offered by 'time-to-penetrate' studies using the pool oscillation frequency as the measurement variable.

6.4 Application to orbital welding

In this section, the sensitivity of the pool oscillation technique as a method of penetration control is discussed, particularly with regard to the 1.65 mm wall thickness materials studied. The reliability and performance of the derived system is then considered with respect to the closed-loop control trials.

6.4.1 Sensitivity of pool frequency to operating variables

In the first section the 'static' sensitivity of the pool oscillation frequency to the level of penetration in travelling weld pools is discussed ie. where welding parameters were maintained at a relatively constant level during the weld run. This can be assessed from the results of the 'basic welding parameters' work (§5.2.4) and also the cast-to-cast work (§5.3.2).

The 'dynamic' behaviour of the pool frequency and state of penetration when the welding parameters were changed significantly *during* the weld run are discussed in the following section, with regard to the results presented in §5.4 and §5.5.

Constant parameter work

The control work presented in this thesis was based on the use of a target penetration frequency (Mode 3). In order to assess the potential performance of the control system in maintaining a constant level of penetration, the sensitivity of the pool frequency in representing the penetration condition is discussed (1.65 mm wall thickness material - only the moving weld pools are examined here). In general, the level of penetration is taken to be represented by the inner bead width, although over-penetration will occur if the inner bead width is too high, causing pool sag or root concavity, depending upon the orbital position.

Figure 45 illustrates both the average inner and outer bead widths for different levels of penetration (according to a variation in the base current, I_b) and the associated average dominant pool frequency (f_d). The sensitivities can be quantified both by the slope of the frequency/inner bead width curve, showing the sensitivity of the resultant frequency output variable to the level of penetration (denoted here as $\Delta f_d / \Delta IBW$), and the slope of the frequency/base current curve, showing the sensitivity of the resultant frequency output variable to the base current input variable ($\Delta f_d / \Delta I_b$).

The slopes derived from the 'basic welding parameters' work for the two dominant modes of oscillation are detailed separately in Table 33.

Note: Δf_d is used to denote the difference between the appropriate dominant frequency values (as $y_1 - y_2$ for a linear relation), ΔIBW and ΔI_b are used to denote the differences between the appropriate average inner bead width and base current values respectively (as $x_1 - x_2$), hence the sensitivity is quoted as the slope of the curves in the relevant place (Mode 1 or 3).

Data is based on the average inner bead widths from the complete orbital welds, with least squares approximations for the appropriate data sets (bead width and frequency) since the results were close to linear for the appropriate data set for each mode. Comparative results from the 'cast-to-cast' work, illustrated in Figure 60, yields the data shown in Table 34.

As shown by the tables, and as highlighted earlier, Mode 1 pool oscillations inherently offer a higher degree of sensitivity to the generated inner bead width (or pool radius), *where an inner bead width has been formed* (as discussed in §6.2.1). However, it does not give an indication of the presence of a lower free surface. A Mode 3 oscillation definitively indicates the presence of the lower free surface, and was therefore used as the target condition for this work. A typical sensitivity of 25 to 40 Hz/mm (Mode 3 - LS and HS casts, $\Delta f_d / \Delta IBW$, from Table 34) therefore offers a *potential* control of approximately ± 0.1 mm of the inner bead width *if* the frequency can be controlled to ± 2 Hz (typical operating resolution from FFT).

The sensitivity of the Mode 3 pool oscillation to the input variable (base current, I_b) is quite low. Interest in the control of the full penetration condition (typically 90 to 70 Hz), would result in the associated operating range of base current of approximately 3.7 Amps or 5.6 Amps (Mode 3 - LS and HS casts, $\Delta f_d / \Delta I_b$, from Table 34) ie. ± 1.9 Amps and ± 2.8 Amps around the target set-point respectively. However, the BDH 320 power source used in the control system was limited to a current resolution of ± 1 Amp, potentially yielding only a minimal ± 2 steps around the desired target - ideally the current resolution would be ± 0.1 Amp for work on this material thickness to provide a greater number of steps for an increased resolution of control.

Mode 3 pool oscillations offer a potentially high degree of sensitivity to the state of penetration (as measured by the inner bead width) for typical ultra high purity tubing material.

Control work

The penetration control system was applied to the 1.65 mm wall thickness casts - 'EP', 'Cast 2', and 'LS Kobe' materials (unfortunately the 'Cast 1' material supply was exhausted). Preliminary open-loop trials were made on 1.65 mm wall thickness ('Cast 1' and 'Cast 2'). Trials were also made on 3.18 mm nominal wall thickness material ('1.5" Thick') to illustrate a larger span of partial and full penetration responses. The results from this work are described in §5.4 (illustrated by Figures 68 to 72 inclusive).

Some time delays were obviously observed when the applied large step changes of base current were made, causing the desired corresponding change in the dominant oscillation mode and Table 35 details a comparative summary of the work on the 1.65 mm wall thickness material ('Cast 1' and 'Cast 2').

The transition from the Mode 3 to the Mode 1 response was made much more quickly after the *decrease* in applied welding current (I_b) than the establishment of the dominance of the Mode 3 response after the step *increase* in welding current. The reasons for this behaviour are discussed below.

This behaviour was more apparent in the greater wall thickness material (nominal 3.18 mm), although an accordingly larger delta-current was used to provide a similar change in the penetration condition. A comparison between a bead-on-tube and a fairly ideal square-butt joint weld (minimal root gap) can be made from Table 36 (the graphical results are shown in Figures 70 and 71, and the inner joint profile in Figure 72).

The behaviour of the square butt joint is evidently very similar to the bead-on-tube, although for some reason there is a significant difference between responses to the first increase in welding current (ie. a. in Table 36 - the results presented are from one bead-on-tube weld and one joint only and not taken to be statistically significant). The long time lags associated with the 3.18 mm thickness material illustrate the potential difficulty in attempting to control or maintain a constant level of full penetration.

It is not surprising that the Mode 1 to 3 transition is made much later after the step change in base current than the Mode 3 to 1 transition. The Mode 1 to 3 transition can only be made once a threshold level of the inner bead width is exceeded. Xiao (1992) estimated this ratio at $a_i/a_b > 0.5$, although as highlighted earlier in the discussion, the figures presented in this thesis for the 1.65 mm wall thickness material (Figure 45 for example) suggest that a_b must nearly approach the value of a_i for the case of the moving weld pool ie. as soon as the lower bead width was less than the upper bead width a Mode 1 response was the dominant result.

Furthermore, the heat losses to the surrounding tube material would result in a delayed response to the positive step change in welding current, as the local heat conditions were gradually built up to create a 'steady-state' full penetration condition. Following the decrease in welding current, the heat losses to the surrounding tube material would contribute to the comparatively rapid response to the negative step change, as the heat was lost reaching a 'steady-state' Mode 1 response more quickly.

As the desired full penetration state is lost after a step decrease in base current, the Mode 3 to 1 transition is quickly apparent, although in accordance with the heat build-up required to establish the desired state of full penetration (Mode 3) after a step increase, the Mode 1 to 3 transition is comparatively slow.

(Suzuki, 1991, also noted variable time constants for GTA welding which were dependent both upon step size and direction - an adaptive control mechanism was implemented to account for the response, using a vision sensor for the back-bead width by controlling the welding current.)

Note: This holds for both 1.65 mm and 3.18 mm WT materials studied - although the associated time lags were obviously much greater for the 3.18 mm WT material.

Frequency data presented in this thesis is based upon the most dominant frequency present in the arc voltage signal after both analogue and mathematical treatments, as determined by a Fast Fourier Transform of the appropriate data set.

6.4.2 Reliability for monitoring/control of penetration

Reliability and smoothing

It is apparent from the real-time frequency plots (ie. each point represents the dominant frequency, f_d , from the FFT of the processed arc voltage result for that current pulse) that the responses for the partial penetration oscillations (Mode 1), were subject to a larger variance than the full penetration oscillations (Mode 3). See Table 37 for a summary of the experimental observations and Figures 68 and 69 in particular.

Despite the variance apparent in the partial penetration frequency, the consistency of the real-time response observed is quite evident. A number of factors would have contributed to the cause of the variance. The small amplitude, short duration signals were more difficult to extract, lasting only 40 milliseconds, with a full penetration oscillation lasting 200 milliseconds or more. The second half of the channel 3 data window was discarded, since it did not contain pool oscillation frequency data, and the first half duplicated. The relatively small amount of data for the Mode 1 oscillations would have resulted in less accuracy (the rest of the data for the 2048 point FFT was zero-padded). A smaller window size and higher sample rate could not have been used to increase the accuracy and resolution of the Mode 1 signals since sufficient data was also required to log the much lower frequency Mode 3 signals (on the fourth channel).

Smoothing the reaction of the control system to the real-time frequency data was necessary to avoid responding to some of the atypical, or chaotic, results. This was performed by rejecting differences of greater than 30 Hz for control decisions (30 Hz was felt to be a reasonable threshold value that would reject single-point, chaotic responses, but allow response to progressive frequency changes which give an accurate reflection of the state of penetration). Ignoring frequency changes of 30 Hz and above proved to be a reasonable control rule - Figures 74 to 76 illustrate many occurrences of frequency responses which are uncharacteristic of the state of the weld pool (from the inner bead width which was measured after welding) ie. a response to these signals would have been inappropriate. Figures 70 and 71 illustrate the 'smoothed' frequency profiles for partial and full penetration conditions on 3.18 mm WT material, and Figure 72 illustrates the associated inner and outer bead surfaces of the joint.

(Figures 73 to 76, 78 and 79, and 81 to 84 illustrate frequency profiles which were not smoothed - the >30 Hz difference rule was applied to the reaction of the control system instead.)

It is possible that these more unexpected elements were caused by the signal conditioning board which was operating at half full scale, making the subsequent analogue processing more susceptible to noise. Some erroneous responses were partly inevitable since the arc itself was being used as the sensing element. It is thought that the absence of this atypical response in other authors' work is due to the generally larger material thicknesses and consequently higher amplitude signals that were studied.

Smoothing the response of the control system is necessary to avoid reaction to atypical frequency data - the >30 Hz difference rule (between successive pulses) was found to operate satisfactorily.

Application of the fuzzy model

The fuzzy logic model applied as the interference engine between the pool frequency input and the derived 'delta-current' output had varying levels of sensitivity to the pool frequency and a non-linear input/output relationship to account for the Mode 1 to Mode 3 transition behaviour. By approximating the input/output relationship to a linear regression in the areas of interest, the sensitivity of the delta-current output to the pool frequency input can be derived and is detailed in Table 38 (for the target frequency of 80 Hz, as defined in Table 22). The derivation of the fuzzy logic model is given in §4.5.1, and illustrated in Figures 30 and 31.

Below 20 Hz a constant output of -3.25 Amps was applied, and above 400 Hz a constant output of +3.75 Amps - these conditions were taken to be considerably removed from the target condition.

Around the target frequency (75 to 85 Hz), the sensitivity of the derived output from the fuzzy logic model to the pool frequency was relatively high, since the density of the input membership functions was correspondingly high - this area covered the 'SO', slightly over-penetrated, 'FP', fully penetrated and 'PP', partially penetrated sets. This was in accordance with the known Mode 3 response of the pool in this area.

A flat response covered the transition area (Mode 1 to Mode 3), and a relatively less sensitive response was generated in the partial penetration area. Although the sensitivity of the fuzzy logic model was lower in this area, the magnitude of the applied control steps was obviously significantly higher (typically +3.0 Amps as noted in the table above) and thought to be adequate to generate a response nearer to the target set-point.

The model applied generated desired welding current changes of 0.1 Amp resolution to control the level of penetration around the target frequency. This level of resolution was offered by the AMI 207, although a way of remotely controlling the power source was not available. The experimental orbital system (described in §3.1.1) used the BDH 320 power source with a software controlled current resolution of ± 1 Amp only. Consequently, a dominant pool frequency (f_d) input of 73 Hz generated a fuzzy logic output of -0.52 Amps (rounded to -1 Amp by the 'delta-reader' software) and a 90 Hz pool frequency generated +0.52 Amps (rounded to +1 Amp).

This limit on the resolution of the base current (I_b) output variable results in a potential best control of the inner bead width of the *HS* cast to +0.3 mm, -0.2 mm around the target, and +0.4 mm, -0.3 mm of the *LS* cast (Table 34 - Mode 3 - *LS* and *HS* casts, $\Delta f_d / \Delta IBW$)². These figures represent the optimum performance and do not take into account overshoot of the pool size.

Performance of control system and full penetration welds

Note: A constant set-point welding current (I_b) was applied for the complete duration of the orbital cycle and the base current was controlled automatically by the user-interface PC running AMOS1 MON (in control mode incorporating the fuzzy interference engine) and 'delta-reader' software.

Despite the extremely high reliability of the power source response to requested current changes across the serial communications link when operated directly (shown in Figure 26), it was evident that there was an element of 'signal queuing' when integrated into the control system (see Figure 27). This was attributed to the decreased time available between pulses for the power source to react to the change demand and the internal prioritisation of communication tasks (by the BDH 320 software) and control of the pulsed welding current output from the inverter modules and error checking etc. Given the occasional observed simultaneous response to two demand signals, the reliability was also thought to be a potential

² Figures calculated from fuzzy logic rule 'firing', example shown below:

The -1 Amp control is generated by a monitored pool frequency (f_d) of 73 Hz (actual fuzzy model output -0.52 Amps). A target frequency of 80 Hz results in a frequency difference of 7 Hz. Therefore an associated sensitivity of 36.6 Hz/mm ($\Delta f_d / \Delta IBW$) results in a potential best control of -0.2 mm (7 Hz \div 36.6 Hz/mm) on the inner bead width for the *HS* Cast (sensitivity from Table 34).

error in the software handling by the power source of the demand signals.

The overall performance of the derived control system and fuzzy logic model can be judged by the full penetration welds made by the system. For the purposes of the discussion, the results provided by the closed-loop trials on the 'Cast 2' material yield the appropriate information.

Inner bead widths were generally controlled to within ± 0.5 mm for the 80 Hz target frequency for Tests I and II on 'Cast 2' material, the 'LS Kobe' material, and the 120 Hz target frequency weld on 'Cast 2' (see Figures 74, 75, 78 and 79). After some initially high pool frequency responses, stability was maintained over the remainder of Test III weld on the 'Cast 2' material (resultant inner bead width 3.5 to 5.1 mm). It is difficult to conjecture the cause of the higher frequency responses present at the start of Test III which caused the over-shoot, since transient arc voltage data was not stored by the AMOS1 MON software. The resultant variation in the inner bead profile would be unacceptable in practice. Despite the initial transgression from the desired target condition, the closed-loop system managed to gain control and establish the desired frequency.

The average bead widths for the three tests on 'Cast 2' were:

Test I	4.3 mm,
Test II	3.8 mm,
Test III	4.2 mm.

Since pool frequencies of between 73 and 90 Hz did not trigger delta-current outputs, there was some deviation of the established pool frequency about the target set-point (80 Hz in this case). For example, the established pool frequency during Test II was generally higher than Test I (resulting in a comparatively lower average inner bead width), although the frequency was several Hertz above the target (Test I frequencies were generally several Hertz *below* the target). It is partly to be expected then that although a consistent full penetration Mode 3 response was maintained for the weld runs some variation in the average inner bead width was produced in practice.

The actual operating performance is below the theoretical potential best as already discussed above (best control of *HS* cast - 0.5 mm range, actual achieved - 1.0 mm range). Some overshoot and variance is inevitable due to the relatively coarse nature of the control of the welding current and firing of the fuzzy logic rules, and the thermal lag associated with the weld pool itself. A 'peak' and 'trough' cycle of overshoot is illustrated by the

inner bead profile of the 'LS Kobe' material - as shown in Figure 78..

Aendenroemer's (1996) work based on frequency mode analysis and pulsed welding (ie. target the generation of a Mode 3 response in the peak current pulse, Mode 1 in the base current pulse) generated an inner bead width of between 2 and 4 mm (± 1 mm) on SS304 tubing that was 60 mm diameter, 3 mm wall thickness material ie. double the range produced here, for a larger wall thickness.

Closed-loop control of the state of penetration based on targeting a constant Mode 3 frequency response produces a variance in the inner bead width which is favourably comparable with work based on frequency mode analysis for pulsed procedures.

Application of the 8 Amp step increase proved too much for the stability of the pool frequency signal in 1.65 mm WT material (illustrated by Figure 81) and consequently resulted in an uncontrolled weld bead. The target frequency of 80 Hz was re-established after the step increases of 6 and 4 Amps were applied, although the sensitivity of the overall system to the pool frequency was such that a significantly long delay was experienced after the +4 Amp step. The response to the step changes is quite consistent with the known characteristics of the fuzzy model in conjunction with the limited resolution of the control variable (I_p), as already discussed. Suzuki's work (1991) also highlighted comparatively long settling times in the width of the lower surface after small step changes, illustrated in this work by the 2 Amp step increase (Figure 84).

In order to avoid the undesired excessively over-penetrated frequency response that is chaotic (when the base current is unreasonably large), a fuzzy logic model might be derived to recognise the *frequency pattern* and reduce the current accordingly by a large step change.

6.4.3 Summary

The Mode 3 frequency response was shown to offer a high degree of sensitivity to the inner bead width. Mode 1 oscillations offer a comparatively higher sensitivity but do not guarantee the formation of a lower free surface and the full penetration condition. Mode 3 target frequencies were used in the closed-loop system, with a fuzzy logic model relating the monitored pool frequency to the desired target and producing an appropriate change in the welding current in real-time. The closed-loop system was applied to several casts of material ('Cast 2', 'EP', and 'LS

Kobe') to produce orbital welds with full penetration for all the orbital positions. Stability of the system was demonstrated by re-establishing the desired target conditions after 'reasonable' step changes.

6.5 Overall discussion summary

Section summaries have been provided at the end of §6.2, §6.3 and §6.4. This summary highlights some of the more important aspects of the research work presented.

6.5.1 Theoretical modelling of pool behaviour

Undetermined variables implicit in the theoretical modelling of pool oscillation behaviour in moving weld pools make the application of even the simplest of the models, in a meaningful way, quite difficult. Variations of the acting surface tension (and the associated surface tension/temperature gradient) - which have been particularly well documented for austenitic stainless steels - complicate the situation further. By examining stationary pool behaviour, a correlation of observed behaviour with theoretical values (based on assumptions about the acting surface tension) derived from the plane circular Mode 3 model is however possible.

Published literature has consistently highlighted the association of the acting surface tension/temperature gradient with the *predominant flow regime* in relatively low current autogenous TIG weld pools, and all the measured pool oscillation variables can be used to make a prediction or assessment of the *overall acting surface tension* (based on the Mode 3 model). However, values calculated for the different material casts used in this research for a range of base currents did not offer much insight into the penetration behaviour of the casts - despite apparent observed differences between the casts. Theoretical predictions of surface tension based on the model of Mode 1 behaviour were also at odds with expectations.

Taken in isolation, theoretical models offer little information that is of use for predicting the frequency behaviour of moving weld pools since they are characteristically quite different in shape from stationary ones, and the only realistic model presented to date in the literature requires a further *empirically derived* parameter (Yoo, 1993). Given the additional unknown variables, singular measurements of frequency from actual weld pools cannot then be reliably employed to make reasonable assessments of surface tension or cast behaviour.

6.5.2 Application of pool frequency to cast behaviour and penetration control

If a 'time-to-penetrate' study is made, using the dominant pool oscillation frequency as a measure of the state of penetration (in a stationary pool) and the Mode 1 to 3 transition as an indicator of 'full' penetration, much more information is offered with regard to the cast/penetration behaviour of the material studied.

The 'time-to-penetrate' studies presented in this thesis produced clear pictures of the penetration behaviour, particularly with regard to the different developments within the pool as the welding current was increased - it is possible that an indication of the change in dominant flow regime in the pool as the welding current is increased may be given by the different transition times (particularly if a surface tension driven flow is being reversed - this was suspected in the 'LS Kobe' 1.65 mm WT low sulphur cast). Observations presented here suggest that cast differences are minimised as the welding current is increased - this was evident both in the stationary and moving pool studies.

Use of the 'time-to-penetrate' characteristic *in conjunction with* theoretical predictions of surface tension (from plane circular pools using the Mode 3 model) provide more data about the response of the material cast studied to welding conditions (and the likely behaviour of the material for the case of the moving weld pool).

Mode 1 and 3 pool oscillations offer a high degree of sensitivity to the inner bead width formed, and a target penetration level can be maintained if the oscillation frequency is closely controlled. This research work shows the *closed-loop control* of penetration, of several casts of material, to ± 0.5 mm inner bead width (38.1 mm diameter, resulting in a weld length of 120 mm), by pulsing at 3 Hz. (An enhanced level of control for this application would be offered by a finer resolution of current from the power source, typically ± 0.1 Amps.)

Stability of the control system was demonstrated by the re-establishment of the target condition after externally imposed step changes in the base current of a reasonable magnitude (an excessively large change, 8 Amps *above* full penetration, produced a chaotic response in the pool frequency signal itself). In the absence of reliable theoretical models of pool oscillation behaviour, fuzzy logic provided a suitable framework for a non-linear control strategy, which accounted for the transition between Mode 1 and 3 pool oscillation behaviour.

SECTION 7.
CONCLUSIONS

7. CONCLUSIONS

The research work presented in this thesis has focused upon the development of the pool oscillation technique to penetration control for orbital welding ultra-high purity tubing. The effect of cast variation has also been studied in detail since it is inherent in the austenitic stainless steel materials that are used. From the work presented, it can be concluded that:

- The full penetration condition can be controlled in a typical ultra-high purity orbital joint using weld pool oscillations, monitored via the arc voltage, and modulating the welding current according to a single-input single-output fuzzy logic model that accounts for the non-linear transition between the Mode 1 and Mode 3 frequency response.
- Additional analogue signal processing circuitry, and the use of software 'post-processing' enhance the clarity of partial penetration signals (Mode 1 oscillation) thereby increasing the sensitivity and repeatability of signals detected from quite small molten pools.
- Cast variations in austenitic stainless steel tubing studied have an effect upon the frequency of pool oscillation that is in accordance with the penetration behaviour, both for stationary and moving weld pools, for example, welds made in casts that are less fully penetrated have comparatively higher pool frequencies (for the same welding conditions).
- The use of the pool oscillation frequency and the geometry of the associated weld pool to predict a value of 'acting' surface tension or the surface tension/temperature behaviour seems difficult, and the behaviour of some of the material casts observed does not necessarily accord with what might be expected if the Marangoni model of surface tension driven flow is assumed to be a dominant factor.
- By monitoring the frequency of the pool oscillation in a stationary 'spot' weld test, a characteristic evaluation of the material weldability can be made by a comparative evaluation of the 'time-to-penetrate' (where this is taken to be a transition from a Mode 1 to Mode 3 frequency response), enabling materials that are difficult to weld to be rapidly identified.

-
- Differences in the penetration behaviour identified in 1.65 mm wall thickness tubing (with different material casts) were minimised at higher levels of welding current - this was apparent in both moving weld pools and identified accordingly in the 'time-to-penetrate' studies by the transition times from a Mode 1 to a Mode 3 response.
 - Software used to monitor pool oscillations and provide a method of penetration control can be integrated into an orbital welding system as an additional utility, with only the addition of signal processing and analogue-to-digital hardware.
 - Both Mode 1 and Mode 3 oscillations offer a high degree of sensitivity to the inner bead width generated in typical ultra high purity welds, although Mode 1 oscillations occur for both partial and full penetration conditions.

IMPLICATIONS OF THE RESEARCH

The software derived was applied to an orbital welding control system effectively as an 'add-on' control function, without disturbing the established performance of the system. Use of a Pentium P90 PC for the user-interface computer enabled an optimised speed of operation - applying pulses at 2 and 3 Hz. Future, faster PCs could enable the application of an FFT with more points and further enhanced mathematical treatments of the pool oscillation signals in the software (given the characteristic difference between Mode 1 and Mode 3 signals). The only additional hardware used was the signal conditioning and analogue-to-digital conversion card.

A more basic and compact system for practical application might comprise a single PC controlling the welding power source, monitoring the pool oscillations and adapting the welding current demand accordingly, without the need for an intermediate control processor.

Control in response to variations in thickness and heat-sinking is still a very desirable objective within industry (see Ushio, 1994, for example). The application of pool oscillations as a top-face sensing technique without intrusion into the welding environment has been shown to offer a potential control solution for orbital tubing, as well as an indicative technique for the evaluation of cast behaviour - other applications (seam welding with variable heat-sinking, for example) might also benefit from the implementation of this technique.

SUGGESTIONS FOR FURTHER WORK

It is suggested that future work should comprise:

- Incorporating more than one characteristic of the pool oscillation response into the control strategy (both the amplitude and the frequency of the response might be used) with a two-input, single-output fuzzy logic control model.
- Hardware FFTs for faster analogue/digital processing could also enable more time for software data storage (storing the transient signals for later analysis for example).
- Using a single PC solution to effect the welding control and the data logging might also offer a straightforward system with minimal data handling / file transfer.
- Developing optimised fuzzy logic models for penetration control that recognise and account for the less predictable patterns of behaviour (frequency response to the severely under- and over-penetrated states).
- Including adaptive algorithms that account for the specific case of the GTA weld pool and alter the developed model accordingly.

It would also be extremely interesting to consider other processes, such as plasma welding (in both the melt-in and the keyhole modes).

REFERENCES

(All the references are arranged alphabetically.)

- a. **Aendenrooier, A.J.R., and den Ouden, G. (1994).** 'Weld pool oscillation during pulsed GTA welding'.
IIW Doc. 212-874-94.
- Aendenrooier, A.J.R. (1996).** *Weld pool oscillation for penetration sensing and control.*
Doctorate Thesis, University of Delft, The Netherlands.
- Allum, C.J. (1981).** 'Gas flow in the column of a TIG welding arc'.
J. Phys. D: Appl. Phys., 14, pp1041 to 1059.
- Andersen, K. (1993).** *Synchronous weld pool oscillation for monitoring and control.*
Doctorate Thesis, Vanderbilt University, Nashville, Tennessee, USA.
- Anderson, P.C.J. (1995).** 'Sensor systems for top-face penetration control'.
Industrial Robot, Vol. 22 No. 4, pp12 to 15.
- b. **Barabokhin, N.S., et al. (1976).** 'The gas-dynamic pressure of an open pulsed arc'.
Welding Production (Svar. Proiz.), No. 2, pp4 to 6.
- Barborak, D., and Richardson, R. (1994).** 'Development of pool dynamics software for weld pool oscillation sensing'.
Computer Technology in Welding, Paris, France, 15-16 June.
- Barnett, R.J., Andersen, K., Cook, G.E., and Strauss, A.M. (1992).** 'Weld quality enhancement using precision multi-parameter control in gas tungsten arc welding'.
Proc. 3rd Int. Conf. on Trends in Welding Research, Gatlinburg, TN, USA, 1-5 June.
- Becker, D.W., and Adams, C.M. (1978).** 'Investigation of pulsed GTA welding parameters'.
Welding Journal, May, pp134-s to 138-s.
-

References

- Bicknell, A., Smith, J.S., and Lucas, J. (1994). 'Arc voltage sensor for monitoring of penetration in TIG welds'.
IEE Proc. - Sci. Meas. Technol., Vol. 141, No. 6, pp513 to 520.
- Bishop, O. (1993). 'How Fourier can help analyse electronic waveforms'.
Electronics World and Wireless World, August, pp692 to 698.
- Boughton P., and Males, B.O. (1973). 'Penetration characteristics of pulsed TIG welding'.
Welding Research International, Volume 3, Number 1, pp47 to 71.
- c. Campbell, R.D., Heiple, C.R., Sturgill, P.L., Robertson, A.M., and Jamsay, R. (1993). 'Surface preparation effects on GTA weld shape in JBK-75 stainless steel'.
Welding Journal, February, pp67-s to 78-s.
- Connelly, C., Fetzer, G.J., Gann, R.G., and Aurand, T.E. (1986). 'Reliable welding of HSLA steels by square wave pulsing using an advanced sensing (EDAP) technique'.
Advances in Welding Science & Technology : TWR '86, Proceedings of an International Conference on Trends in Welding Research, S.A. David ed., ASM International, pp419 to 423.
- Cornu, J. (1988). *Advanced welding systems: TIG and related processes*.
IFS Publications, Bedford, UK.
- d. Deam, R.T. (1989). 'Weld pool frequency: a new way to define a weld procedure'.
Proc. 2nd Int. Conf. on Trends in Welding Research, Gatlinburg, TN, USA.
- Doumanidis, C.C. (1994). 'Multiplexed and distributed control of automated welding'.
IEEE Control Systems, IEEE, p14.
- e. Ecer, G.M., Tzavaras, A., Gokhale, A., and Brody, H.D. (1981). 'Weld pool fluid motion and ripple formation in pulsed current GTAW'.
Proceedings of Conference on Trends in Welding Research in The United States, New Orleans, Louisiana, 16 to 18 November, pp419 to 442.
- g. Glickstein, S.S. (1982). 'Basic studies of the arc welding process'.
Trends in Welding Research in the United States, S.A. David ed., ASM, pp3 to 51.
-

References

- h. **Hardt, D.E., Garlow, D.A. and Weinert, J.B. (1985).** 'A model of full penetration arc-welding for control system design'.
Journal of Dynamic Systems, Measurement and Control, Vol. 107, pp40 to 46.
- Heiple, C.R., and Roper, J.R. (1982).** 'Mechanism for minor element effect on GTA fusion zone geometry'.
Welding Journal, April, pp97-s to 102-s.
- Heiple, C.R., Roper, J.R., Stagner, R.T., and Aden, R.J. (1983).** 'Surface active element effects on the shape of GTA, laser, and electron beam welds'.
Welding Journal, March, pp72-s to 77-s.
- Hiraoka, K., Okada, A., Inagaki, M. (1986).** 'Effect of electrode geometry on maximum arc pressure in Gas Tungsten Arc welding'.
Transactions of National Research Institute for Metals, Vol. 28, No. 1, pp63 to 70.
- Hirata, Y., and Maruo, H., (1994).** 'Gas Tungsten Arc discharge phenomena by pulsed current supplied from experimental power source with pulse forming network circuit'.
IIW Doc. 212-865-94, Welding and Production Department, Osaka University, Osaka, Japan.
- Hinata, T., Yasuda, K., Kasuga, Y., and Onzawa, T. (1994).** 'Penetration shape and welding of real joints by a travelling TIG arc (2nd Report). Study of low-speed DC TIG welding'.
Welding International, 8(9), pp684 to 689.
- Hooijmans, J.W., and den Ouden, G. (1995).** 'Influence of hydrogen on arc properties and weld pool geometry during GTA welding of austenitic stainless steel'.
Unpublished.
- i. **Iida, T. (1994).** 'Physical properties of liquid metals [IV] - surface tension and electronic transport properties of liquid metals'.
Welding International, 8(10), pp766 to 770.
- k. **Kaneko, Y., Iisaka, T., Oshima, K., and Yamane, S. (1995).** 'Neuro-fuzzy control of the weldpool in pulsed MIG welding'.
Welding International, 9(3), pp191 to 196.
-

References

- Keene, B.J., Mills, K.C., and Brooks, R.F. (1985). 'Surface properties of liquid metals and their effects on weldability'.
Materials Science and Technology, July, Vol. 1.
- Key, J.F. (1980). 'Anode/cathode geometry and shielding gas interrelationships in GTAW'.
Welding Journal, December, pp364-s to 370-s.
- Kosko, B. (1994). *Fuzzy thinking*.
Harper Collins.
- Kotecki, D.J., Cheever, D.L. and Howden, D.G. (1972). 'Mechanism of ripple formation during weld solidification'.
Welding Journal, 51(8) pp386-s to 391-s.
- Kovacevic, R., Zhang, Y.M. and Li, L. (1996). 'Monitoring of weld joint penetration based on weld pool geometrical appearance'.
Welding Journal, October, pp317-s to 328-s.
- Krüger, J. and Marya, S.K. (1994). 'On recent trends in orbital TIG welding of tubes'.
International Journal for the Joining of Materials, Vol. 6(1), pp27 to 32.
- Kulik, V.I., Ostrovskii, O.E., Novikov, O.M., and Borisov, E.M. (1993). 'Orbital arc welding pipelines'.
Welding International, 7(11), pp901 to 904.
- I. Lambert, J.A. (1991). 'Cast-to-cast variability in stainless steel mechanized GTA welds'.
Welding Journal, May, pp41 to 51.
- Lancaster, J.F. (1984). *The physics of welding*.
Pergamon Press Ltd, Oxford, UK.
- Lee, H.J., and Na, S.J. (1991). 'A study on heat flow in circumferential pipe welding using a semi-analytical finite element method'.
Proc. Instn. Mech. Engrs, Vol. 205, pp179 to 185.
- Lho, T.J., and Na, S.J. (1992). 'A study on parameter optimization with numerical heat conduction model for circumferential Gas Tungsten Arc (GTA) welding of thin pipes'.
Proc. Instn. Mech. Engrs, Vol. 206, pp102 to 111.

References

Lillquist, R.D., and Case, A.W. (1987). *Method and apparatus for measuring weld penetration in an arc welding process*.

U.S. Patent N° 4,711,986.

Lin, W., Dexiang, D., and Dinghus, C. (1987). 'Detection and analysis of weld penetration in stationary TIG arc welding - a preliminary study'.

Welding International, No. 5, pp475 to 479.

Lucas, W. (1992). 'Shielding gases for arc welding - part 1'.

Welding and Metal Fabrication, June, pp218 to 225.

Luijendijk, T., and Holt, M. (1995). 'Shielding gas and weld pool penetration during GTA welding of stainless steel'.

IIW Doc. XII-1407-95, Delft University of Technology, The Netherlands.

Lundin, C. (1990). 'Weldability of austenitic stainless steels for the 1990s and beyond'.

Proceedings from the First United States - Japan Symposium on Advances in Welding Metallurgy, San Francisco, California, 7 to 8 June, and Yokohama, Japan, June 12 to 13, p420 to 438.

m. Madigan, R.B., Renwick, R.J., Farson, D.J., and Richardson, R.W. (1986). 'Computer based control of full penetration GTA welds using pool oscillation sensing'.

Proceedings of the 1st International Conference on Computer Technology in Welding, June.

Maruo, H., and Hirata, Y. (1985). 'Study on pulsed TIG welding'.

IIW Doc. SG212-621-85, Welding Department, Osaka University, Japan.

Maruo, H., and Hirata, Y. (1993). 'Natural frequency and oscillation in fully penetrated pool'.

IIW Doc. 212-834-93, Welding Department, Osaka University, Japan.

Matsunawa, A. (1982). 'The role of surface tension in fusion welding'.

Transactions of JWRI, Vol. 11, No. 2.

Mills, K.C. (1993). 'The effects of welding parameters on penetration in GTA welds'.

Welding Journal, July, pp347-s to 353-s.

Motorola, (1992). *Fuzzy logic education program*.

(Software for Windows 3.1).

References

- n. Nakata, K., Matsuda, F., Jogan, S., Harada, S., and Ueyama, T. (1994). 'Improvement of weld solidification crack susceptibility of Al-Zn-Mg ternary alloy by low-frequency pulsed GMA (MIG) welding with trial-manufactured Zr-added Al-high-Mg welding wire'.
Welding International, 8(9), pp690 to 696.
- Nomura, H., (1994). *Sensors and control systems in arc welding*.
Chapman and Hall, London, UK.
- Norrish, J. (1992). *Advanced welding processes*.
IOP Publishing Ltd, Bristol, UK.
- o. Omar, A.A., and Lundin, C.D. (1979). 'Pulsed plasma - pulsed GTA arc: a study of the process variables'.
Welding Journal, April, pp97-s to 105-s.
- den Ouden, G., Xiao, Y.H., and Hermans, M.J.M., (1993). 'The role of weld pool oscillation in arc welding'.
International Journal for the Joining of Materials, Vol 5(4), pp123 to 129.
- p. Pitscheneder W., DebRoy, T., Mundra, K., and Ebner, R. (1996). 'Role of sulfur and processing variables on the temporal evolution of weld pool geometry during multikilowatt laser beam welding of steels'.
Welding Journal, March, pp71-s to 80-s.
- Pollard, B. (1988). 'The effects of minor elements on the welding characteristics of stainless steel'.
Welding Journal, September, pp202-s to 213-s.
- Postacioglu, N., Kapadia, P., and Dowden, J. (1991). 'Theory of the oscillations of an ellipsoidal weld pool in laser welding'.
Journal of Physics D.: Applied Physics, 24, pp1288-1292.
- q. Quigley, M.B.C. (1977). 'Physics of the welding arc'.
Welding and Metal Fabrication, December.
- r. Richardson, I.M. (1991). *Properties of the constricted Gas Tungsten (Plasma) welding arc at elevated pressures*.
Ph.D. Thesis, Cranfield University, UK.

References

- Richardson, R.W., and Ludewig, H.K. (1989). 'The effect of weld parameter variations on pool oscillations in full-penetration welds.'
Edison Welding Institute Research Report, MR8901, January, USA.
- s. Saedi, H.R., and Unkel, W. (1988). 'Arc and weld pool behaviour for pulsed current GTAW'.
Welding Journal, November, pp247-s to 255-s.
- Sandford, A. (1994). 'Hi-tech, low tech or no tech ?'
Metalworking Production, May.
- Savage, W.F., Nippes, E.F., and Agusa, K. (1979). 'Effect of arc force on defect formation in GTA welding'.
Welding Journal, July, pp212-s to 224-s.
- Semak, V.V., Hopkins, J.A., McCay, M.H., McCay, T.D., and West, J.C. (1995). 'Weld pool oscillations in laser welding'.
Laser Materials Processing Conference (ICALEO '95), San Diego, California, 13 to 16 November, pp739 to 748.
- Shirali, A.A., and Mills, K.C. (1993). 'The effect of welding parameters on penetration in GTA welds'.
Welding Journal, July, pp347-s to 353-s.
- Sorensen, C.D., and Eagar, T.W. (1989). 'Digital signal processing as a diagnostic tool for gas tungsten arc welding'.
Proceedings of the 1st International Conference on Trends in Welding Research, Gatlinburg, Tennessee, USA, 14 to 18 May, pp967 to 971.
- Suga, Y., and Tokiwa, T. (1996). 'Penetration control by detecting oscillation of weld pool in automatic TIG arc welding'.
Proceedings of the 6th International Offshore and Polar Engineering Conference, Los Angeles, USA, 26 to 31 May, pp185 to 189.
- Suzuki, A., Hardt, D.E., and Valavani, L. (1991). 'Application of adaptive control theory to on-line GTA weld geometry regulation'.
Journal of Dynamic Systems, Measurement and Control, March, Vol. 113, pp93 to 103.
- t. Takeuchi, Y., Takagi, R., and Shinoda, T. (1992). 'Effect of bismuth on weld joint penetration in austenitic stainless steel'.
Welding Journal, August, pp283-s to 289-s.
-

References

- Tam, A.S., and Hardt, D.E. (1989).** 'Weld pool impedance for pool geometry measurement: stationary and non-stationary pools'.
Journal of Dynamic Systems, Measurement and Control, December, Vol. 111, pp545 to 553.
- Tapp, J. (1996).** The Welding Institute - private communication.
- Tsuruha, M. (1990).** *Standard welding procedure based on OSK ultra-clean gases technology, Vol. 1 - general outline.*
OSK Technical Centre, Japan.
- Turner, I.W. (1985).** *An investigation of the interaction between pulsed-TIG welding parameters and the effect of arc gap.*
M.Sc. Thesis, Cranfield University, UK.
- u. **Ushio, M., et al. (1994).** 'The state-of-the-art and the subjects of arc welding automation in various industries in Japan.'
IIW Doc. XII-1359-94.
- w. **Wareing, A.J. (1989).** *Investigations into changes in the GTAW process parameters on the effects of cast/cast variation in austenitic stainless steels.*
M.Sc. Thesis, Cranfield University, UK.
- Wang, Q.L, Zhang, J.H., and Yang, C.L. (1988).** 'Detection of the weld full penetration signals of a travelling arc in GTAW'.
IIW Asian Pacific Regional Welding Congress and 36th AWI Conference,
Hobart, 14-18 November.
- Wang, Q.L., Yang, C.L., and Geng, Z. (1993).** 'Separately excited resonance phenomenon of the weld pool and its application'.
Welding Journal, Research Supplement, September, pp455-s to 462-s.
- Wen, J., and Lundin, C.D. (1986).** 'Technical note: surface tension of 304 stainless steel under welding conditions'.
Welding Journal, Research Supplement, May, p138-s.
- Wu, C. S., and Liu, Y.C. (1996).** 'Rule-based control of weld bead width in pulsed gas tungsten arc welding (GTAW).'
Proc. Instn. Mech. Engrs Part B: Journal of Engineering Manufacture,
Vol 210, p93 to 98.
-

References

- x. **Xiao, Y.H., and den Ouden, G. (1993).** 'Weld pool oscillation during GTA welding of mild steel'.
Welding Journal, Research Supplement, August, pp428-s to 434-s.
- Xiao, Y.H. (1992).** *Weld pool oscillation during Gas Tungsten Arc welding*.
Doctorate Thesis, University of Delft, The Netherlands.
- Xiao, Y.H., and den Ouden, G. (1994).** 'Measurement of surface tension of liquid metals & alloys under arc welding conditions'.
IIW Doc. 212-875-94.
- y. **Yamane, S., Ohshima, K. and Kohashi, Y. (1993).** 'Sensing and fuzzy logic control of weld pools in pulsed MIG welding'.
Welding International, No. 7, p378 to p383.
- Yasuda, K., Hinata, T., Jimma, T., and Onzawa, T. (1989).** 'Investigations into the phenomena of high speed one-sided welding of thin sheet, paying attention to arc force'.
Welding International, No. 10, p866 to 871.
- Yoo, C.D., and Richardson, R.W. (1993).** 'An experimental study on sensitivity and signal characteristics of weld pool oscillation'.
Transactions of the Japan Welding Society, Vol. 24, No. 2.
- z. **Zacksenhouse, M., and Hardt, D.E. (1983).** 'Weld pool impedance identification for size measurement and control'.
Journal of Dynamic Systems, Measurement and Control, September, Vol. 105, pp179 to 184.
- Zacharia, T., David, S.A., Vitek, J.M., and Kraus, H.G. (1995).** 'Surface temperature distribution of GTA weld pools on thin-plate 304 stainless steel'.
Welding Journal, Research Supplement, November, pp353-s to 362-s.
- Zacharia, T. and David, S.A. (1993).** 'Heat and fluid flow in welding'.
Mathematical modelling of weld phenomena.
Institute of materials, UK, pp4 to 38.
- Zadeh, L.A. (1965).** 'Fuzzy sets'.
Information and Control, Vol. 8, pp338 to 353.
-

References

Zhao, J., Zhao, J., Sun, D., Lu, D., and Hu, S. (1988). 'A study of diagnosing pulsed high-frequency TIG welding arc plasma by microcomputer image processing'.

IIW Asian Pacific Regional Welding Congress 1988, Australian Welding Institute, pp584 to 593.

Zijp, J., and Hiraoka, K. (1994). 'Basic parameters of heat transport in argon-helium mixed gas arcs'.

Welding International, 8 (7), pp518 to 524.

Zimmerman, H.J. (1991). *Fuzzy set theory and its applications*.

Kluwer Academic Publishers Group, The Netherlands.

APPENDED TABLES AND FIGURES

SS316 Material	Temperature Range	Surface Tension γ	dy/dT
sample A (poor weldability) ie. low surface activity	1500°C to 1800°C	2.00 to 1.90 N/m	-ve
sample B (good weldability) ie. high surface activity	- as above -	1.60 to 1.70 N/m	+ve

Table 1 Surface tension and cast, Keene (1985)

Power sources & controllers	Arc Machines AMI 207 Orbital TIG welder (Inverter) Migatronik BDH 320 Triple Commander (Inverter) Isotek control rack
Torches/heads	Arc Machines AMI 9-1500, 9-4500 orbital heads Migatronik manual TIG torch
Shielding gases	Argon (BOC Pureshield) Argon with 5% hydrogen addition (BOC Special Gas) Argon with 10% hydrogen addition (BOC Special Gas) Helium (Commercial Grade) (99.999% Purity)
Purge gas	Argon (99.999% Purity)
Tungstens	2% Thoriated (ϕ 1.6, 2.4 mm) <i>unless otherwise specified in the Experimental programme section, a standard geometry of 30° tip angle with a 0.7 mm flat was used</i>
Signal conditioning	ArcWatch™ signal conditioning interface (passive RC filter) Migatronik signal conditioning interface (active 4th order, 6-Pole Butterworth 10 kHz low pass filter)
A/D Conversion	Amplicon PC30D A/D converter (200 kHz maximum sampling frequency)
Processors	Elonex 486 DX 33MHz, 16MB RAM, 500MB HDD Pentium P90, 8MB RAM, 1000MB HDD
Software	ArcWatch™ (version 4.0) ArcWatch™ (for selected FFT sampling) Fortran programs for FFT conversion Brite LOG (real-time graphical logging FFT for pool oscillation detection, analysis and data output) AMOS1 MON (real-time text based logging for analysis, data and control function output) Microsoft Excel™ (Version 4.0 and 5.0)
Square butt joint preparation	Tri-Tool tube/pipe facing machine GA-3075 tool bits

Table 2 Overview of equipment

Real-time Performance of Oscillation Software (Pentium P90 Processor)

Sample Rate (kHz)	Window Size (points)	Logging Time (ms)	FFT Sample Size	N°. of Windows per Minute				Max. Operating Frequency (Hz)				Computation Time (Secs)			
				1	2	3	4	1	2	3	4	1	2	3	4
8	256	128	210	316	345	308	298	5.3	5.8	5.1	5.0	19.6	15.8	20.6	21.9
10	256	102	210	360	410	354	342	6.0	6.8	5.9	5.7	23.1	18.0	23.8	25.0
16	256	64	210	484	555	456	430	8.1	9.3	7.6	7.2	29.0	24.5	30.8	32.5
20	256	51	210	530	630	500	475	8.8	10.5	8.3	7.9	32.9	27.7	34.4	35.7
8	512	256	400	188	195	183	178	3.1	3.3	3.1	3.0	11.9	10.1	13.2	14.4
10	512	205	400	220	242	218	215	3.7	4.0	3.6	3.6	14.9	10.4	15.4	16.0
16	512	128	400	308	340	300	291	5.1	5.7	5.0	4.9	20.6	16.5	21.6	22.8
20	512	102	400	360	401	345	330	6.0	6.7	5.8	5.5	23.1	18.9	24.7	26.2
8	1024	512	978	103	105	100	99	1.7	1.8	1.7	1.7	7.3	6.2	8.8	9.3
10	1024	410	978	124	130	123	117	2.1	2.2	2.1	2.0	9.2	6.8	9.6	12.1
16	1024	256	978	179	194	178	176	3.0	3.2	3.0	2.9	14.2	10.3	14.4	14.9
20	1024	205	978	212	233	210	208	3.5	3.9	3.5	3.5	16.6	12.3	17.0	17.4

- 1 'Brite AMOS' Graphics Program on Pentium P90
- 2 'AMOS1 MON' Text Program running as DOS Session on C:\
- 3 'AMOS1 MON' Text Program running as DOS Session on RAMDRIVE under OS/2
- 4 - as for 3 - with User-Interface Orbital Welding Software running (COMMS line open)

Table 3 Real-time performance of oscillation software

N°	Experimental identification	Certified type	Specified size	Manufacturer
1	'Cast 1'	316L (S)	ϕ1.5" x 16SWG <i>ϕ38.1mm x 1.63mm WT</i>	Schoeller Bleckmann, Germany
2	'Cast 2'	316L (S)	ϕ1.5" x 16SWG <i>ϕ38.1mm x 1.63mm WT</i>	Schoeller Bleckmann, Germany
3	'LS Kobe'	316L (S)	ϕ1.5" x 16SWG <i>ϕ38.1mm x 1.63mm WT</i>	Kobe Steel, Japan
4	'EP' (Electro-polished bore)	316L (S)	ϕ1.5" x 16SWG <i>ϕ38.1mm x 1.63mm WT</i>	AST (Avesta Sandvik Tube), Sweden
5	'35 mill.'	316L (S)	ϕ35mm x 2mm WT	Sandvik, Sweden
6	'280410'	304 (W)	2" Pipe x 40 Schedule <i>ϕ60.3mm x 3.91mm WT</i>	Mannesman
7	'MS097'	304 (W)	2" Pipe x 40 Schedule <i>ϕ60.3mm x 3.91mm WT</i>	Sandvik
8	'2" Pipe 2'	316L (W)	2" Pipe x 40 Schedule <i>ϕ60.3mm x 3.91mm WT</i>	AST, Sweden
9	'2" Pipe 4'	304L (W)	2" Pipe x 40 Schedule <i>ϕ60.3mm x 3.91mm WT</i>	AST, Sweden
10	'1.5" Thick'	316 (S)	ϕ1.5" x 0.125" <i>ϕ38.1mm x 3.18mm WT</i>	Kobe Steel, Japan

Table 4 Tube and pipe material description

Notes: the units for diameter and wall thickness (WT) are those used by the suppliers (ie. both metric and imperial) - where imperial units are the declared material size, a metric conversion is supplied below *in italics*.

(S) - seamless tube, (W) - welded pipe/tube

N°.	Experimental identification	C	Si	Mn	P	S	Cr	Mo	Ni
1	'Cast 1'	0.010	0.42	1.41	0.025	0.011	16.97	2.11	11.30
2	'Cast 2'	0.025	0.30	1.43	0.027	0.006	17.11	2.11	12.12
3	'LS Kobe'	0.032	0.38	1.63	0.030	0.001	16.91	2.13	11.53
4	'EP' (Electro-polished bore)	0.024	0.58	1.57	0.024	0.007	17.17	2.55	13.59
5	'35 mill.'	0.001	0.40	1.56	0.023	0.006	17.24	2.52	12.92
6	'280410'	0.010	0.30	1.66	0.014	0.003	18.32	0.02	10.71
7	'MS097'	0.012	0.50	1.17	0.010	0.004	18.24	0.06	10.13
8	'2" Pipe 2'	0.018	0.38	1.49	0.026	0.006	17.28	2.04	11.18
9	'2" Pipe 4'	0.020	0.39	1.38	0.028	0.006	18.44	-	9.07
10	'1.5" Thick'	0.037	0.40	1.66	0.027	0.002	16.55	2.12	11.24

Table 5 Tube and pipe material certificate chemical composition
(as supplied)

Note: the Molybdenum content of 9. '2" Pipe 4' was not declared by the steel suppliers and is presumed to be close to zero as it is SS304 certified.

SG:	Ar 5% H ₂ @ 12 l/min	PG:	Ar @ 4 l/min
I_p:	100 A. for 0.01 s	I_b:	25 A. for 1.00 s
S:	60 mm/min	L_{arc}:	1.3 mm
PS:	AMI 207	Head:	9-1500

| **Anode:** SS316L ϕ 1.5" 16SWG tube ('Cast 1') | | | |

Table 6 Initial pool oscillation welding parameters

SG:	Ar 10% H ₂ @ 12 l/min		
I:	17.5, 20.0, 25.0, 30, 35, 40, 50, 60, 80 and 100 Amps		
L_{arc}:	1.0, 1.5 and 2.0 mm		
PS:	AMI 207	Head:	9-1500

| **Anode:** solid copper cylinder ϕ 1.5" | | | |

Table 7 AMI 207 V/I characteristic static arc parameters

SG:	Ar, Ar 1.5% H ₂ and Ar 10% H ₂ @ 12 l/min		
I_p:	125 Amps for 0.01 s	I_b:	25 Amps for 0.49 s
S:	-	L_{arc}:	1.3 mm
PS:	AMI 207 & BDH320 Head: 9-1500		

| **Anode:** solid copper cylinder ϕ 1.5" | | | |

Table 8 Pulsed current on copper static arc parameters

SG:	Ar 10% H ₂ @ 12 l/min	PG:	Ar @ 4 l/min
I_p:	125 A. for 0.01 s	I_b:	12.5 and 27.5 A. for 0.49 s
S:	90 mm/min	L_{arc}:	1.3 mm
PS:	AMI 207	Head:	9-1500

Anode: SS316L ϕ 1.5" 16SWG tube ('Cast 1')

Table 9 Typical partial and full penetration pool oscillation welding parameters used for the optimisation of the arc voltage signal response

SG:	Ar 5% & 10% H ₂ @ 12 l/min	PG:	Ar @ 4 l/min
I_p:	75, 100, 125 and 150 A.	I_b:	15.0 Amps for 4 s (no pulse) followed by 30.0 Amps for 10 s (with pulse)
t_p:	5, 10, 15 and 20 ms (pulsing @ 2 Hz)		
S:	-	L_{arc}:	1.3 mm
PS:	AMI 207, BDH 320	Head:	9-1500

Anode: SS316L ϕ 35mm 2 mm WT tube ('35 mill.')

Table 10 Stationary spot welding parameters
- peak current and time study

SG:	Ar 10% H ₂ @ 12 l/min	PG:	Ar @ 4 l/min
I_p:	125 A. for 0.01 s	I_b:	10.0, 12.5, 15.0, 17.5, 20.0, 22.5, 25.0 and 27.5 A. for 0.49 s (32.5 A. for '35 mill.')
S:	90 mm/min	L_{arc}:	1.3 mm
PS:	AMI 207	Head:	9-1500

**Anode: SS316L ϕ 1.5" 16SWG tube ('Cast 1') and
 ϕ 35mm 2 mm WT tube ('35 mill.')**

Table 11 Standard welding parameters
- variation in penetration and orbital position

1.	I_p : 100 A.	I_b : 30 A.	S: 90 mm/min
2.	I_p : 100 A.	I_b : 25 A.	S: 60 mm/min
3.	I_p : 100 A.	I_b : 20 A.	S: 30 mm/min
4.	I_p : 125 A.	I_b : 30 A.	S: 90 mm/min
5.	I_p : 125 A.	I_b : 25 A.	S: 60 mm/min
6.	I_p : 125 A.	I_b : 20 A.	S: 30 mm/min

Table 12 Travel speed and peak current magnitude effect on inner bead profile

SG:	Ar 10% H ₂ @ 12 l/min	PG:	Ar @ 4 l/min
I_p :	125 A. for 0.01 s	I_b :	1. 28.0 A. 2. 36.0 A. 3. 44.0 A. for 0.49 s
S:	90 mm/min	L_{arc} :	1.3 mm
PS:	AMI 207	Head:	9-4500
Anode: SS316L 2 inch pipe 2.5 mm WT tube ('2" Pipe 2')			

Table 13 Base current and penetration effect on outer bead appearance

SG:	Ar 10% H ₂ @ 12 l/min	PG:	Ar @ 4 l/min
I_p :	125 A. for 0.01 s	I_b :	1. 32.5 A. 2. 43.5 A. 3. 55.0 A. 4. 65.0 A. for 0.49 s
S:	1. 83 mm/min 2. 110 mm/min 3. 165 mm/min 4. 220 mm/min	L_{arc} :	1.3 mm
PS:	AMI 207	Head:	9-1500
Anode: SS316L ϕ 35 mm 2 mm WT tube ('35 mill.')			

Table 14 Welding parameters - travel speed variation and signal quality

SG:	Ar 10% H ₂ @ 12 l/min	PG:	Ar @ 4 l/min
I_p:	125 A. for 0.01 s	L_{wo}:	1.3 mm
I_b:	15.0, 17.5, 20.0, 22.5 and 25.0 A. (16SWG material), plus 27.5, 30.0, 32.5 and 35 A. (2.0 mm WT) for 0.49 s		
PS:	AMI 207	Head:	9-1500

Anode: SS316L ϕ 1.5" 16SWG tube ('Cast 1, Cast 2, LS Kobe, EP')
and ϕ 35mm 2 mm WT tube ('35 mill.')

Table 15 Time-to-penetrate and surface tension
study parameters (Part 1)

SG:	Ar 10% H ₂ @ 14 l/min	PG:	Ar @ 4 l/min
I_p:	135 A. for 0.01 s	L_{wo}:	1.8 mm
I_b:	40 A. for 0.49 s		
PS:	AMI 207	Head:	9-4500

Tungsten: ϕ 2.4mm 2% thoriated with 30° tip angle
and ϕ 0.7mm tip flat

Anode: 2 Inch schedule 10 pipe - ('280410', 'MS097',
'2" Pipe 2' and '2" Pipe 4')

Table 16 Time-to-penetrate and surface tension
study parameters (Part 2)

SG:	Ar @ 12 l/min	PG:	Ar @ 4 l/min
I_p:	74 A. for 0.20 s	I_b:	20 A. for 0.20 s
S:	120 mm/min	L_{arc}:	1.3 mm
PS:	AMI 207	Head:	9-1500

Anode: SS316L ϕ 1.5" 16SWG tube ('Cast 1' and 'LS Kobe')

Table 17 Standard pulsed TIG welding procedure

SG:	Ar 10% H₂ @ 12 l/min	PG:	Ar @ 4 l/min
I:	15.0, 20.0 and 25.0 A.		
S:	90 mm/min	L_{arc}:	1.3 mm
PS:	AMI 207	Head:	9-1500

Anode: SS316L ϕ 1.5" 16SWG tube ('Cast 1' and 'LS Kobe')

Table 18 Straight d.c. welding procedures

SG:	Ar 10% H₂ @ 12 l/min	PG:	Ar @ 4 l/min
I_p:	125 A. for 0.01 s	I_b:	15.0, 17.5, 20.0, 22.5, 25.0 and 27.5 A. for 0.49 s
S:	90 mm/min	L_{arc}:	1.3 mm
PS:	AMI 207	Head:	9-1500

Anode: SS316L ϕ 1.5" 16SWG tube ('Cast 1' and 'LS Kobe')

Table 19 Pool oscillation procedures

SG:	Ar 10% H ₂ @ 12 l/min	PG:	Ar @ 4 l/min
I_p:	125 A. for 0.01 s @ 2 Hz	I_b:	1. 15.0 A. for 40 s 2. 27.5 A. for 40 s
S:	90 mm/min	L_{gro}:	1.3 mm
PS:	AMI 207	Head:	9-1500

Anode: SS316L ϕ 1.5" 16SWG tube ('Cast 1' and 'Cast 2')

Table 20 Pool oscillation procedure - PARTIAL and FULL penetration conditions (2 conditions, 1 pass)

SG:	Ar 10% H ₂ @ 12 l/min	PG:	Ar @ 4 l/min
I_p:	125 A. for 0.01 s @ 2 Hz	I_b:	1. 32.0 A. for 20 s 2. 52.5 A. for 20 s 3. 32.0 A. for 20 s 4. 52.5 A. for 20 s
S:	90 mm/min	L_{gro}:	1.3 mm
PS:	AMI 207	Head:	9-1500

Anode: SS316L ϕ 1.5" 0.125" WT tube ('1.5" Thick')

Table 21 Pool oscillation procedure - PARTIAL and FULL penetration conditions (4 conditions, 1 pass)

CRISP INPUT: Fuzzification of Weld Pool Frequency
(SEE FIGURE 30 FOR GRAPHICAL PRESENTATION
OF INPUT MEMBERSHIP FUNCTIONS)

CRISP OUTPUT: Delta-Current
(SEE FIGURE 30 FOR GRAPHICAL PRESENTATION
OF OUTPUT MEMBERSHIP FUNCTIONS)

MEMBERSHIP FUNCTIONS

Input Membership Functions				Output Membership Functions				
WELD POOL FREQUENCY				DELTA BASE CURRENT				
		VARIABLE PARAMETERS				VARIABLE PARAMETERS		
OP	x-intercept	40		-LG	x-intercept	-4.5		
	slope	0.03	-ve		slope	1.00	+ve	
SO	x-intercept	20			x-intercept	-2.0		
	slope	0.03	+ve		slope	1.00	-ve	
	x-intercept	80		-SM	x-intercept	-2.8		
	slope	0.03	-ve		slope	1.00	+ve	
FP	x-intercept	40			x-intercept	-0.5		
	slope	0.03	+ve		slope	1.00	-ve	
	x-intercept	120		ZE	x-intercept	-1.0		
	slope	0.03	-ve		slope	1.00	+ve	
PP	x-intercept	80			x-intercept	1.0		
	slope	0.02	+ve		slope	1.00	-ve	
	x-intercept	400		+SM	x-intercept	0.5		
	slope	0.01	-ve		slope	1.00	+ve	
SP	x-intercept	300			x-intercept	2.8		
	slope	0.01	+ve		slope	1.00	-ve	
				+LG	x-intercept	2.0		
					slope	1.00	+ve	
					x-intercept	5.5		
					slope	1.00	-ve	

TARGET FREQUENCY: 80 Hz

FULLY PENETRATED INPUT MEMBERSHIP FUNCTION CENTRED ABOUT 80 Hz
MORE SENSITIVITY IS ALLOCATED TO LOWER FREQUENCY RANGE BY
INCREASING THE DENSITY OF MEMBERSHIP FUNCTIONS IN THIS AREA
LESS SENSITIVITY IS ALLOCATED TO MID FREQUENCY RANGE WHERE
TRANSITION BETWEEN OSCILLATION MODES 1 AND 3 USUALLY OCCURS

Table 22 Fuzzy logic model

SG:	Ar 10% H ₂ @ 12 l/min	PG:	Ar @ 4 l/min
I_p:	125 A. for 5 ms @ 2 Hz	I_p:	25.0 A. for 90 s
S:	90 mm/min	L_{arc}:	1.3 mm
PS:	BDH320 †	Head:	9-1500

† As part of the control system (with the rack and user-interface PC)

Anode: SS316L ϕ 1.5" 16SWG tube ('EP')

Sample rate: 16 kHz (4 kHz per channel)
Window size: 512 Points
Post trigger delay: 40 Points
FFT size: 400 Points

Control Parameters:

fuzzy logic variables as shown in Table 22 and Figure 30,
target frequency centred about 80 Hz

Table 23 Open-loop oscillation procedure and monitoring parameters - full and over-penetration conditions

SG:	Ar 10% H ₂ @ 12 l/min	PG:	Ar @ 4 l/min
I_p:	125 A. for 10 ms @ 3 Hz	I_b:	22.0 A. for 90 s <i>(initial set current)</i>
S:	90 mm/min	L_{arc}:	1.3 mm
PS:	BDH320 †	Head:	9-1500

† As part of the control system (with the rack and user-interface PC)

Anode: SS316L ϕ 1.5" 16SWG tube ('Cast 2', 'LS Kobe', and 'EP')

Sample rate: 16 kHz (4 kHz per channel)
Window size: 256 Points
Post trigger delay: 40 Points
FFT size: 210 Points

Control Parameters:

fuzzy logic variables as shown in Table 22 and Figure 30,
target centred about 80 Hz

Table 24 Closed-loop oscillation procedure - full penetration conditions - target frequency 80 Hz

Input Membership Functions
WELD POOL FREQUENCY

OP	x-intercept	40	
	slope	0.025	-ve
SO	x-intercept	20	
	slope	0.025	
	x-intercept	120	
	slope	0.025	-ve
FP	x-intercept	80	
	slope	0.025	
	x-intercept	160	
	slope	0.025	-ve
PP	x-intercept	120	
	slope	0.022	
	x-intercept	400	
	slope	0.0075	-ve
SP	x-intercept	300	
	slope	0.0075	

Output Membership Functions - DELTA BASE CURRENT - not changed, as per Table 22, and Figure 30

Table 25 Fuzzy logic control parameters
for 120 Hz target frequency

Peak Current (I _p)		Peak Pulse Time (t _p)		Subjective Description (see below for key)				Pool Frequency (Hz) (Mode 3 Behaviour)				Typical Damping Time (ms)			
				AMI 207		BDH 320		AMI 207		BDH 320		AMI 207		BDH 320	
				5%	10%	5%	10%	5%	10%	5%	10%	5%	10%	5%	10%
75.0 A.		5 ms					2, 3								
75.0 A.		10 ms		1	2	1	2	-	-	-	-	-	-	-	-
75.0 A.		15 ms					2, 3								
75.0 A.		20 ms		2, 3	2, 3	2, 3	2, 3	94.5	85.6	83.7	78.7	216	200	150	209
100.0 A.		5 ms					3								
100.0 A.		10 ms		2, 3	2	2, 3	3	97.4	104.3	82.7	76.8	160	153	164	316
100.0 A.		15 ms					5								
100.0 A.		20 ms		3	3	2, 3	3	85.0	83.7	80.7	67.9	227	284	220	356
125.0 A.		5 ms					3								
125.0 A.		10 ms		2, 3	3	3	3	89.6	75.8	83.7	73.8	198	323	249	490
125.0 A.		15 ms					3, 4								
125.0 A.		20 ms		3	3	3	4, 5	81.7	67.9	74.8	65.9	334	440	310	430
150.0 A.		5 ms					3								
150.0 A.		10 ms		3	3	3	3	79.7	72.8	78.7	65.0	280	460	355	387
150.0 A.		15 ms					3, 4								
150.0 A.		20 ms		3	3, 4	3	3	75.8	66.9	69.9	59.1	341	480	386	480

1 - No Oscillations Observable

2 - Only Small Amplitude Signal Present

3 - Stable Regular Response to Each Pulse

4 - Mixed-Mode Oscillations

5 - Chaotic Response ie. Stable Signal Deterioration

Calculated on Most Dominant Pool Frequency using FFT Routine in Modified ArcWatch™ Software

Table 26 Stationary spot welding - effect of pulse magnitude and duration

MATERIAL - BASE CURRENT (A.) -	Electro-Polished ('EP')					Low-Sulphur ('LS Kobe')				
	15.0	17.5	20.0	22.5	25.0	15.0	17.5	20.0	22.5	25.0
O.B.W. 1 (mm)	4.0	4.3	4.4	4.7	5.3	4.0	4.5	5.0	5.2	5.6
O.B.W. 2 (mm)	4.0	4.3	4.6	4.8	5.5	4.0	4.6	5.0	5.2	5.9
I.B.W. 1 (mm)	4.0	4.0	4.5	4.6	5.0	2.0	3.2	4.0	5.2	5.4
I.B.W. 2 (mm)	4.0	4.5	4.5	5.0	5.5	2.1	3.5	4.2	5.0	5.5
Equivalent Dia (mm)	4.0	4.3	4.5	4.8	5.3	3.0	4.0	4.6	5.2	5.6
Frequency (Hz)	109.4	91.8	82.0	76.2	69.3	288.1	109.4	93.8	93.8	67.4
Surface Tension (N/m) (Membrane Model)	2.07	1.66	1.47	1.43	1.47	-	2.02	1.97	1.78	1.54
Surface Tension (N/m) (Yoo's Model)	2.99	2.41	2.13	2.07	2.12	-	2.39	2.61	2.57	2.21

MATERIAL - BASE CURRENT (A.) -	'Cast 1'					'Cast 2'				
	15.0	17.5	20.0	22.5	25.0	15.0	17.5	20.0	22.5	25.0
O.B.W. 1 (mm)	3.8	4.0	4.5	4.5	5.5	3.7	3.9	4.4	5.0	5.7
O.B.W. 2 (mm)	3.8	4.0	4.5	4.6	5.5	4.0	4.0	4.5	5.0	6.0
I.B.W. 1 (mm)	3.1	3.7	4.2	4.6	5.3	2.5	3.8	4.0	5.0	5.6
I.B.W. 2 (mm)	3.1	3.9	4.3	5.1	5.6	2.9	3.8	4.2	5.0	5.6
Equivalent Dia (mm)	3.5	3.9	4.4	4.7	5.5	3.3	3.9	4.3	5.0	5.7
Frequency (Hz)	117.2	99.6	92.8	78.1	67.4	129.9	102.5	89.8	77.1	67.4
Surface Tension (N/m) (Membrane Model)	1.77	1.63	1.70	1.46	1.47	1.96	1.70	1.59	1.61	1.61
Surface Tension (N/m) (Yoo's Model)	2.33	2.34	2.43	2.09	2.13	2.17	2.46	2.27	2.32	2.32

Table 27 Surface tension predictions from membrane and Yoo’s model for electro-polished ('EP'), low sulphur ('LS Kobe'), Cast 1 and 2 materials

RUN DESCRIPTION		BEAD WIDTH DATA				HEAT INPUT			FREQUENCY		
		Ave. OBW mm	S.D. OBW mm	Ave. IBW mm	S.D. IBW mm	Ave. Current Amps	Ave. Voltage Volts	Heat Input kJ/mm	Ave. Overall (Hz)	S.D. Overall (Hz)	
Standard Pulsed Procedure LS Ar/Ar											
74/71/68/65 A. I _p 20 A. I _b		4.4	0.1	3.5	0.2	44.8	7.8	0.175	-	-	
Standard Pulsed Procedure HS Ar/Ar											
74/71/68/65 A. I _p 20 A. I _b		3.9	0.1	3.3	0.1	44.8	7.7	0.173	-	-	
Non-Pulsed Procedure LS Ar Hyd/Ar											
15.0 A. I _p 15.0 A. I _b		2.1	0.1	0.0	0.0	14.8	13.2	0.130	-	-	
20.0 A. I _p 20.0 A. I _b		2.8	0.1	2.4	0.3	19.5	12.8	0.166	-	-	
25.0 A. I _p 25.0 A. I _b		3.5	0.2	3.9	0.2	24.2	12.0	0.194	-	-	
Non-Pulsed Procedure HS Ar Hyd/Ar											
15.0 A. I _p 15.0 A. I _b		2.2	0.1	0.0	0.0	14.8	13.6	0.134	-	-	
20.0 A. I _p 20.0 A. I _b		2.6	0.1	2.9	0.3	19.5	12.4	0.162	-	-	
25.0 A. I _p 25.0 A. I _b		2.9	0.1	3.3	0.2	24.2	11.4	0.184	-	-	
Oscillation Procedure LS Ar Hyd/Ar											
125 A. I _p 15.0 A. I _b		3.2	0.1	0.5	0.5	14.8	13.1	0.130	410	12	
125 A. I _p 17.5 A. I _b		3.4	0.1	2.3	0.2	17.1	12.6	0.144	353	13	
125 A. I _p 20.0 A. I _b		3.7	0.1	3.3	0.1	19.5	12.3	0.160	297	10	
125 A. I _p 22.5 A. I _b		4.1	0.2	3.8	0.2	21.9	12.1	0.177	94	3	
125 A. I _p 25.0 A. I _b		4.3	0.2	4.4	0.2	24.2	11.9	0.192	79	5	
125 A. I _p 27.5 A. I _b		4.8	0.3	4.9	0.3	26.6	11.7	0.207	67	7	
Oscillation Procedure HS Ar Hyd/Ar											
125 A. I _p 15.0 A. I _b		3.2	0.2	2.2	0.2	14.8	14.4	0.141	385	15	
125 A. I _p 17.5 A. I _b		3.3	0.1	2.6	0.1	17.1	12.9	0.147	367	14	
125 A. I _p 20.0 A. I _b		3.4	0.2	3.1	0.2	19.5	12.1	0.158	347	15	
125 A. I _p 22.5 A. I _b		3.7	0.2	3.6	0.2	21.9	11.7	0.170	98	5	
125 A. I _p 25.0 A. I _b		3.9	0.1	3.9	0.1	24.2	11.3	0.182	86	4	
125 A. I _p 27.5 A. I _b		4.0	0.1	4.1	0.1	26.6	11.0	0.195	81	4	

Table 28 Cast-to-cast variation - effect of standard, straight d.c., and oscillation procedures on bead width and frequency - low sulphur LS ('LS Kobe') and high sulphur HS ('Cast 1') casts

	Material	Heat Input (kJ/mm)	Average OBW (mm)	Average IBW (mm)
non-pulsed procedure	'LS Kobe'	0.166	2.8	2.4
	'Cast 1'	0.162	2.6	2.9
pulsed procedure	'LS Kobe'	0.160	3.7	3.3
	'Cast 1'	0.158	3.4	3.1

Table 29 Lower pool surface and Mode 1 to 3 transition - example results
(20 Amps set current)

	Mode 3 frequency response				
	04:30 Position	07:30 Position	10:30 Position	01:30 Position	Overall Average
'LS Kobe'					
$I_b = 22.5$ A.	93 Hz	98 Hz	91 Hz	94 Hz	94 Hz
$I_b = 25.0$ A.	82 Hz	81 Hz	81 Hz	72 Hz	79 Hz
$I_b = 27.5$ A.	66 Hz	73 Hz	73 Hz	57 Hz	67 Hz
'Cast 1'					
$I_b = 22.5$ A.	92 Hz	99 Hz	100 Hz	103 Hz	99 Hz
$I_b = 25.0$ A.	79 Hz	88 Hz	88 Hz	90 Hz	86 Hz
$I_b = 27.5$ A.	73 Hz	83 Hz	83 Hz	83 Hz	81 Hz

Table 30 Orbital position and Mode 3 frequency
response ('cast-to-cast' work)

	'EP'	'LS Kobe'	'Cast 1'	'Cast 2'
$I_b = 15.0$ Amps				
Average OBW	4.0 mm	4.0 mm	3.8 mm	3.9 mm
Average IBW	4.0 mm	2.1 mm	3.1 mm	2.7 mm
$I_b = 17.5$ Amps				
Average OBW	4.3 mm	4.6 mm	4.0 mm	4.0 mm
Average IBW	4.3 mm	3.4 mm	3.8 mm	3.8 mm

Table 31 Cast behaviour and stationary pool sizes

	First occurrence of Mode 3 frequency (Pulse N°.)				
I_b (Amps)	15.0	17.5	20.0	22.5	25.0
'EP'	10	6	4	3	2
'LS Kobe'	-	16	9	5	5
'Cast 1'	13	6	5	4	2
'Cast 2'	19	9	6	3	2

Table 32 Time-to-penetrate (1.65 mm wall thickness)

	$\Delta f_d / \Delta IBW$	$\Delta f_d / \Delta I_b$
Mode 1	48.2 Hz/mm	17.8 Hz/Amp
Mode 3	29.5 Hz/mm	4.4 Hz/Amp

Table 33 Sensitivity of pool frequency to inner bead width, and frequency to base current (1.65 mm WT material)

	$\Delta f_d / \Delta IBW$	$\Delta f_d / \Delta I_b$
Mode 1 (HS Cast)	39.8 Hz/mm	7.6 Hz/Amp
Mode 3 (HS Cast)	36.6 Hz/mm	3.6 Hz/Amp
Mode 1 (LS Cast)	40.7 Hz/mm	22.6 Hz/Amp
Mode 3 (LS Cast)	26.2 Hz/mm	5.4 Hz/Amp

Table 34 Sensitivity of pool frequency to inner bead width and base current (cast-to-cast comparison)

	'Cast 1'	'Cast 2'
Mode 1 to Mode 3 ($I_b = 15.0$ to 27.5 Amps)	12 pulses 6.0 seconds	8 pulses 4.0 seconds
Mode 3 to Mode 1 ($I_b = 27.5$ to 15.0 Amps)	4 pulses 2.0 seconds	4 pulses 2.0 seconds

Table 35 Delay in frequency response with change in base current
(Step change in $I_b = 12.5$ Amps for 1.65 mm WT)

	'Bead-on-tube'	'Butt Joint'
a. Mode 1 to Mode 3 ($I_b = 32.5$ to 52.5 Amps)	13 pulses 6.5 seconds	25 pulses 12.5 seconds
b. Mode 3 to Mode 1 ($I_b = 52.5$ to 32.5 Amps)	7 pulses 3.5 seconds	6 pulses 3.0 seconds
c. Mode 1 to Mode 3 ($I_b = 32.5$ to 52.5 Amps)	11 pulses 5.5 seconds	12 pulses 6.0 seconds

Table 36 Delay in frequency response with change in base current
(Step change in $I_b = 20.0$ Amps for 3.18 mm WT)

	'Cast 1'		'Cast 2'	
	Average	S.D.	Average	S.D.
<i>PARTIAL to FULL PEN.</i>				
Mode 1 (Hz)	408.2	27.8	399.9	11.2
Mode 3 (Hz)	79.3	1.3	78.2	0.8
<i>FULL to PARTIAL PEN.</i>				
Mode 1 (Hz)	389.6	28.9	392.9	20.1
Mode 3 (Hz)	79.9	1.7	78.4	0.7

Table 37 Real-time frequency response of 1.65 mm WT tubing -
average and standard deviation

<i>Region of interest</i>	<i>Typical Output</i>	<i>Sensitivity</i> $\Delta f_d / \Delta I_b$
Mode 3 - Full penetration 50 to 75 Hz 75 to 85 Hz (around the target) 85 to 110 Hz	-0.9 Amps 0.0 Amps + 0.8 Amps	31.9 Hz/Amp 14.0 Hz/Amp 29.5 Hz/Amp
Mode 1 - Partial penetration 120 to 300 Hz (transition) 300 to 400 Hz	+ 1.6 Amps + 3.0 Amps	constant output 50 Hz/Amp

Table 38 Sensitivity of fuzzy logic model to pool frequency
(80 Hz target)

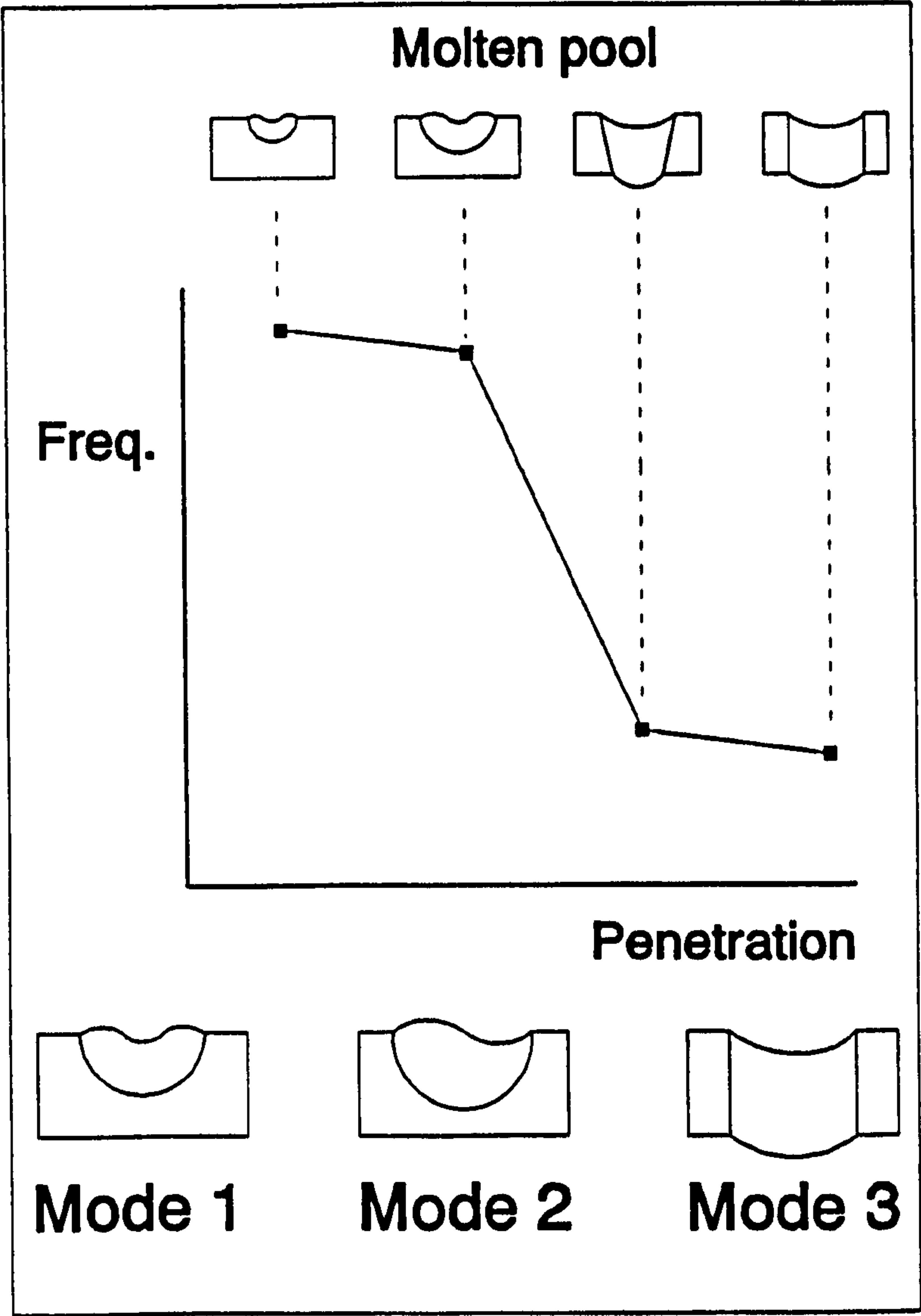


Figure 1 Generalised frequency behaviour

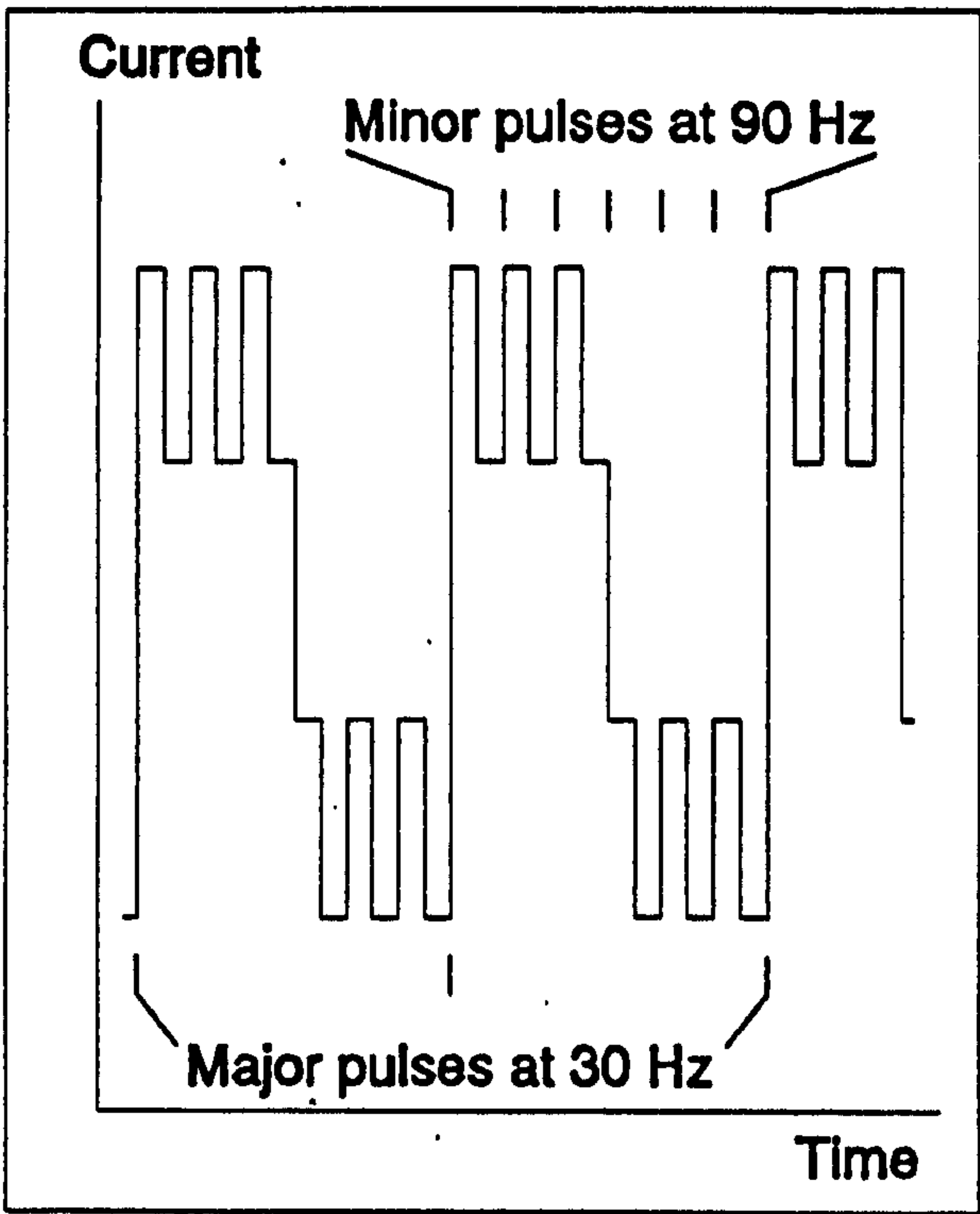


Figure 2 Modified current pulsing - Nakata (1994)

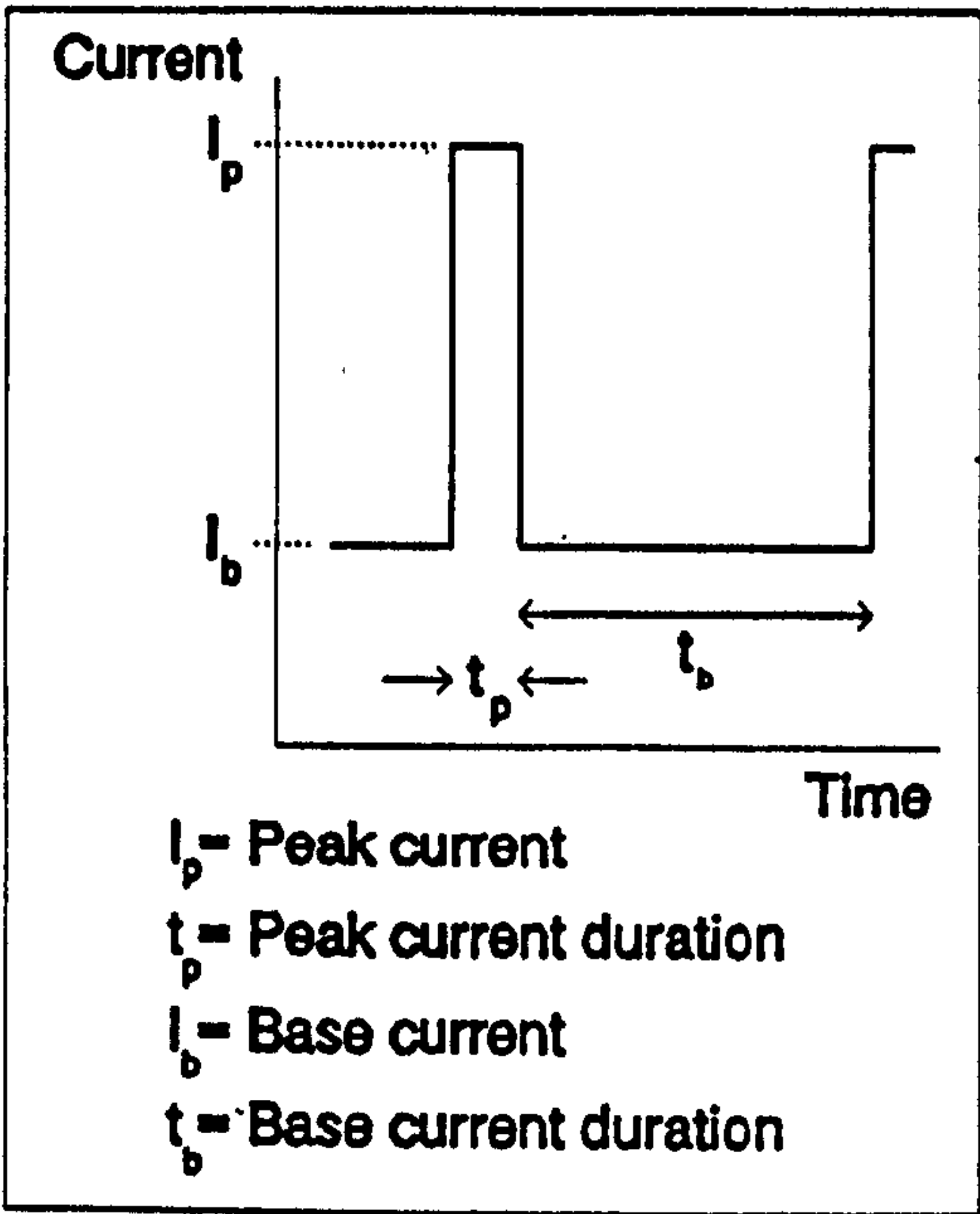


Figure 3 Pulsed current designation

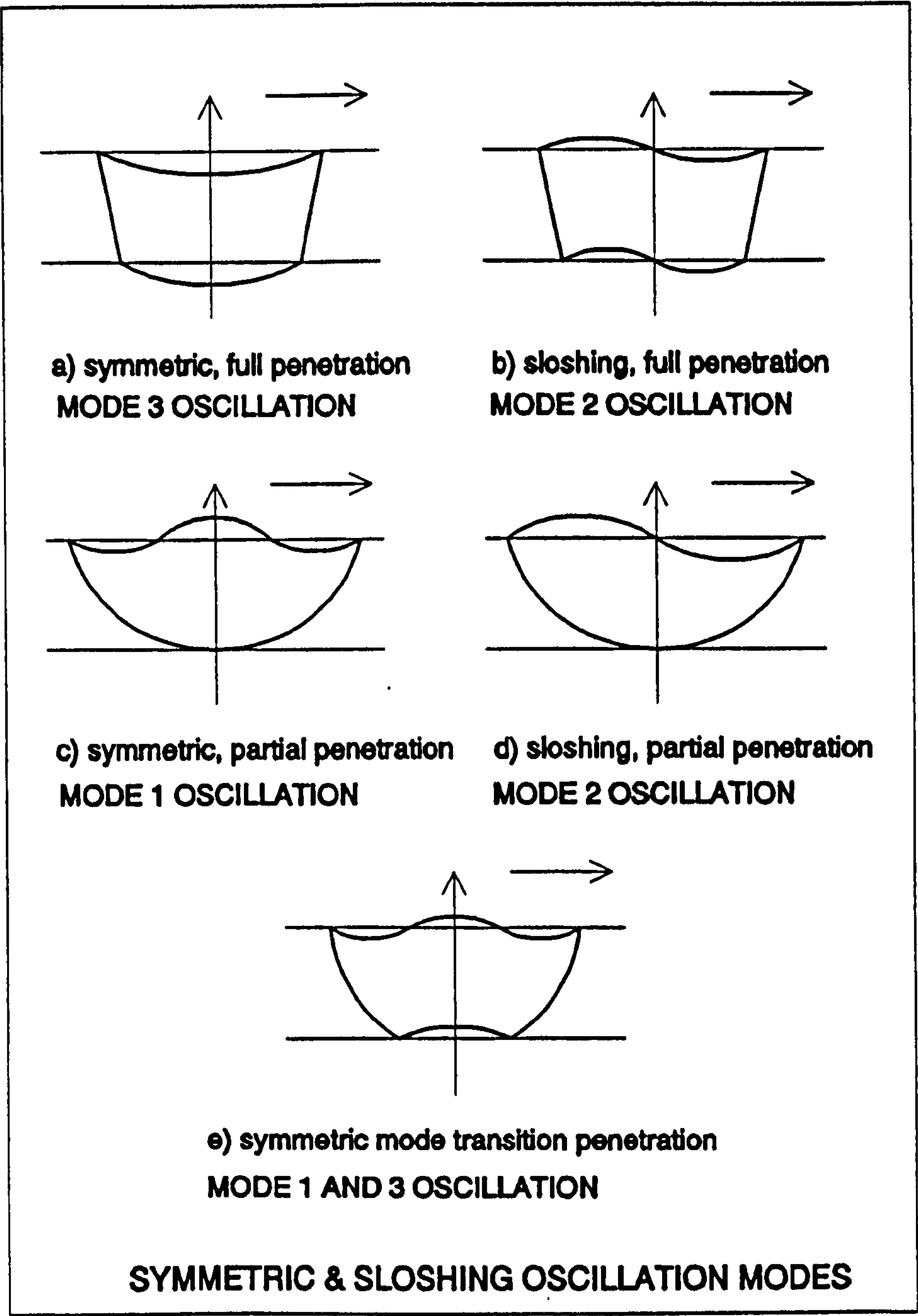


Figure 4 Symmetric & sloshing oscillation modes - Yoo (1993)

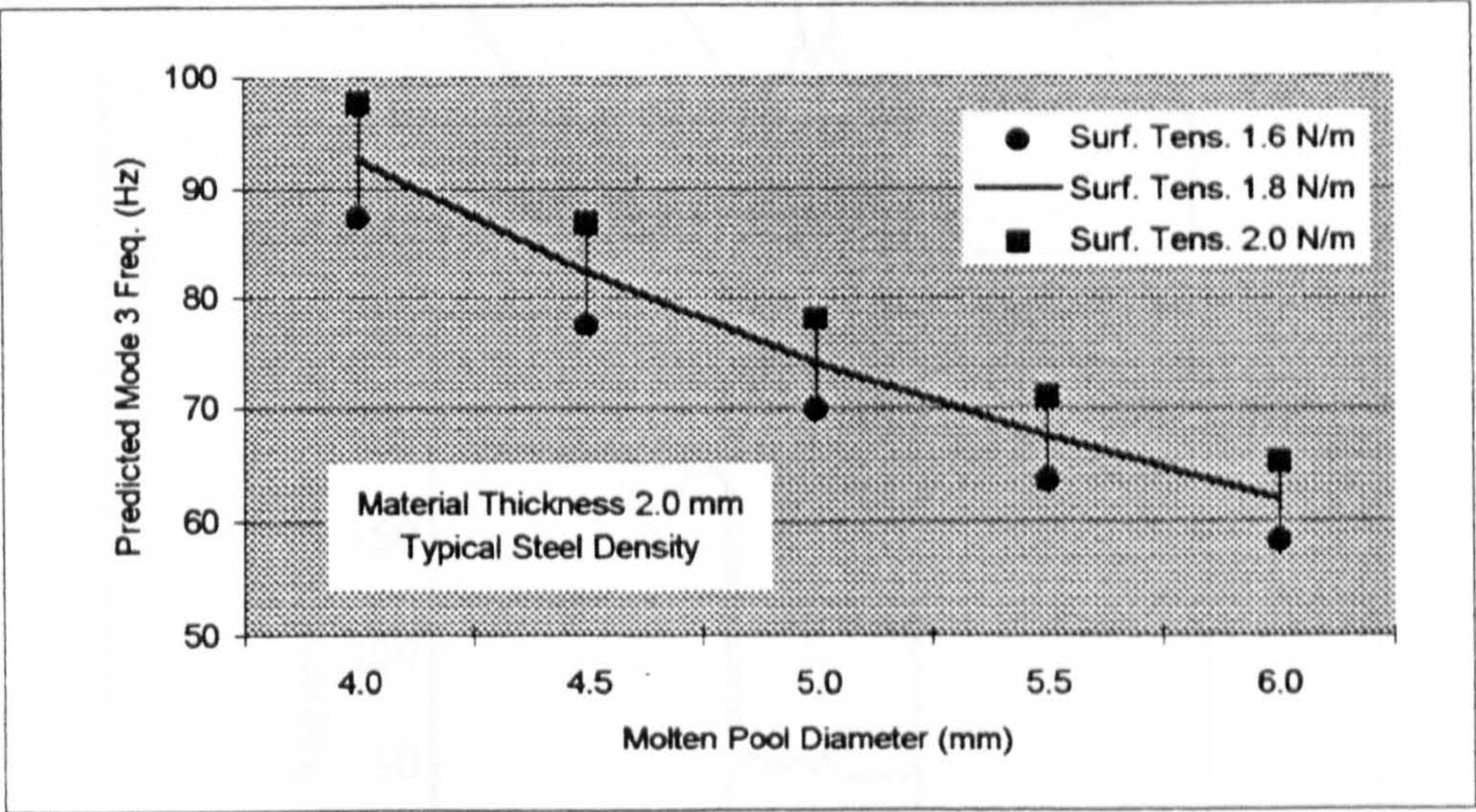


Figure 5 Error in predicted frequency with surface tension variation

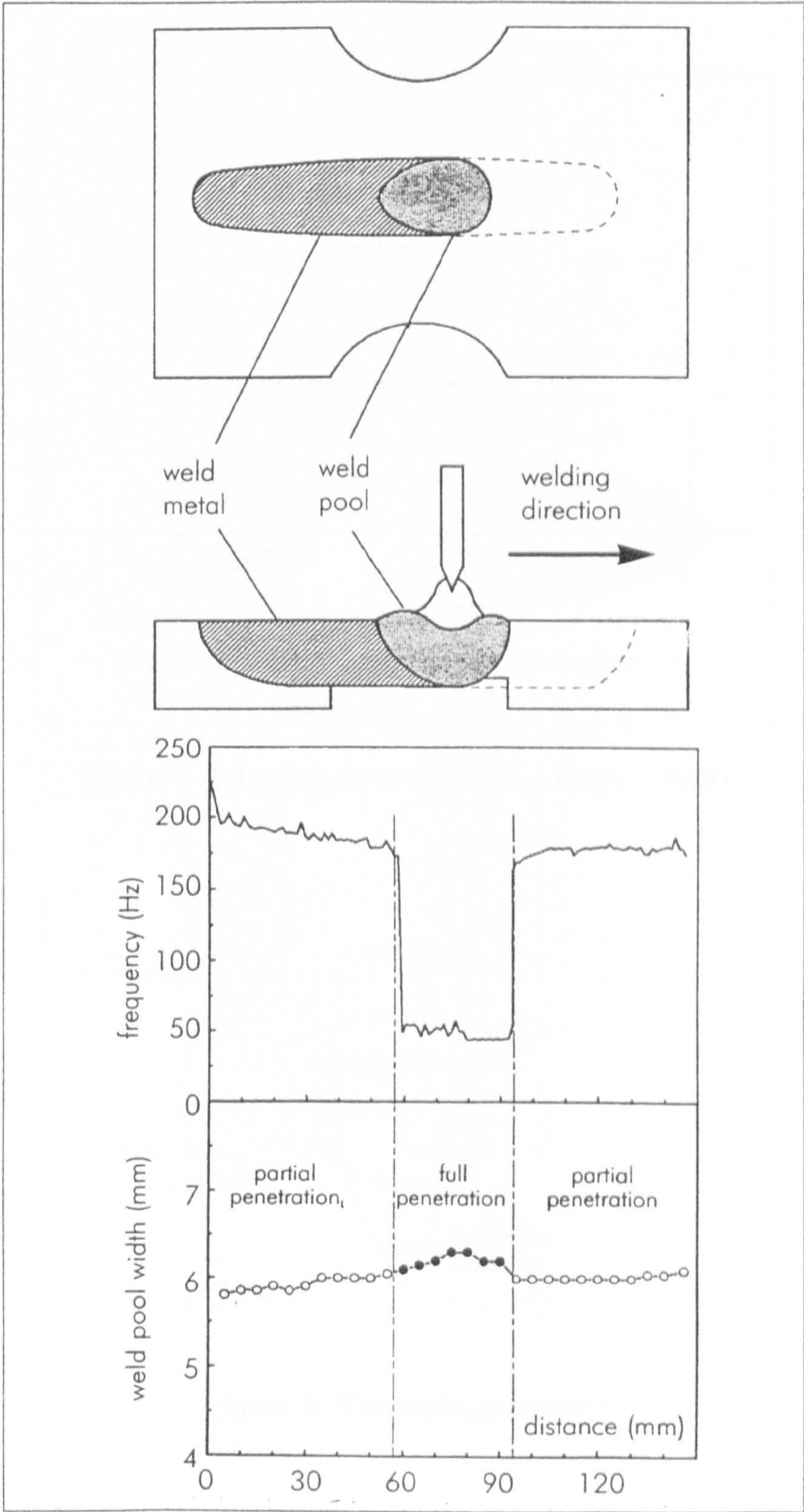


Figure 6 Partial and full penetration conditions - Xiao (1993)

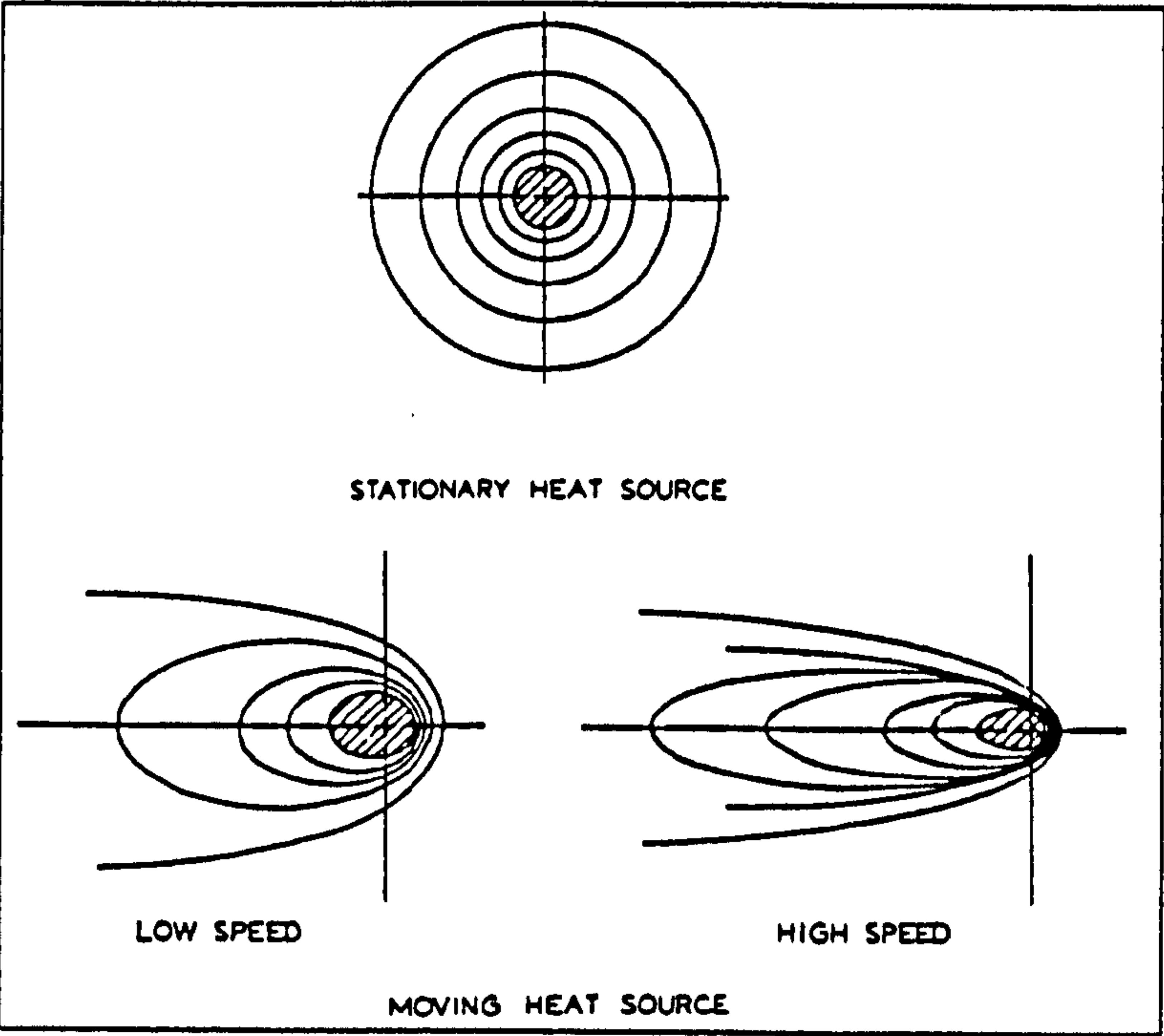


Figure 7 Effect of welding speed - Hardt (1985)

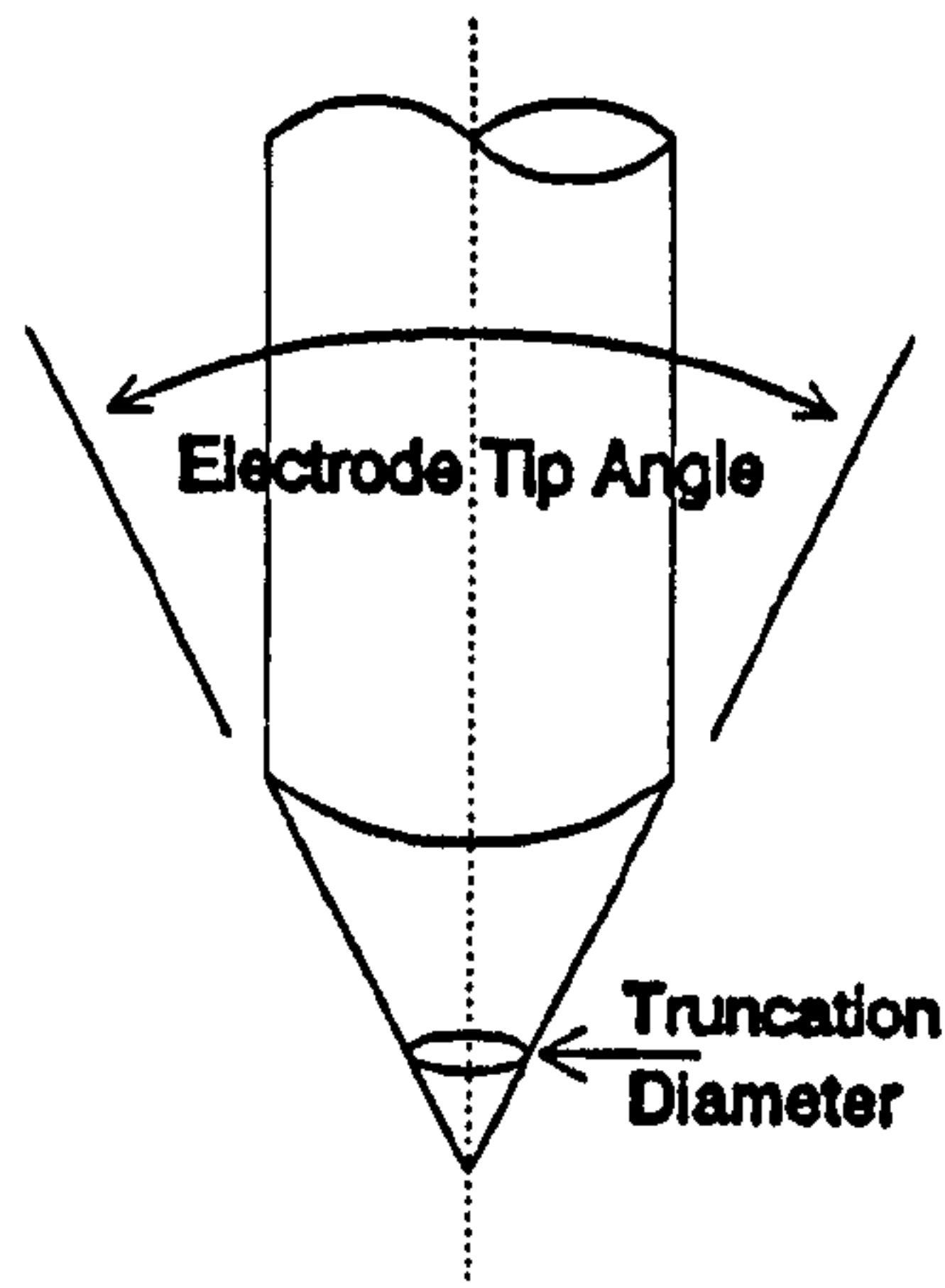
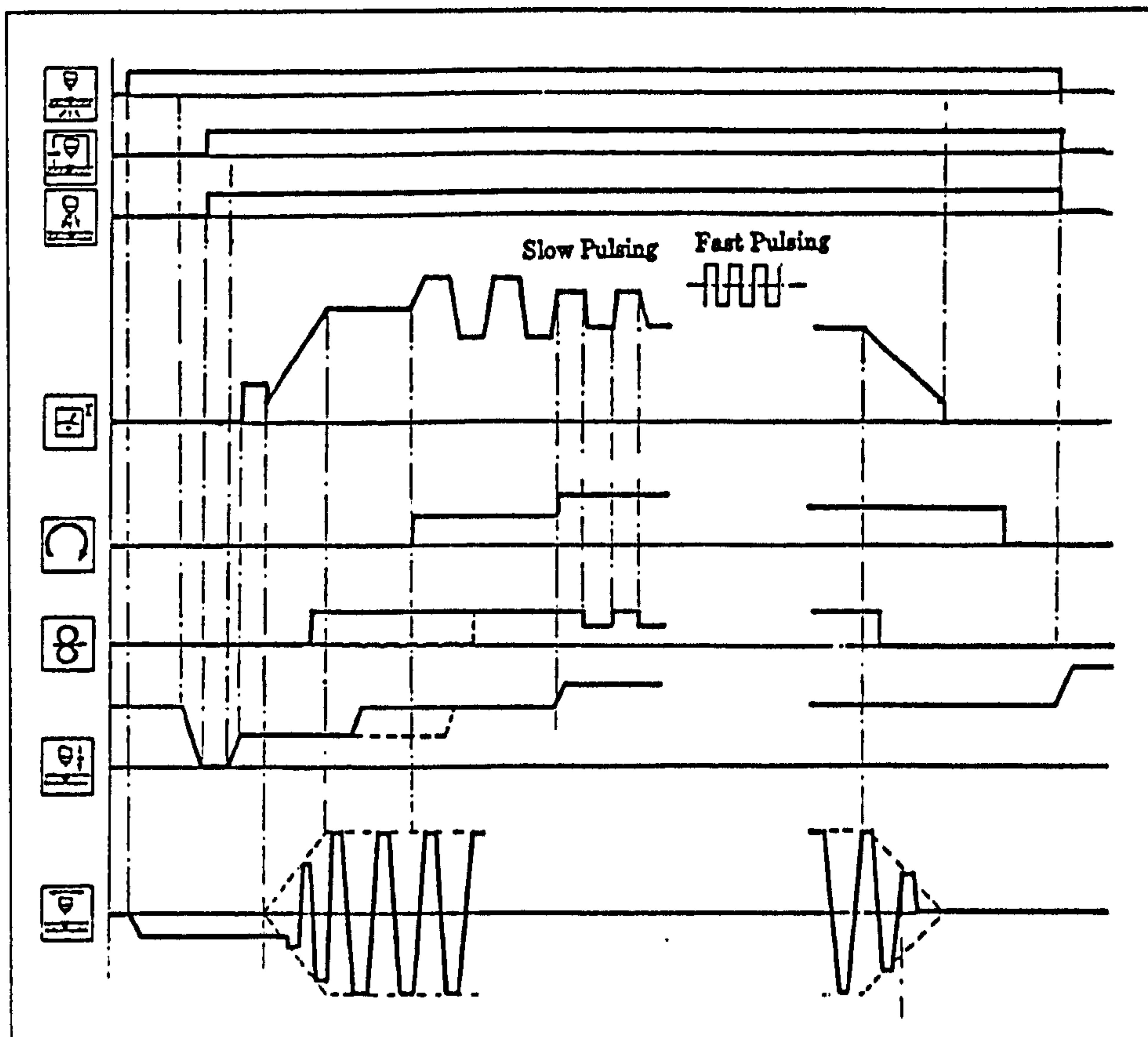


Figure 8 Tungsten geometry



Symbolically from the top: backing or purge gas, chamber gas, torch shielding gas, welding current, rotation of the head, filler wire, arc voltage control, weaving.

Figure 9 Orbital welding control variables - Krüger (1994)

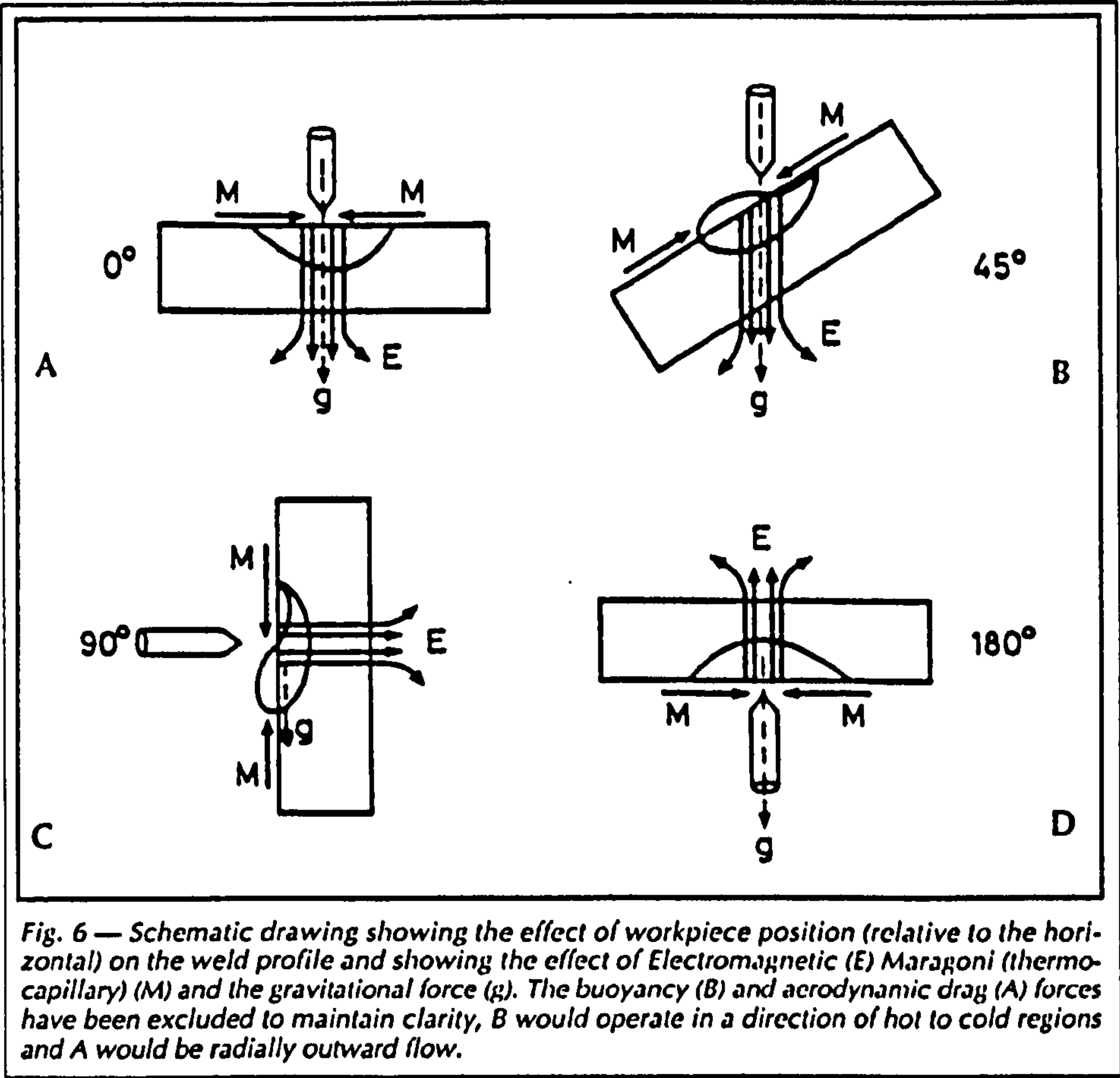


Figure 10 Effect of workpiece position - Shirali and Mills (1993)

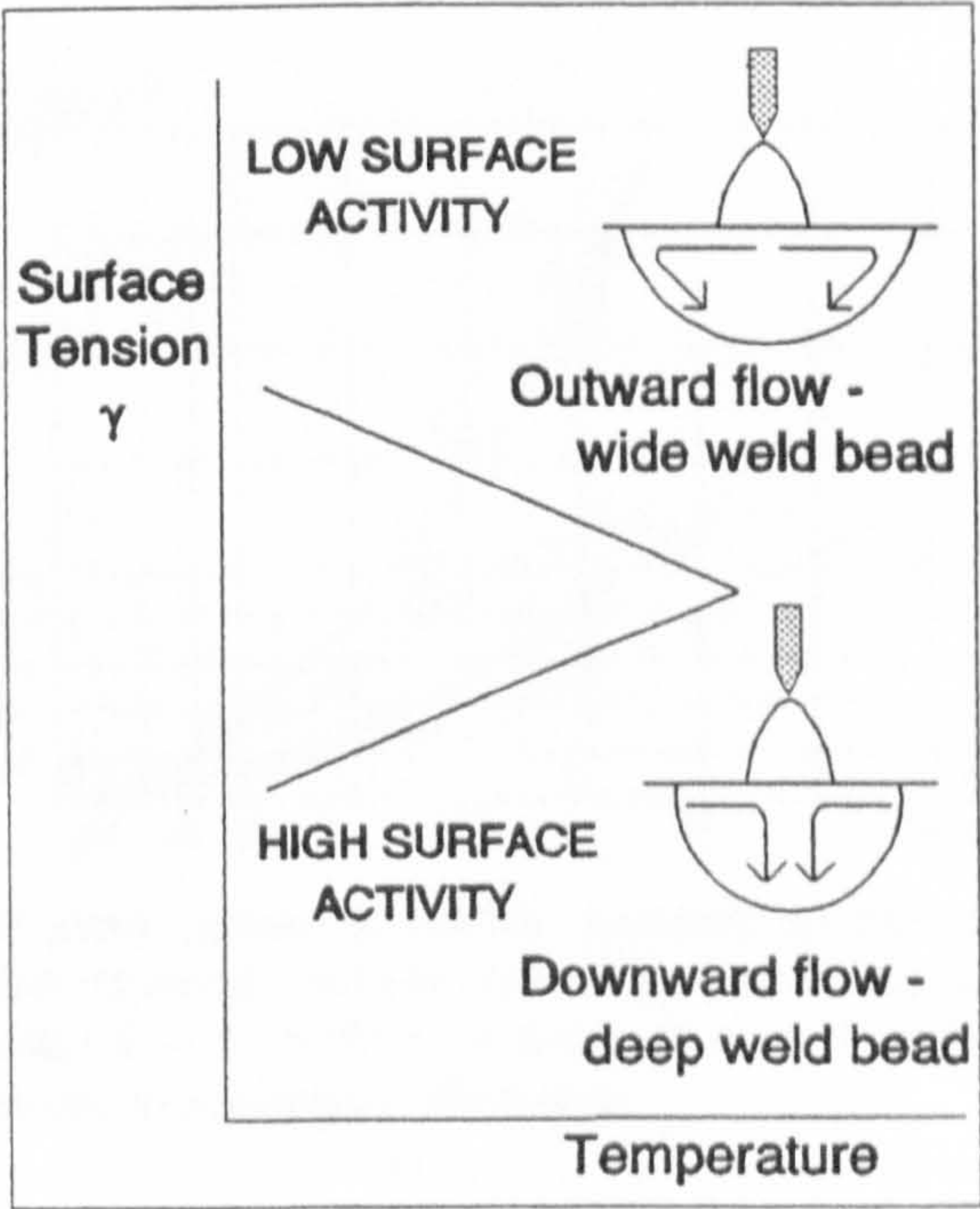


Figure 11 Surface tension / temperature behaviour


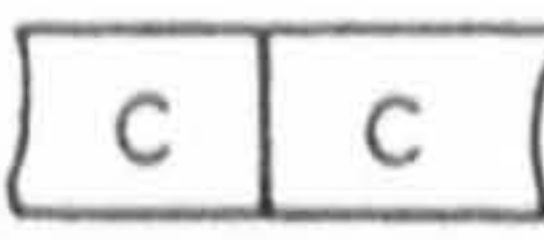
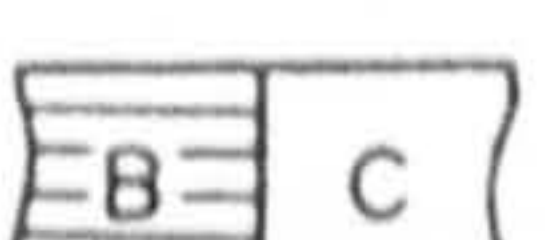
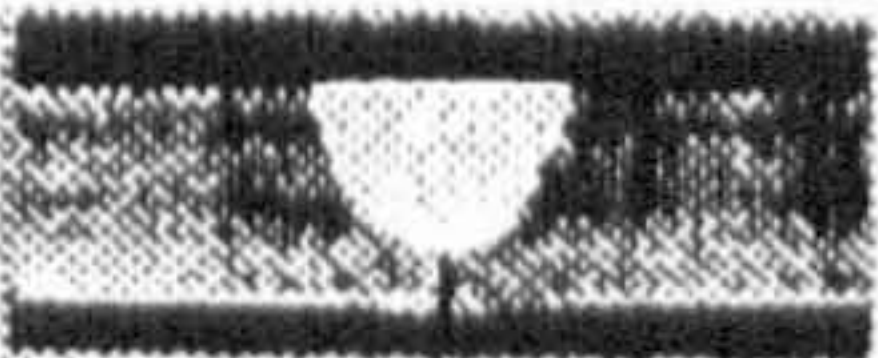
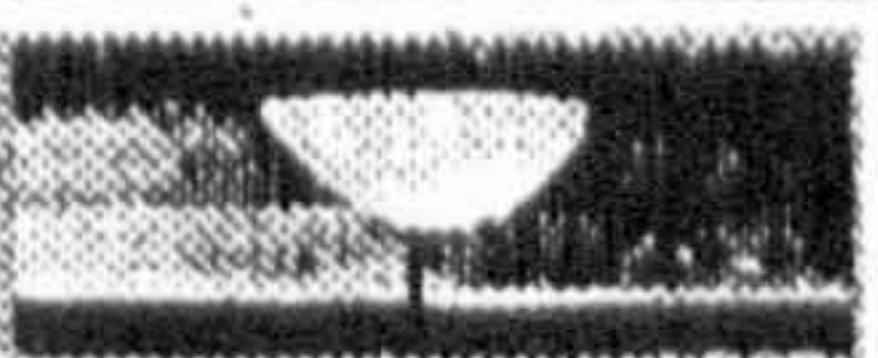

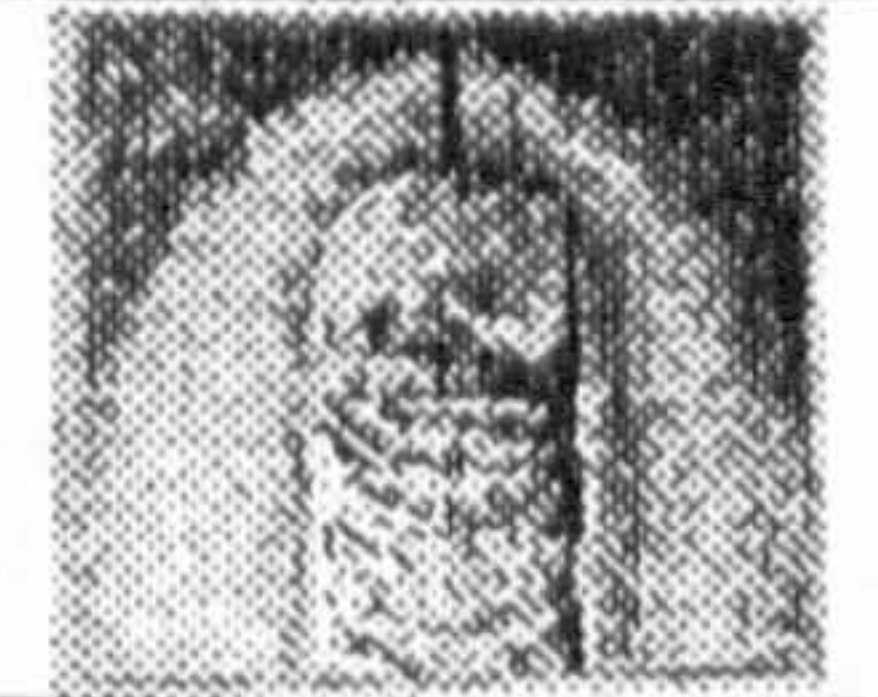

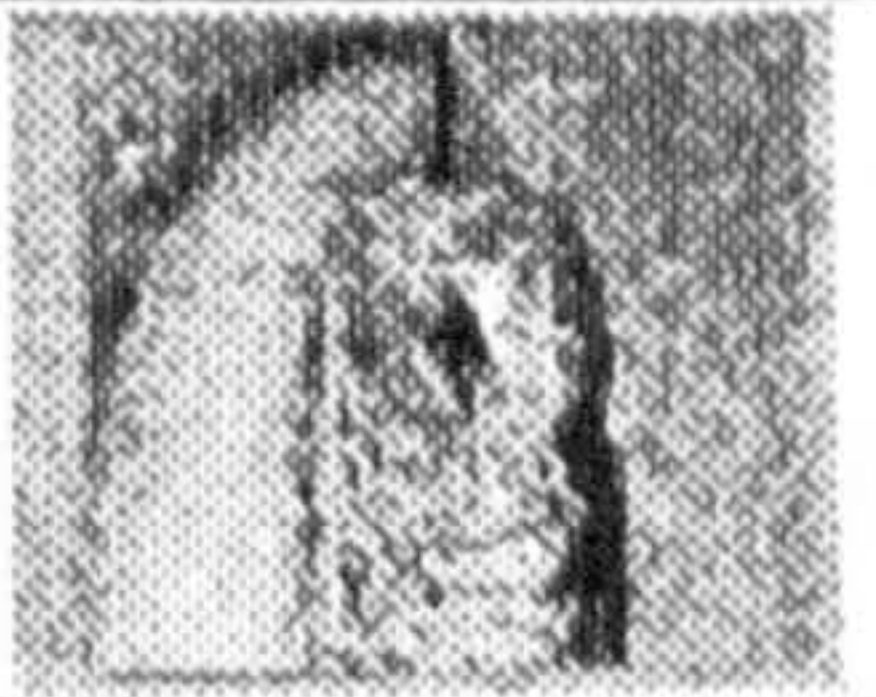
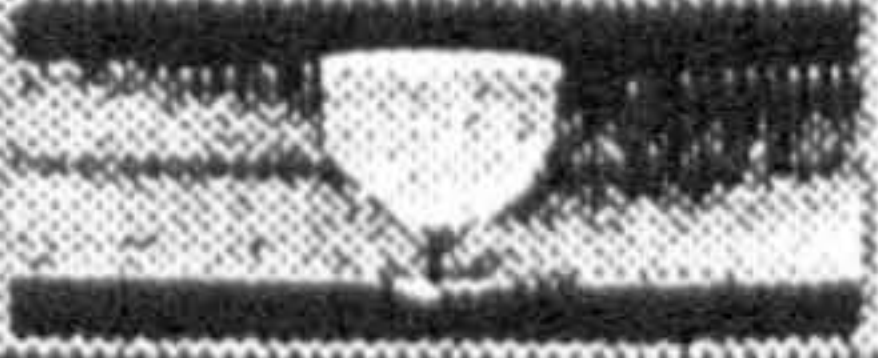
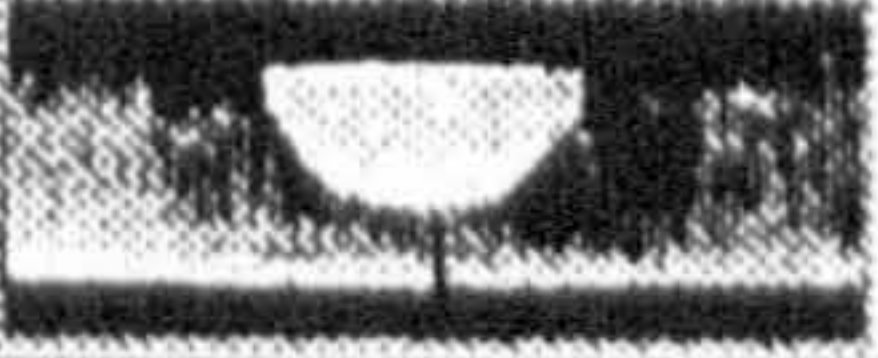
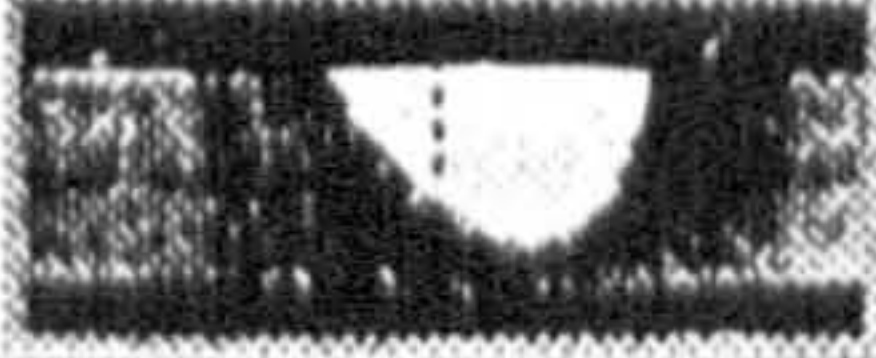
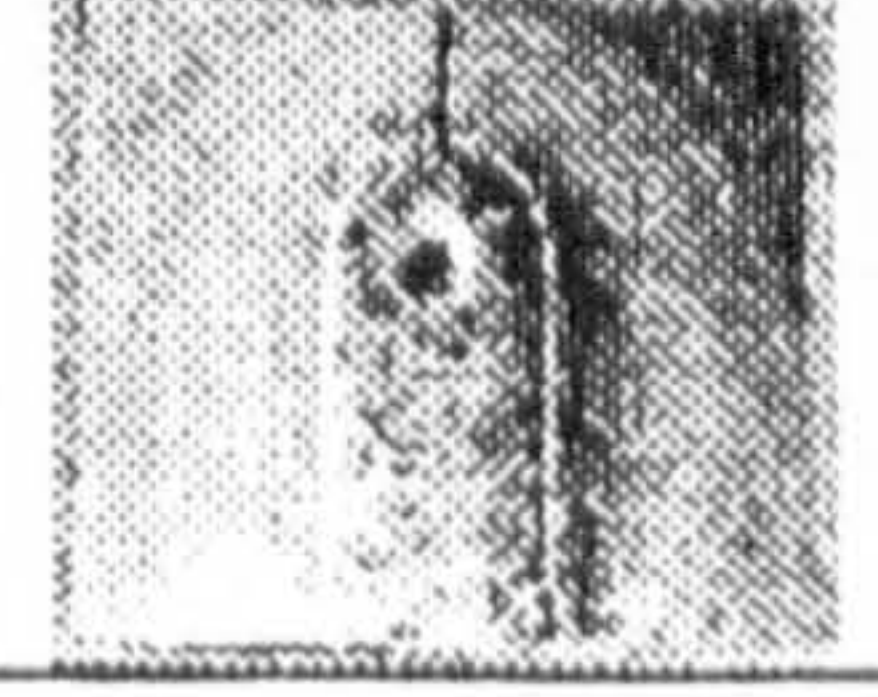
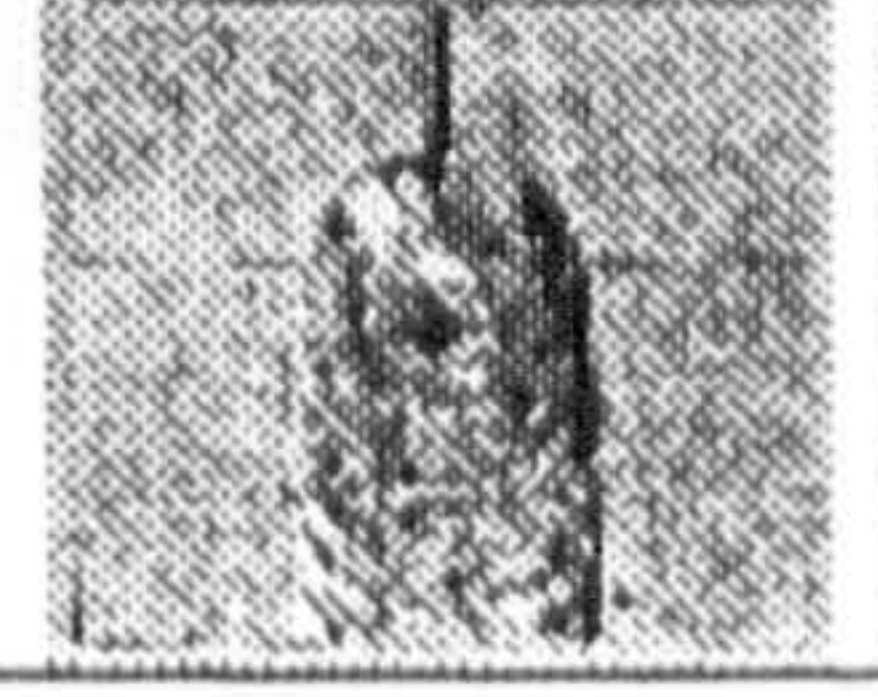

Joint Welding condition	 (S=0.008%)	 (S=0.001%)	
Ar – DC · TIG (I = 150 A v = 2.5 cm/min)			
			
He – DC · TIG (I = 100 A v = 2.5 cm/min)			
			

Figure 12 Effect of cast variation - Hinata (1994)

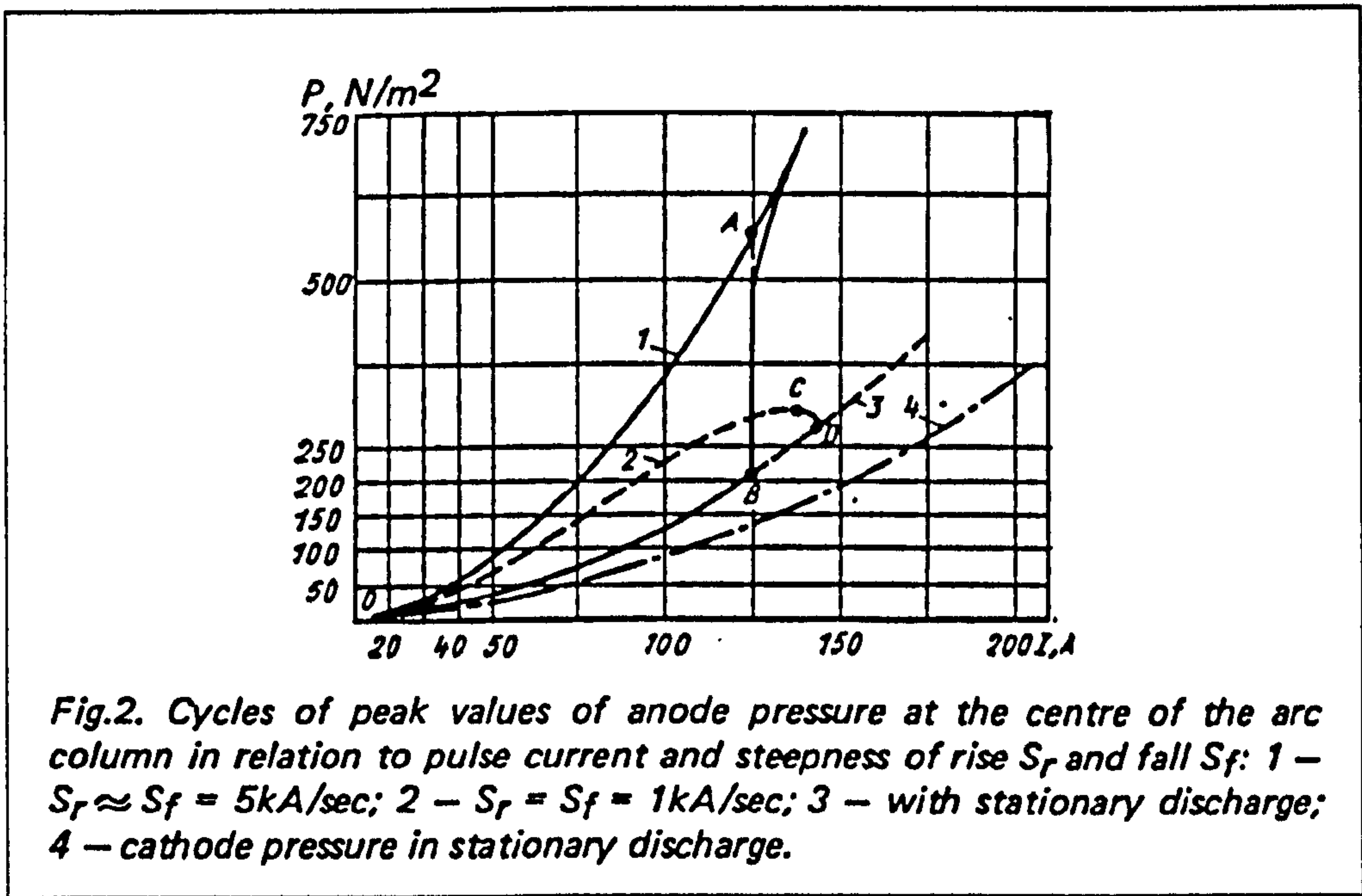


Figure 13 Reported effect of rate of rise of current on arc pressure - Barabokhin (1976)

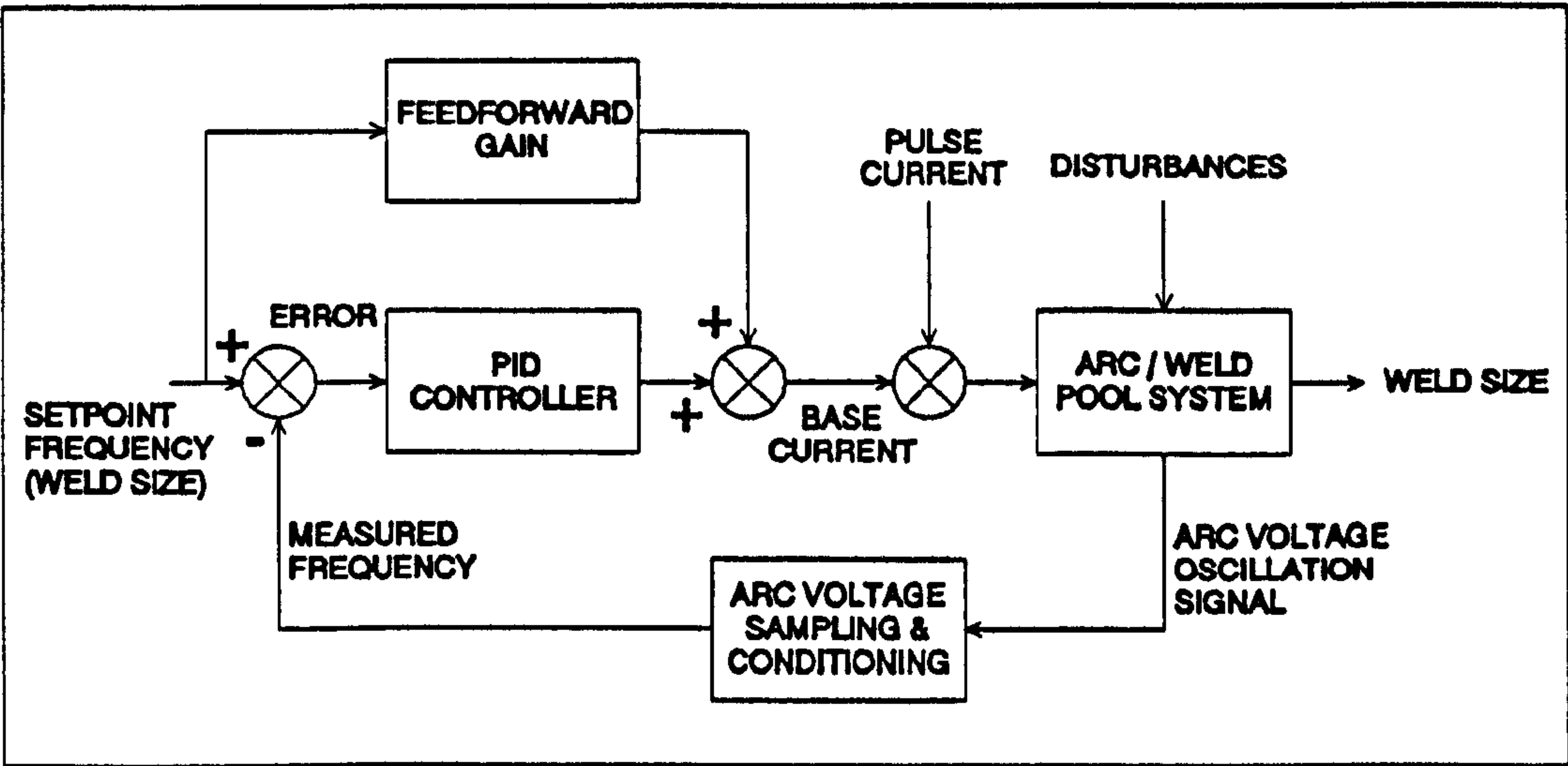


Figure 14 Weld pool frequency control system - Madigan (1986)

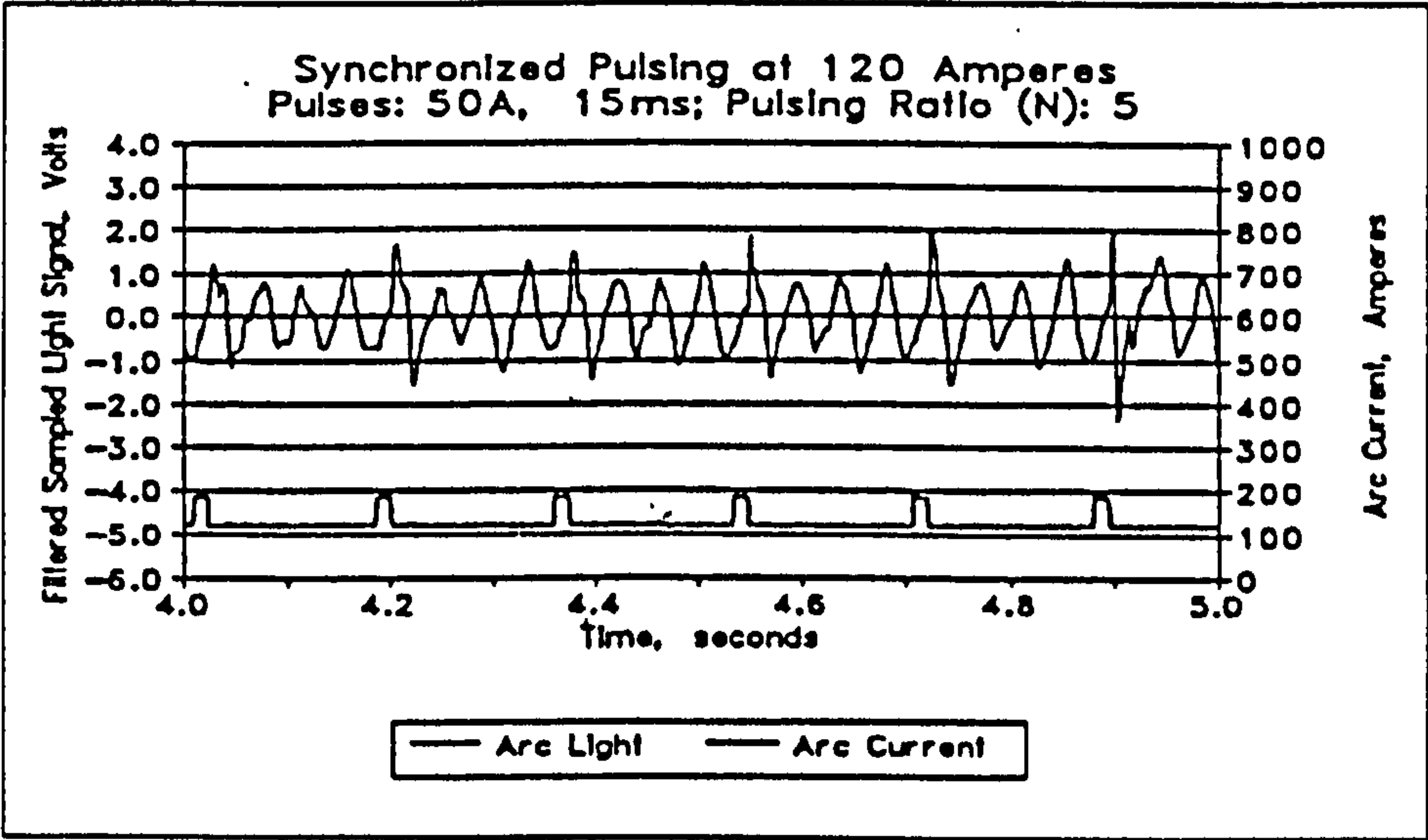


Figure 15 Synchronized pulsing and pool oscillations - Andersen (1993)

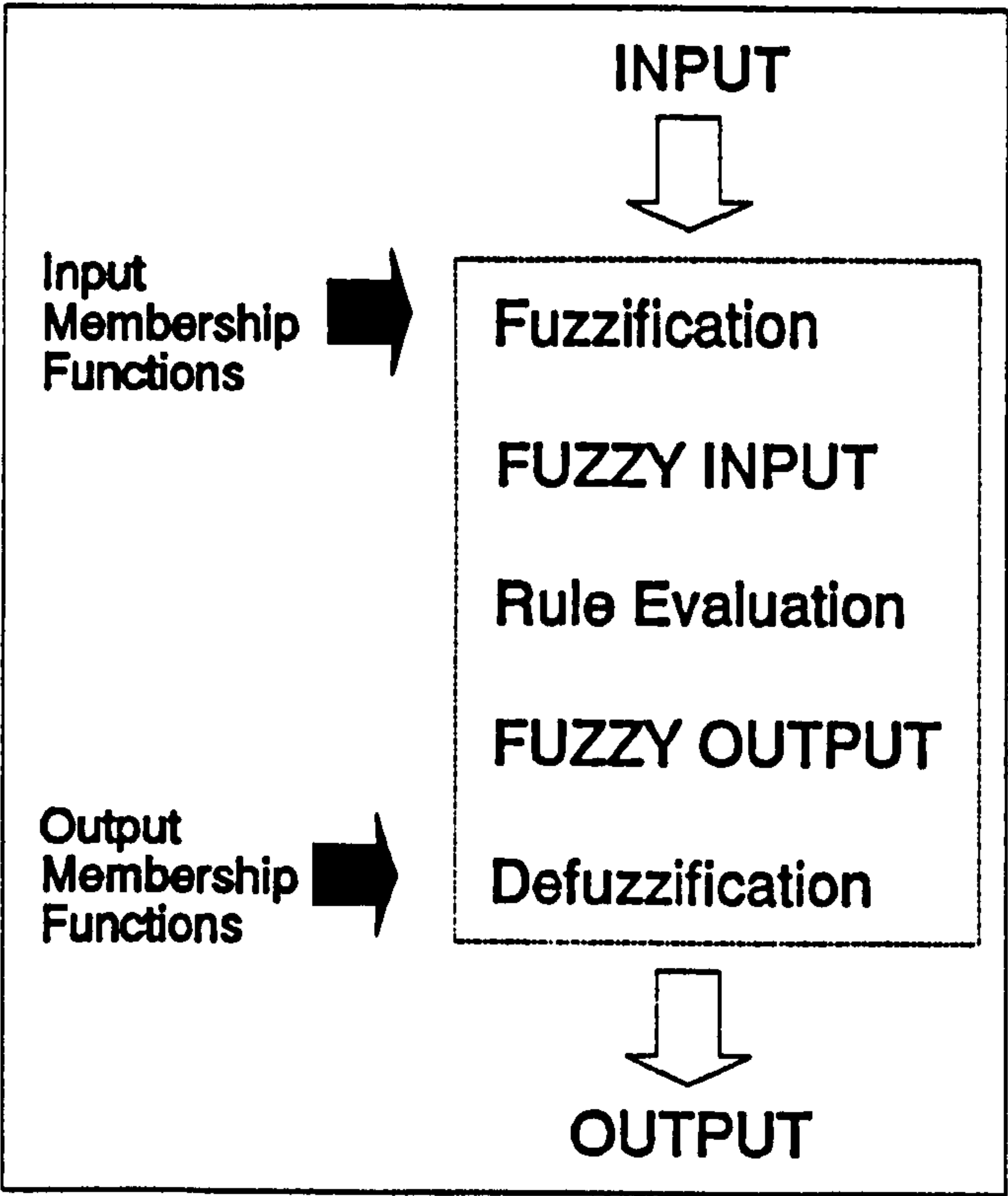


Figure 16 Fuzzy logic strategy

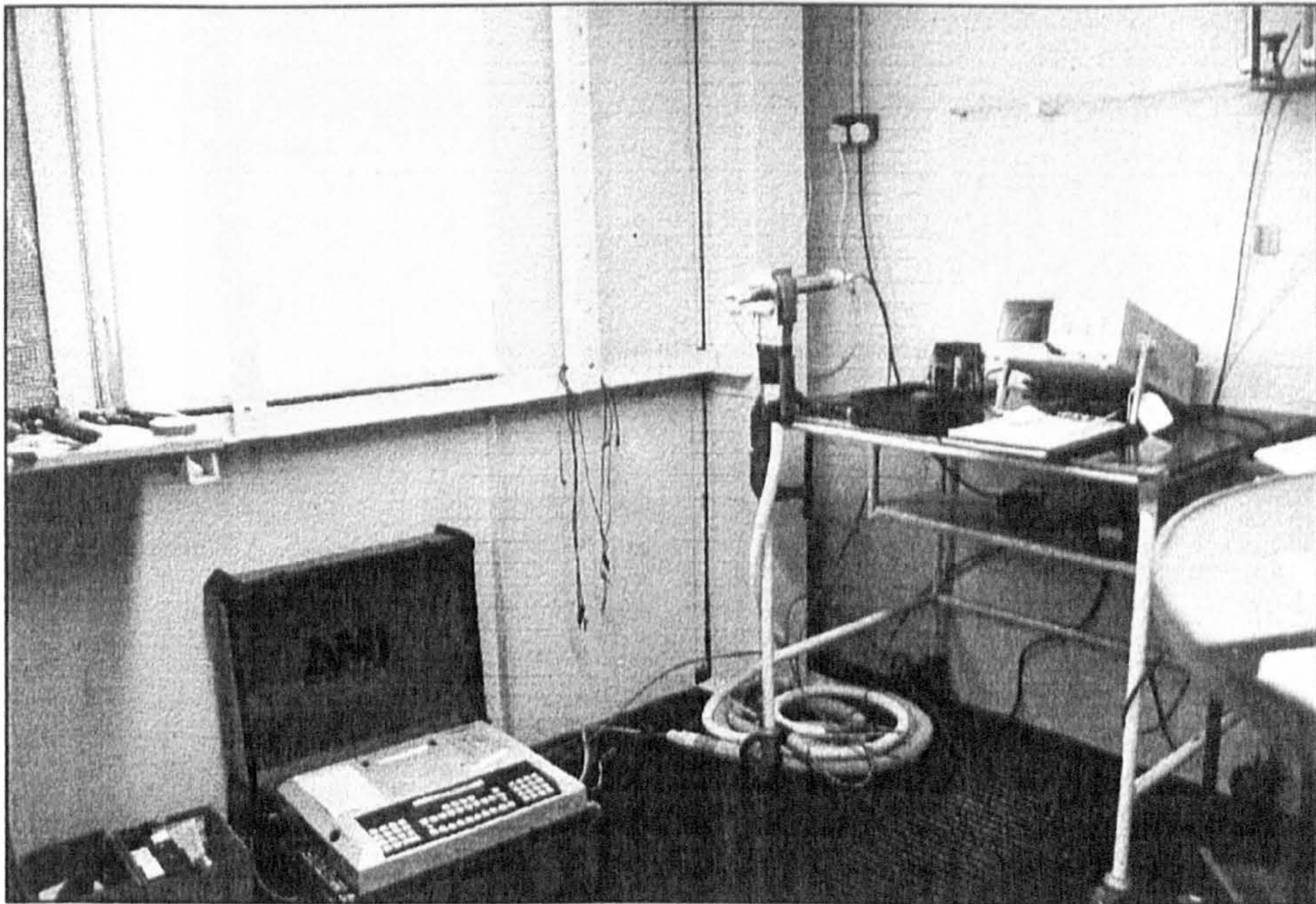


Figure 17 Arc Machines 207 power source and AMI head in laboratory

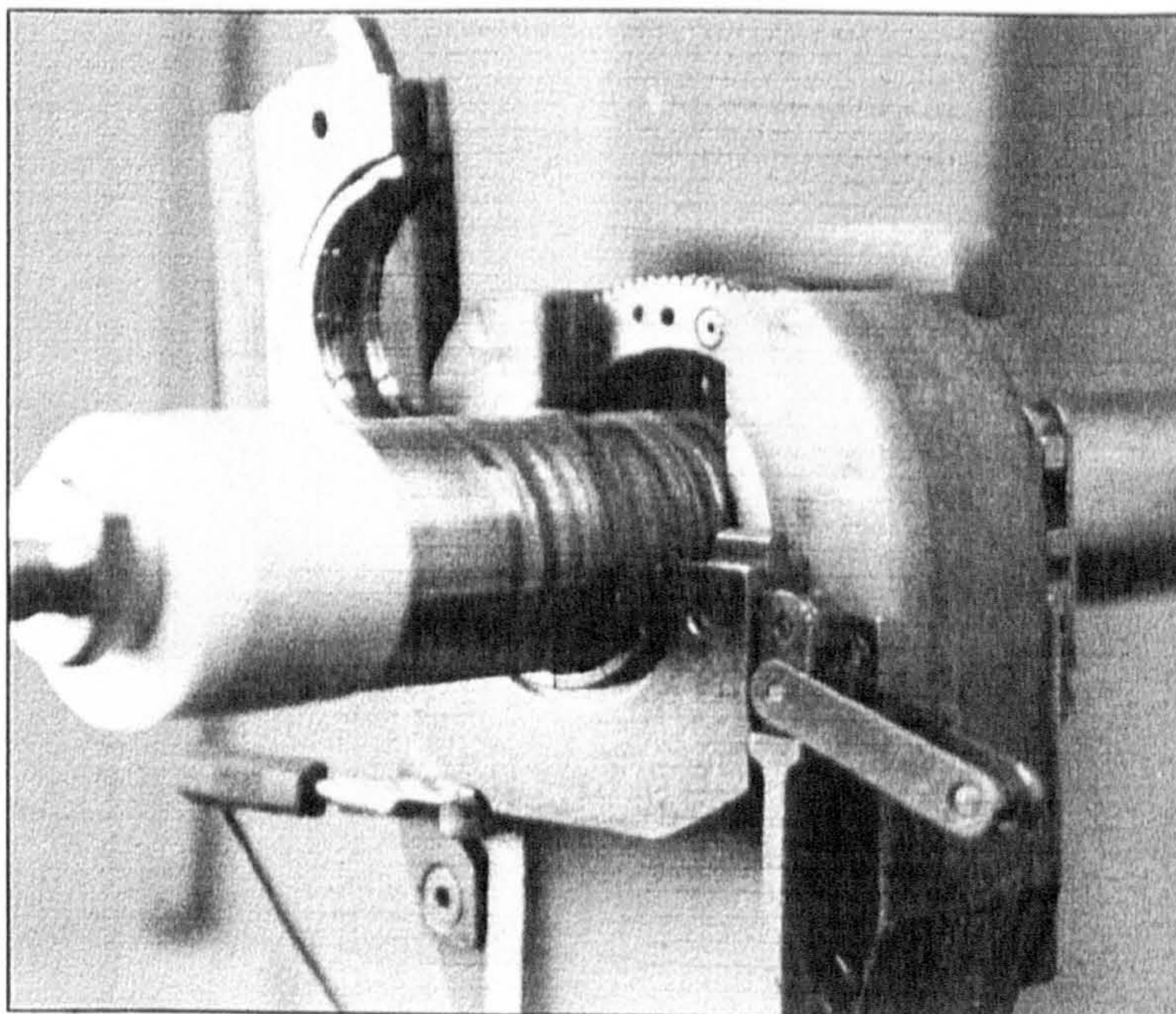


Figure 18 AMI 9-1500 orbital head

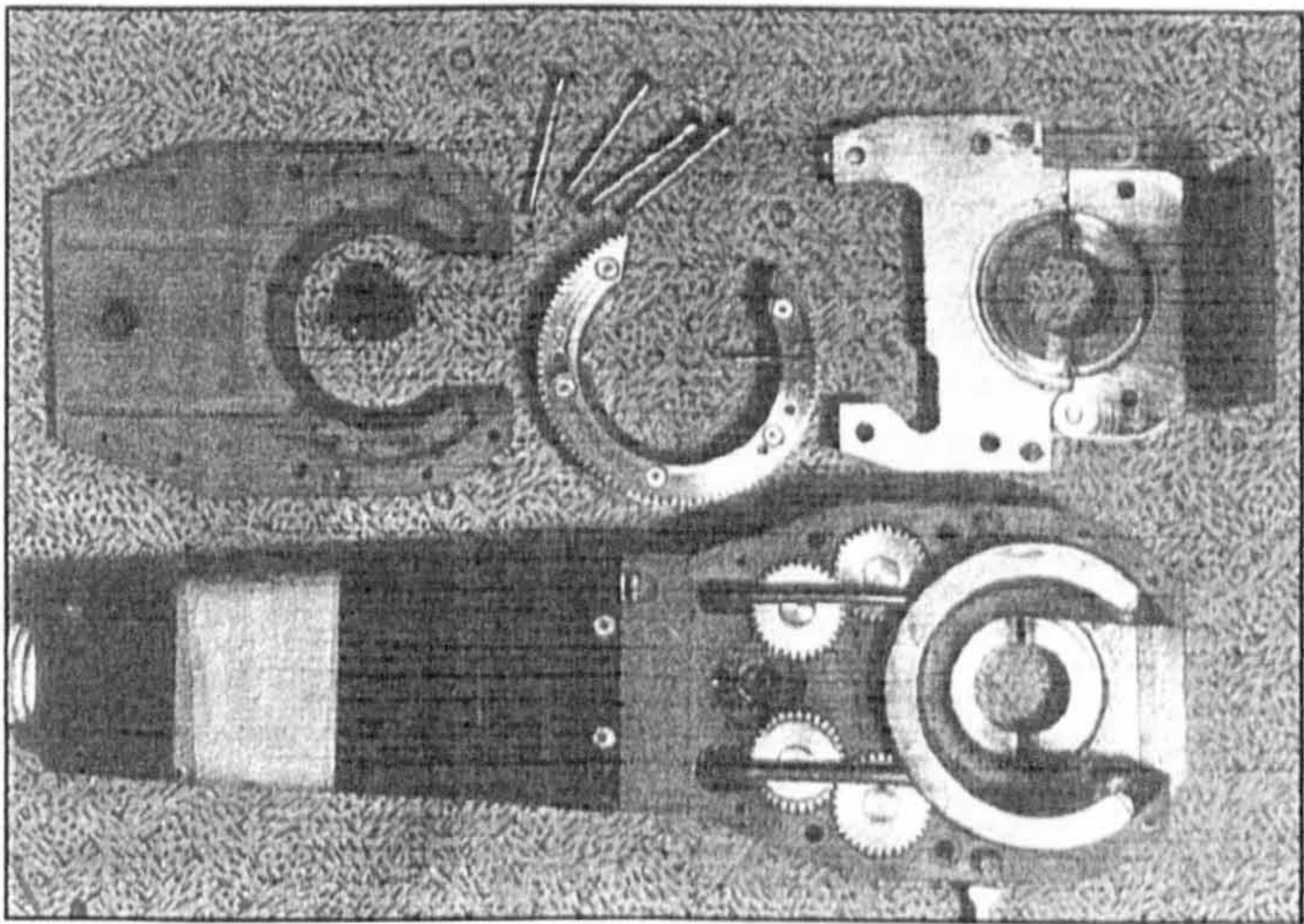


Figure 19 Exploded view - 9-1500 head

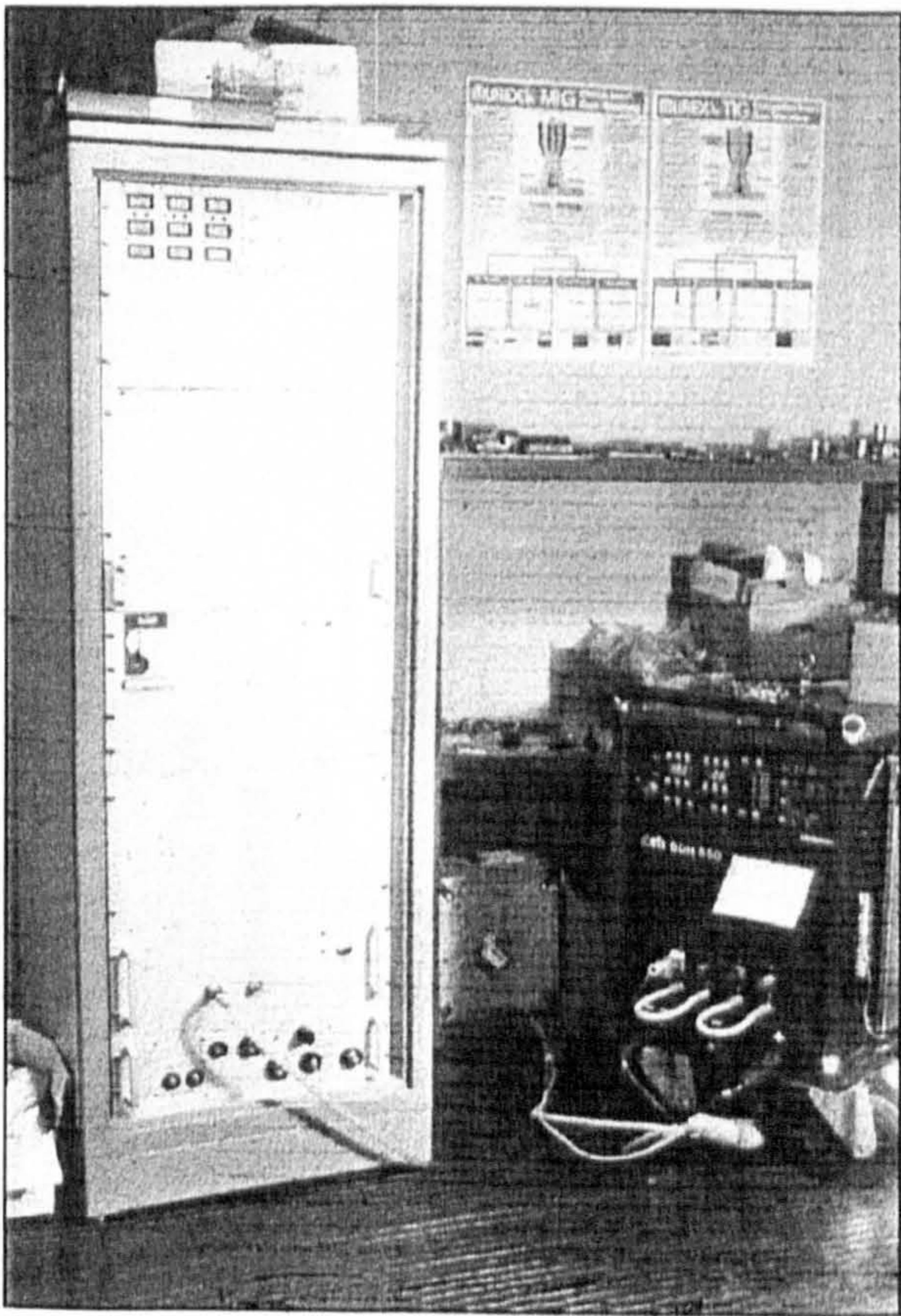


Figure 20 Isotek VME-Bus control rack (19") and Migatron BDH320 Commander power source

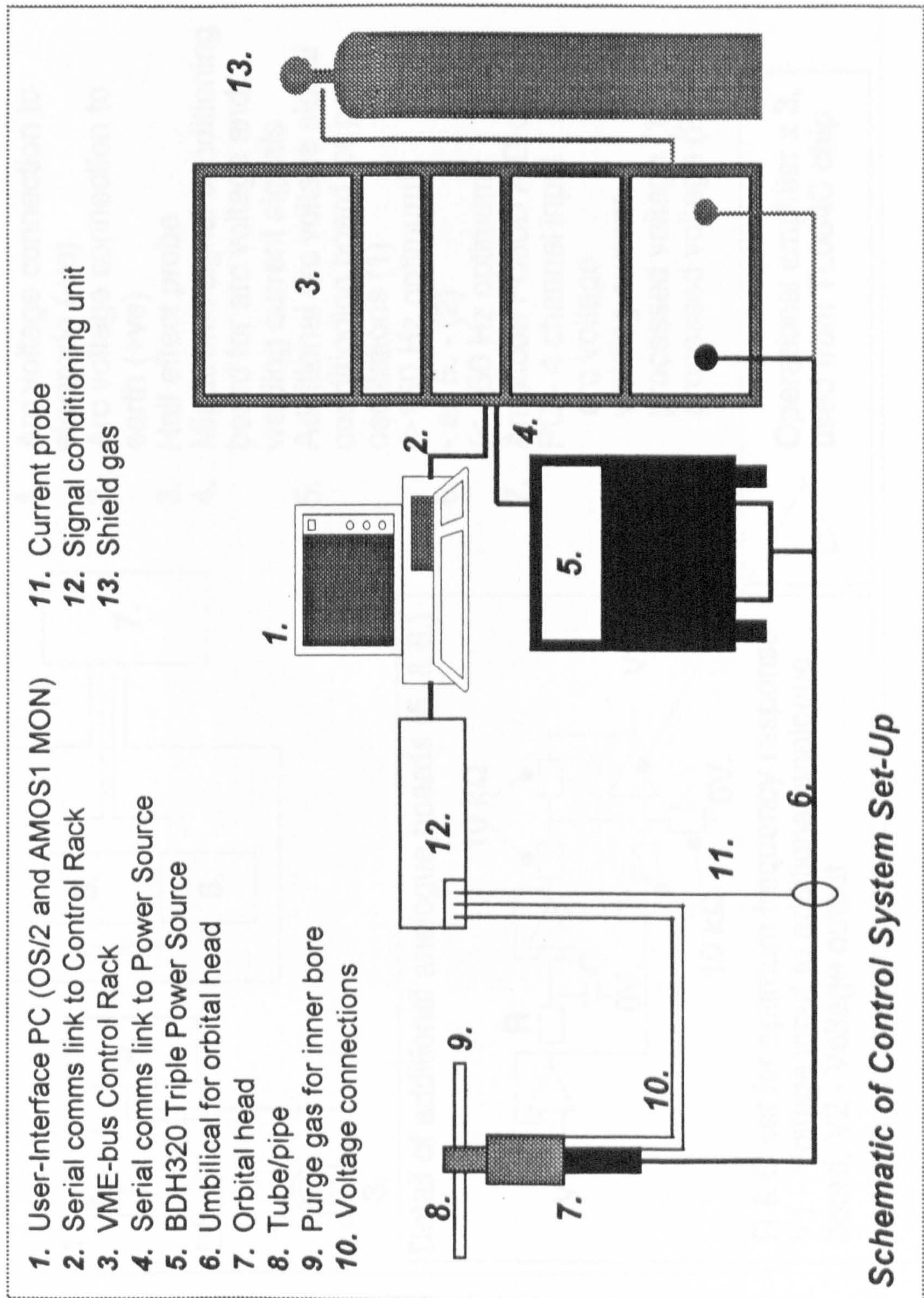


Figure 21

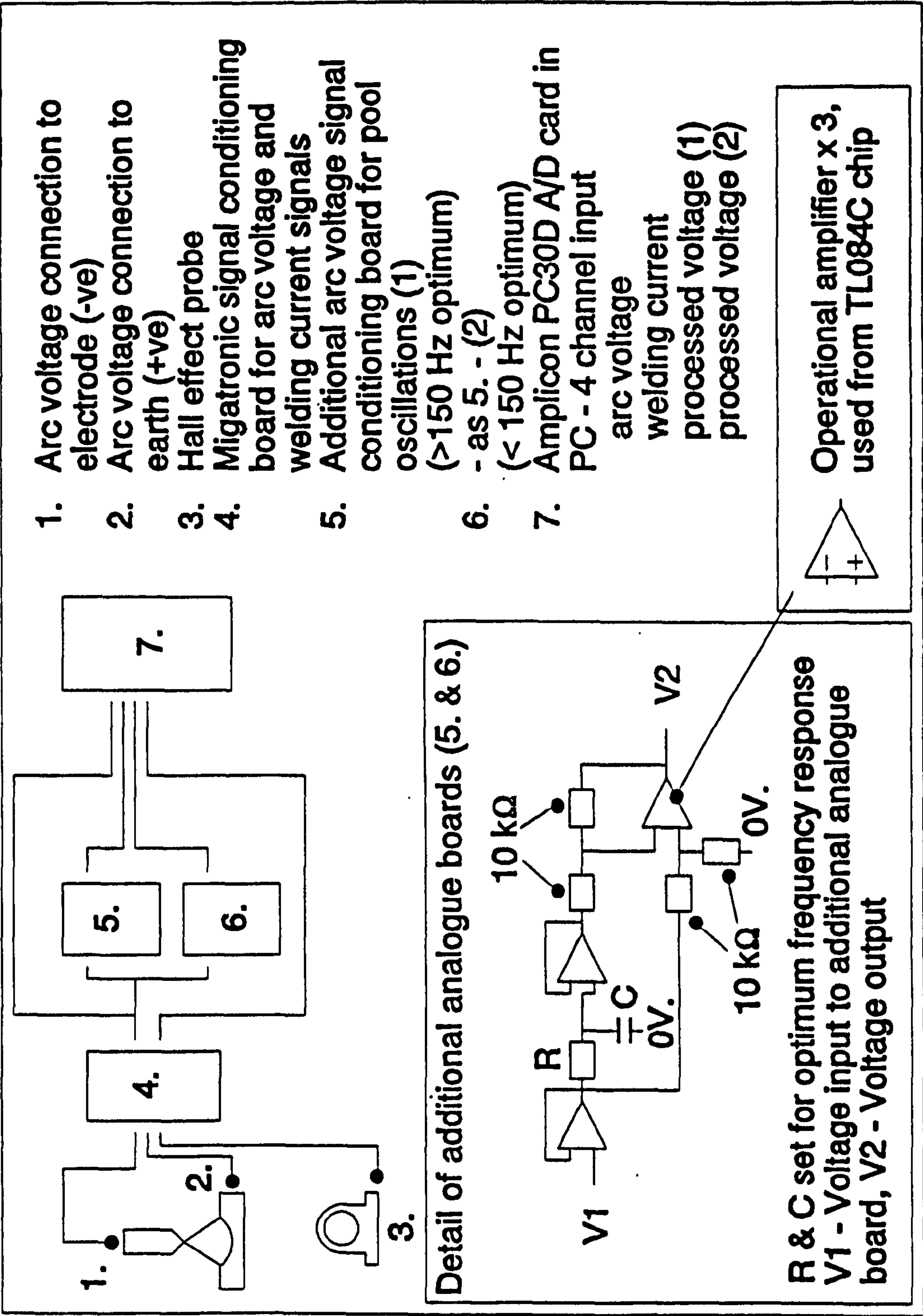


Figure 22 Layout of signal processing hardware

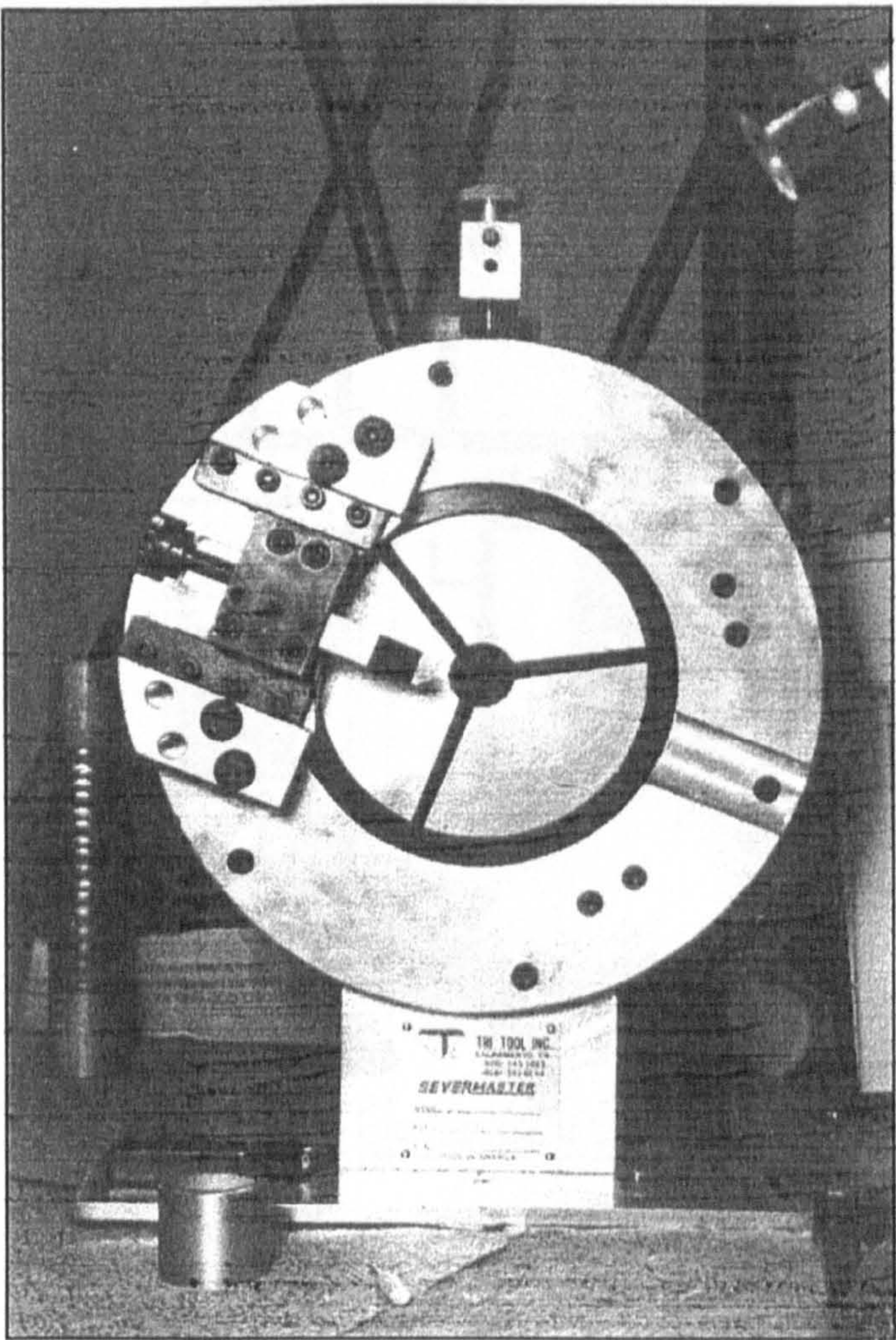


Figure 23 Tri-Tool facing machine for butt joint preparation

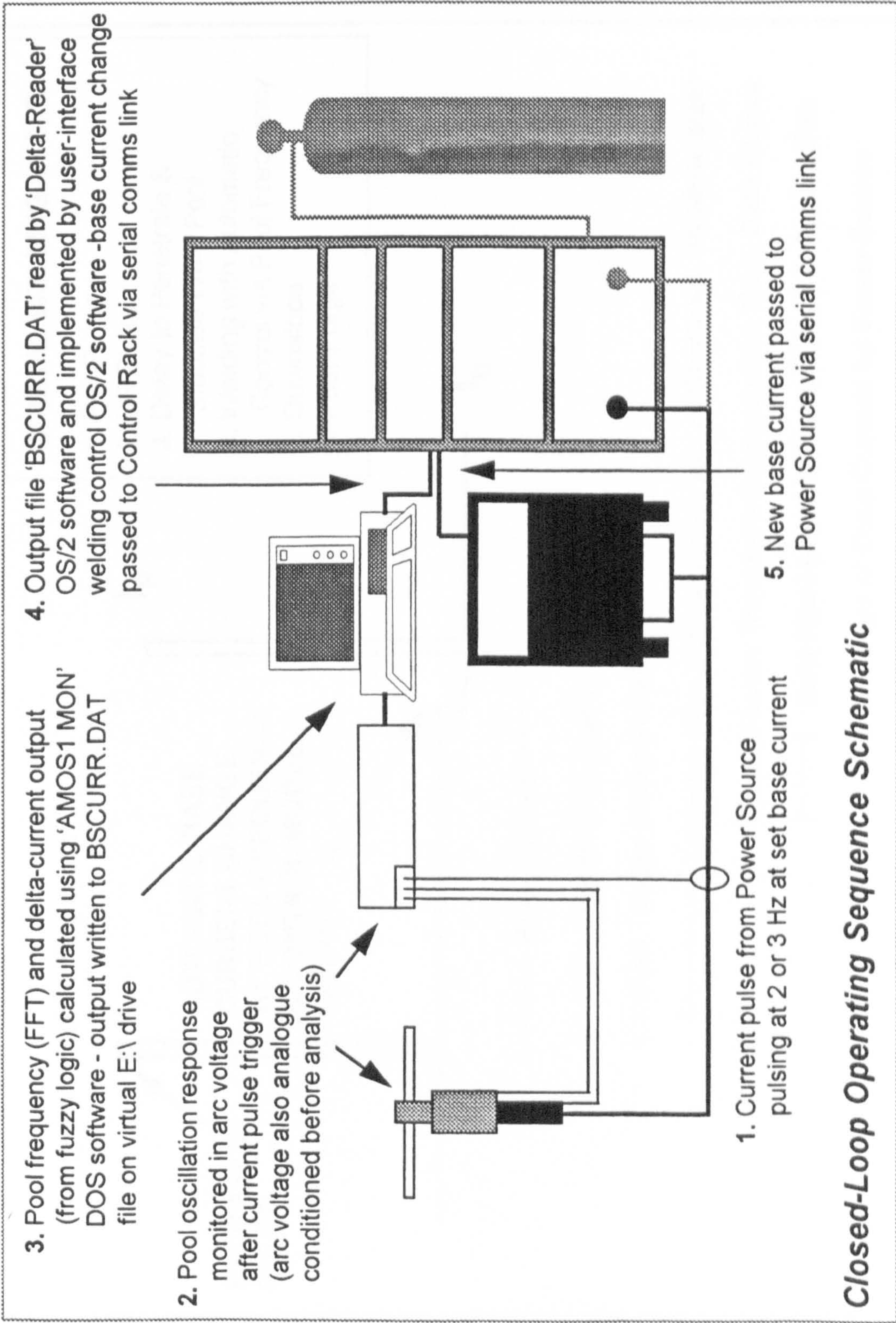


Figure 24

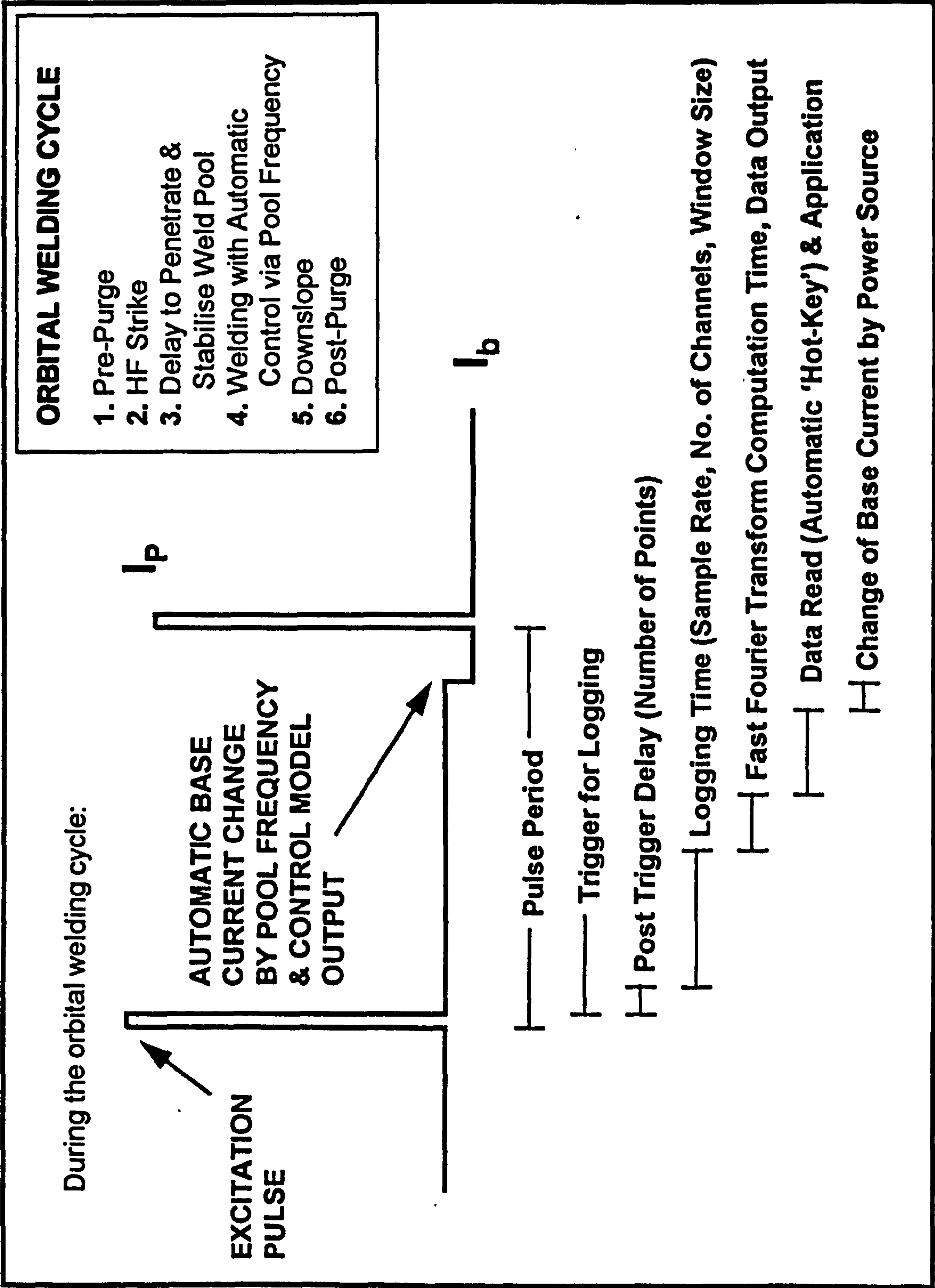


Figure 25 Control of orbital welding (event cycle)

Calibration of Power Source using Serial Comms

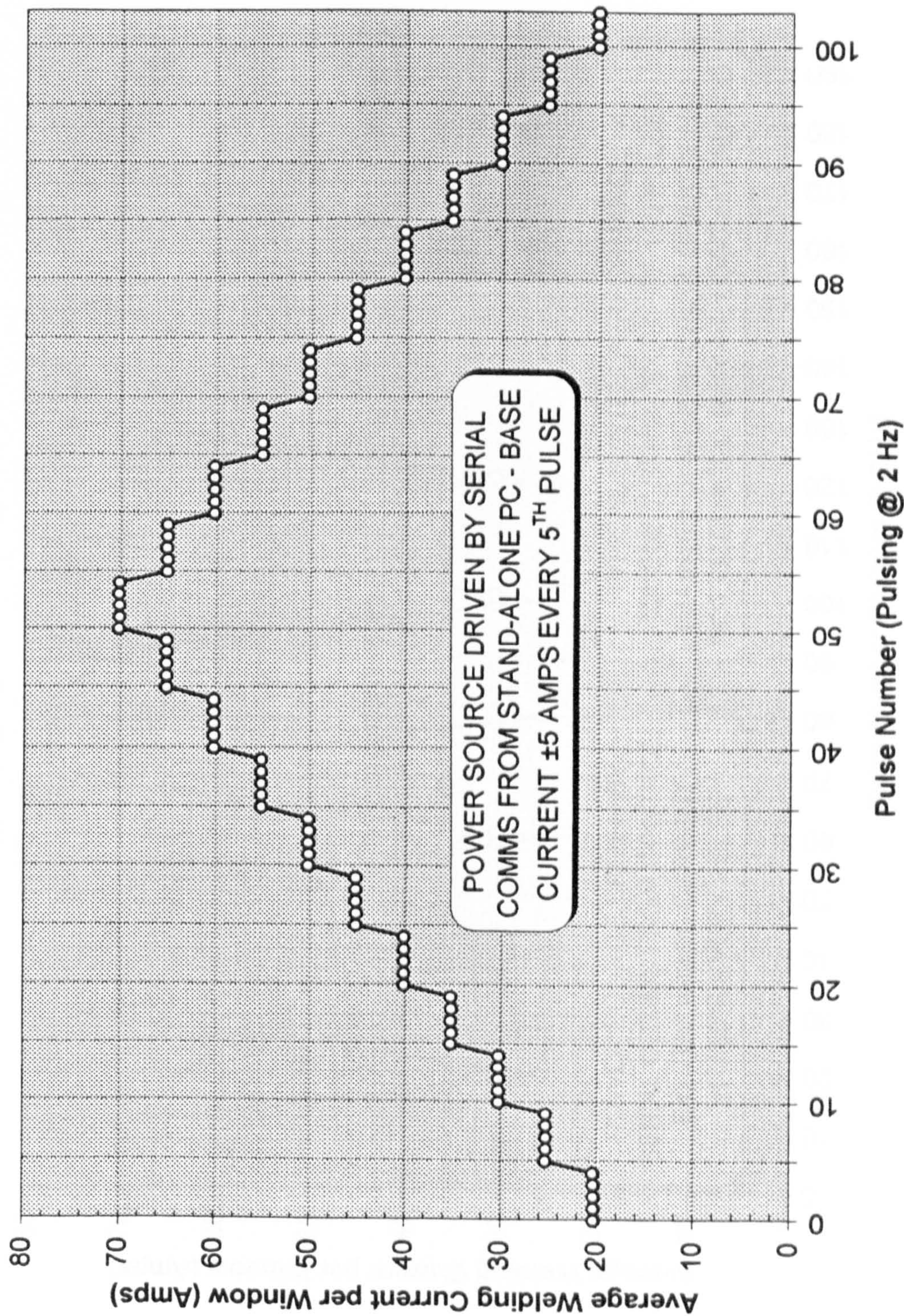


Figure 26

Calibration of Control of Power Source using User-Interface PC
Automatic 'Hot-Key' Command and Control Rack

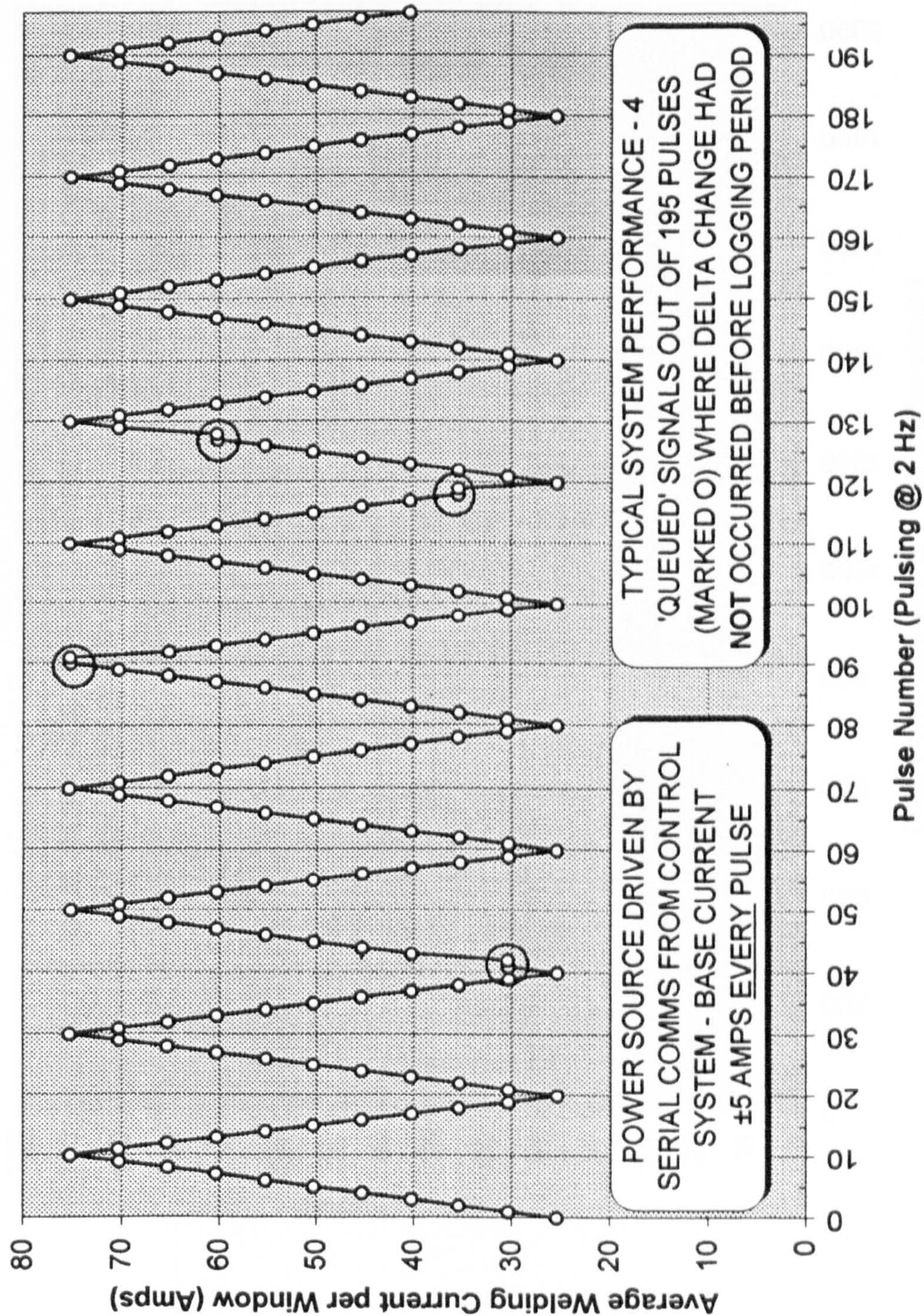


Figure 27

Transient Current Signal - Forced Output ± 5 Amps
Ideal System Response for Closed-Loop Control

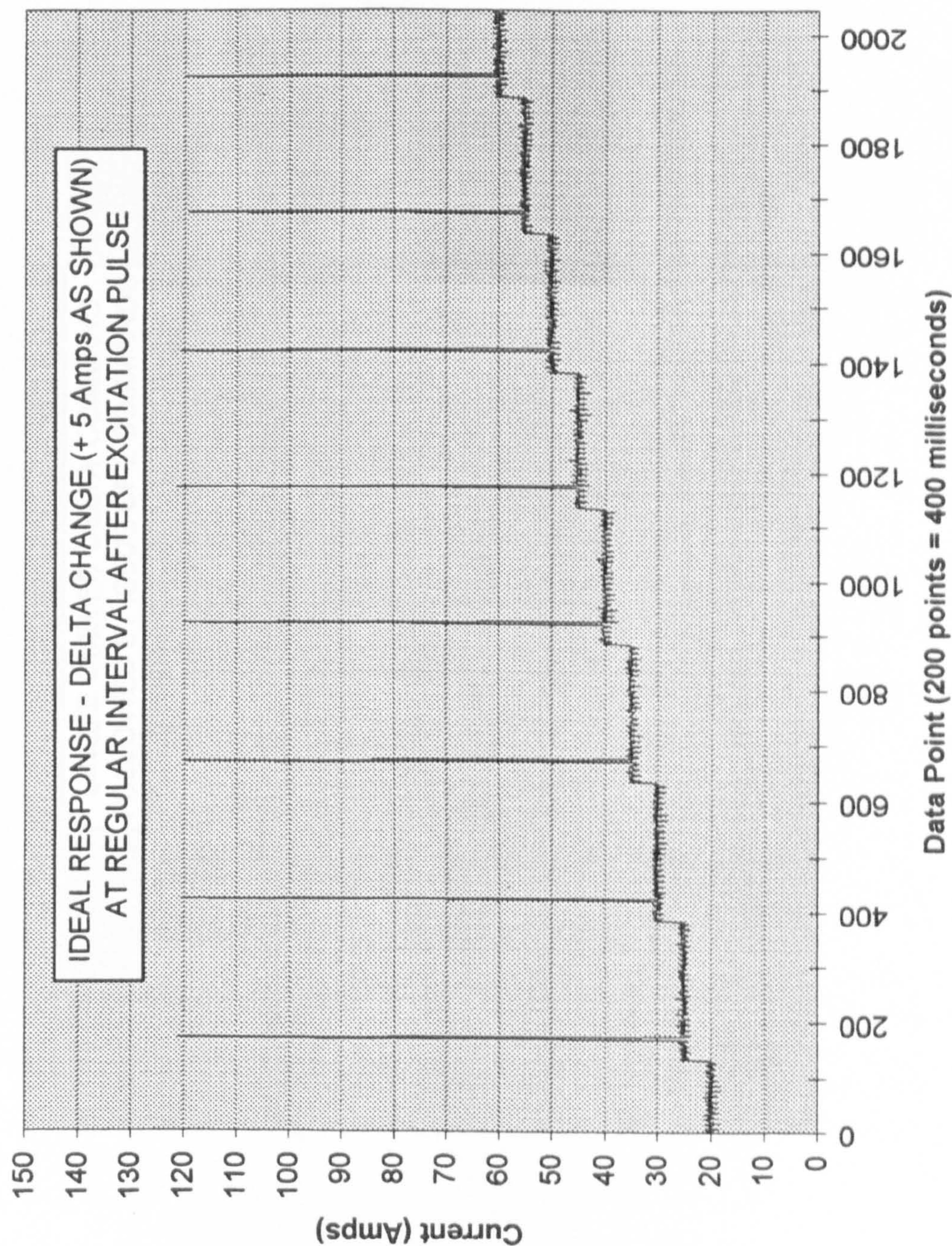


Figure 28

Transient Current Signal - Forced Output ± 5 Amps
Typical System Response for Closed-Loop Control

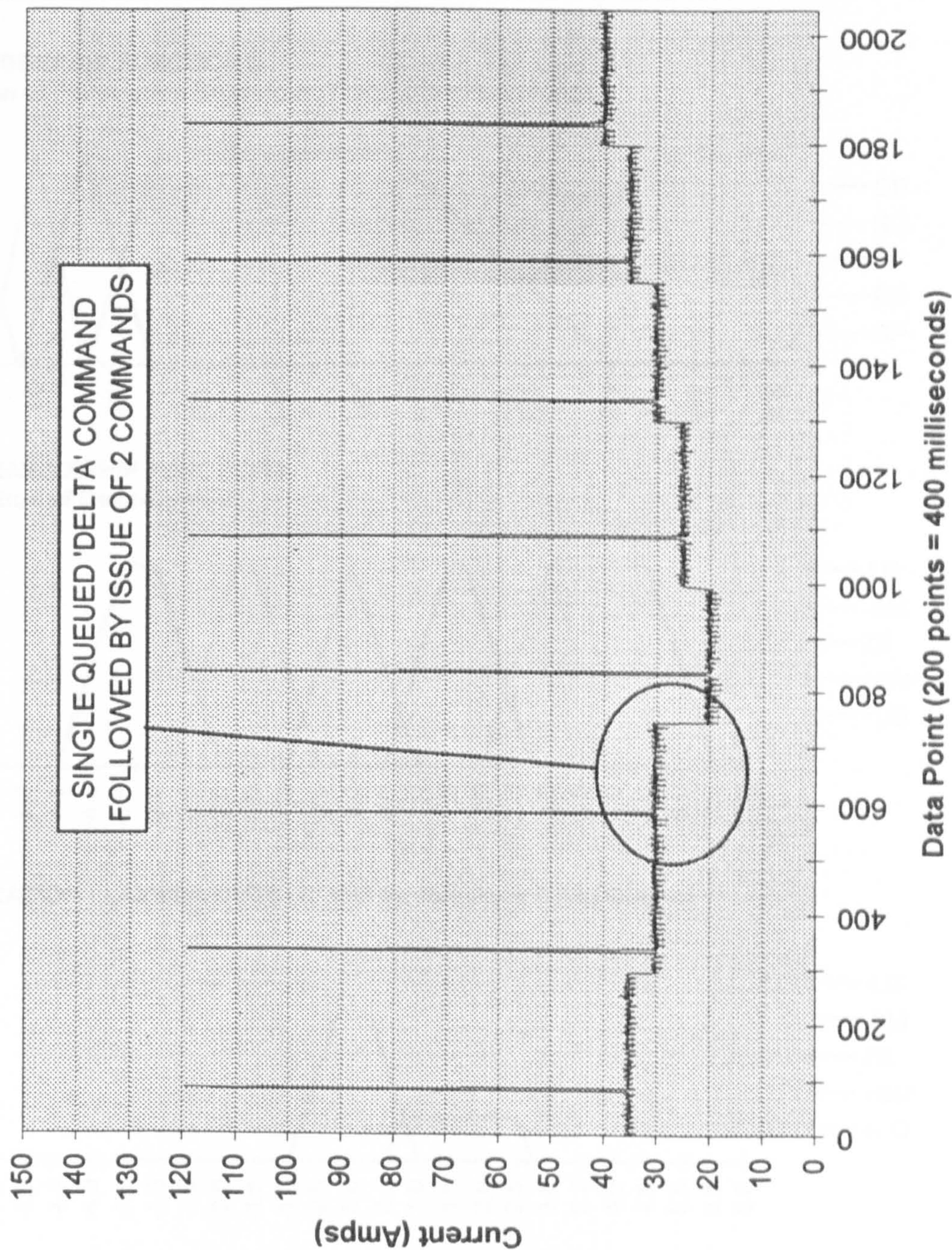
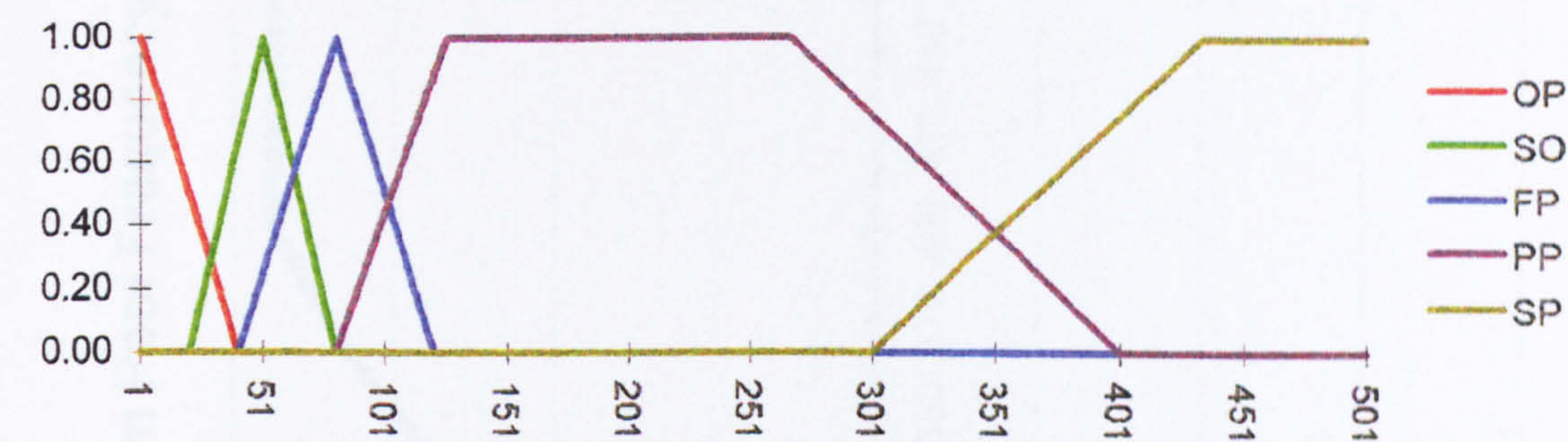


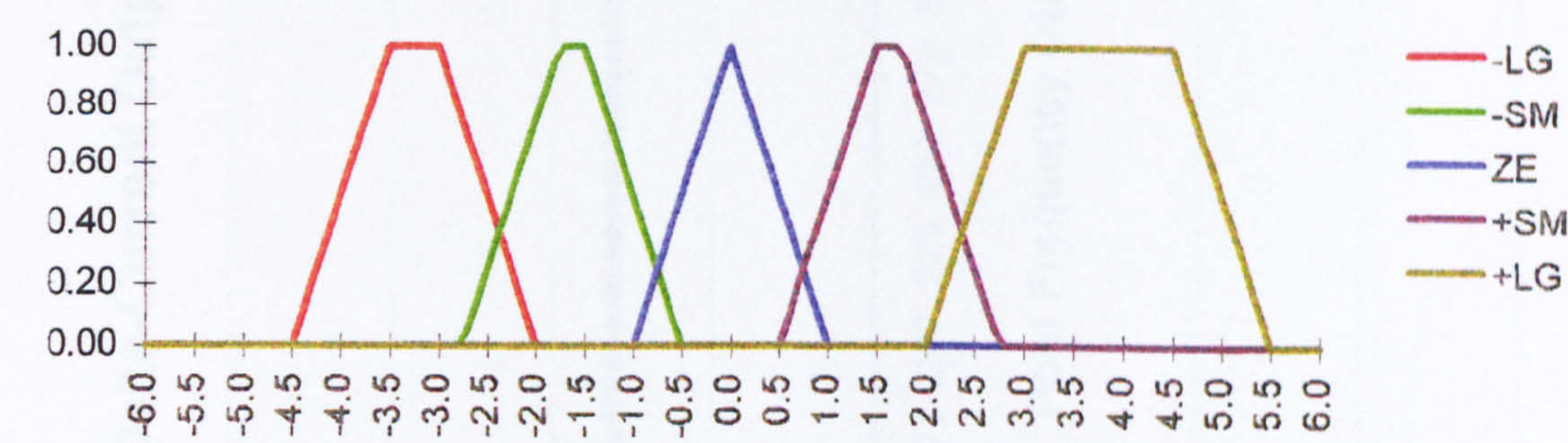
Figure 29

Example Input	OP	SO	FP	PP	SP	Resultant Output
90.0 Hz	0.00	0.00	0.75	0.22	0.00	0.52 Amps

INPUT MEMBERSHIP FUNCTIONS
(Fuzzification of Penetration Behaviour / Oscillation Frequency)



OUTPUT MEMBERSHIP FUNCTIONS
(Defuzzification of Delta-Current)



DEFUZZIFICATION : LAMBDA CUTS (C of G for Resultant Crisp Output)

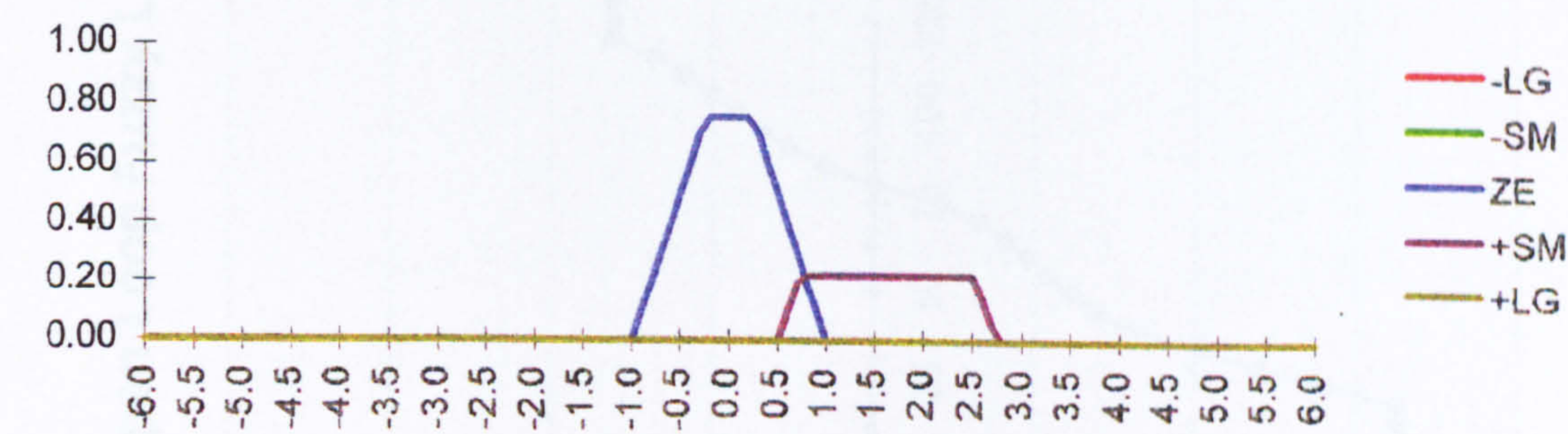


Figure 30 Graphical presentation of input and output membership functions, example input and resulting lambda cuts for resultant crisp output (target frequency of 80 Hz)

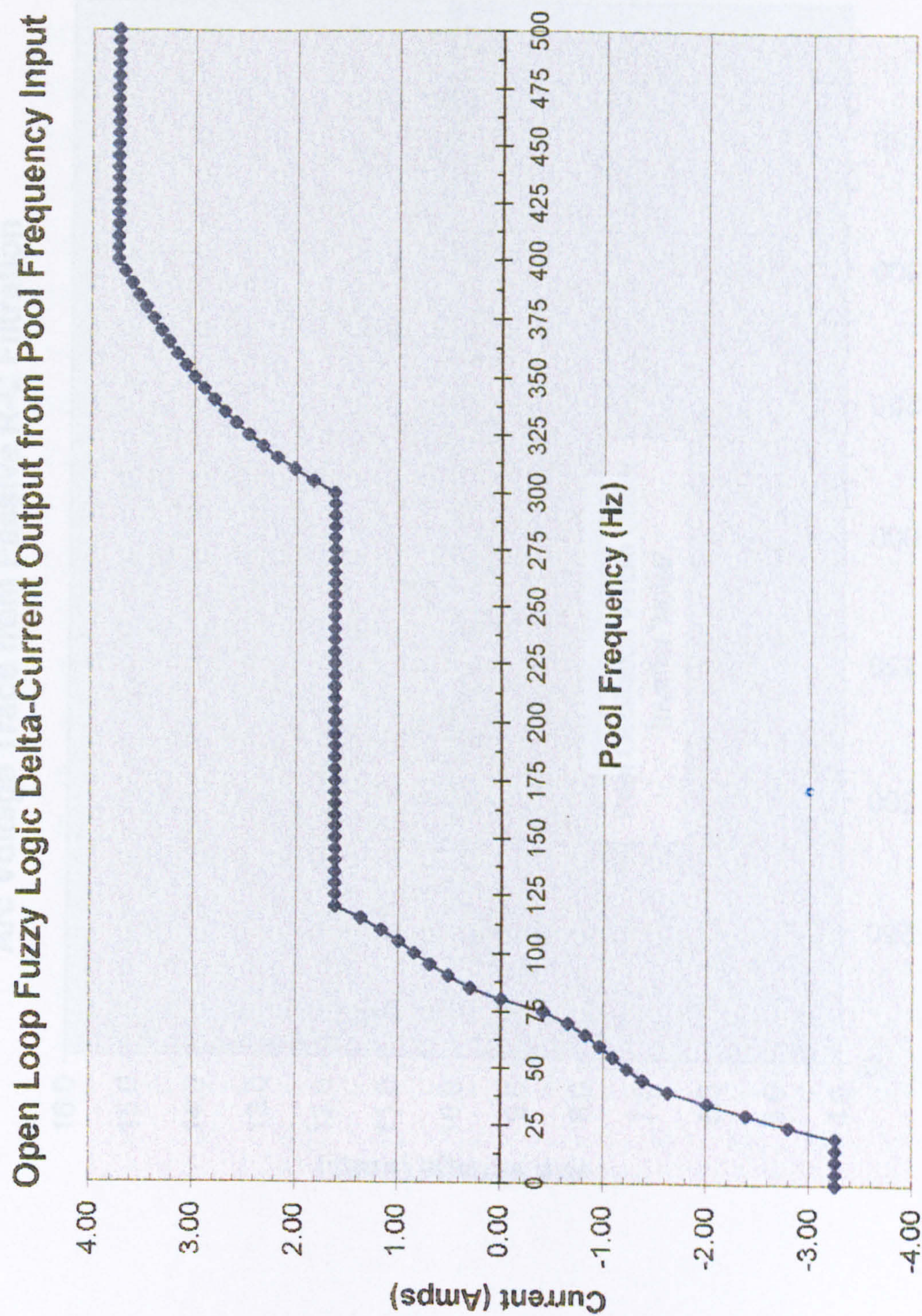


Figure 31 Input/Output curve for fuzzy logic model

Arc Voltage Trace from Passive R-C Filtration

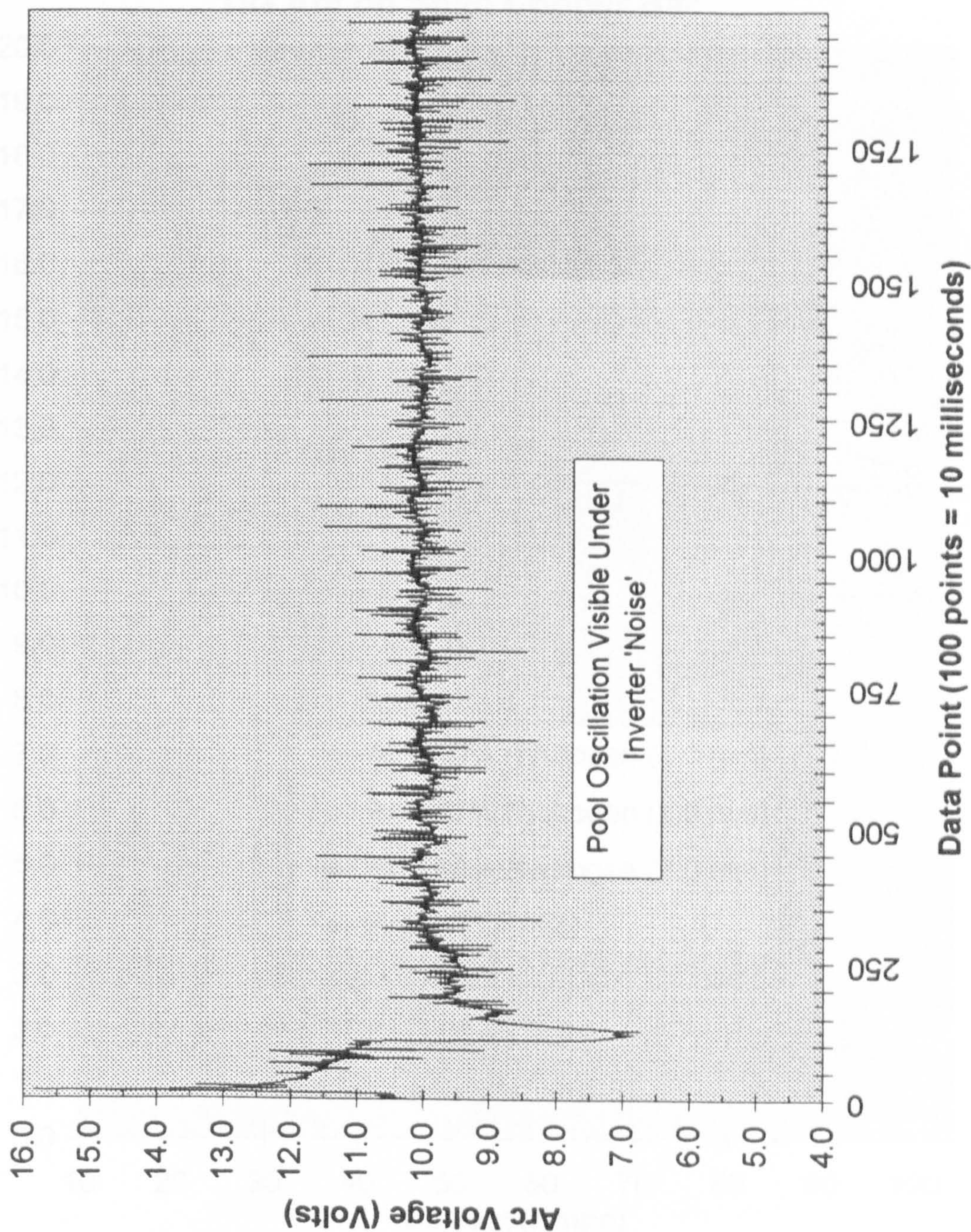


Figure 32

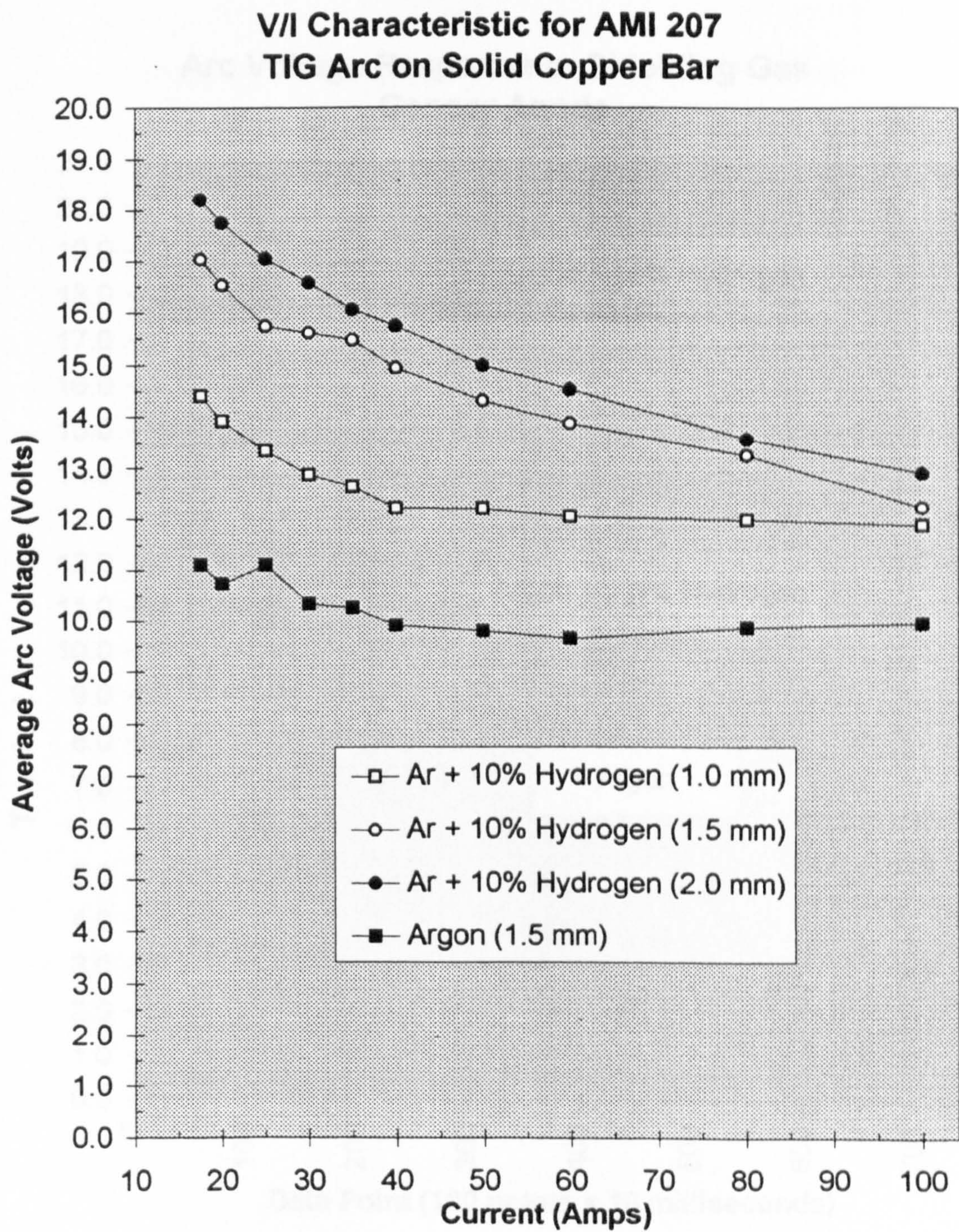


Figure 33

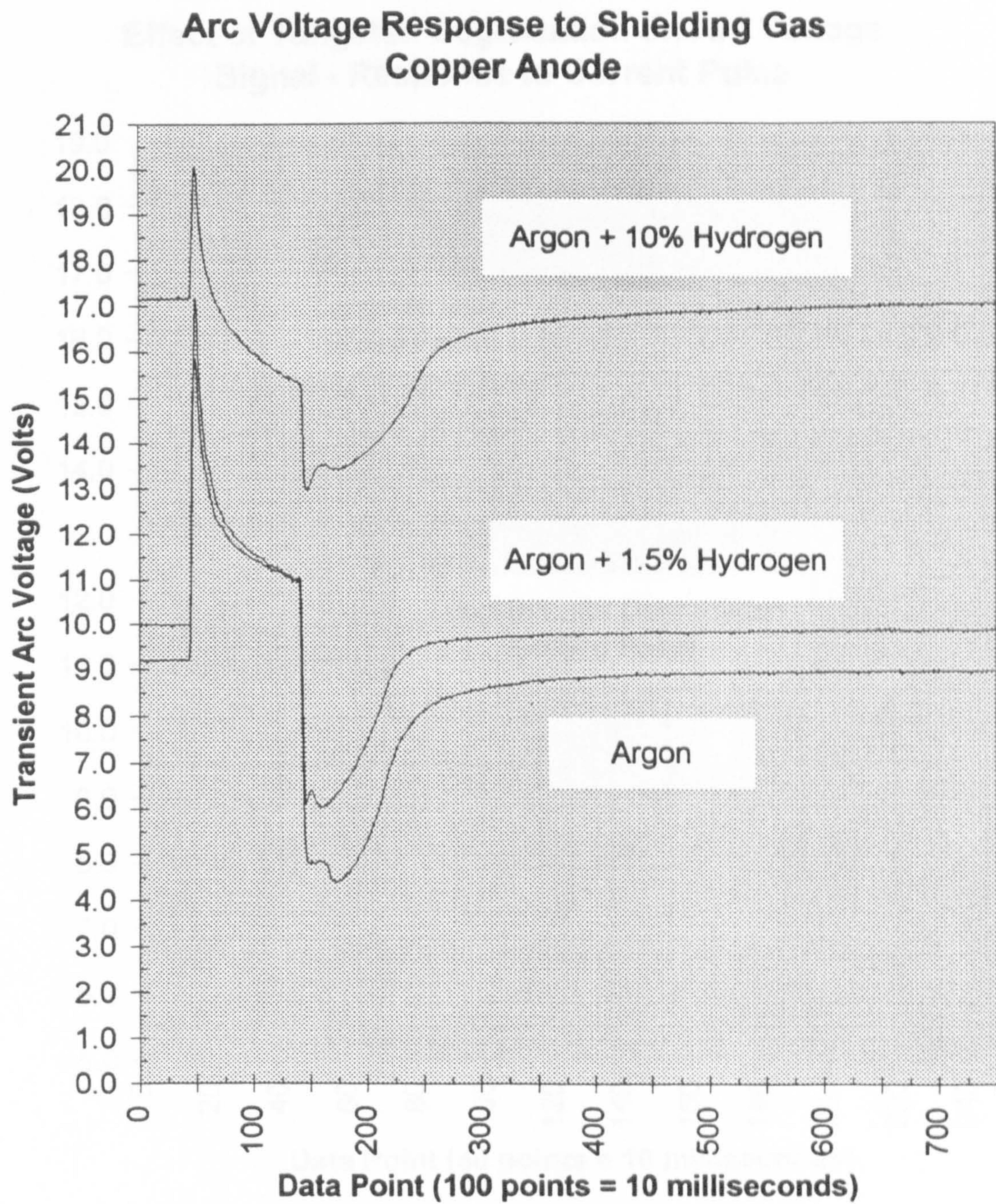


Figure 34

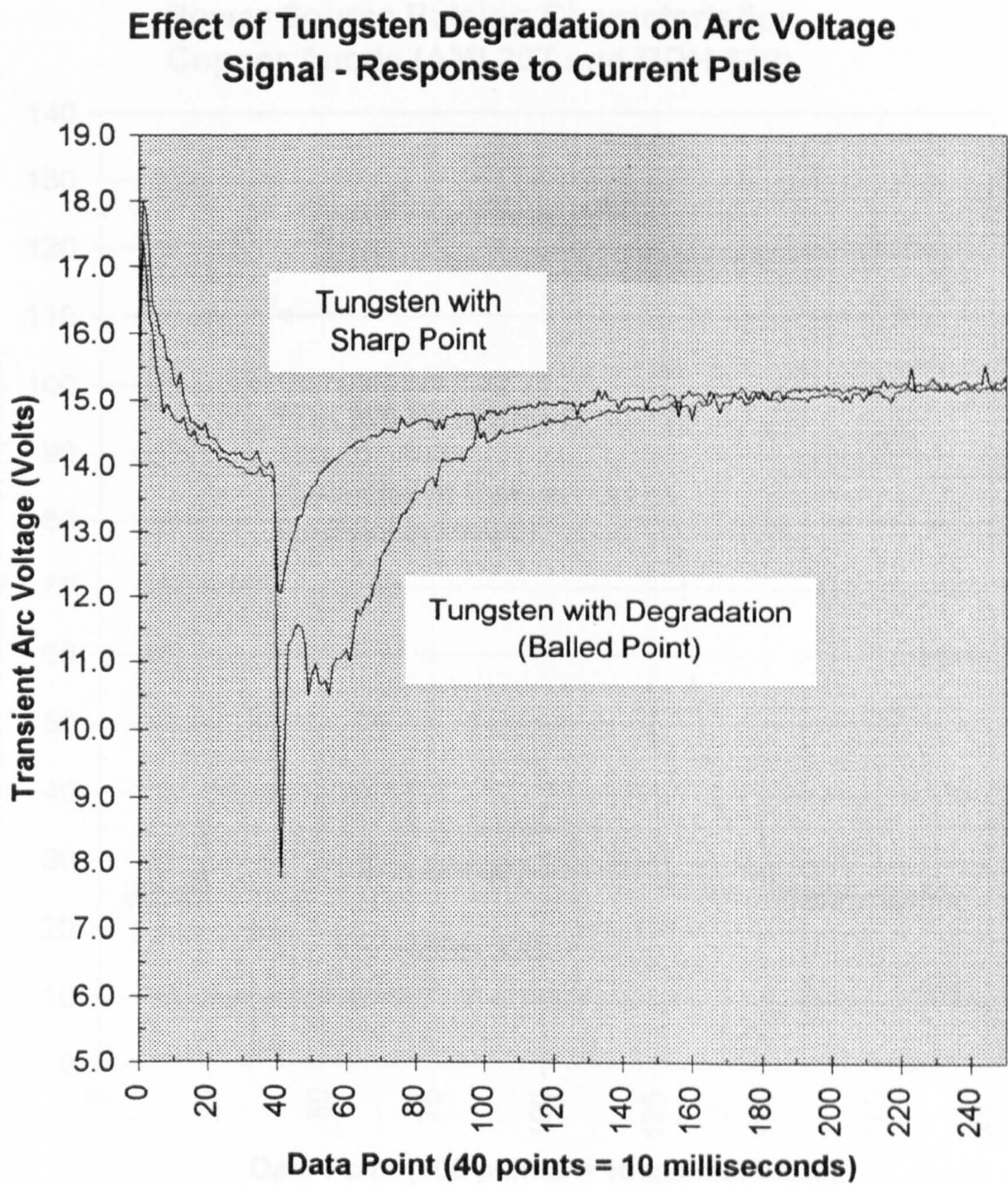


Figure 35

**Power Source Pulsing Characteristics
Copper Anode (AMI 207 and BDH 320)**

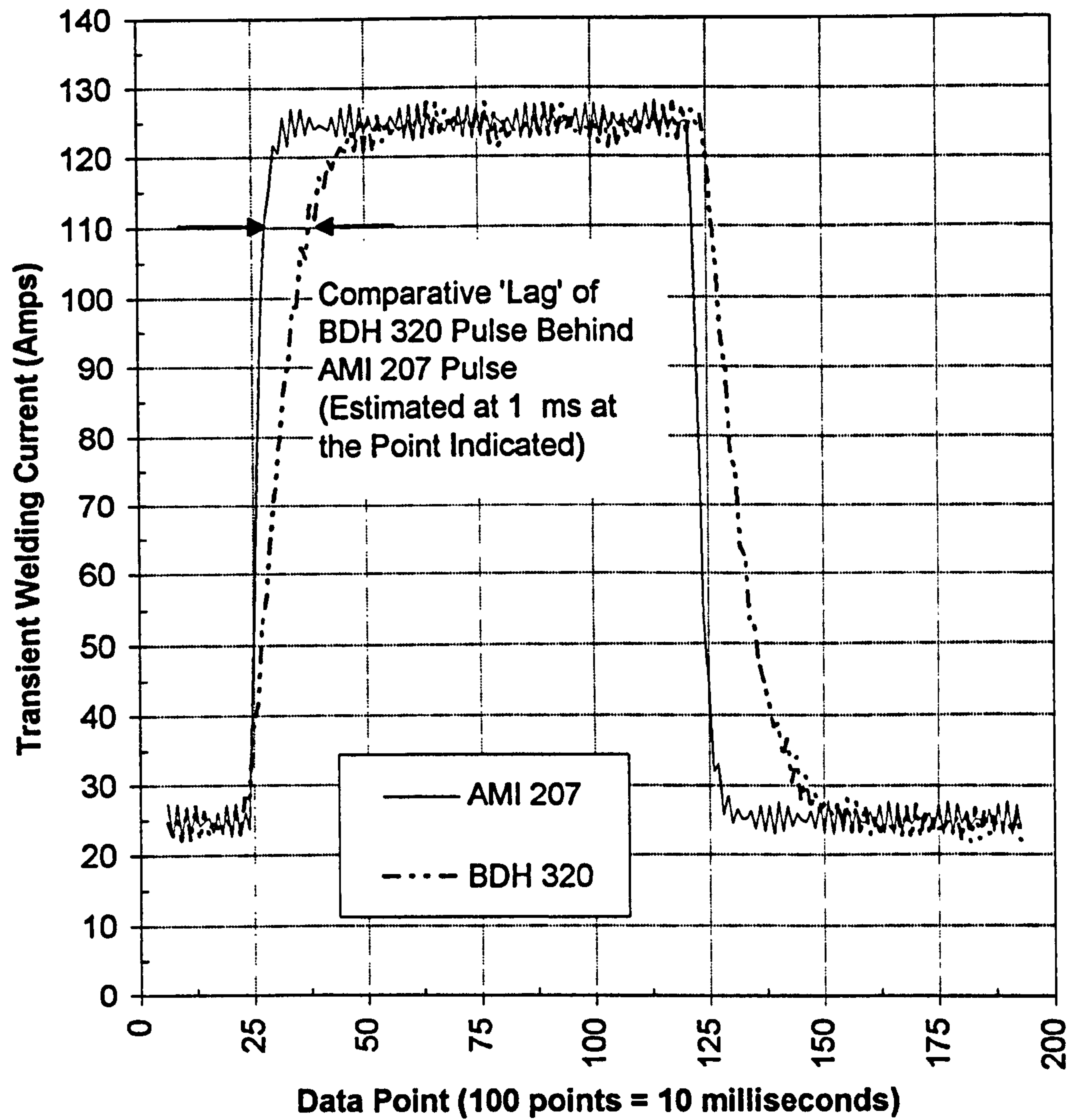


Figure 36

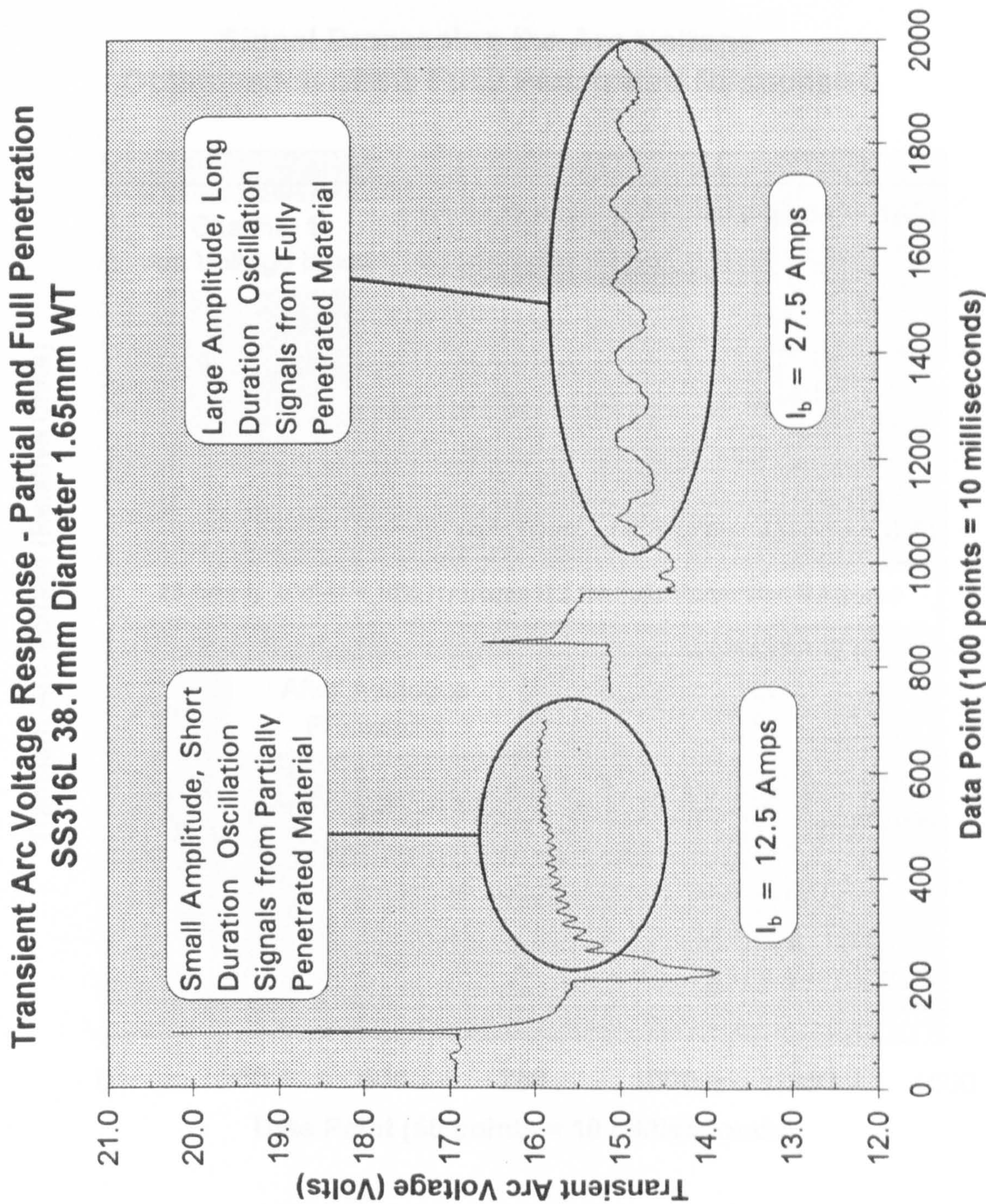


Figure 37

Signal Processing the Arc Voltage
Optimisation of the Fully Penetrated Response

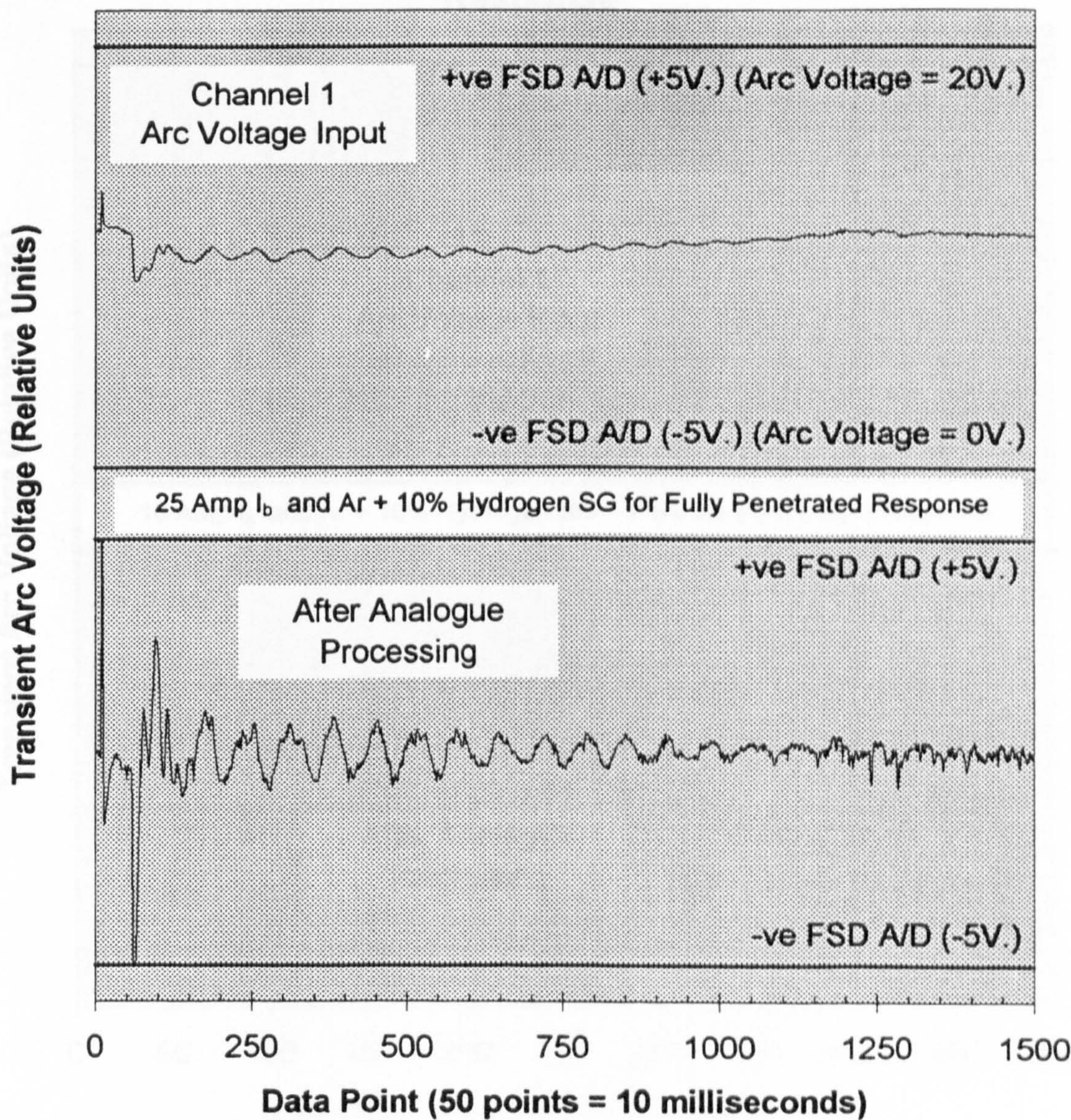


Figure 38

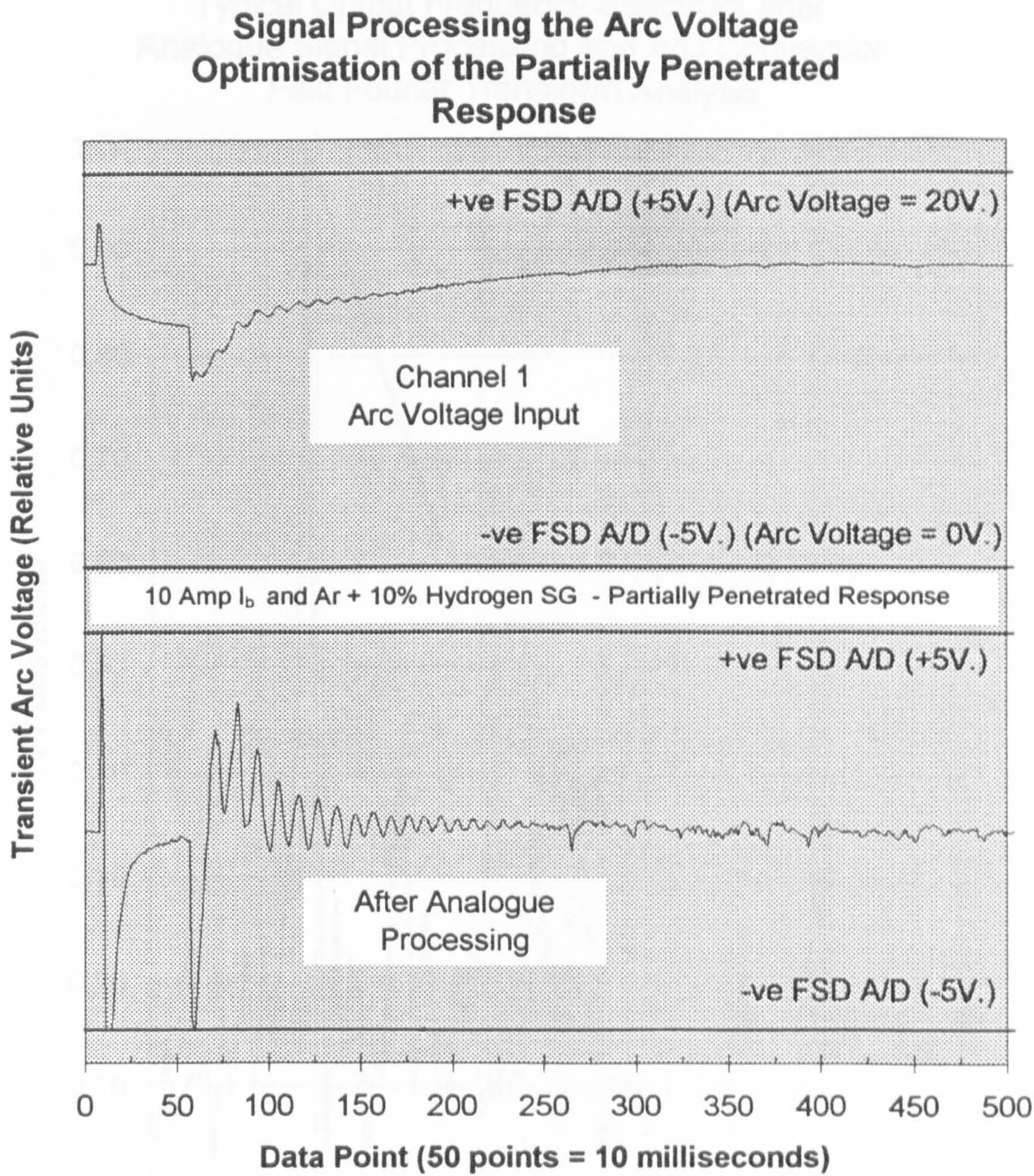


Figure 39

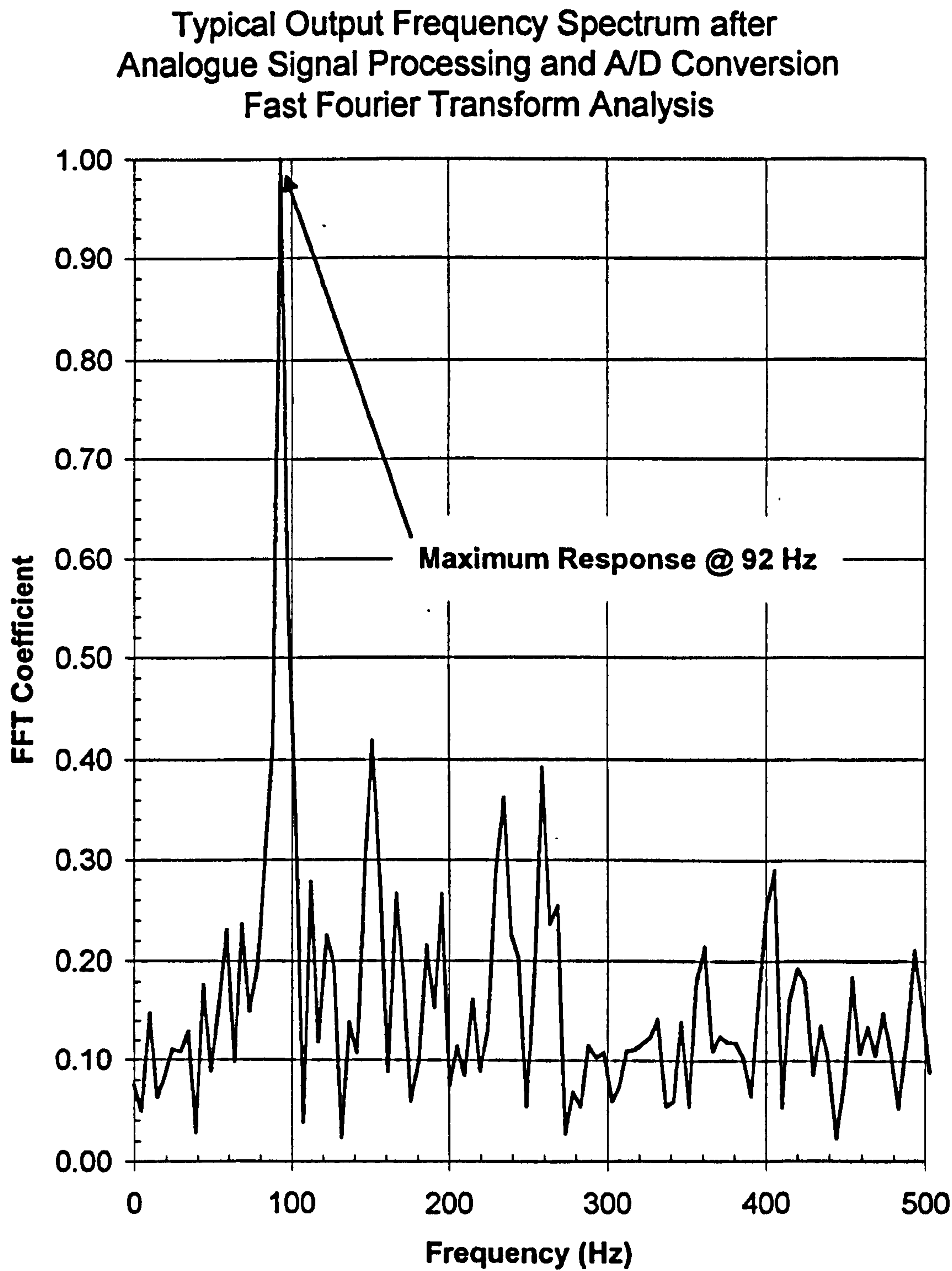


Figure 40

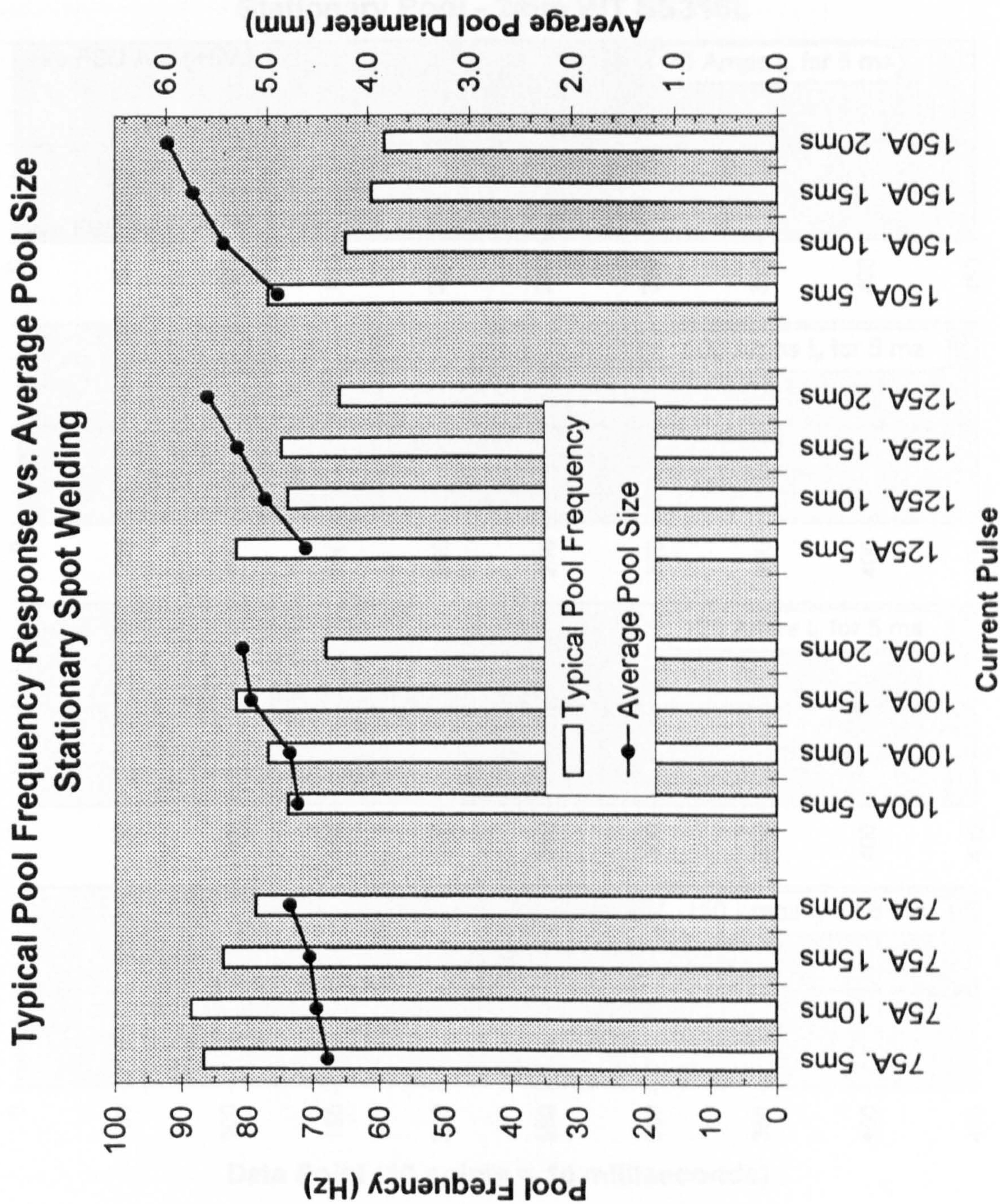


Figure 41

Effect of Pulse Magnitude on Pool Oscillation
Stationary Pool - 2mm WT SS316L

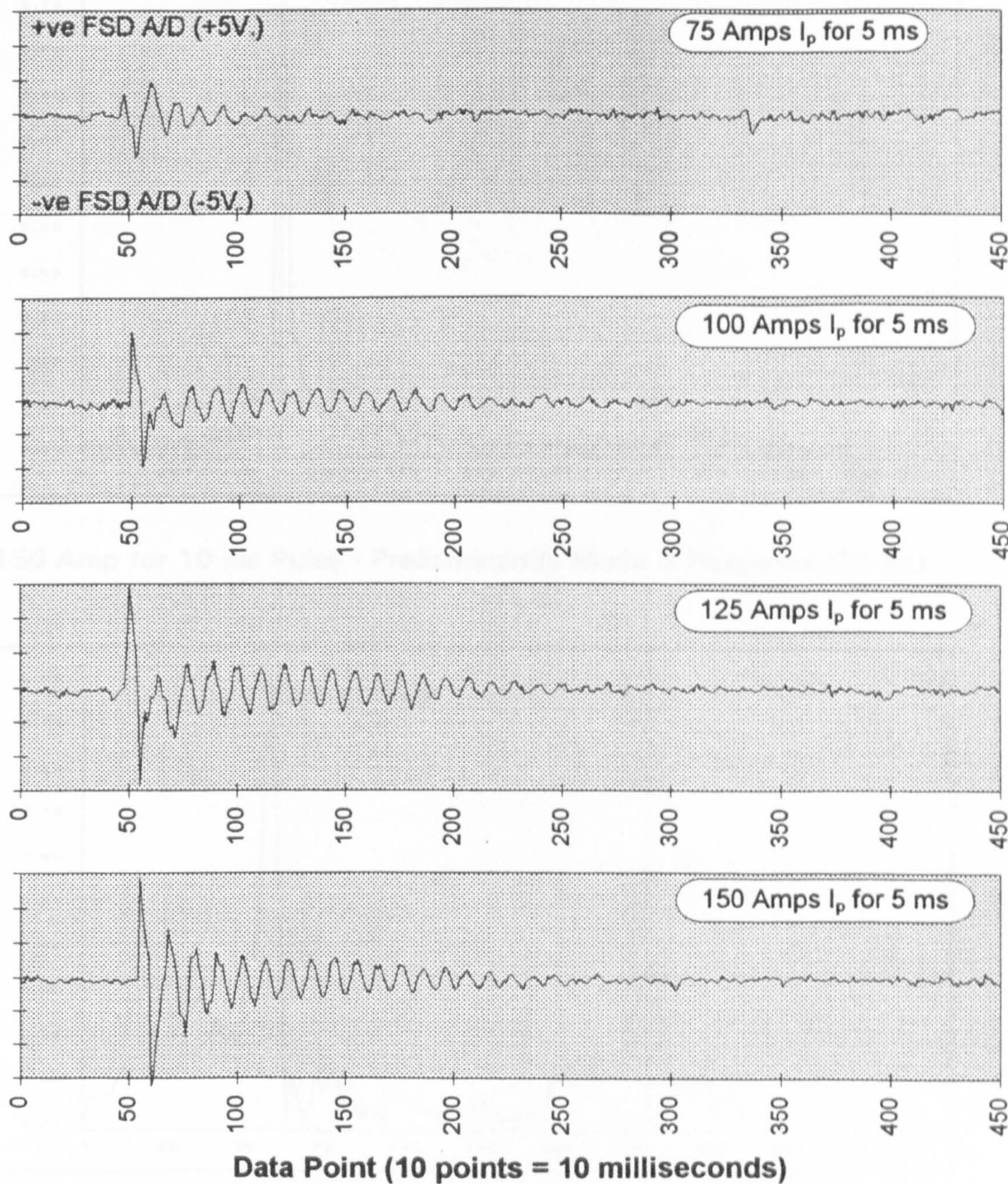
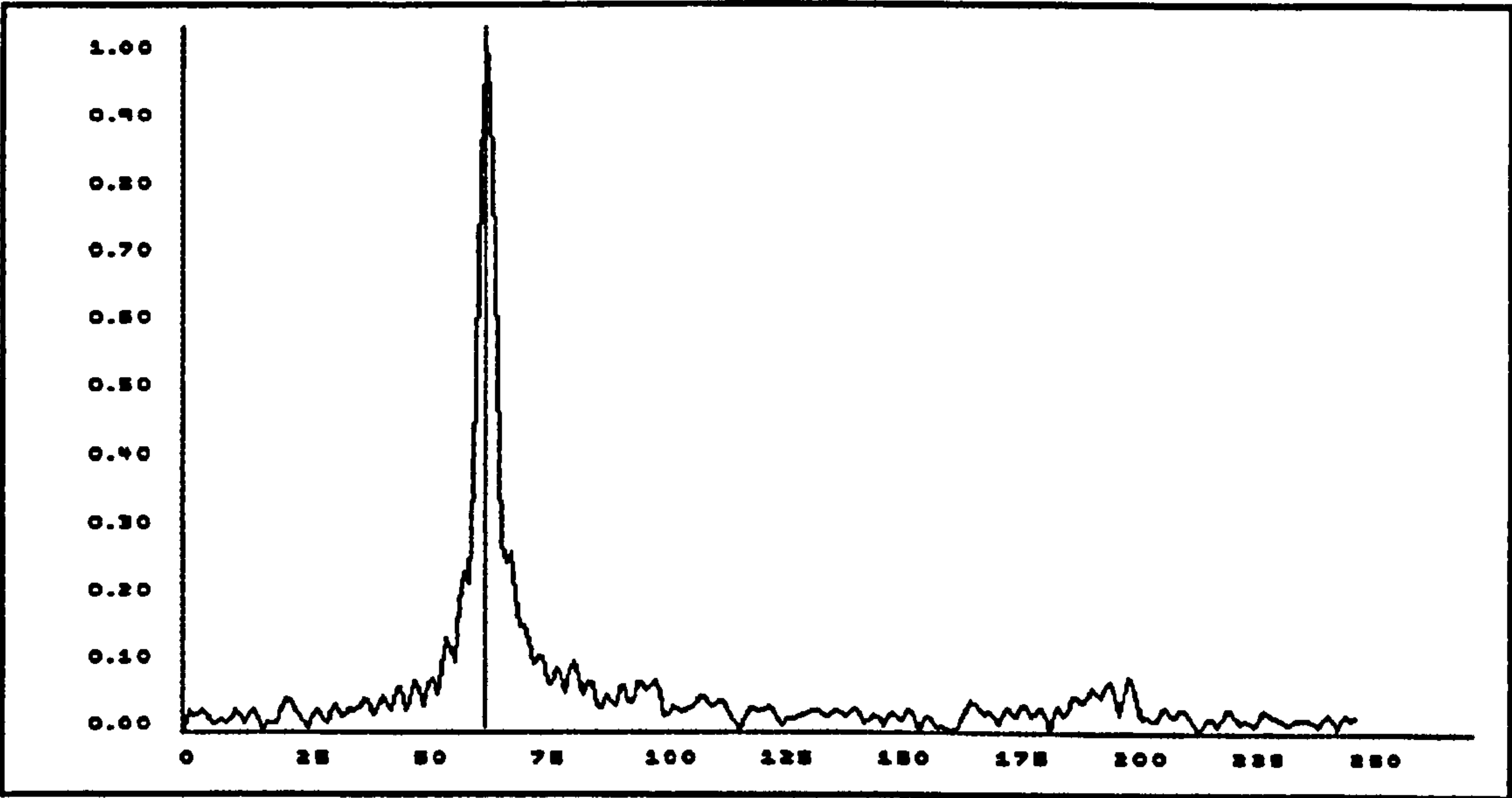
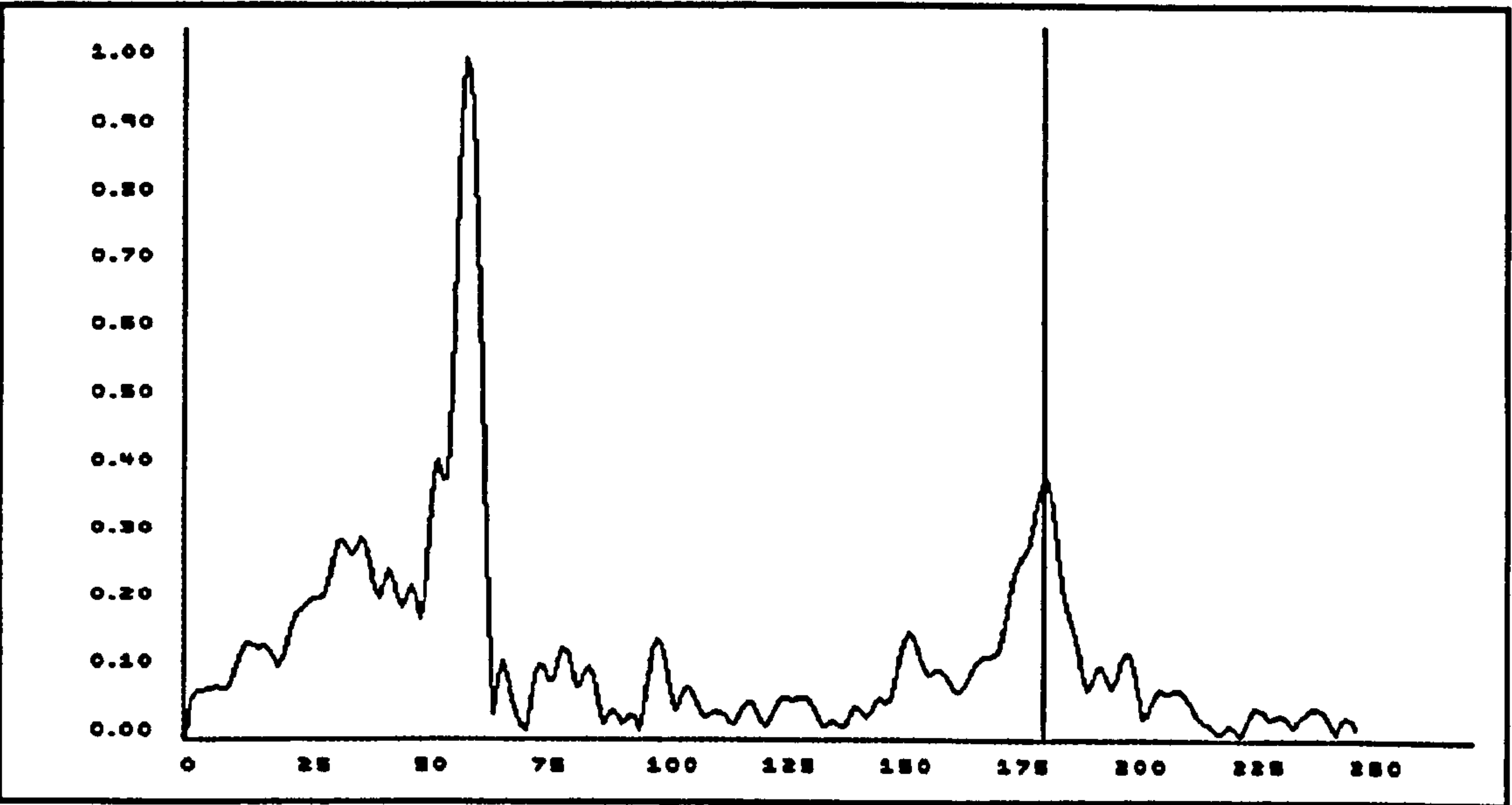


Figure 42

Y-Axis - FFT Co-efficient (0.00 to 1.00)
X-Axis - Frequency (0 to 250 Hz)



150 Amp for 10 ms Pulse - Predominantly Mode 3 Response (65 Hz)



150 Amp for 15 ms Pulse - Mixed-Mode Response (61 Hz and 185 Hz)

Figure 43 FFT spectra for two stationary pools
- predominantly Mode 3 and a mixed-mode response

Basic Welding Parameters
Effect of Welding Current upon Pool Frequency
04:30 Position

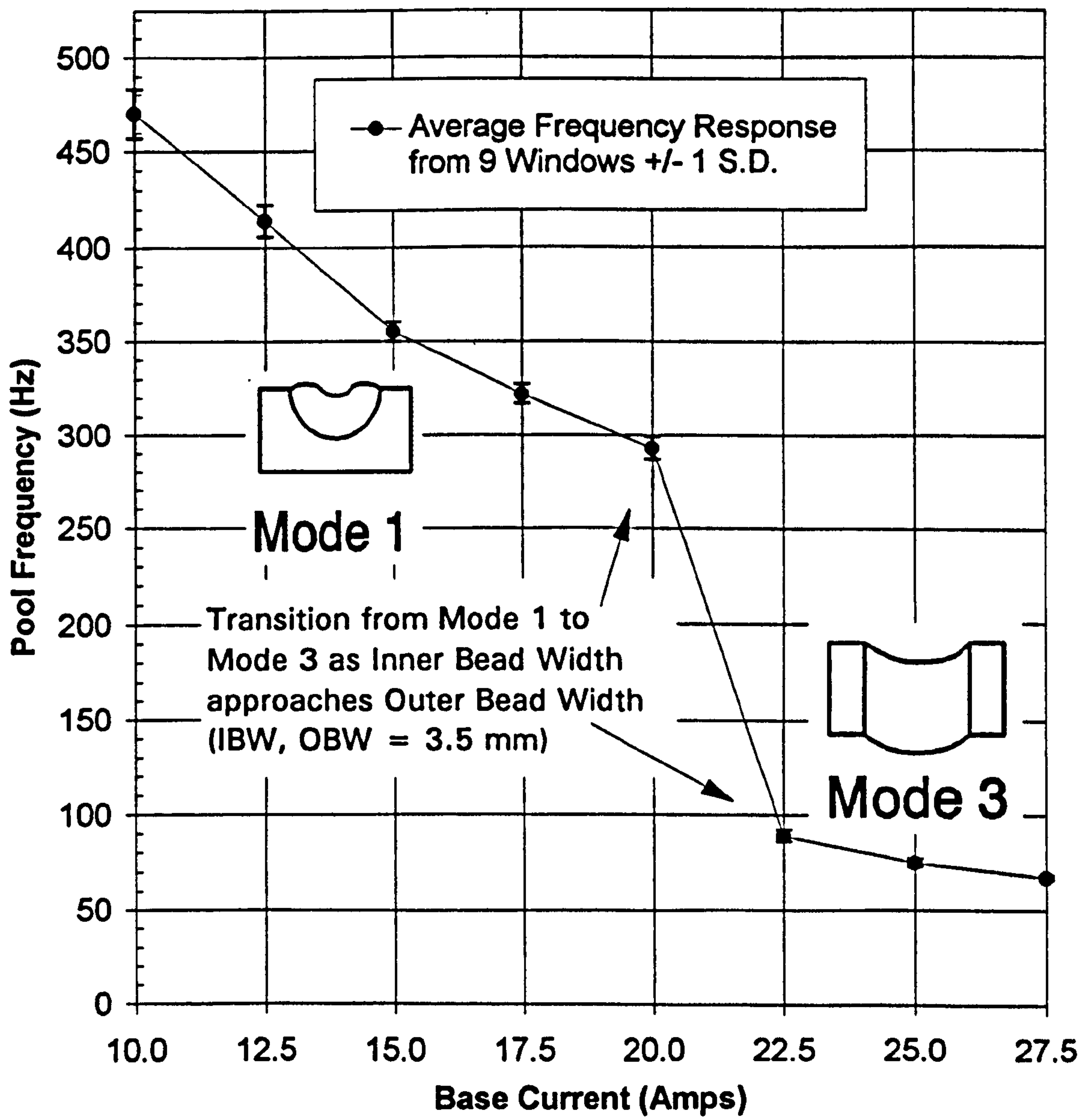


Figure 44

Basic Welding Parameters
Effect of Welding Current upon Pool Frequency
04:30 Position

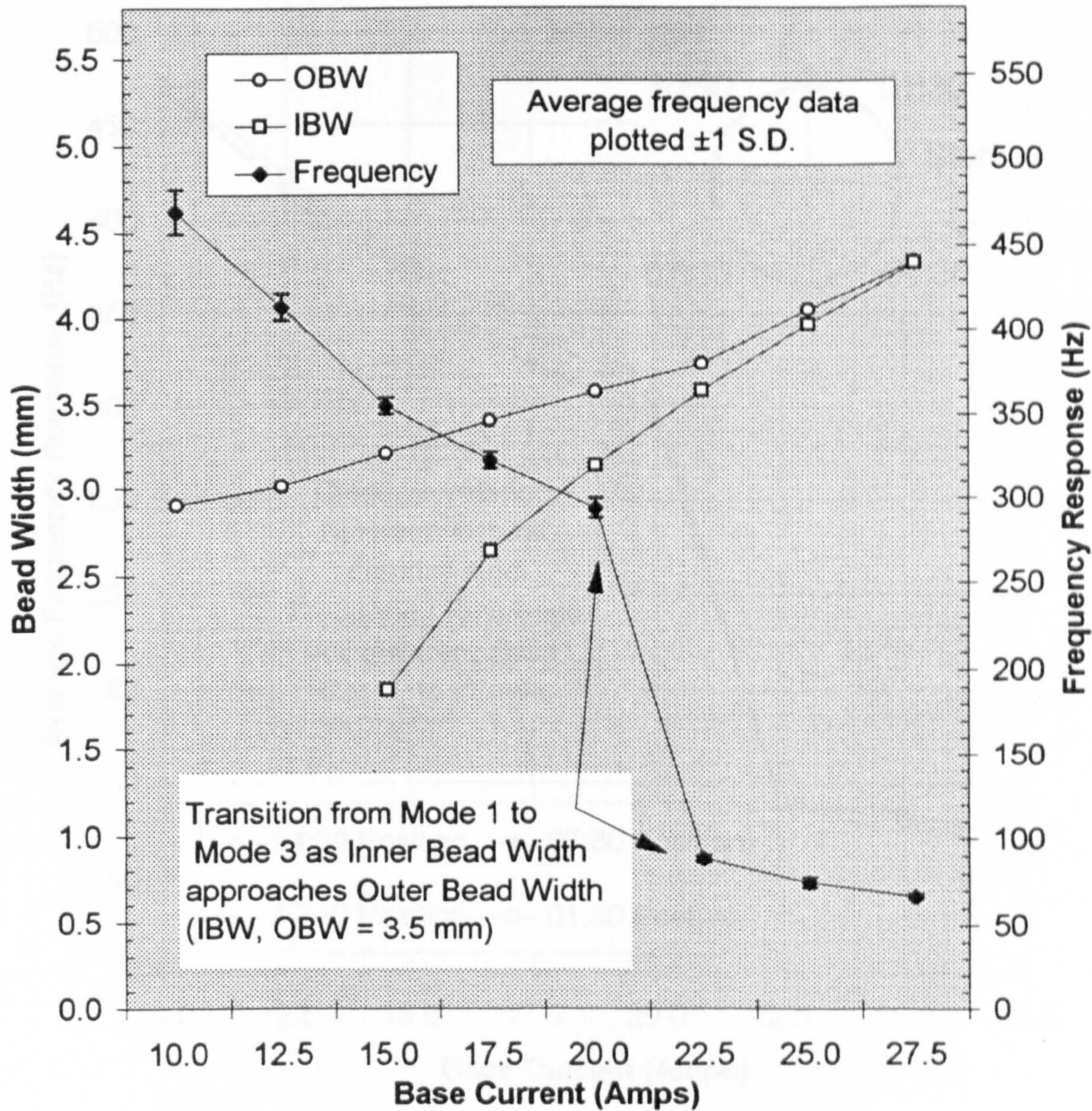


Figure 45

Frequency Response for 4 Orbital Positions
SS316L 38.1 mm Diameter 1.65 mm WT

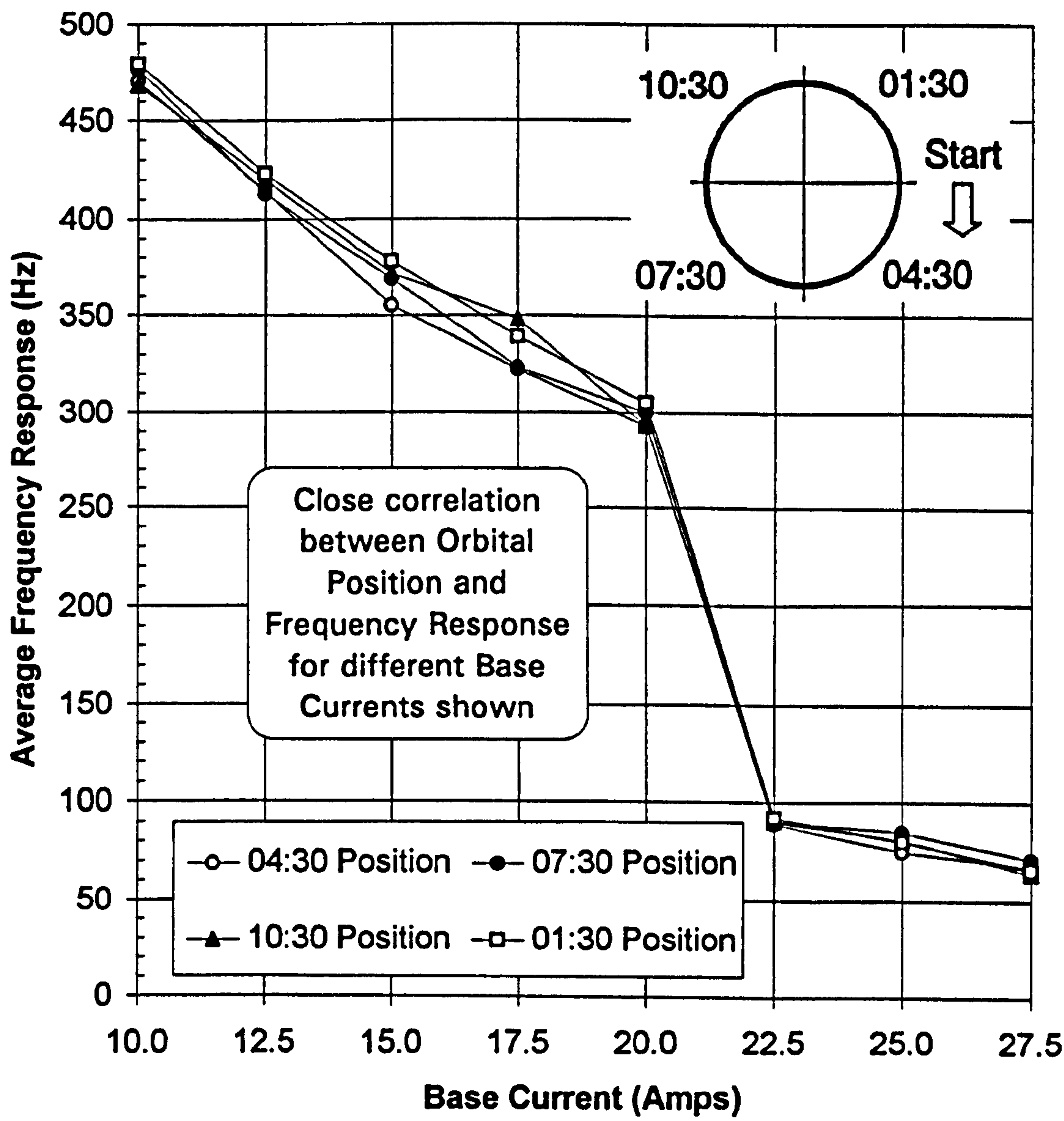


Figure 46

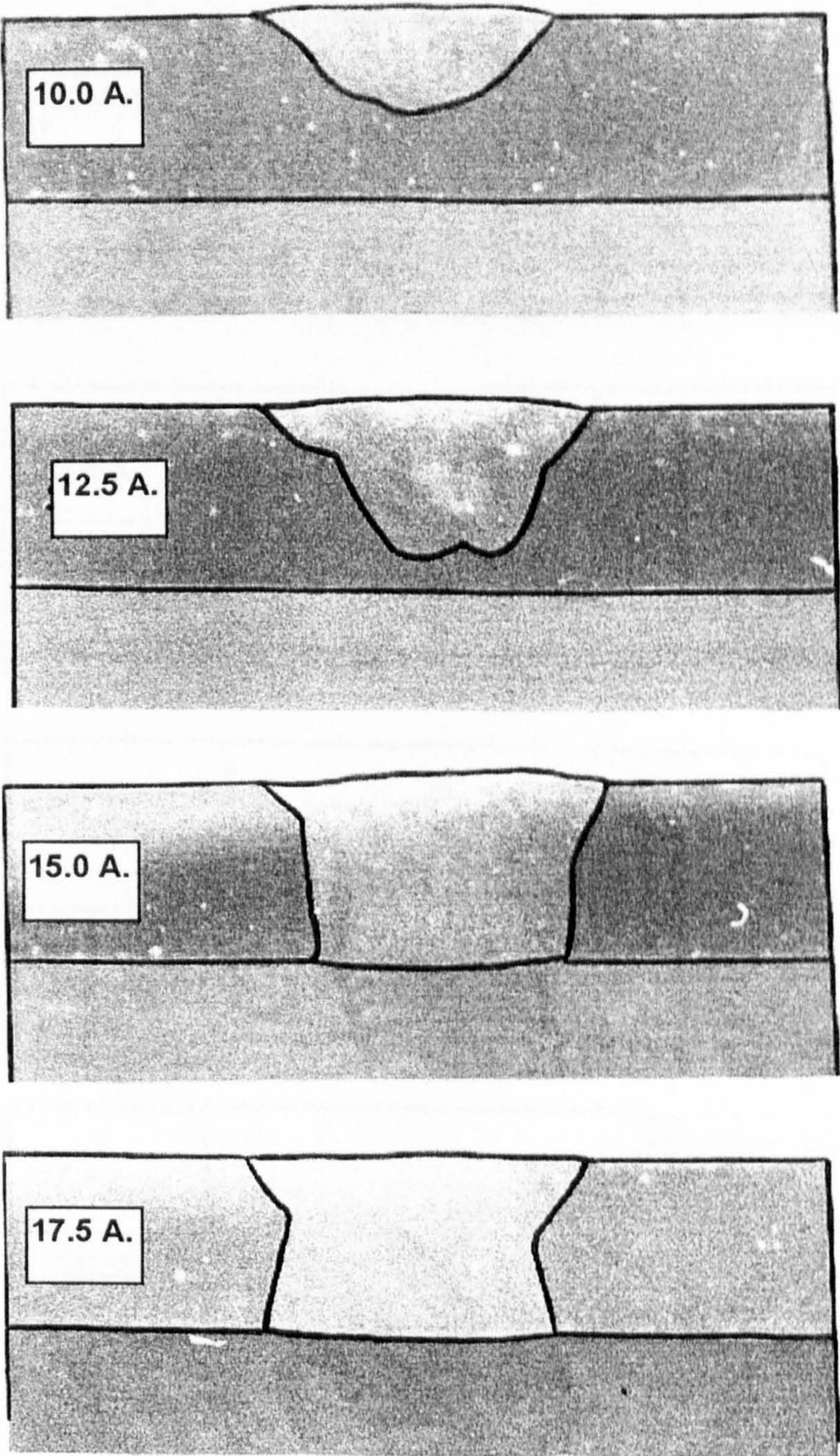


Figure 47 Penetration profiles from the effect of penetration upon frequency (1) - Base Current 10.0 to 17.5 Amps

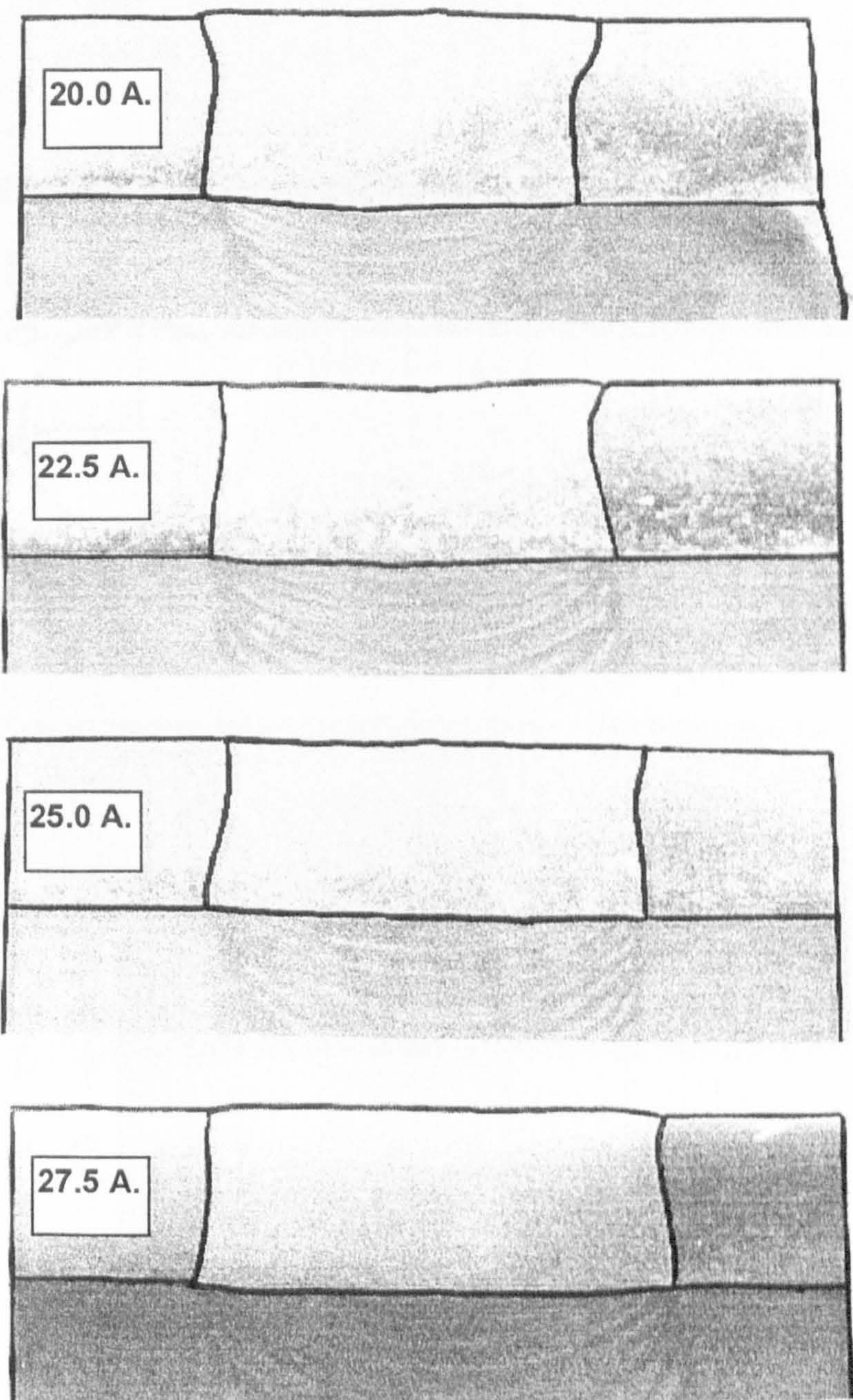


Figure 48 Penetration profiles from the effect of penetration upon frequency (2) -
Base Current 20.0 to 27.5 Amps

Effect of Orbital Position - Full Penetration Weld on SS316L
35 mm Diameter 2 mm Wall Thickness Material

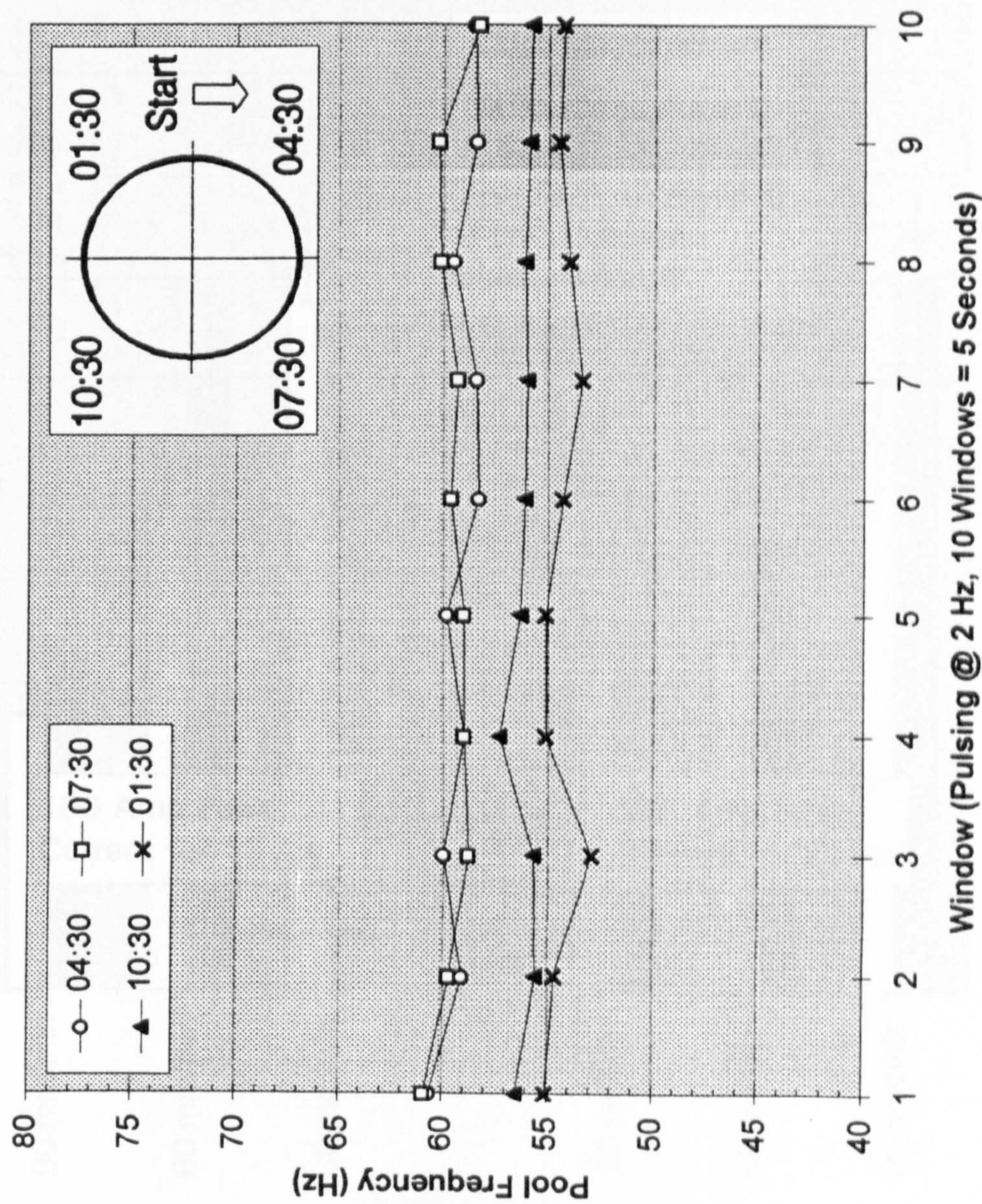


Figure 49

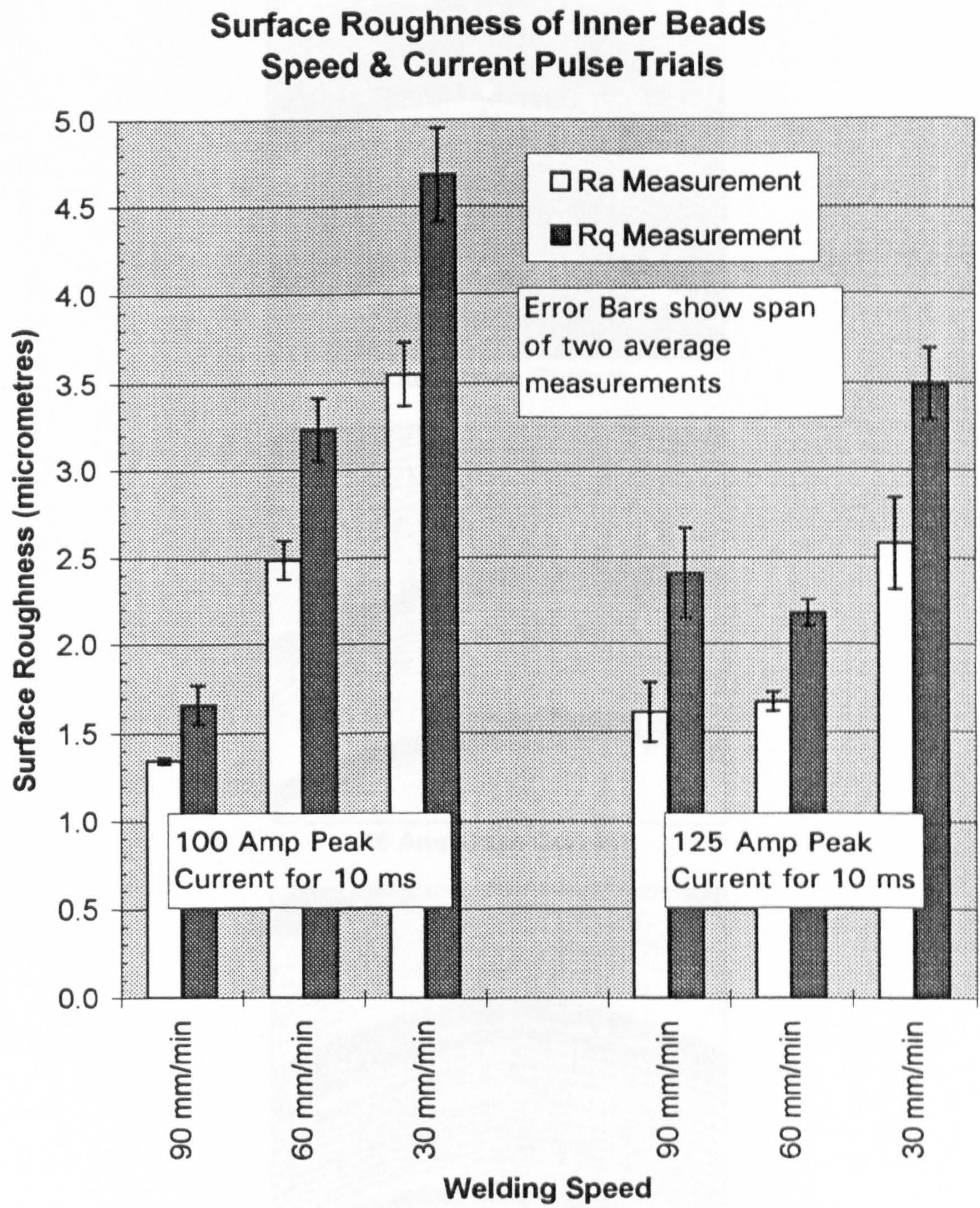
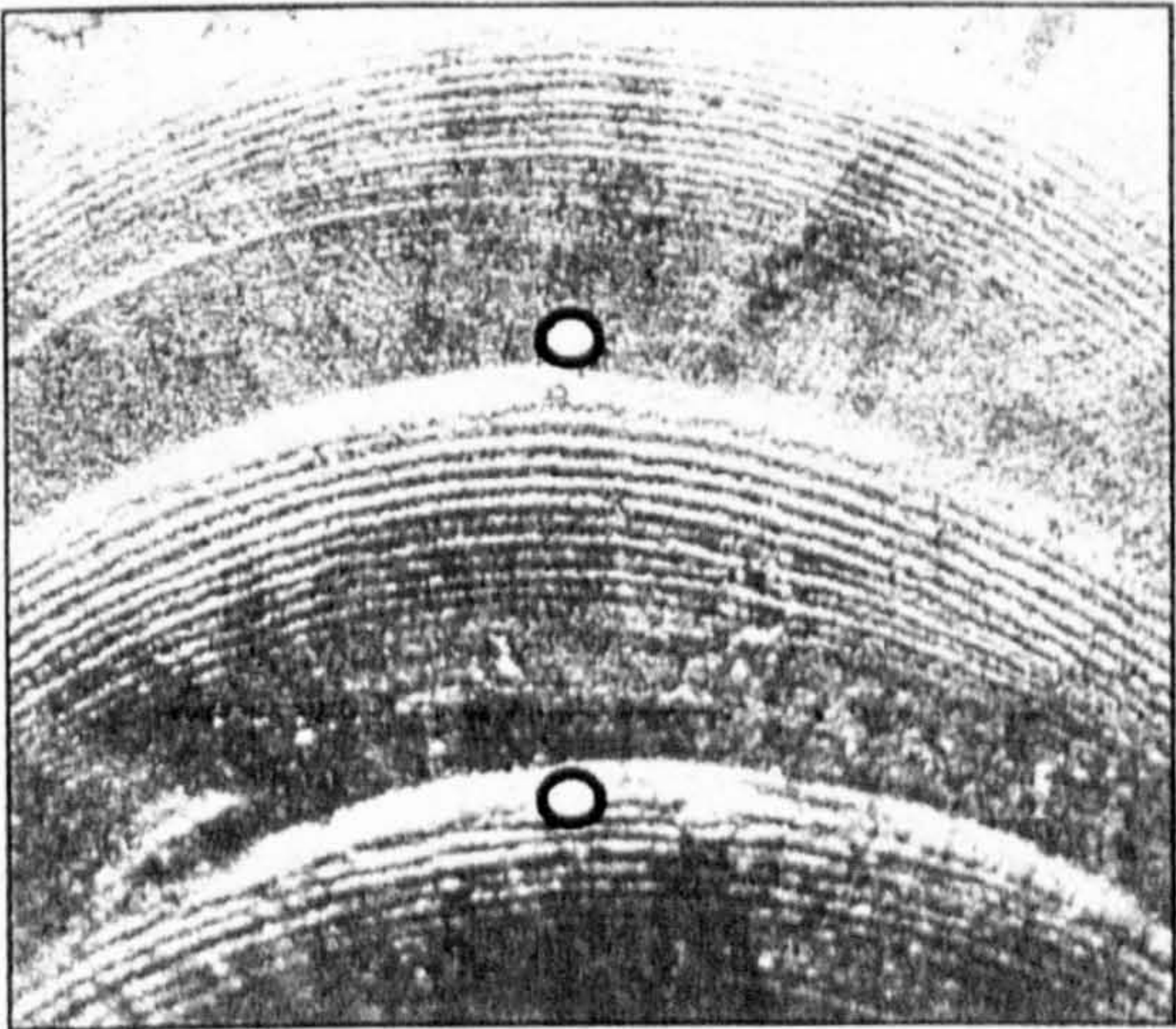
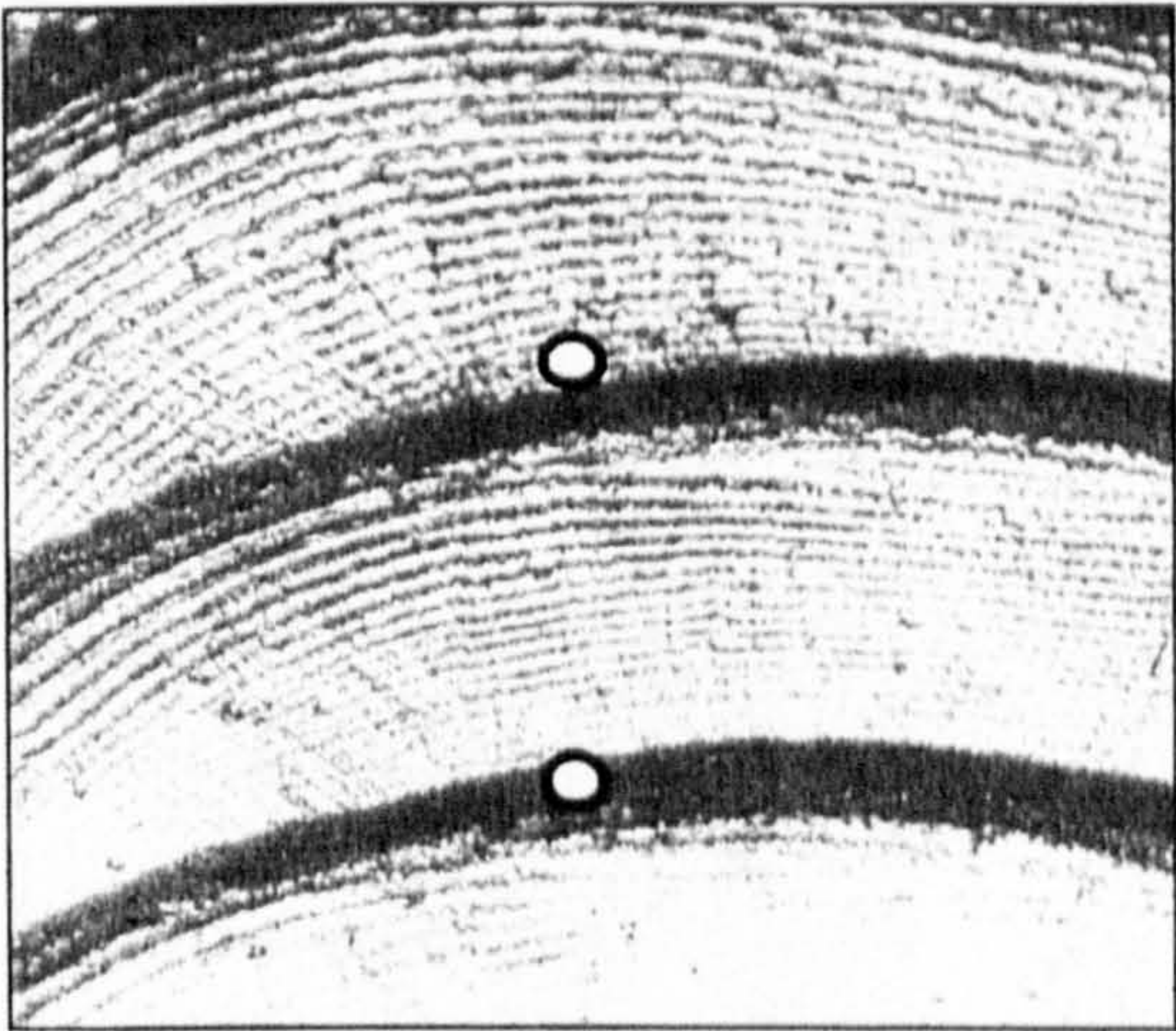


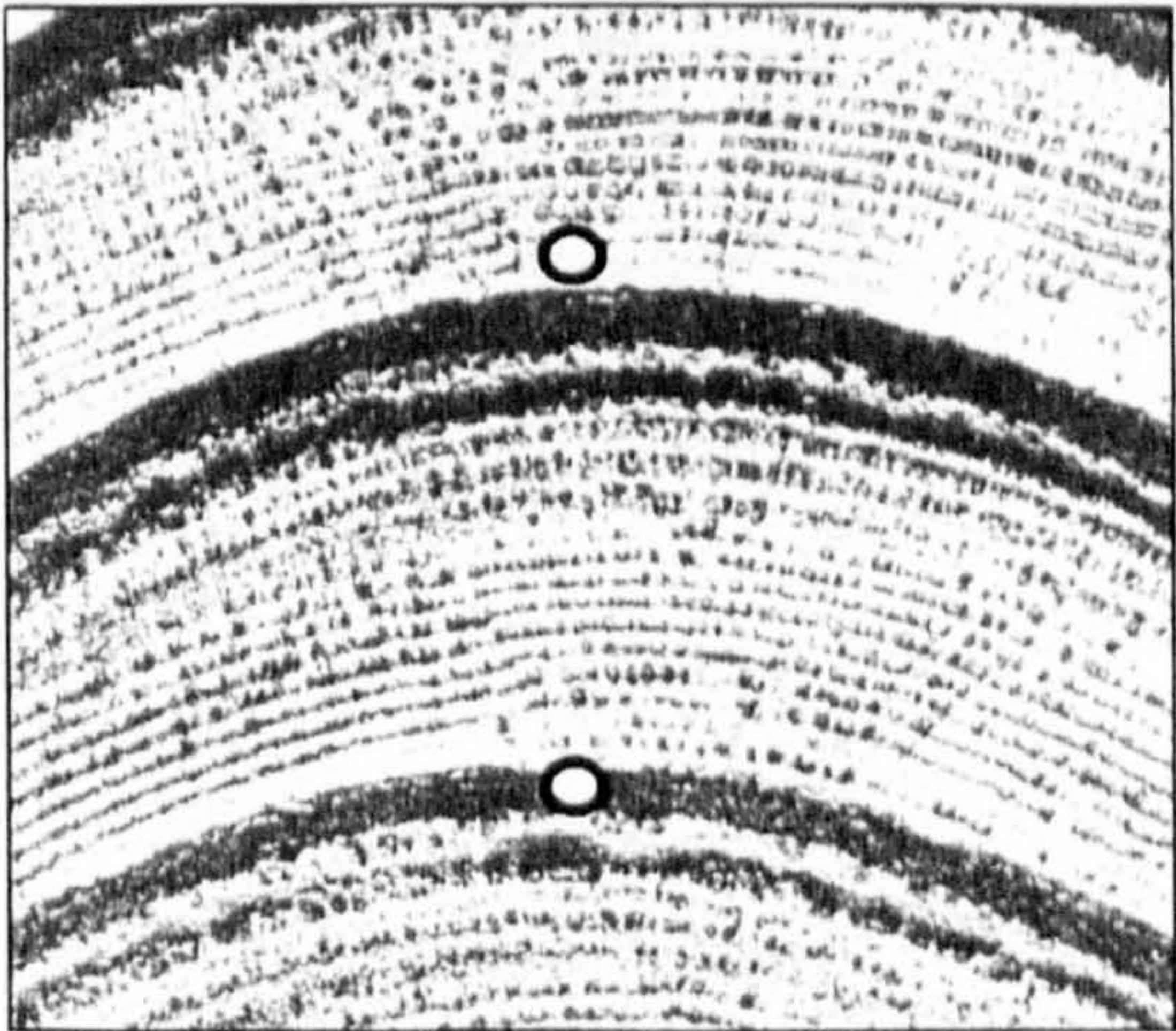
Figure 50



28 Amp Base Current



36 Amp Base Current



44 Amp Base Current

Figure 51 Effect of penetration upon outer bead appearance

**Effect of Welding Speed Upon Quality of
Arc Voltage Signal**

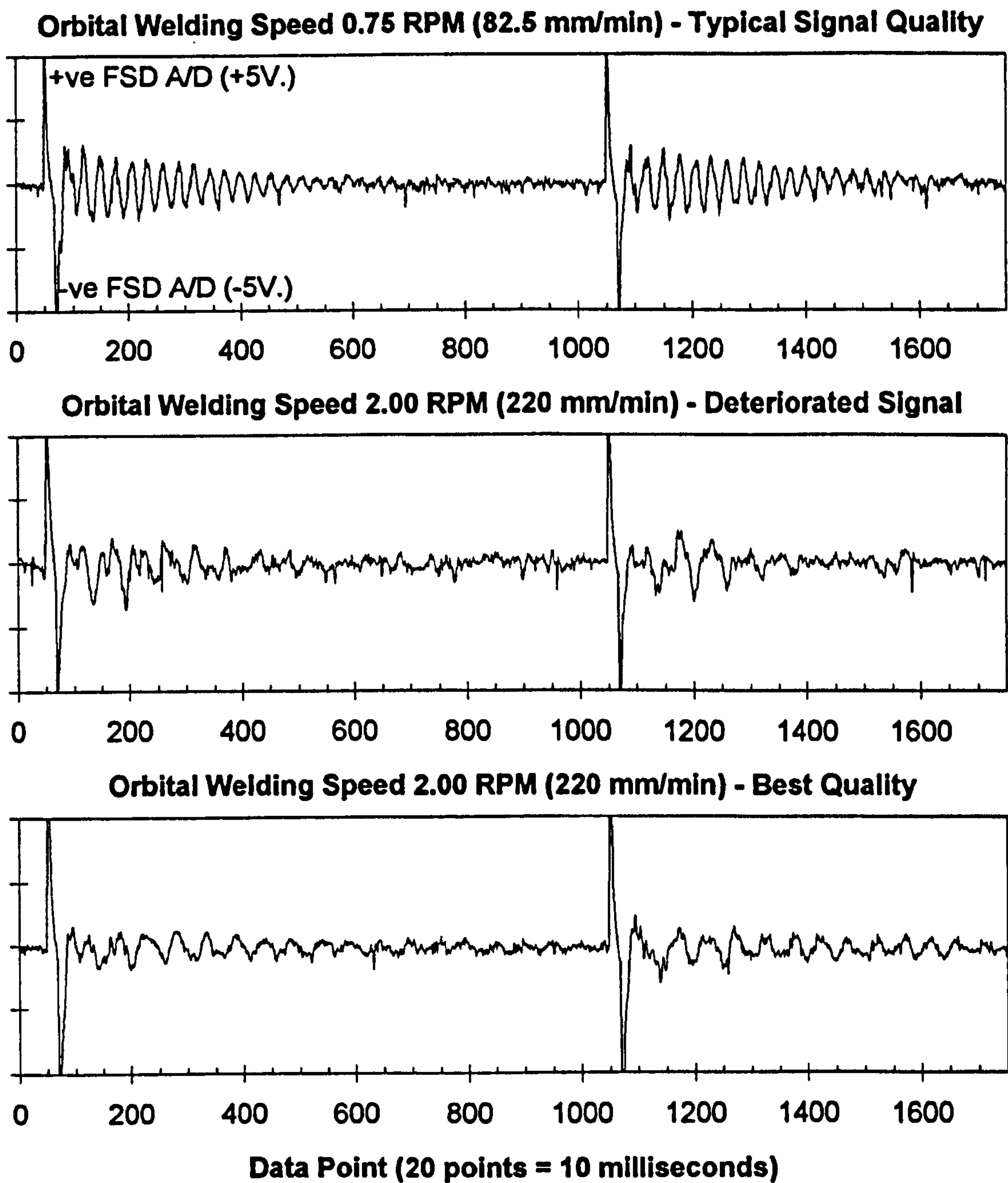


Figure 52

Stationary Weld Pool Behaviour
Electro-Polished ('EP') Material

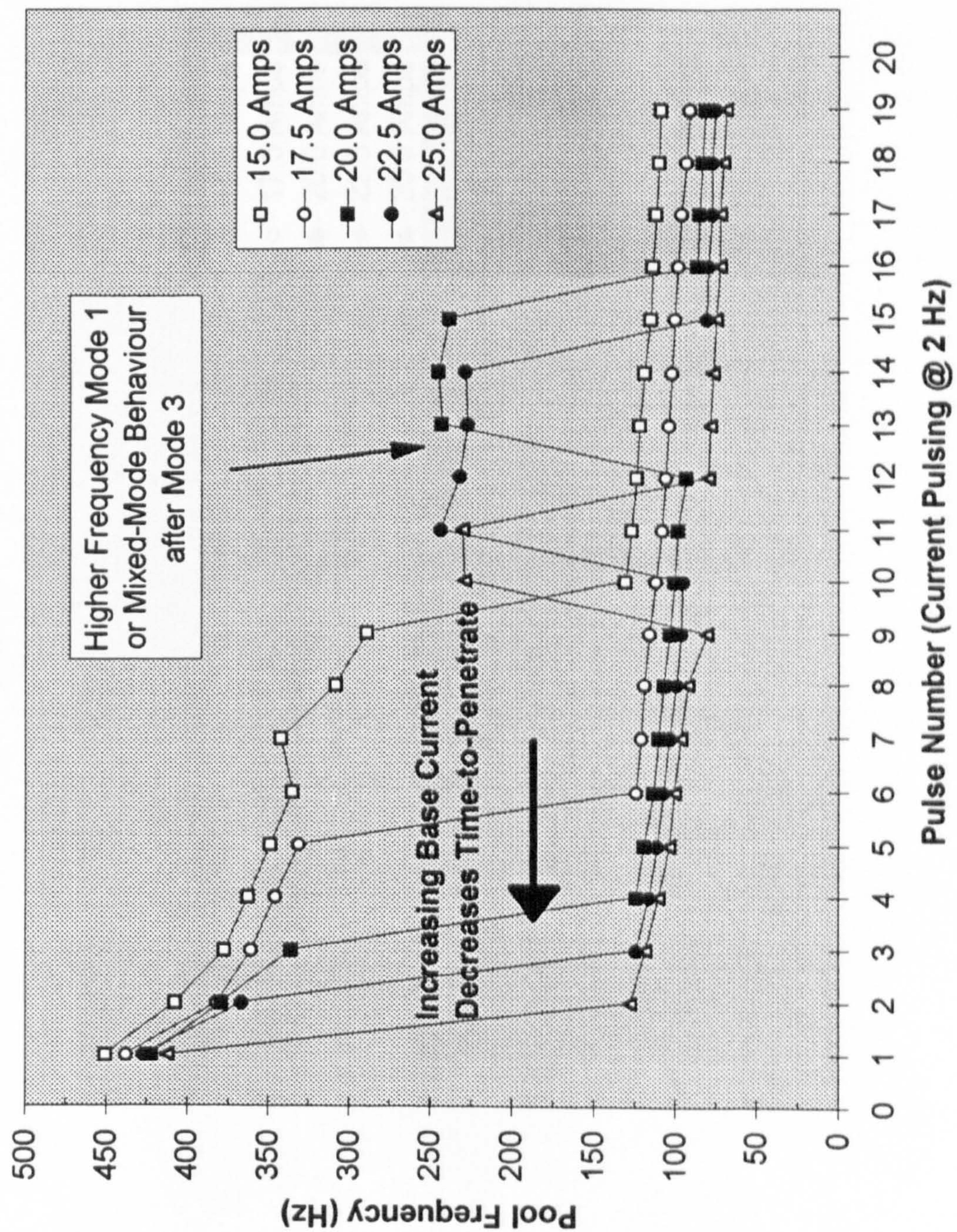


Figure 53

Stationary Weld Pool Behaviour
'Cast 1' Material

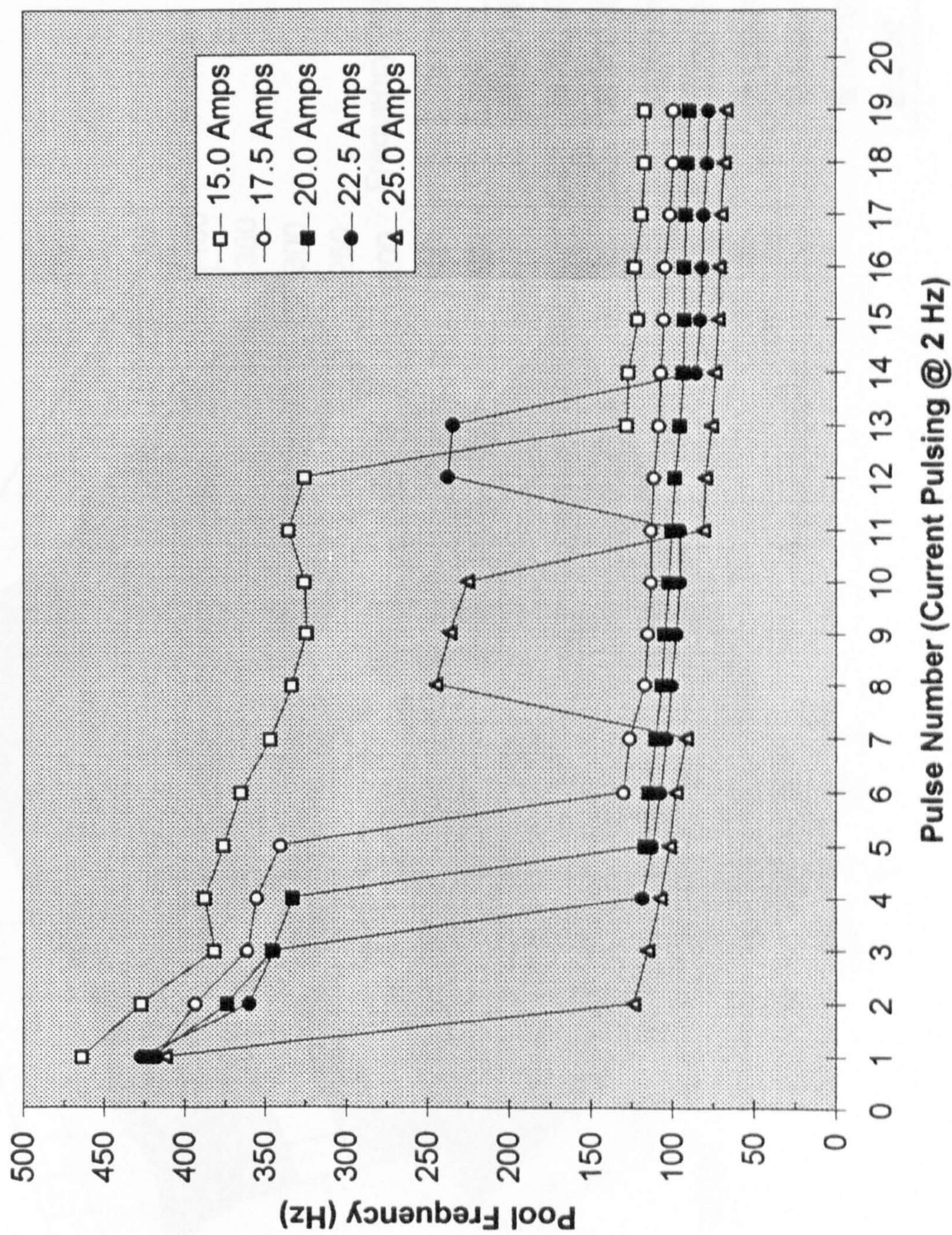


Figure 54

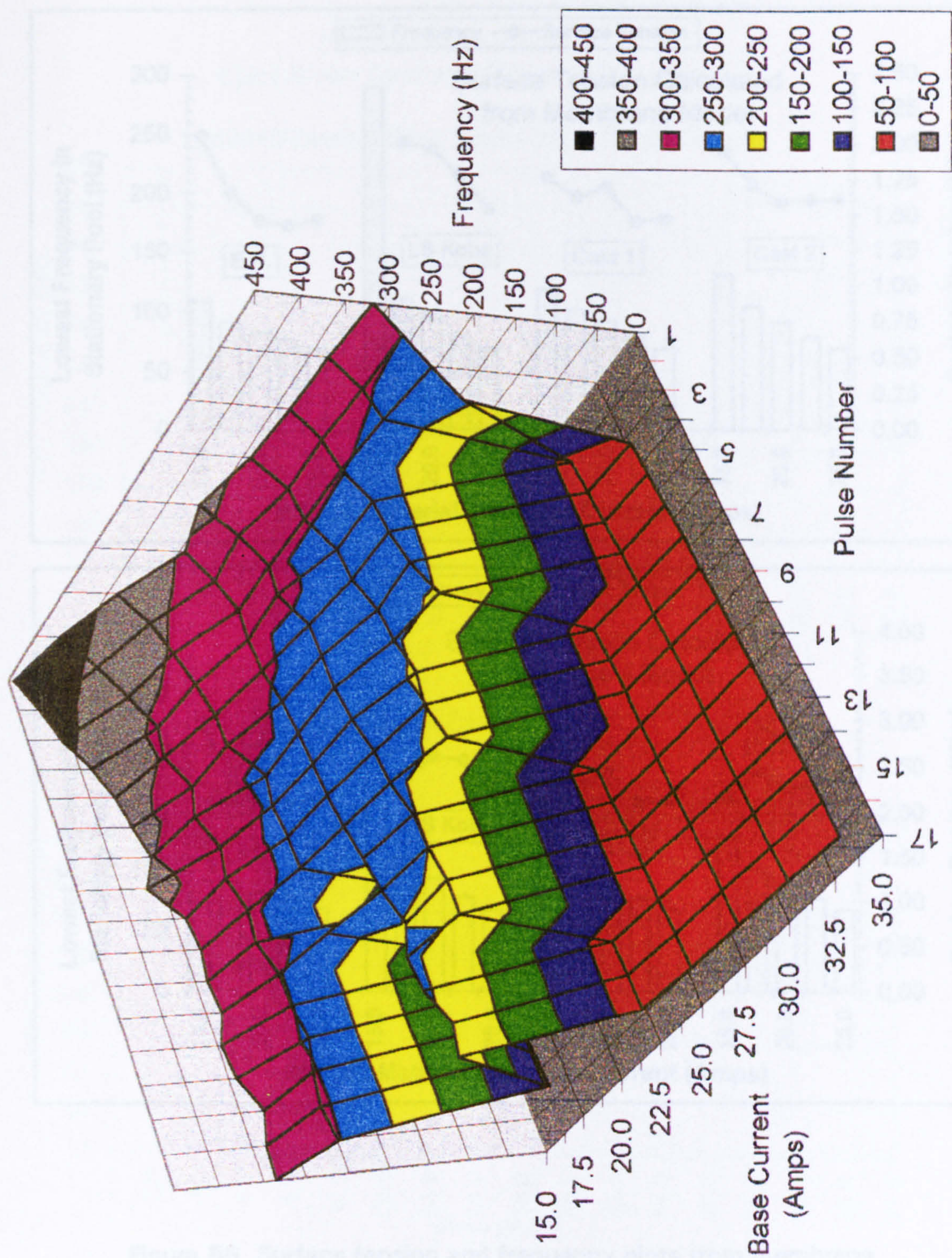


Figure 55 Stationary weld pool - 3D time (pulse number) & base current versus frequency plot (SS316L 35mm diameter 2mm WT)

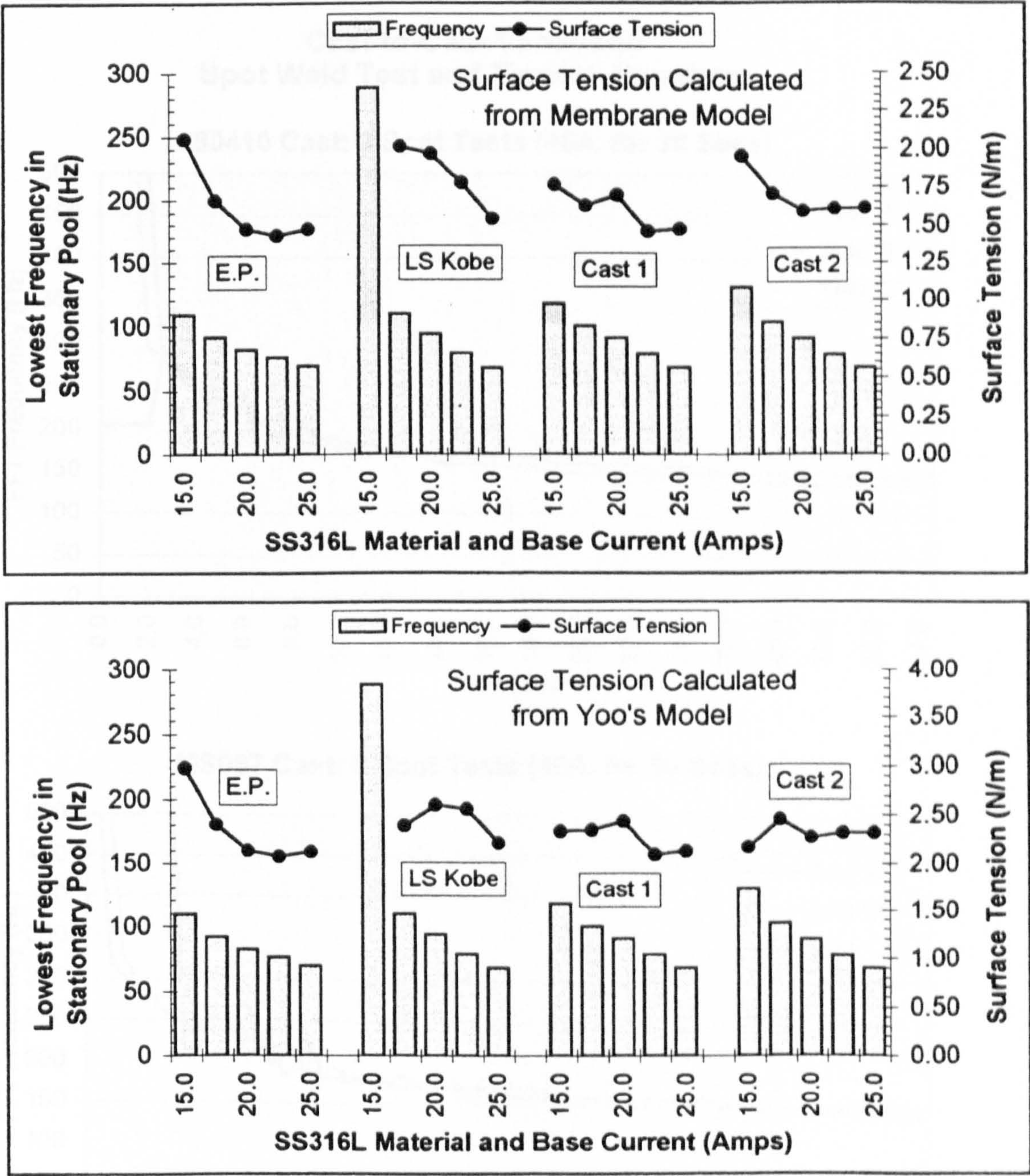
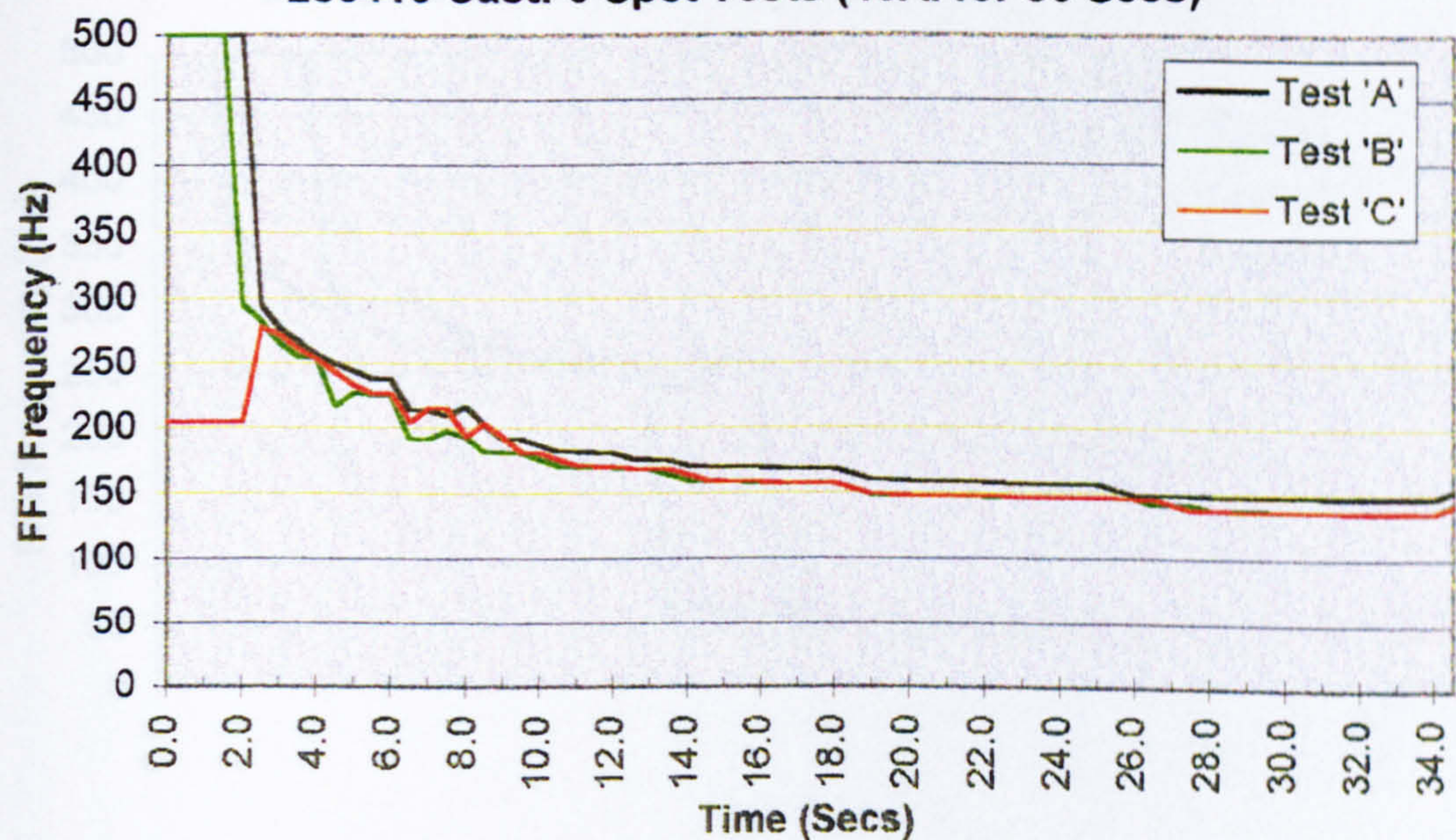


Figure 56 Surface tension and frequency plots from membrane and Yoo's model for electro-polished ('EP'), low sulphur ('LS Kobe'), 'Cast 1' and 'Cast 2' materials

**Cast-to-Cast Variations
Spot Weld Test and Time-to-Penetrate**

280410 Cast: 3 Spot Tests (40A. for 30 Secs)



MS097 Cast: 3 Spot Tests (40A. for 30 Secs)

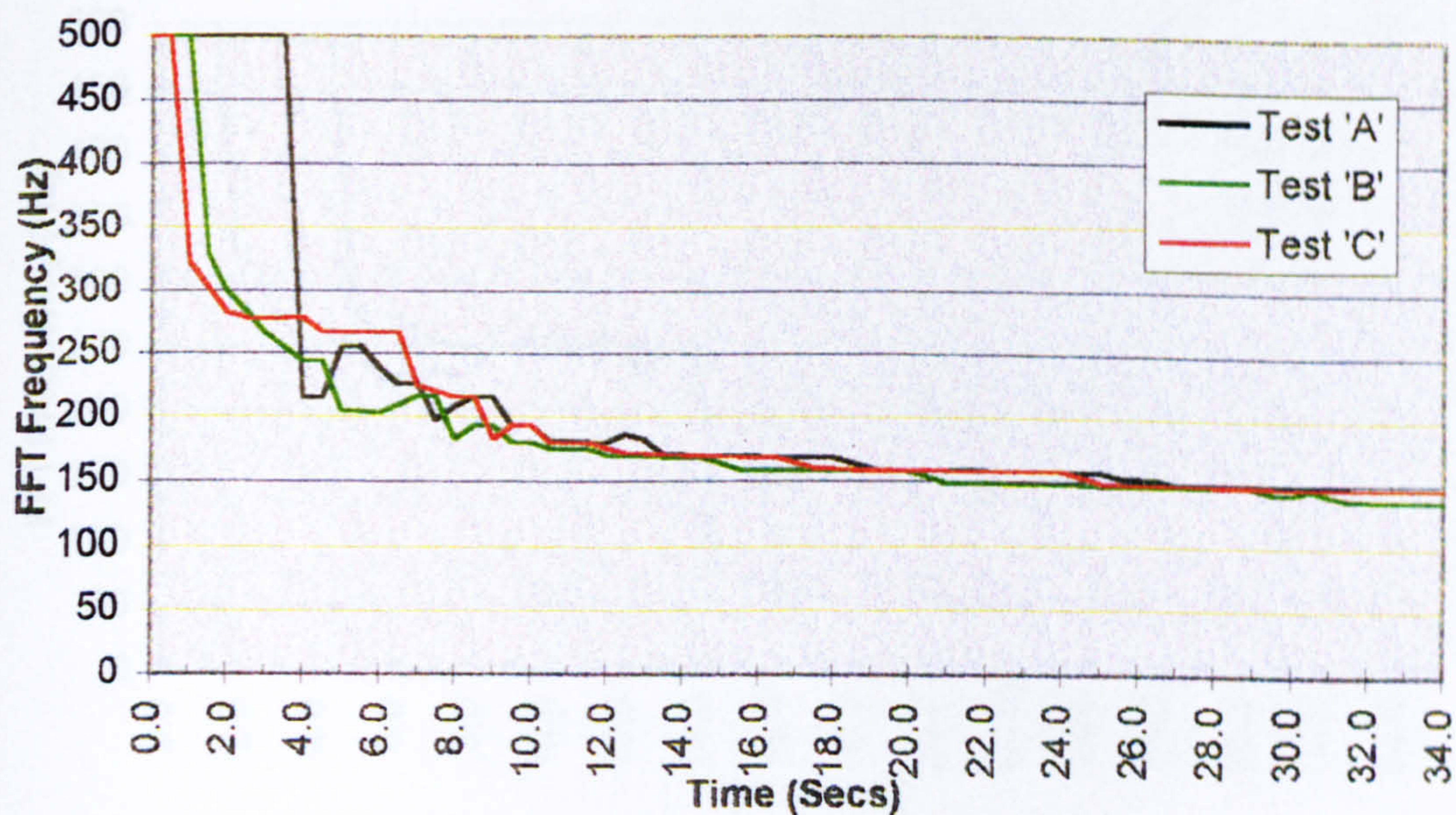
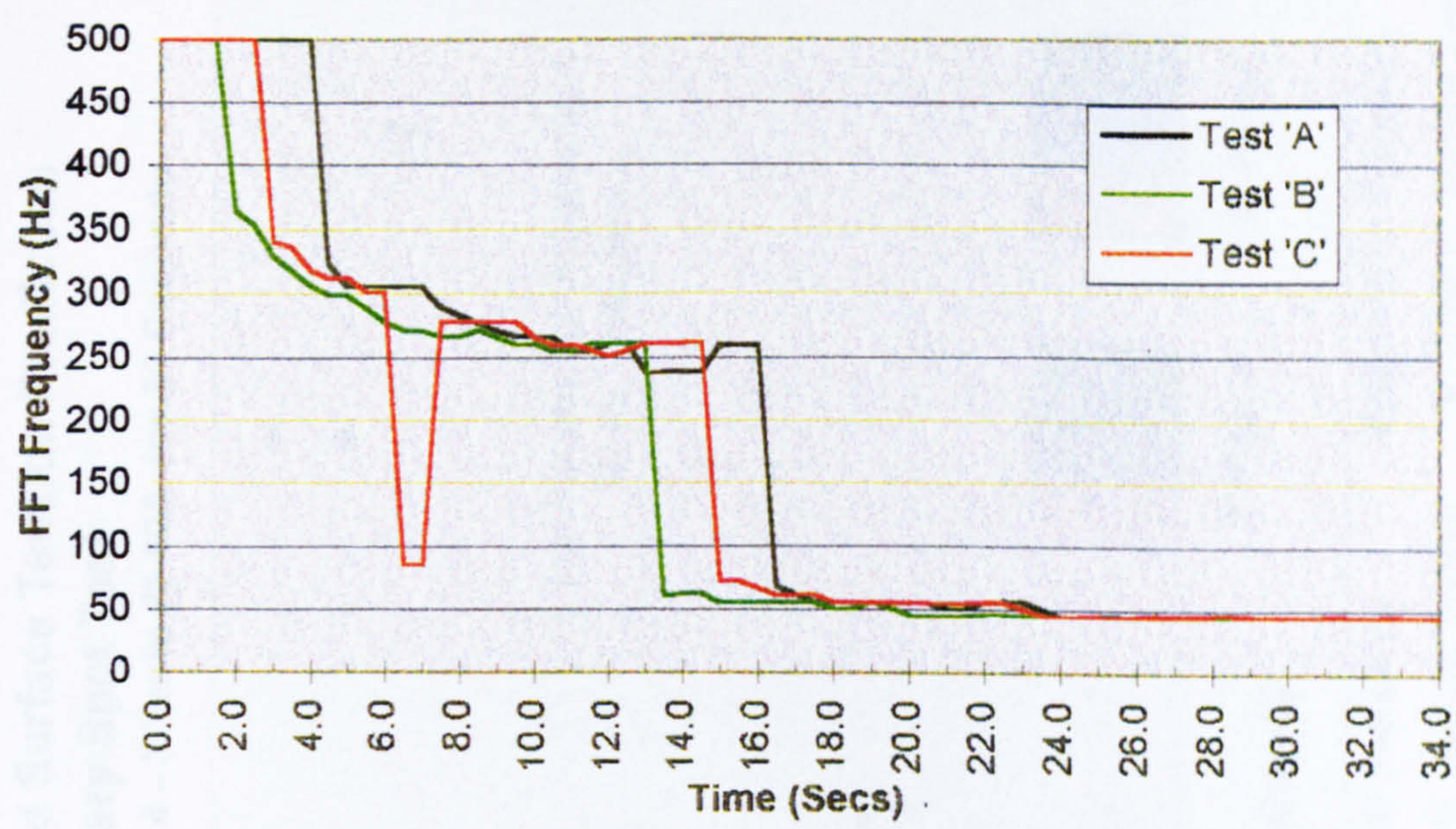


Figure 57

Cast-to-Cast Variations
Spot Weld Test and Time-to-Penetrate

2" Pipe 2 Cast: 3 Spot Tests (40A. for 30 Secs)



2" Pipe 4 Cast: 3 Spot Tests (40A. for 30 Secs)

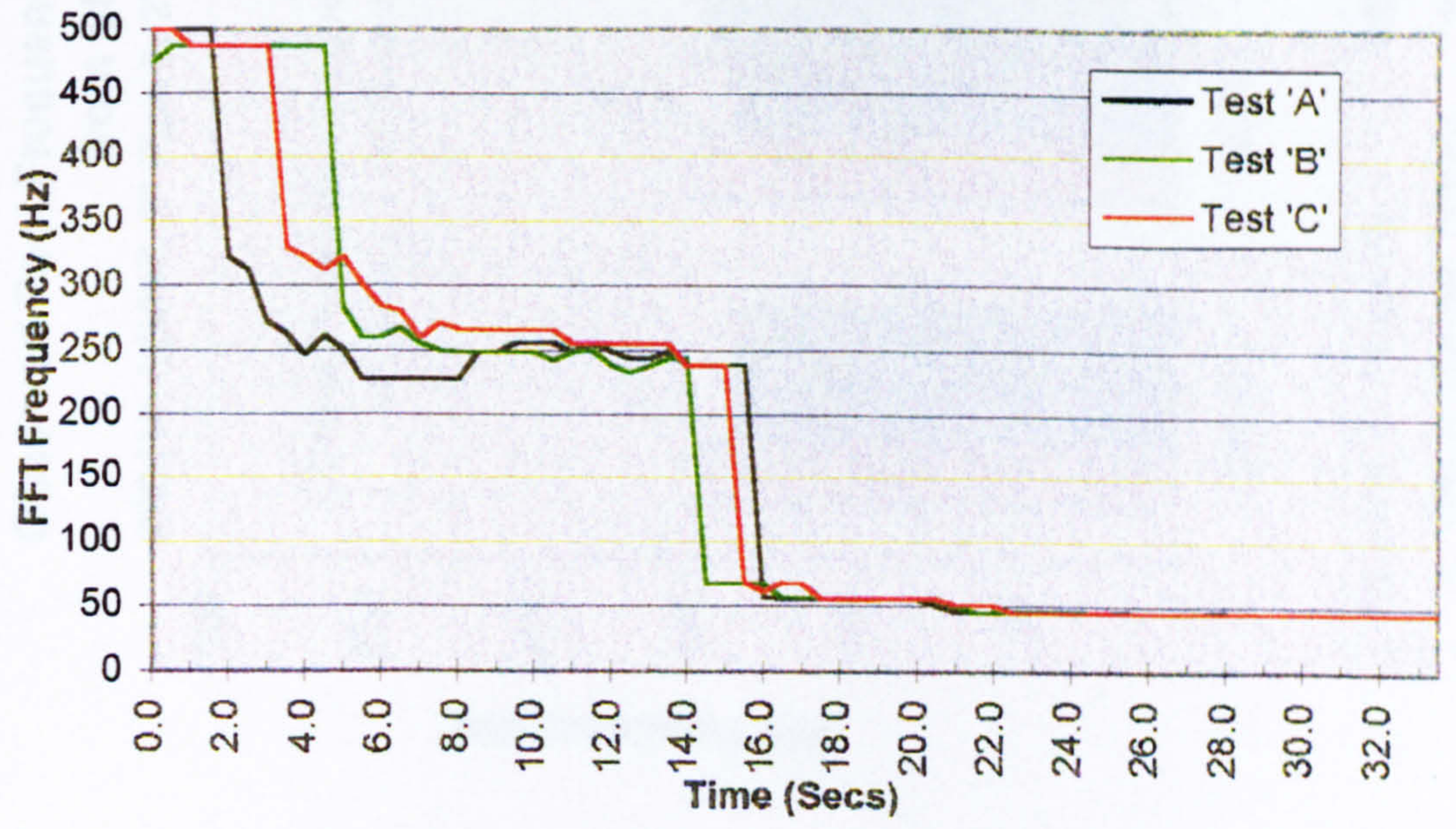


Figure 58

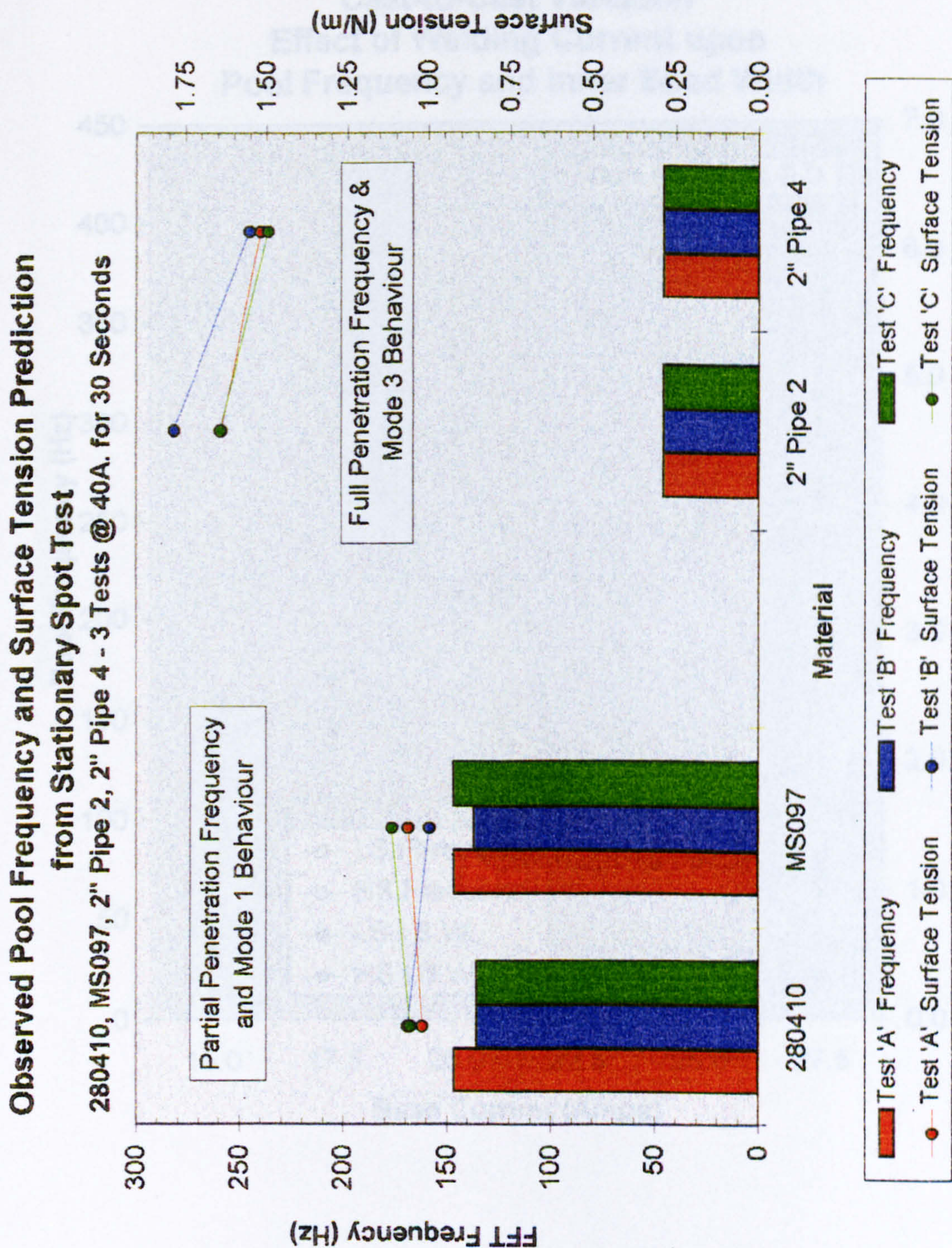


Figure 59

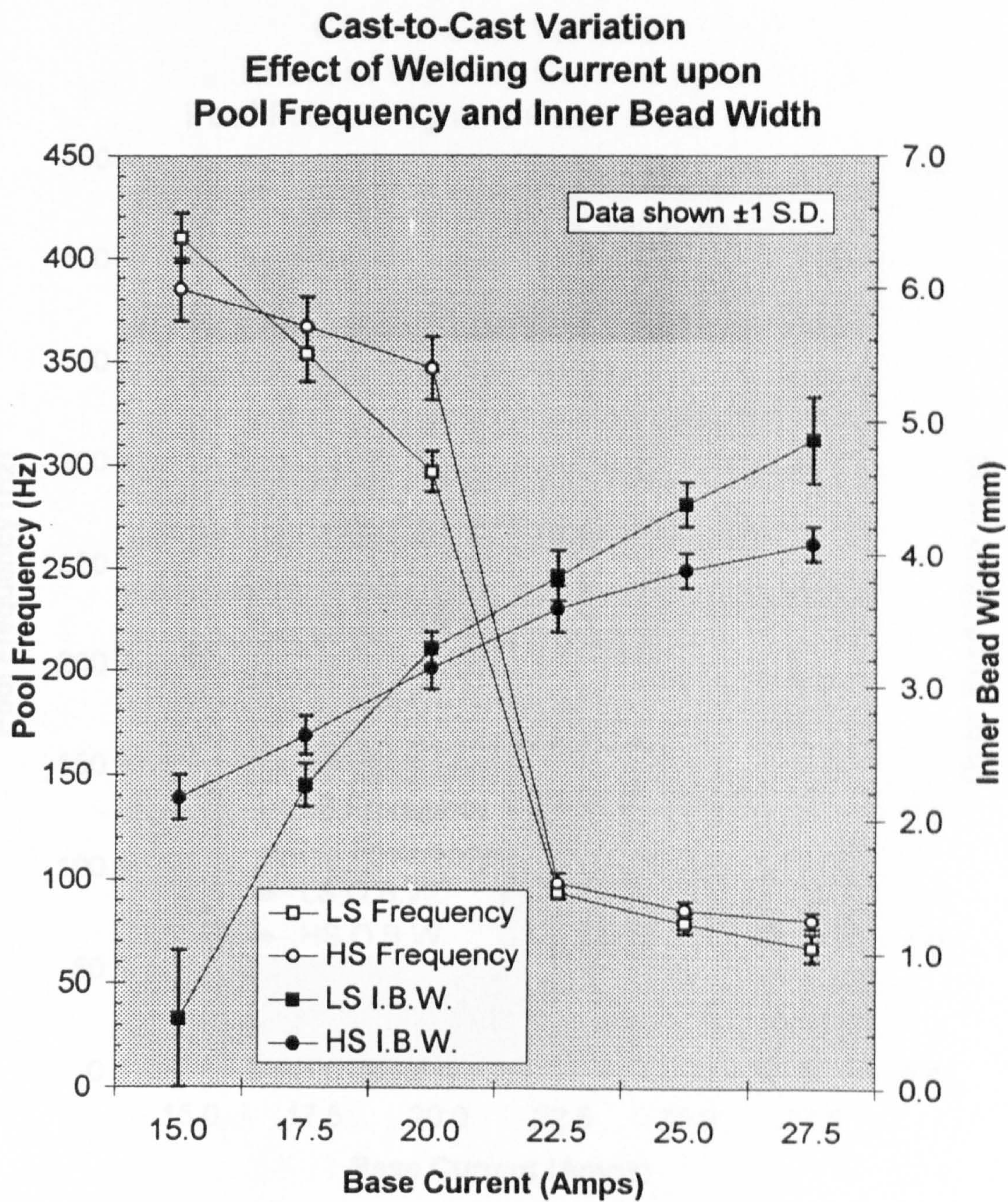


Figure 60

(Low sulphur *LS* 'LS Kobe' and
high sulphur *HS* 'Cast 1' casts)

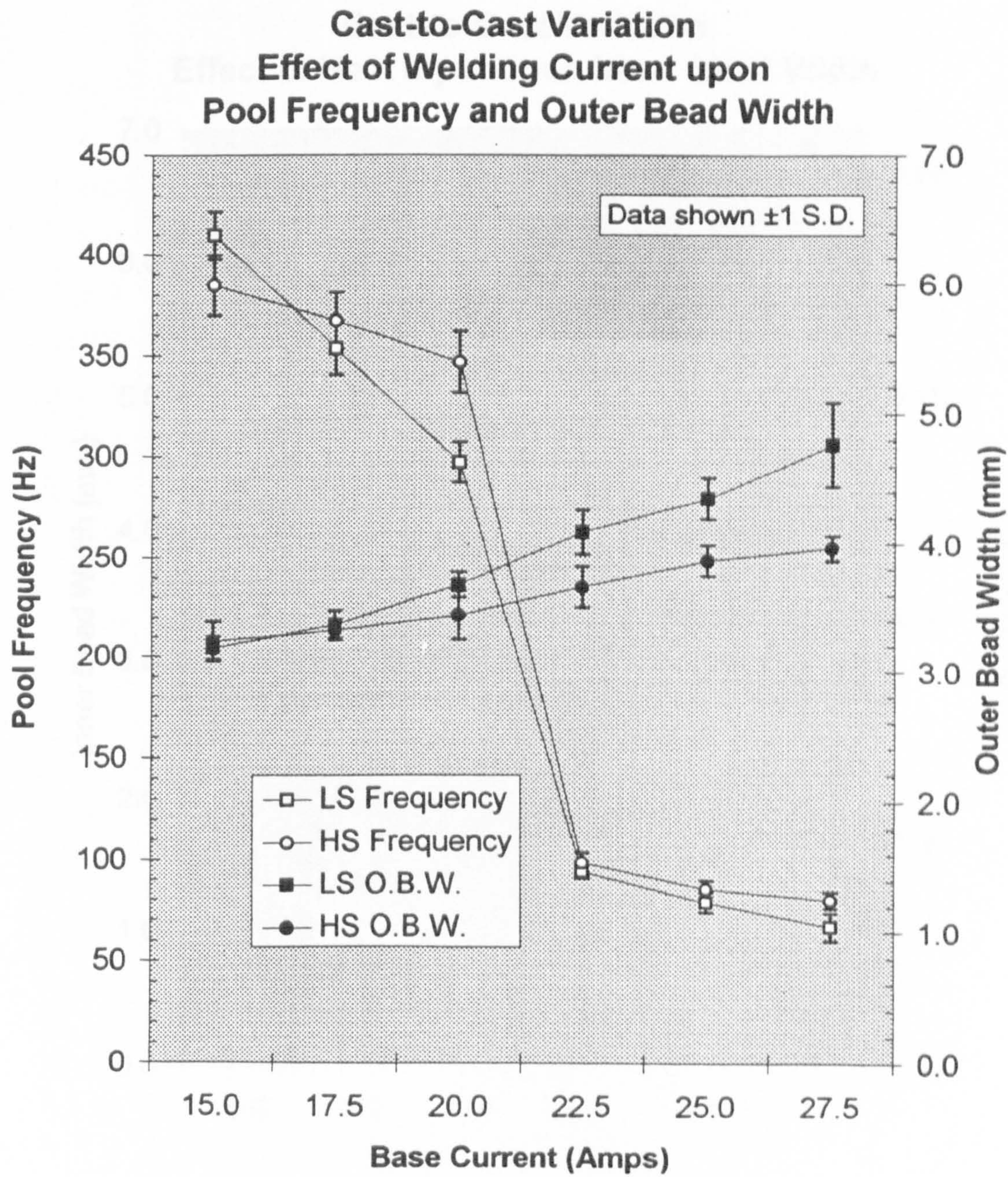


Figure 61

(Low sulphur *LS* 'LS Kobe' and
high sulphur *HS* 'Cast 1' casts)

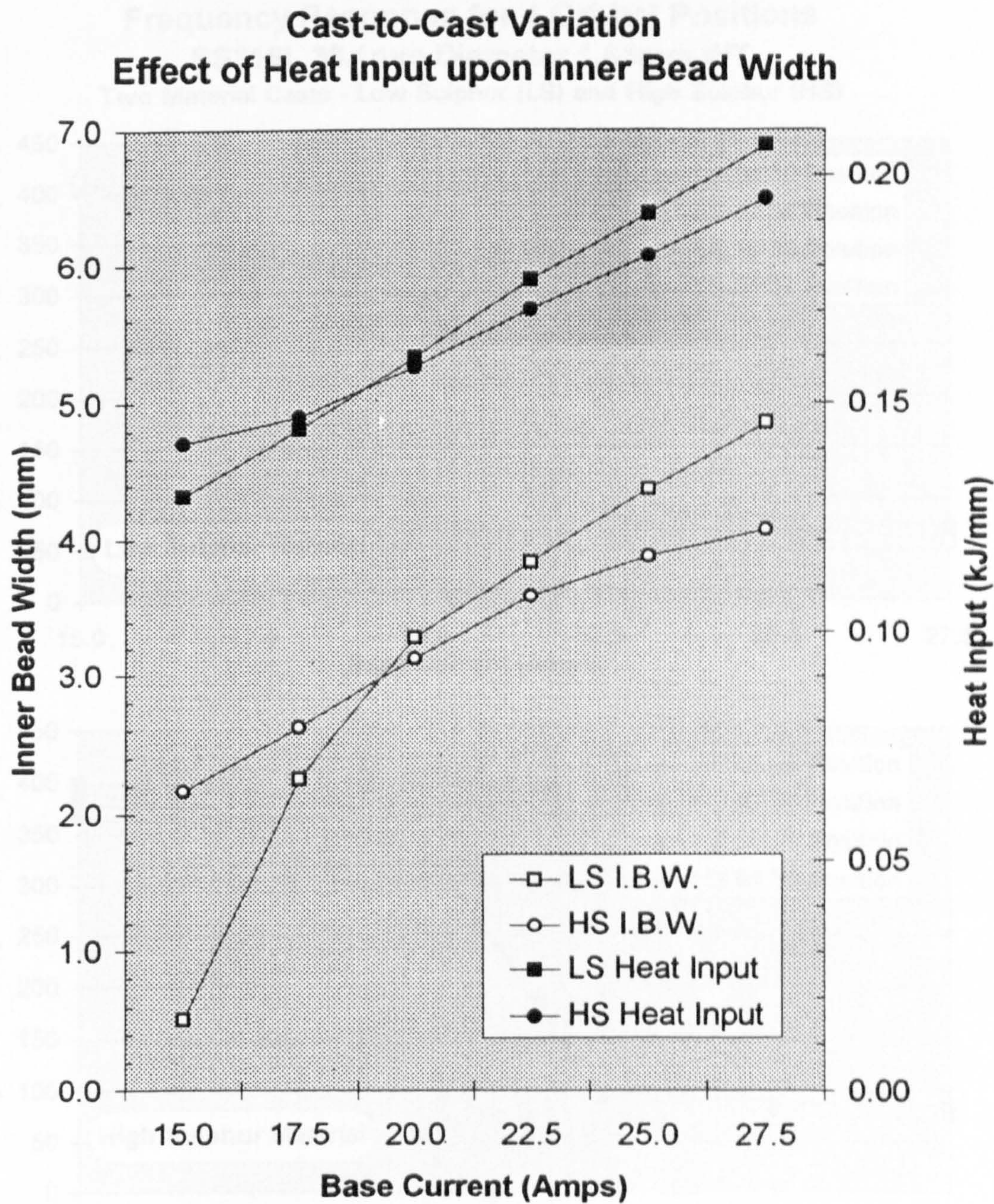


Figure 62

(Low sulphur *LS* 'LS Kobe' and
high sulphur *HS* 'Cast 1' casts)

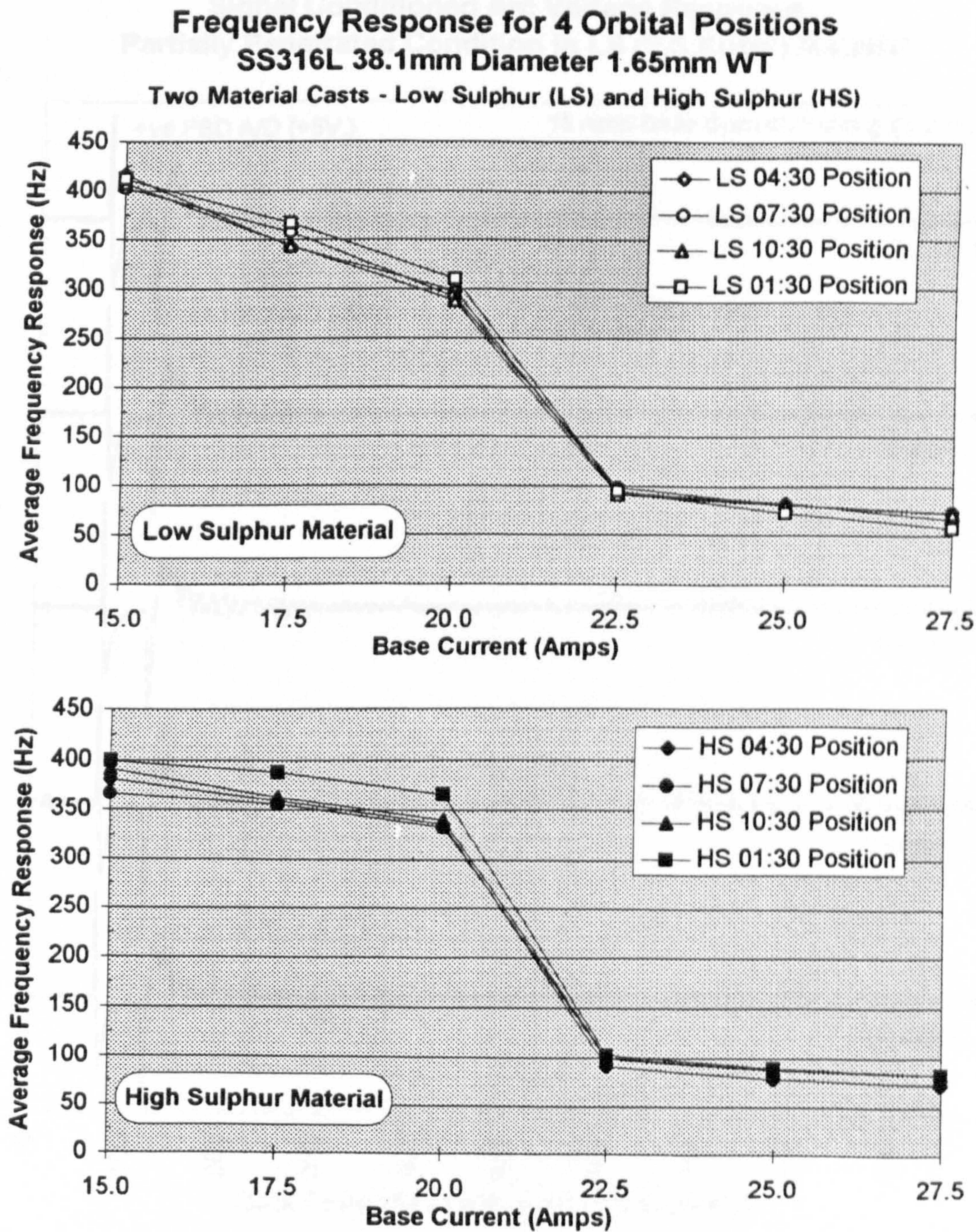


Figure 63

(Low sulphur *LS* 'LS Kobe' and
high sulphur *HS* 'Cast 1' casts)

**Signal Conditioned Arc Voltage Response -
Partially Penetrated Condition in LS ('LS Kobe') Material**

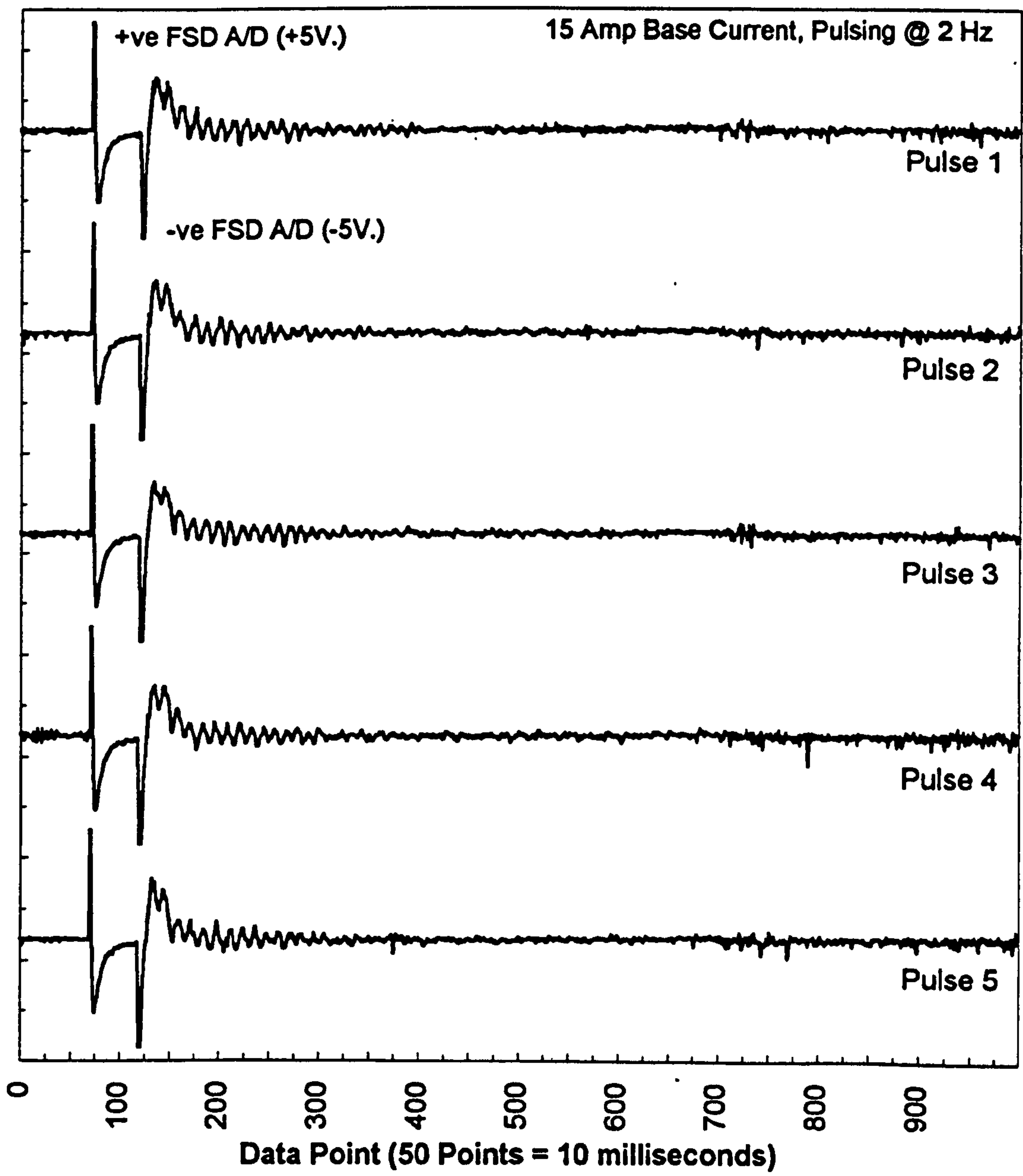


Figure 64

**Signal Conditioned Arc Voltage Response -
Partially Penetrated Condition in HS ('Cast 1') Material**

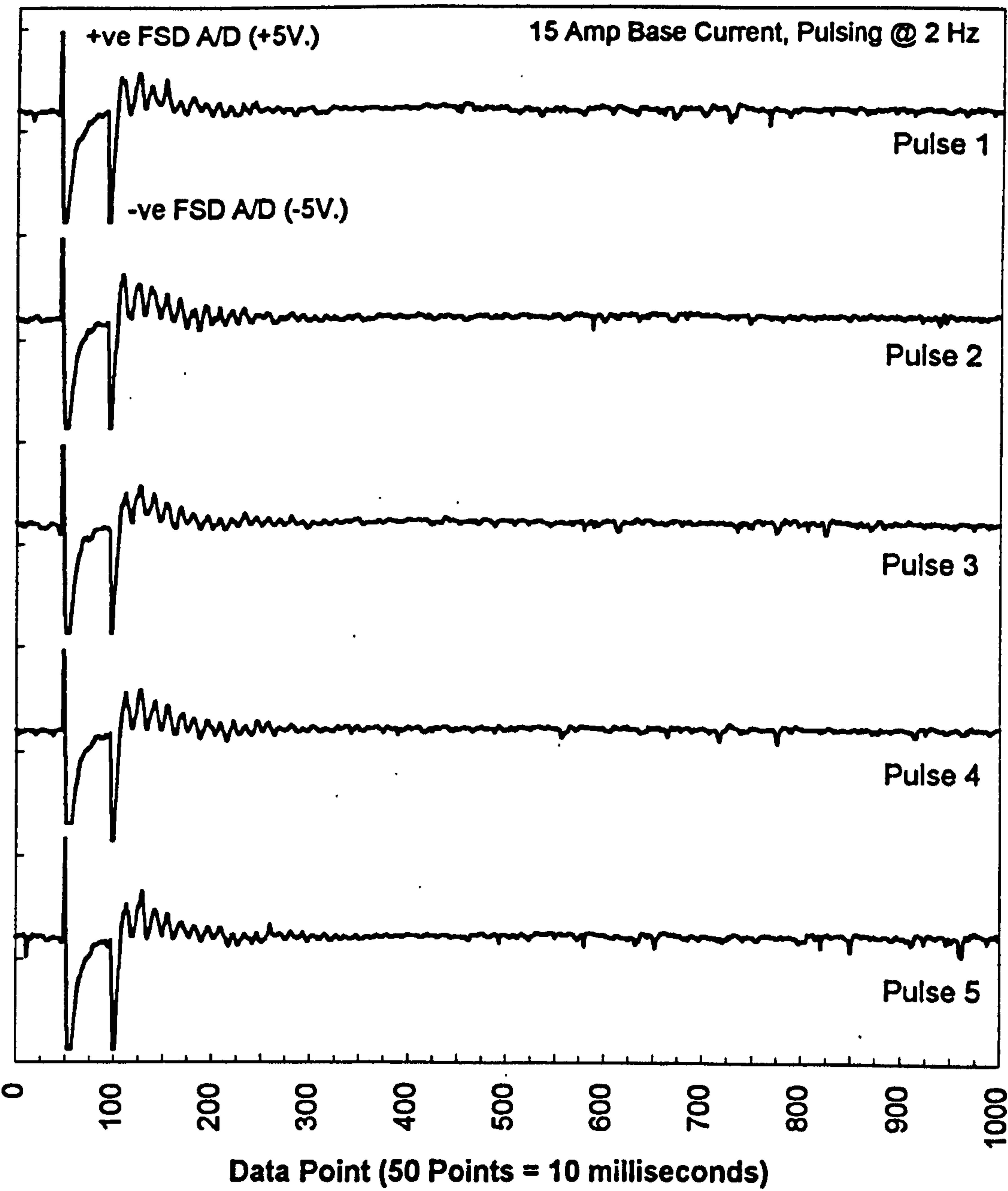


Figure 65

**Arc Voltage Response -
Fully Penetrated Condition in LS ('LS Kobe') Material**

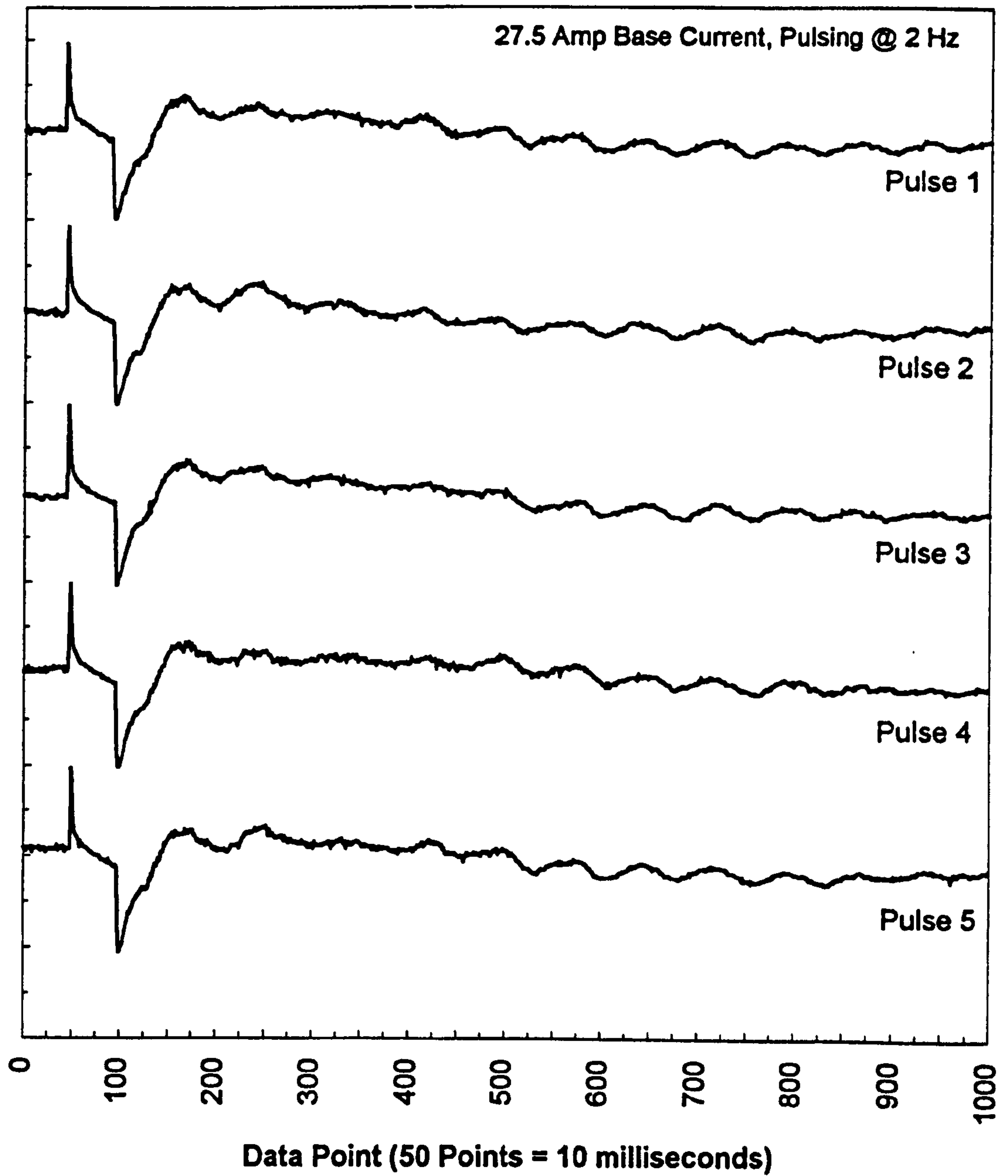


Figure 66

**Arc Voltage Response -
Fully Penetrated Condition in HS ('Cast 1') Material**

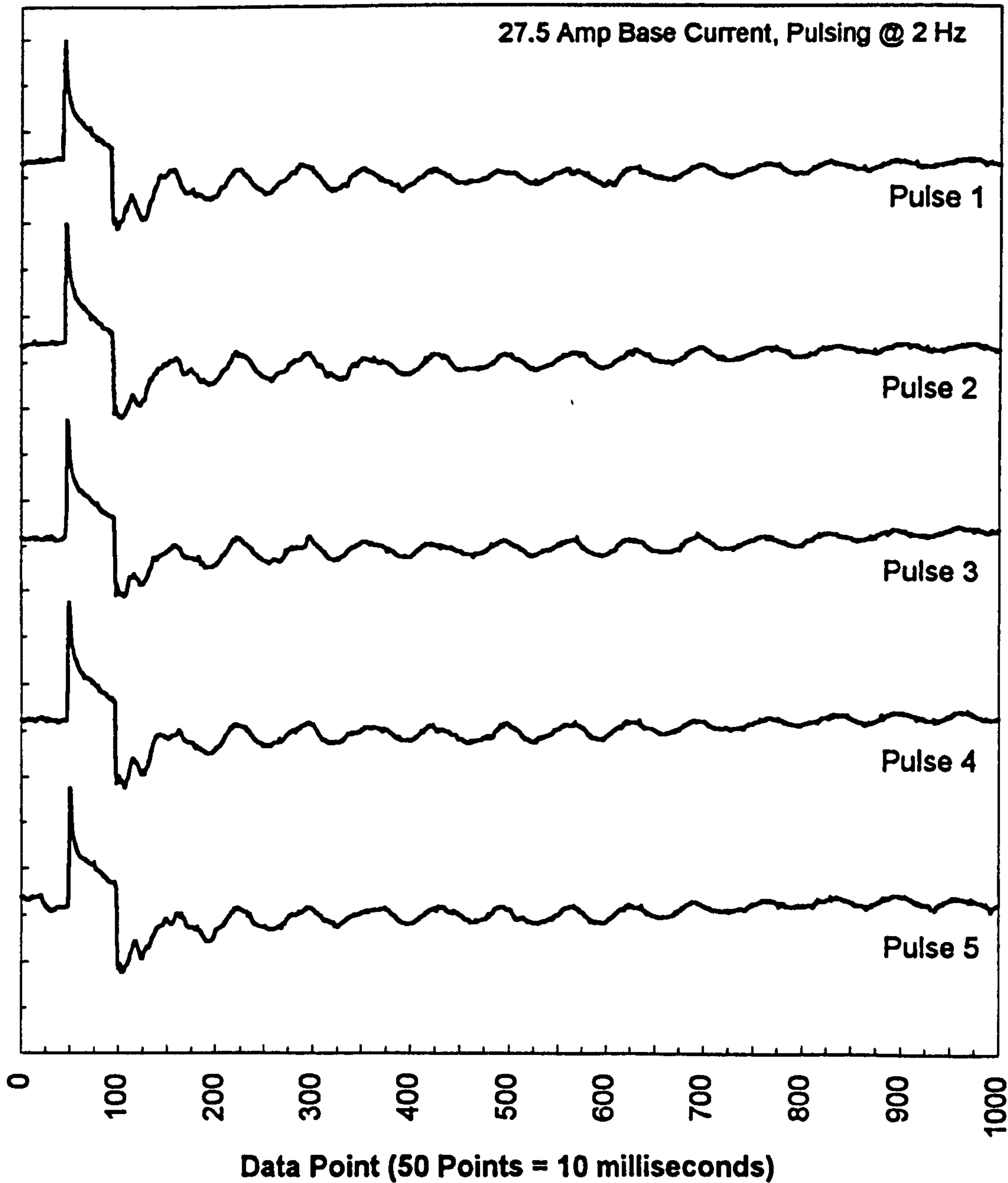
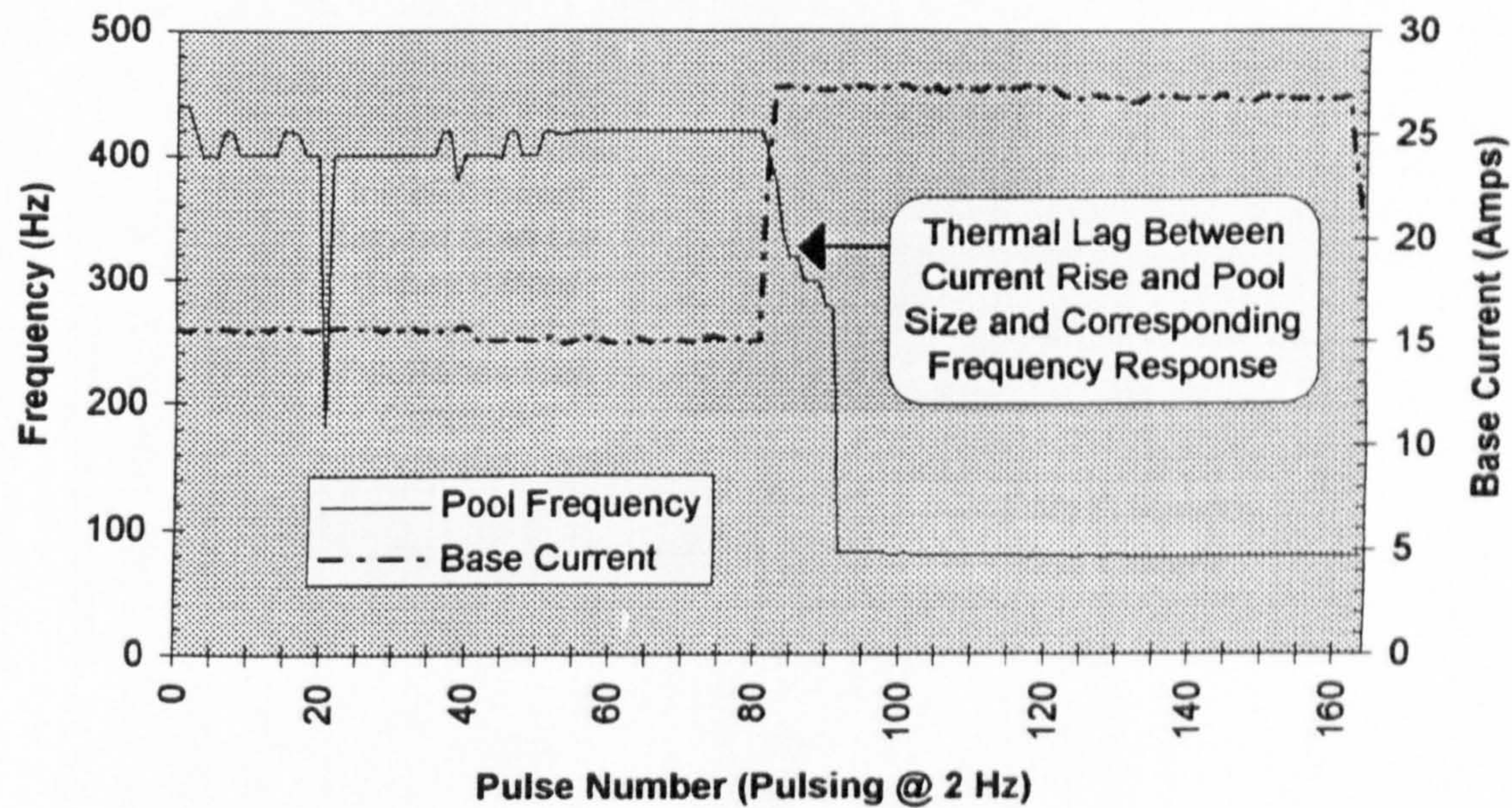


Figure 67

Real-Time Frequency Response - PARTIAL to FULL Penetration
CAST 1



CAST 2

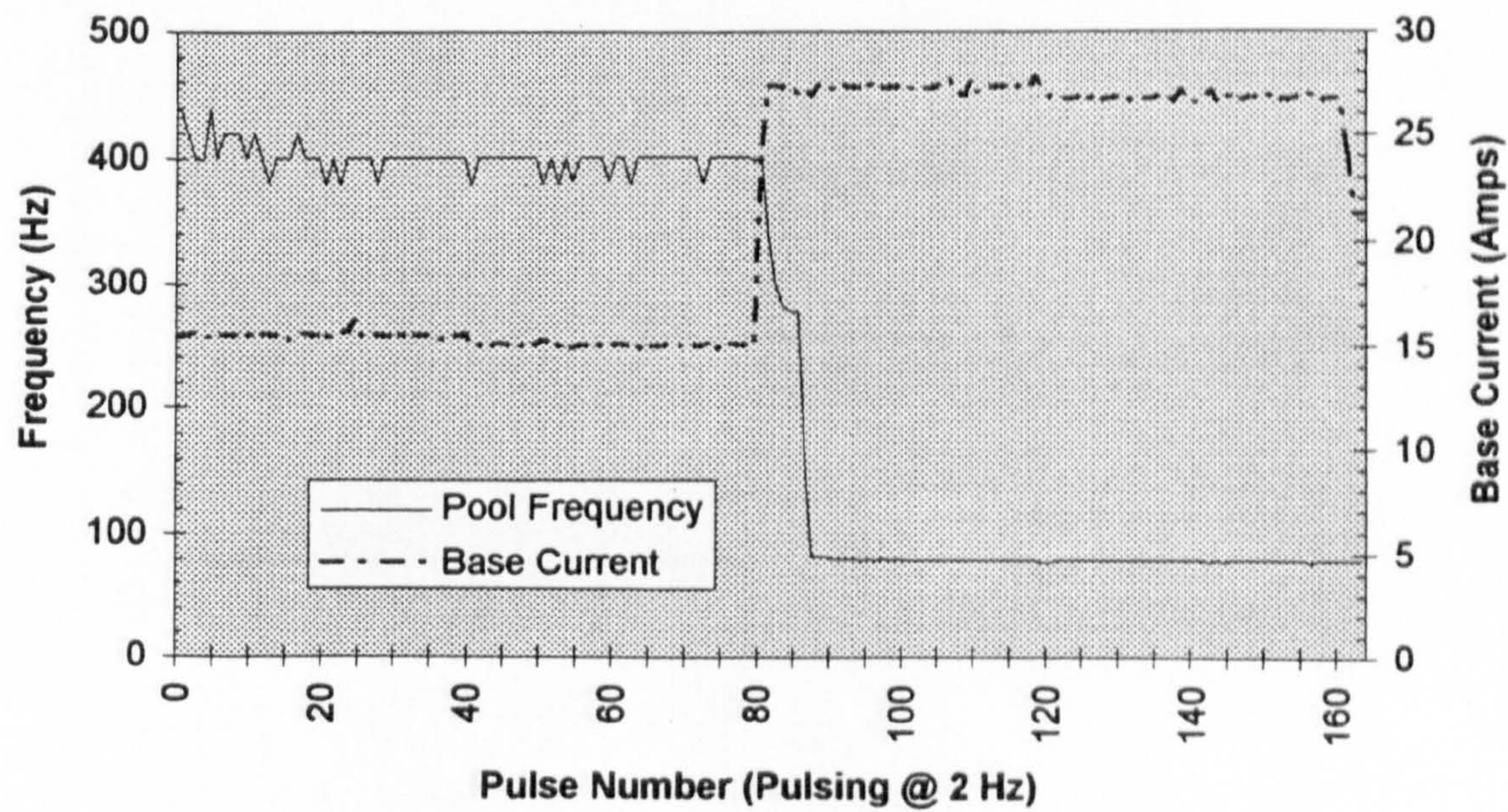


Figure 68

Real-Time Frequency Response - FULL to PARTIAL Penetration

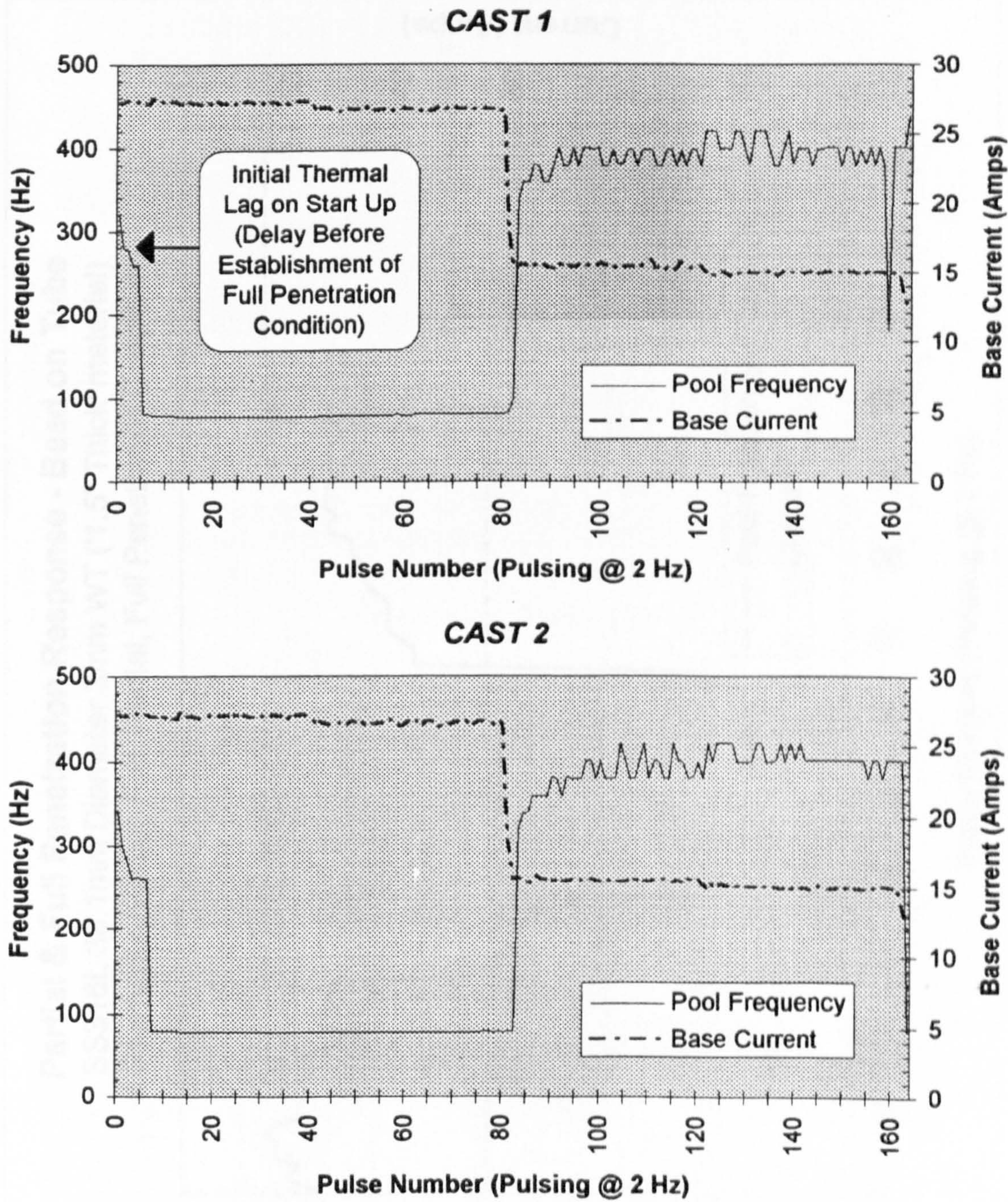


Figure 69

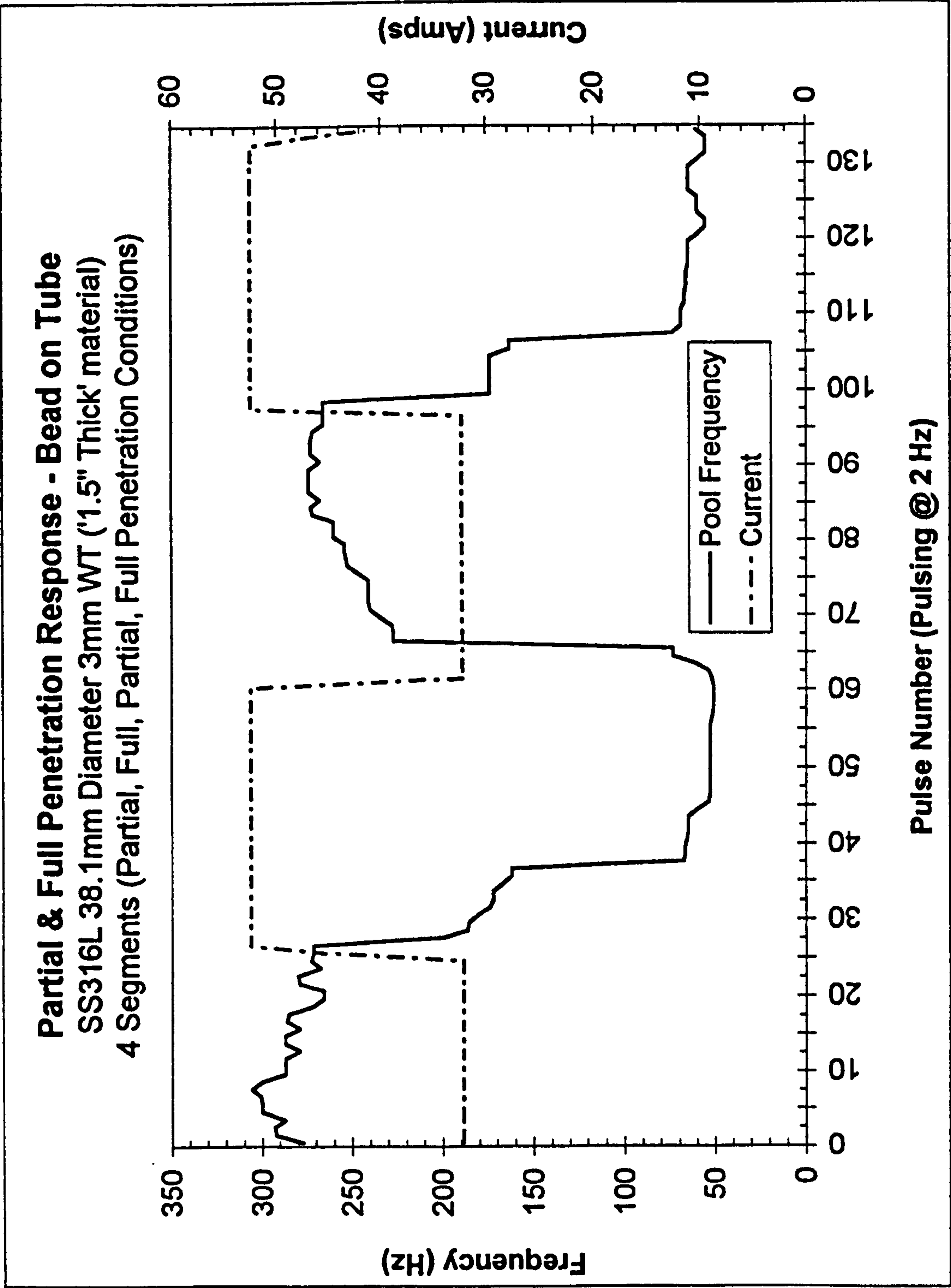


Figure 70

Partial & Full Penetration Response - SQUARE BUTT JOINT
SS316L 38.1mm Diameter 3mm WT ('1.5" Thick' material)
4 Orbital Segments (Partial, Full, Partial, Full Penetration Conditions)

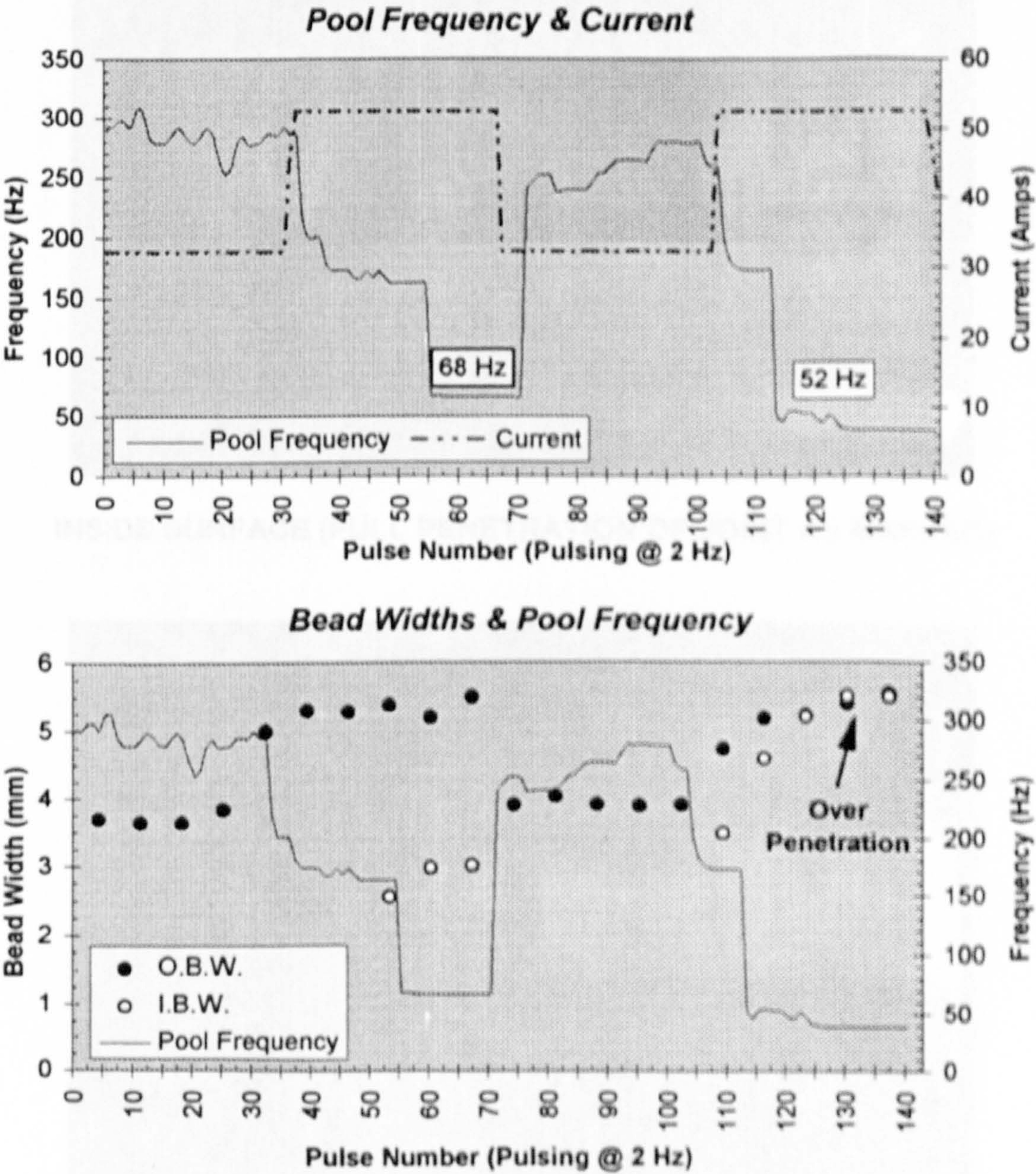
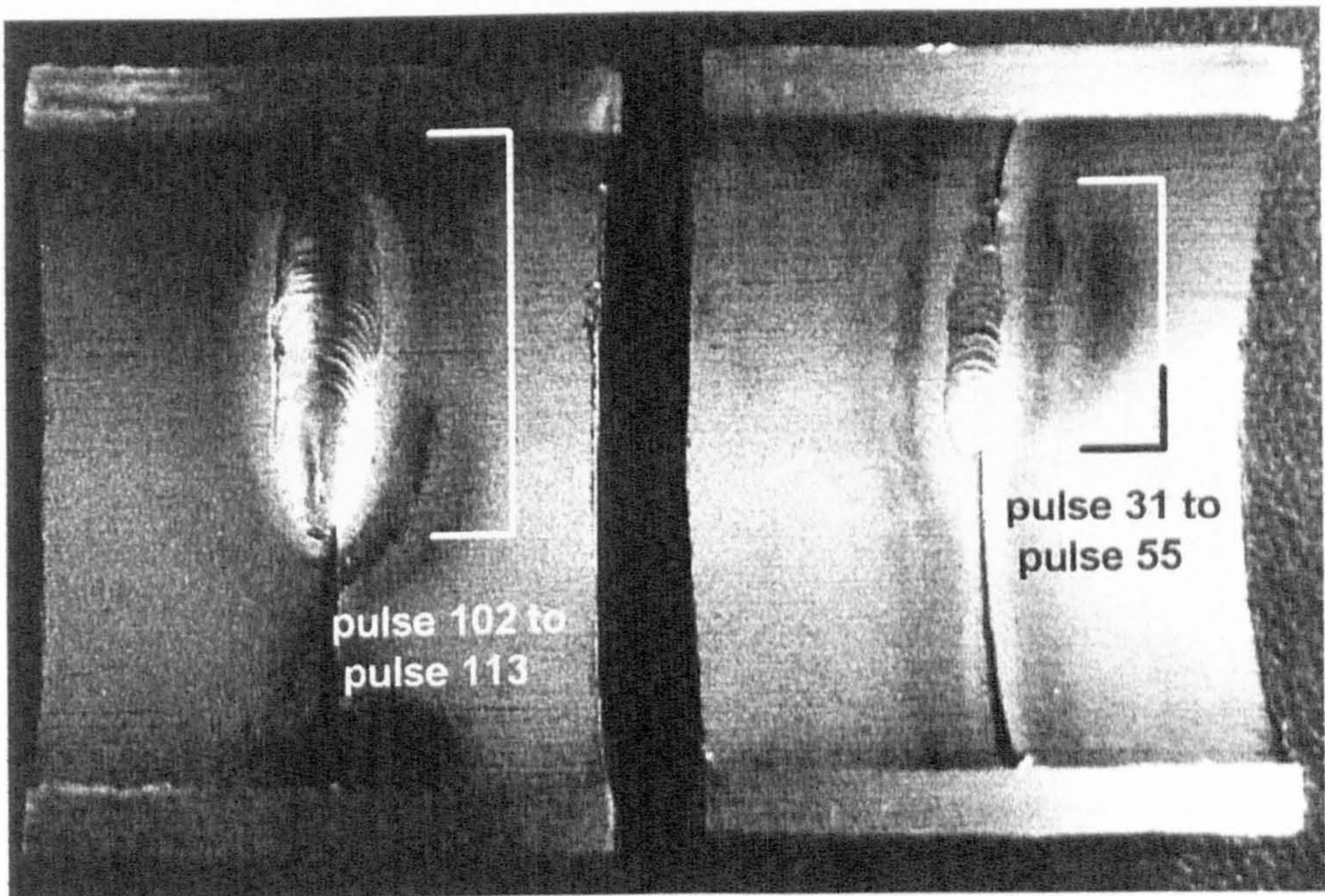
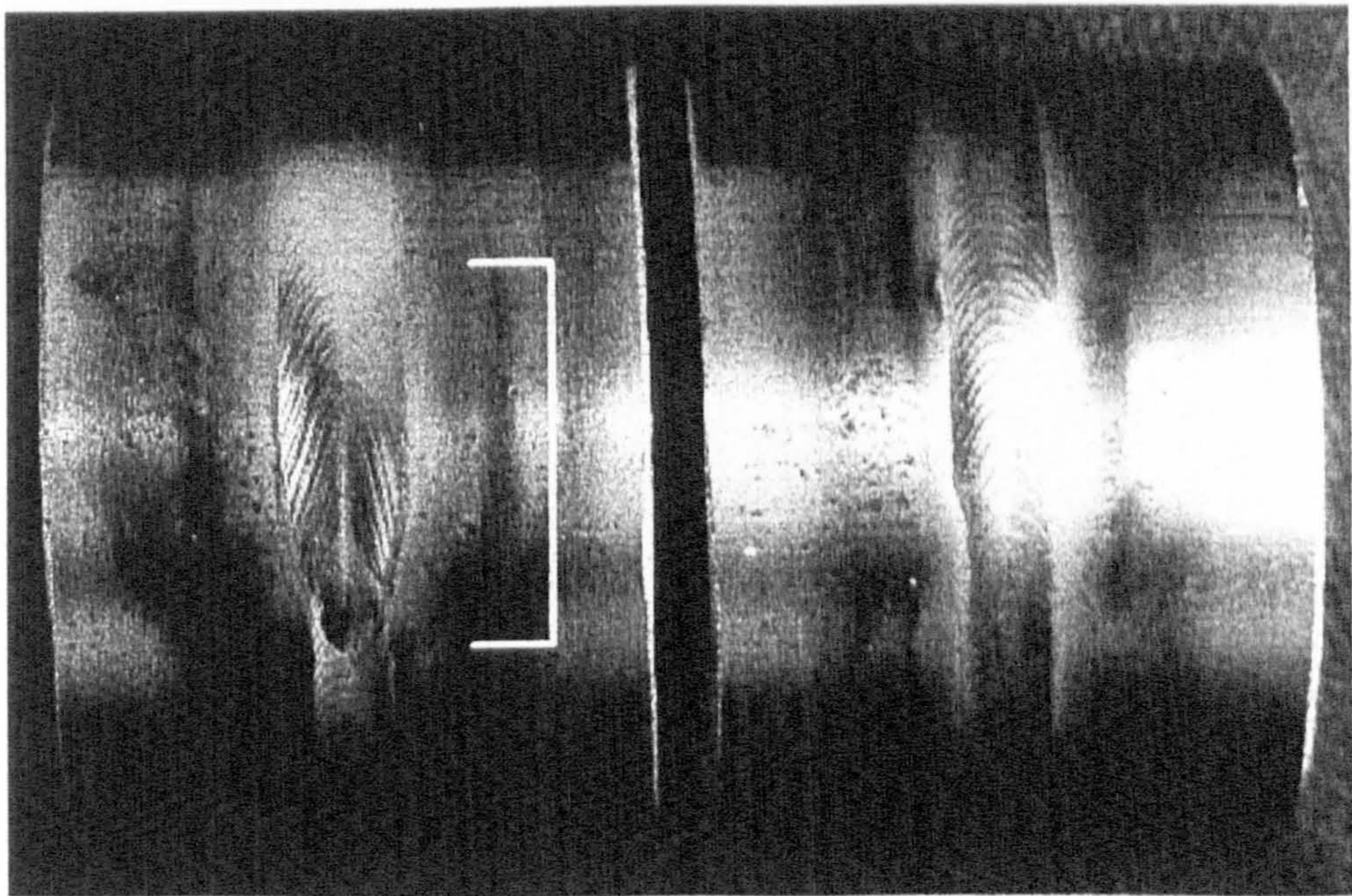


Figure 71



INSIDE SURFACE (FULL PENETRATION OF JOINT AS MARKED)



OUTSIDE SURFACE (OVER-PENETRATION AT WELD END MARKED)

Figure 72 Inner and outer beads of square butt joint in '1.5" Thick' material for partial and full penetration response

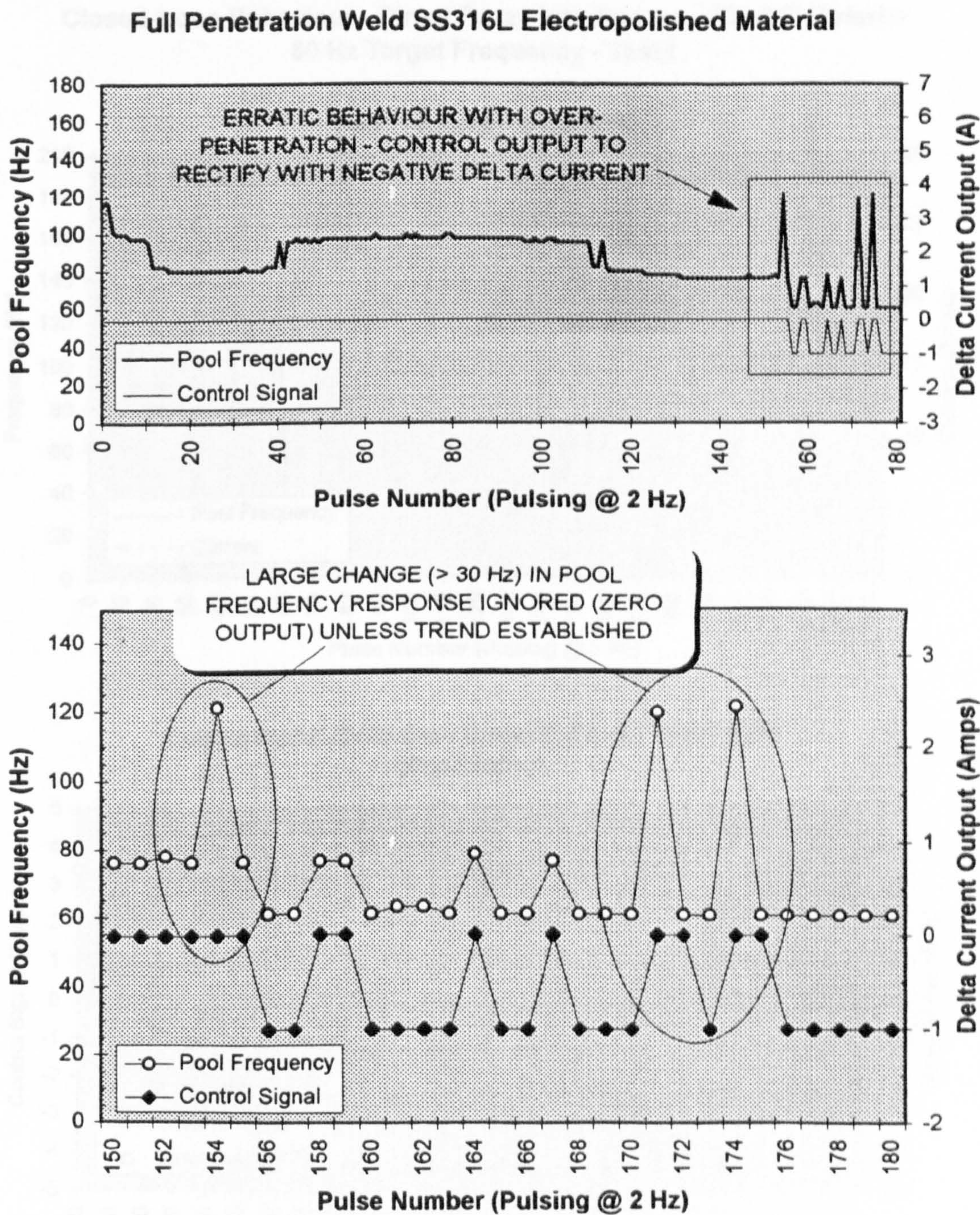


Figure 73 Open-loop control output - full penetration leading to over-penetration weld on electro-polished material

Closed-Loop Behaviour - Direct Fuzzy Interference - 'Cast 2' Material
80 Hz Target Frequency - Test I

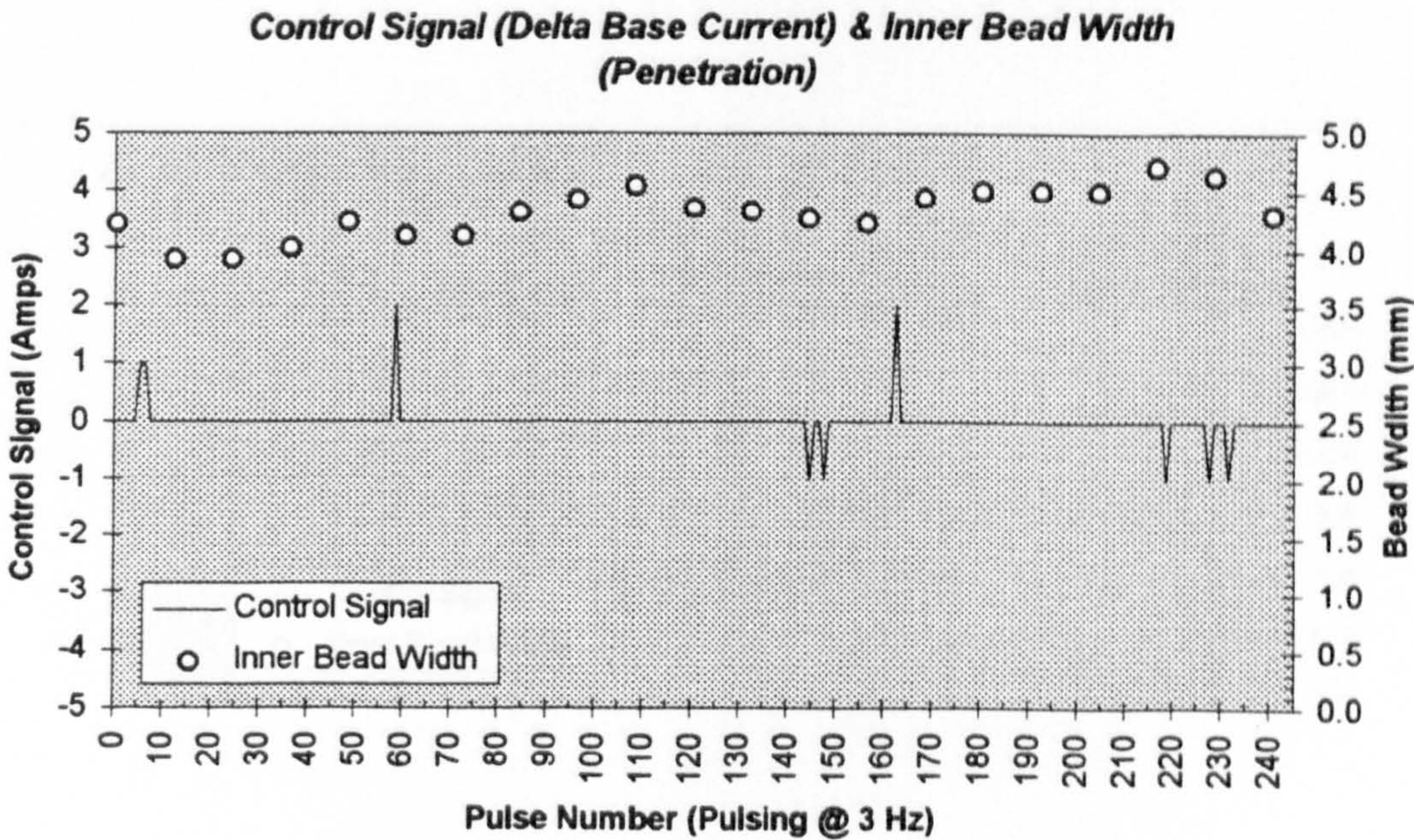
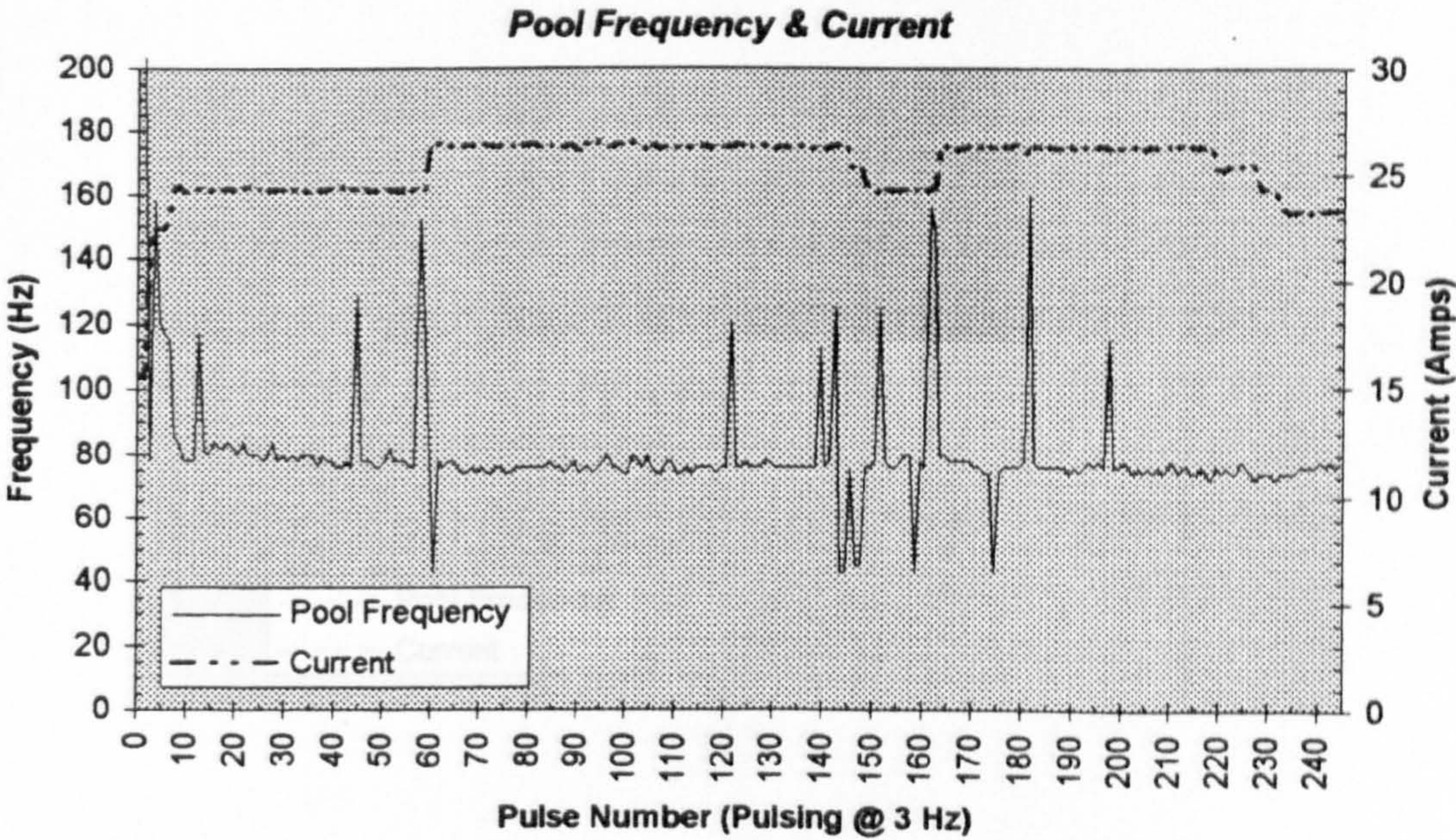


Figure 74

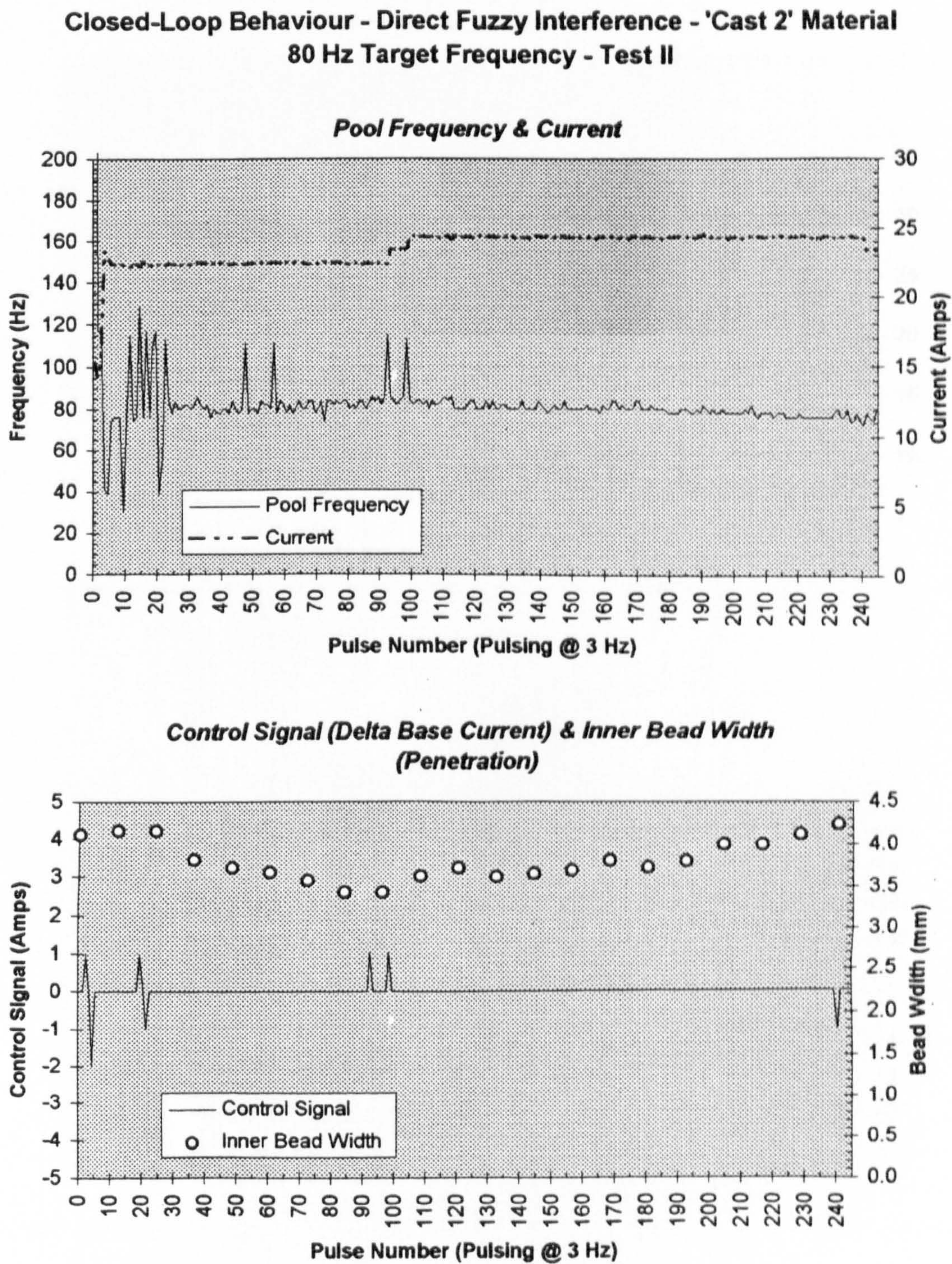


Figure 75

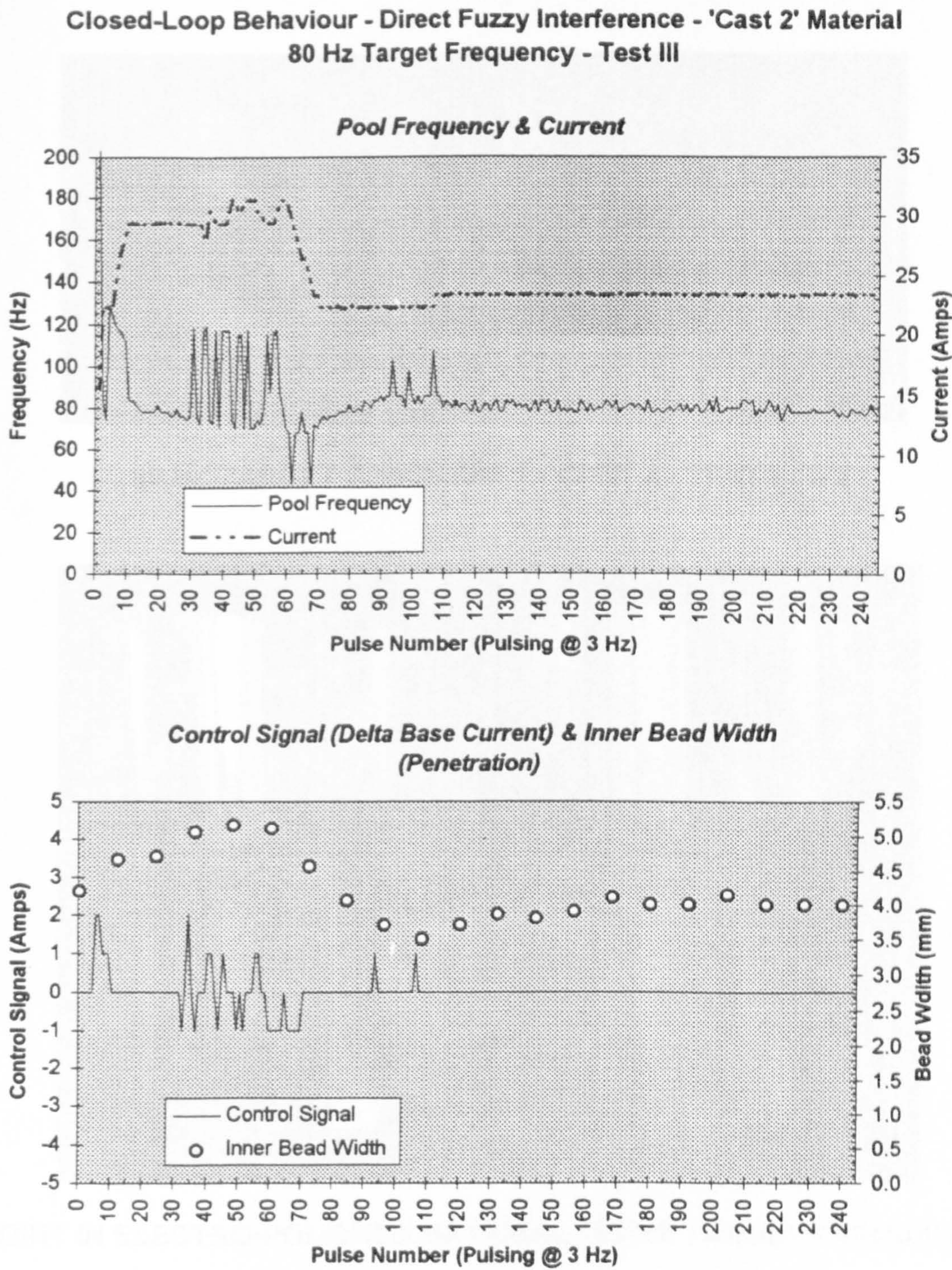
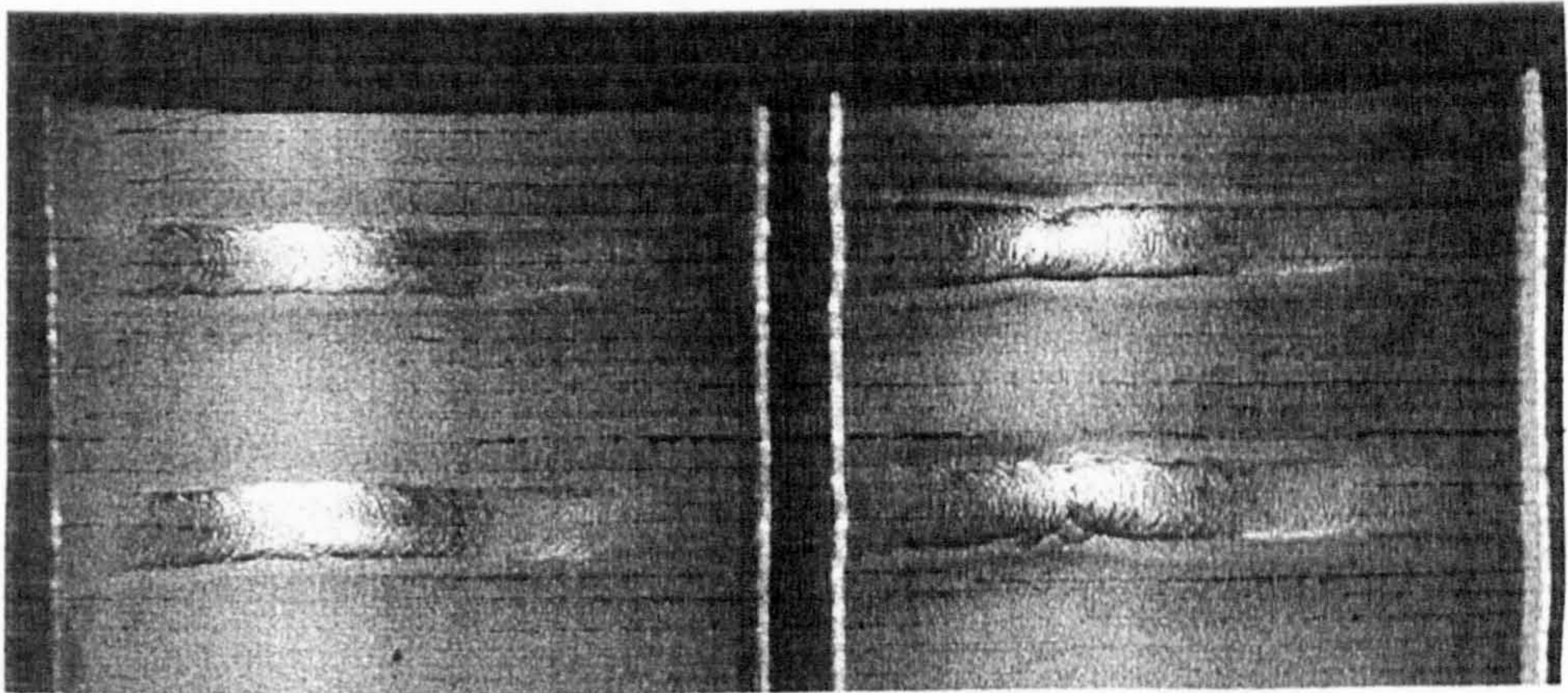
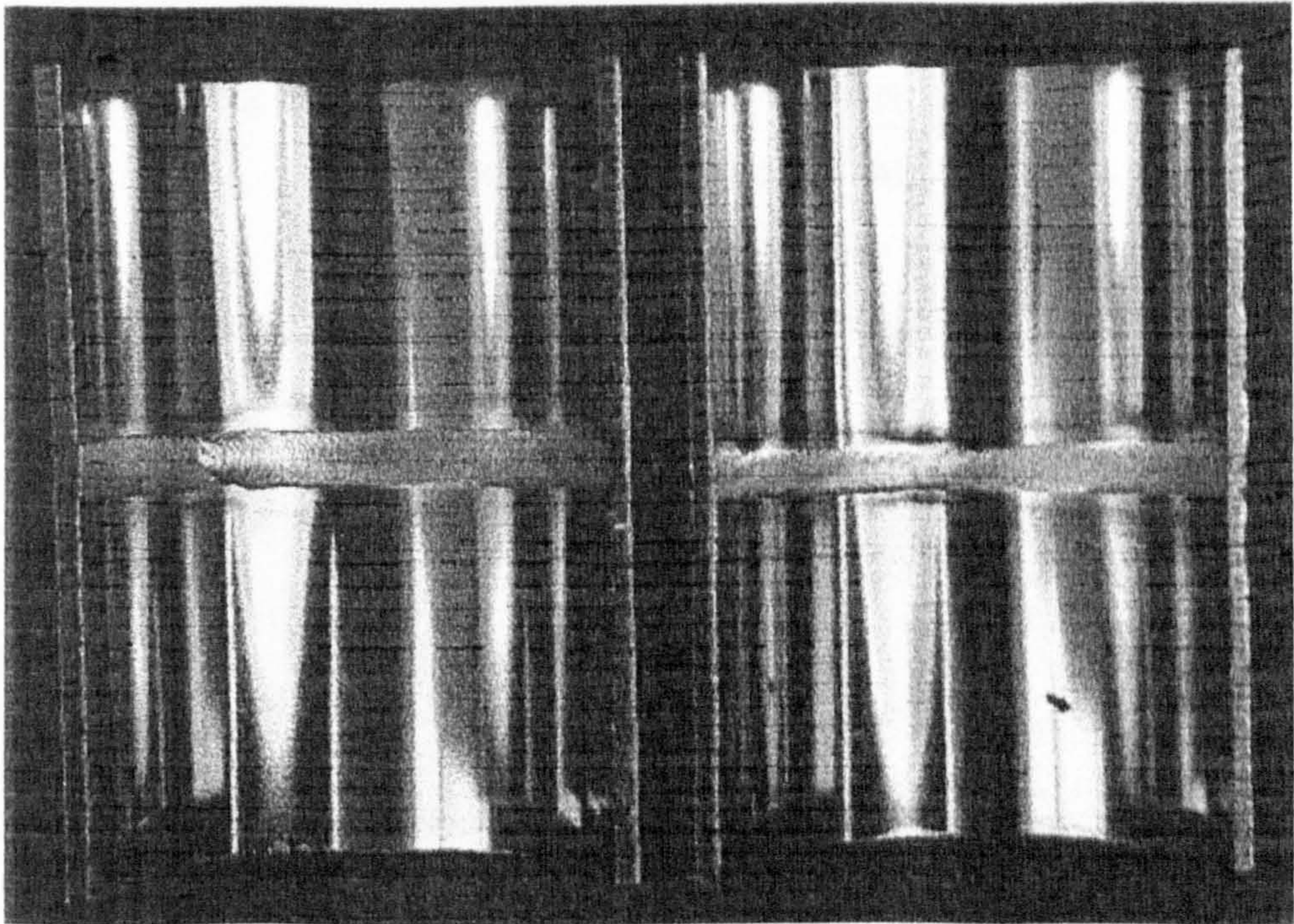


Figure 76



80 HZ TARGET FREQUENCY - CAST 2 - TESTS I & II



JOINT IN ELECTRO-POLISHED MATERIAL - 80 HZ TARGET FREQUENCY

Figure 77 Inner beads of 'Cast 2' and Electro-polished material using closed-loop control

Closed-Loop Behaviour - Direct Fuzzy Interference - 'LS Kobe' Material
80 Hz Target Frequency

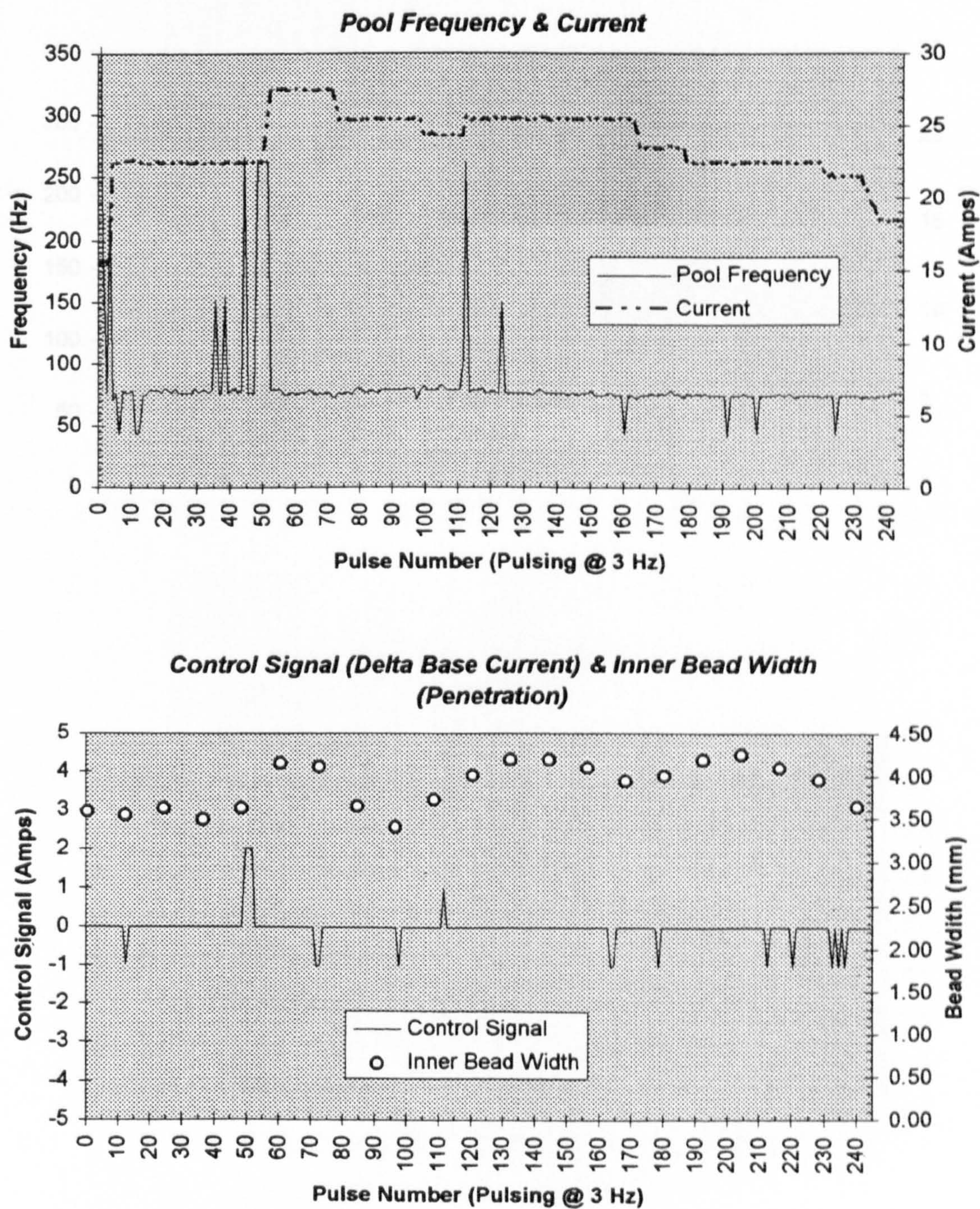


Figure 78

Closed-Loop Behaviour - Direct Fuzzy Interference - 'Cast 2' Material
Modified Parameters - 120 Hz Target Frequency

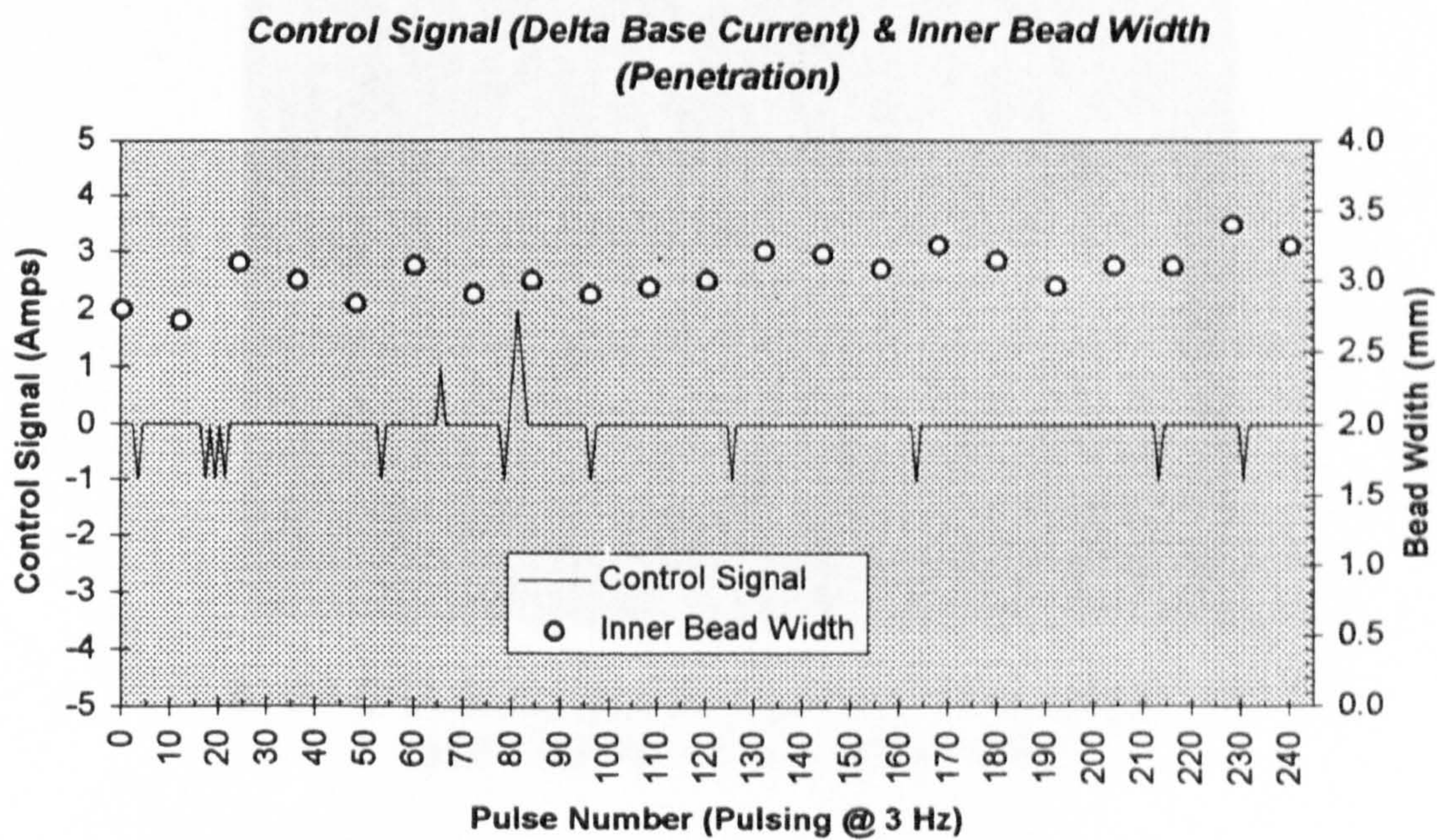
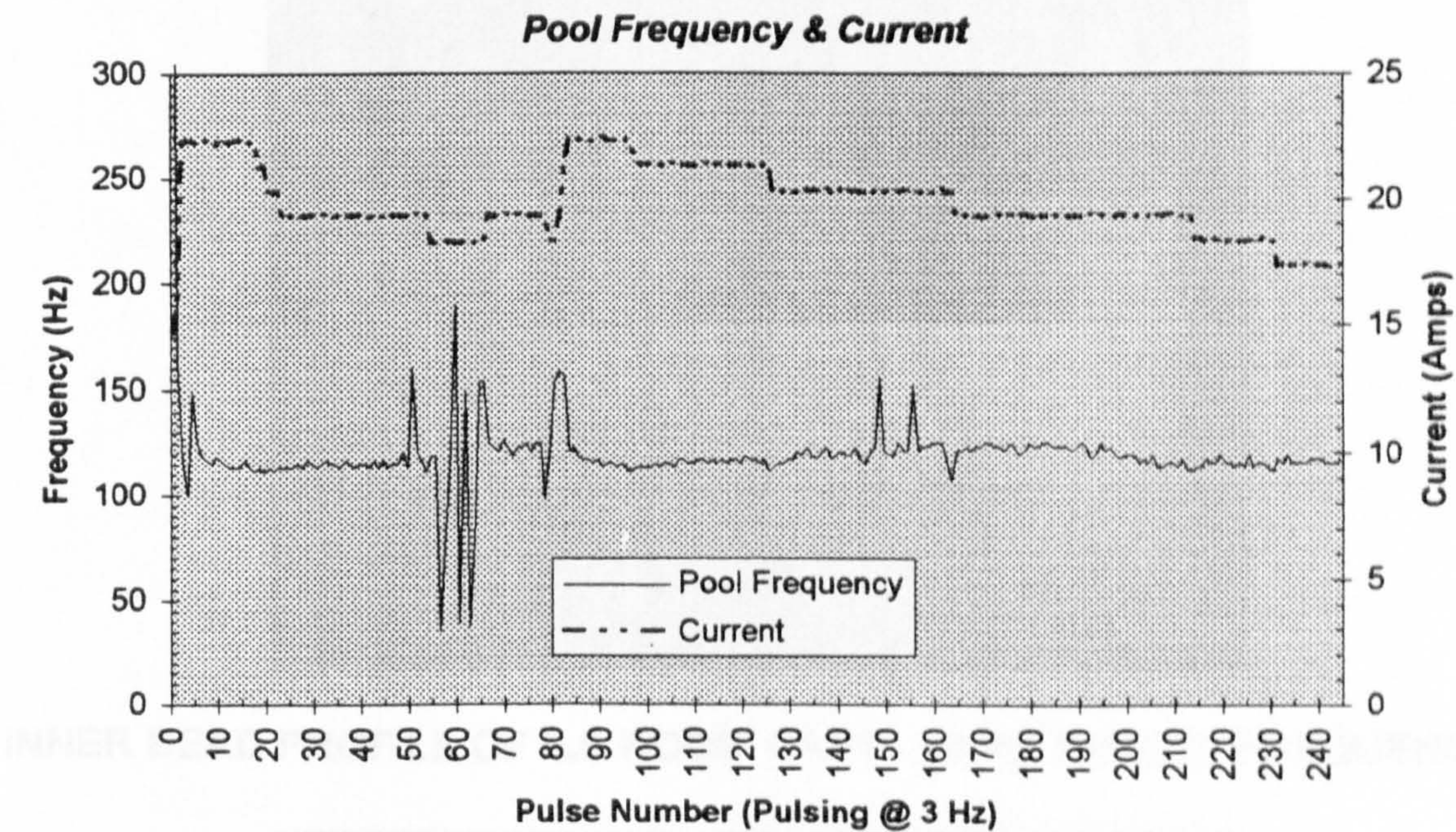
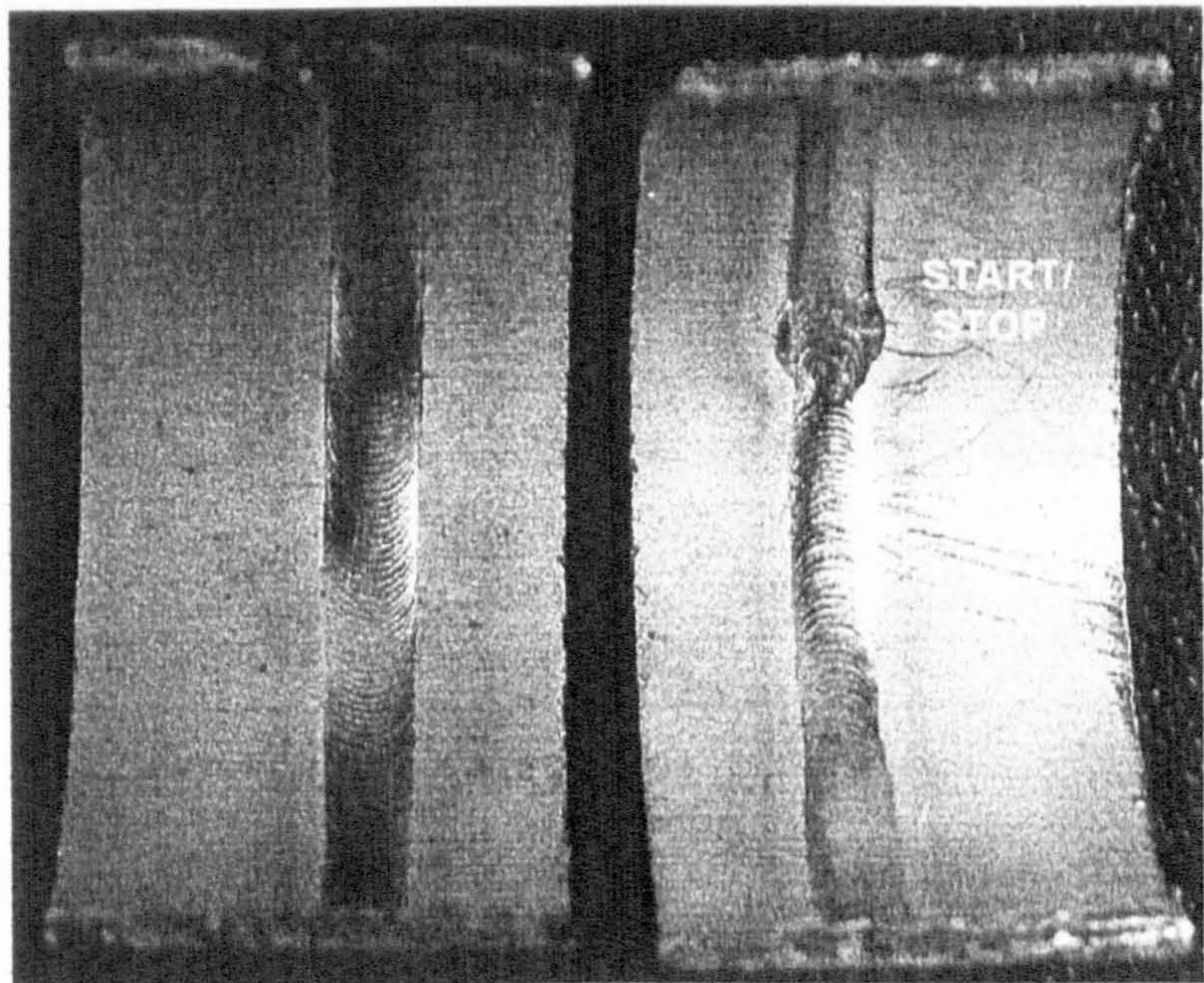
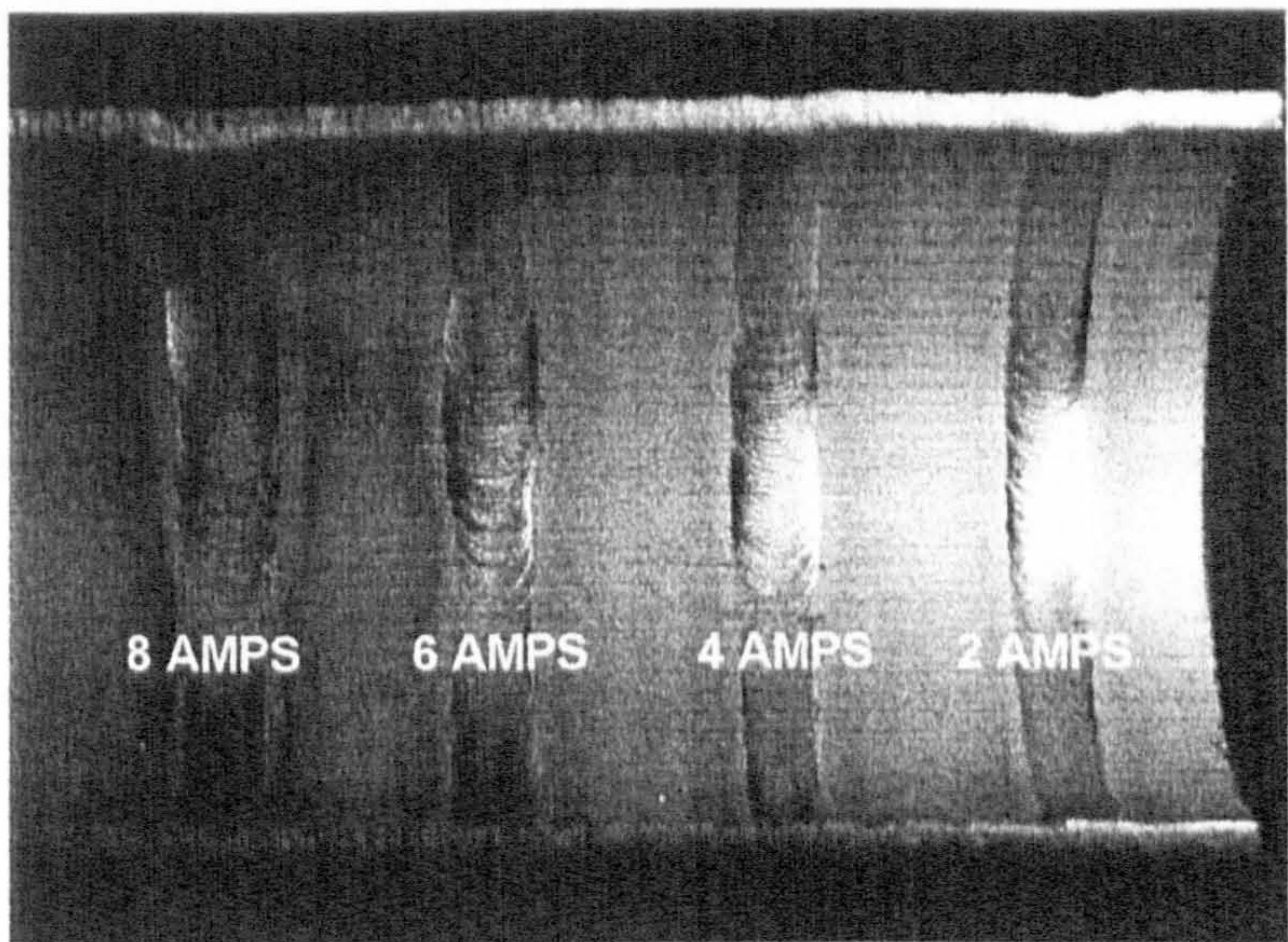


Figure 79



INNER BEAD PROFILE OF 'LS KOBE' CAST - 80 HZ TARGET FREQUENCY



STEP CHANGES IN BASE CURRENT IMPOSED BY SOFTWARE - 8, 6, 4 AND 2 AMP

Figure 80 Inner beads of 'LS Kobe' material (closed-loop control with set target frequency) and 'Cast 2' material with imposed base current step changes

Closed-Loop Behaviour - Direct Fuzzy Interference - 'Cast 2' Material
80 Hz Target Frequency - 8 Amp Step Increase

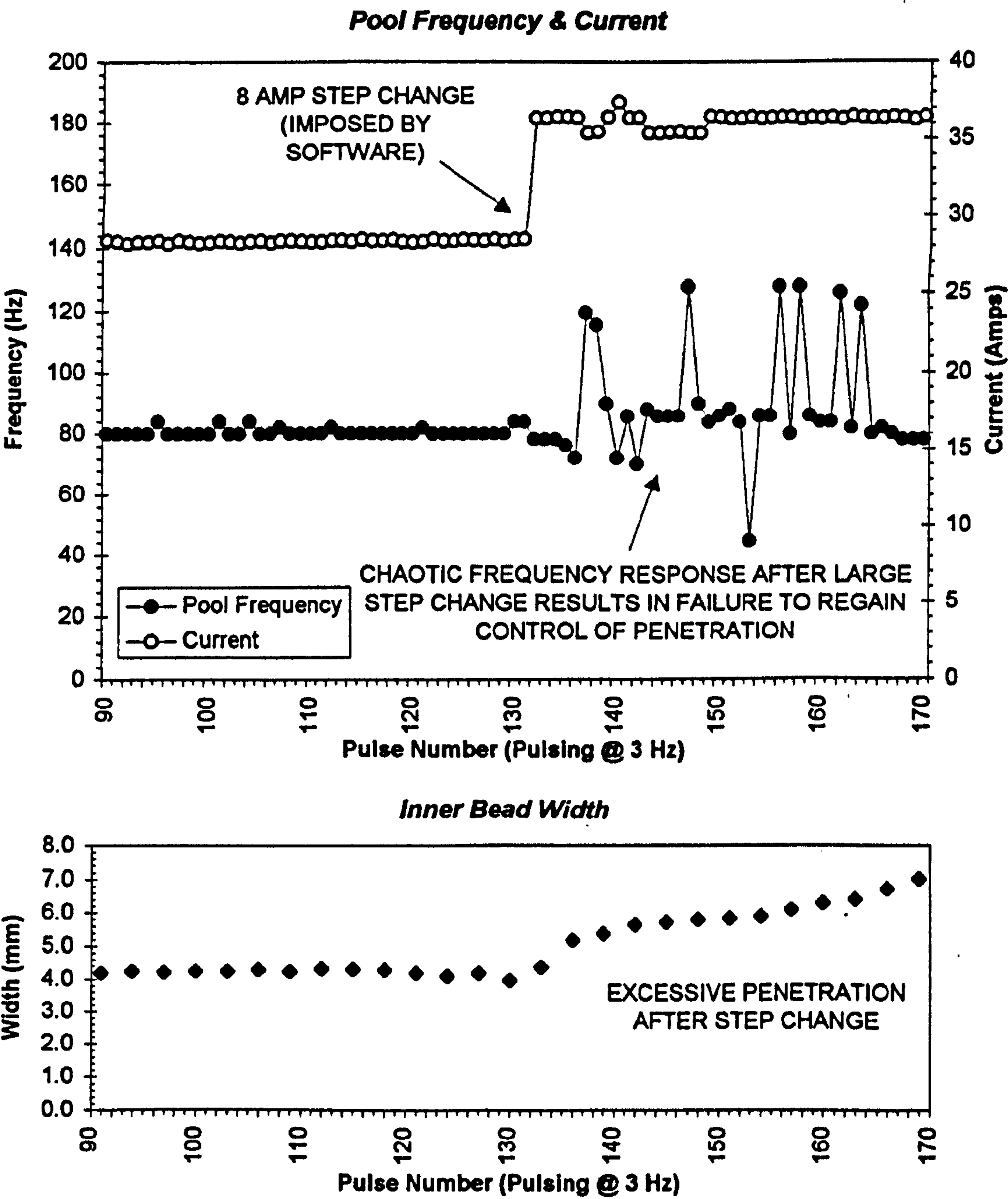


Figure 81

**Closed-Loop Behaviour - Direct Fuzzy Interference - 'Cast 2' Material
80 Hz Target Frequency - 6 Amp Step Increase**

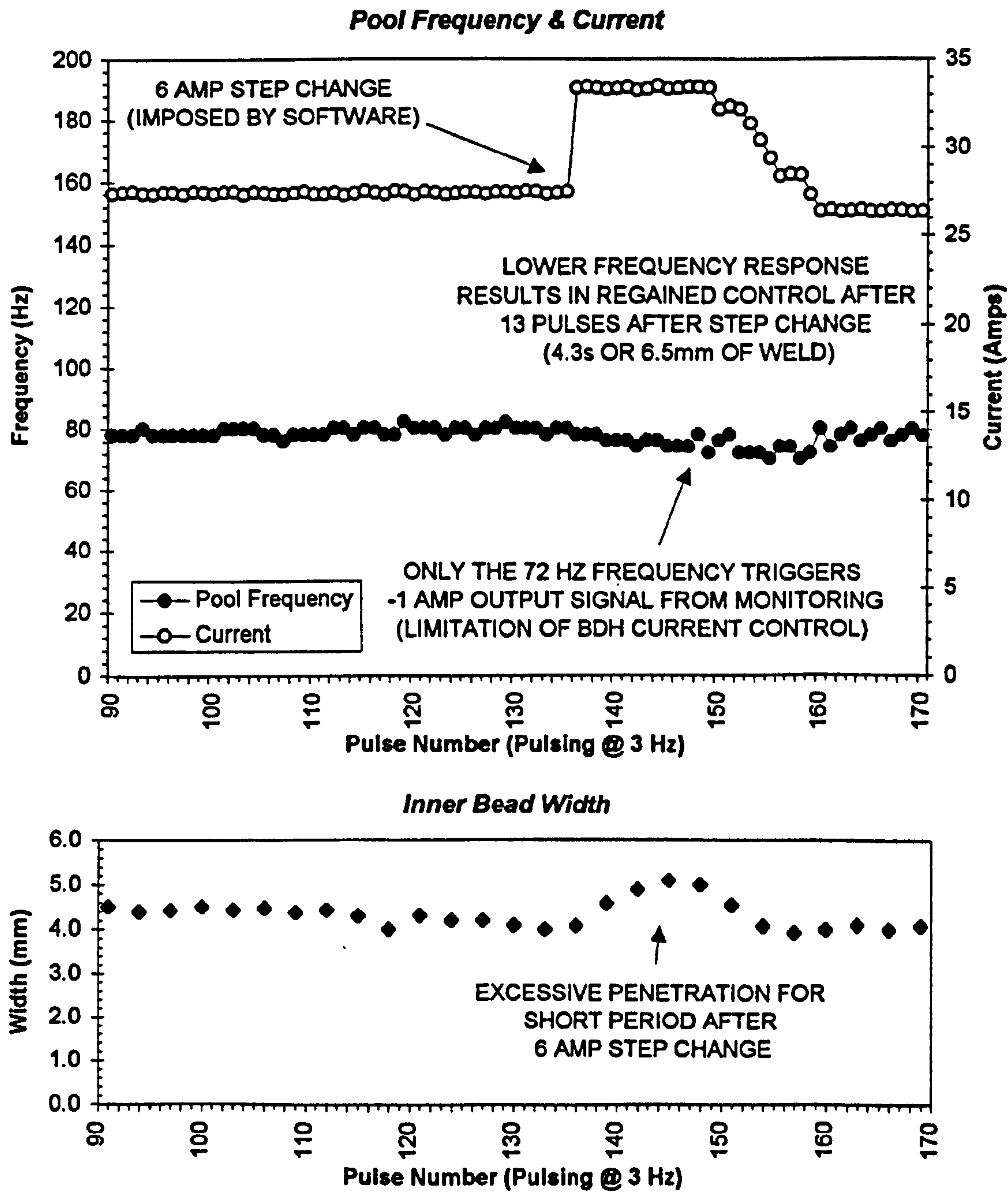


Figure 82

Closed-Loop Behaviour - Direct Fuzzy Interference - 'Cast 2' Material
80 Hz Target Frequency - 4 Amp Step Increase

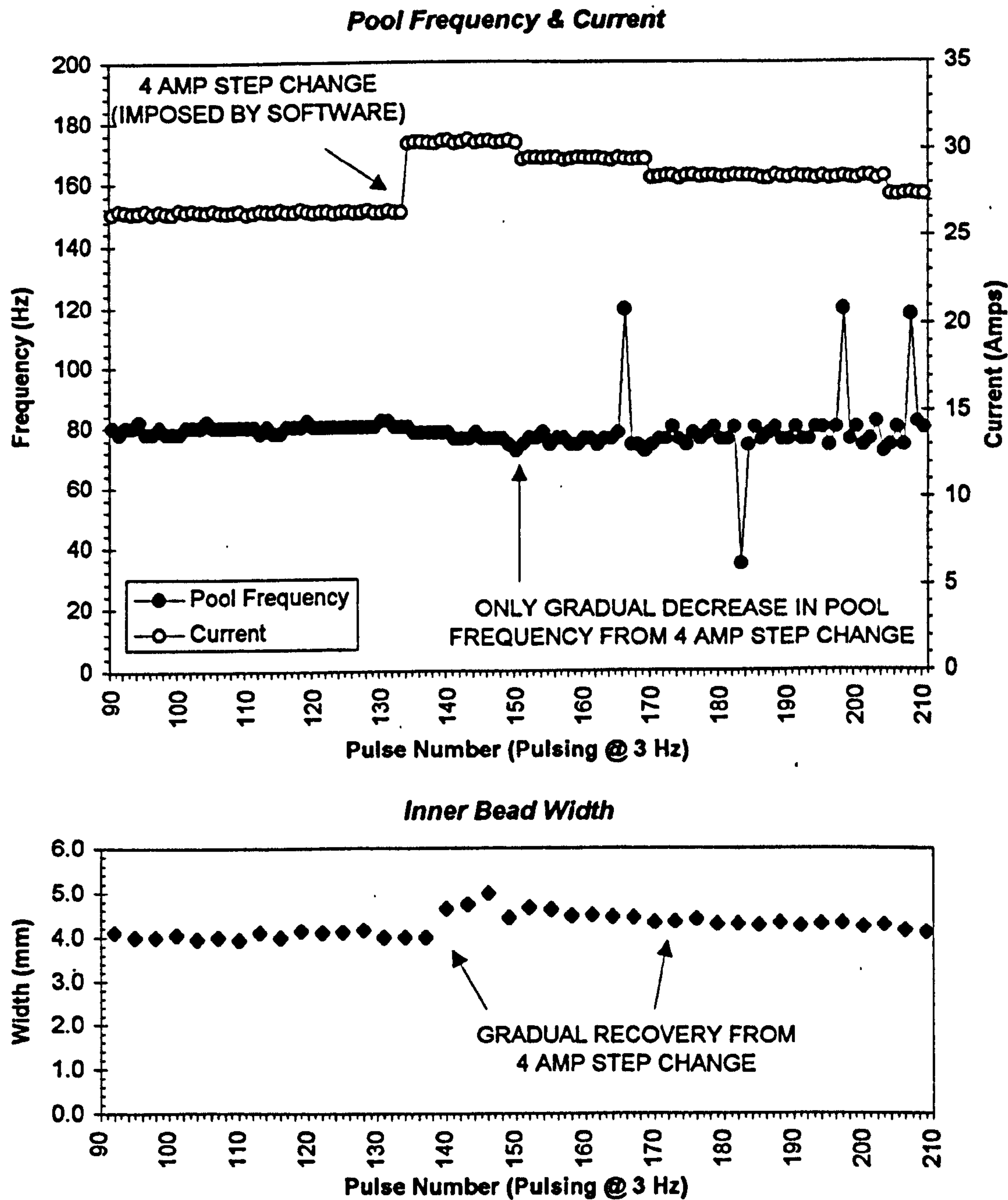


Figure 83

Closed-Loop Behaviour - Direct Fuzzy Interference - 'Cast 2' Material
80 Hz Target Frequency - 2 Amp Step Increase

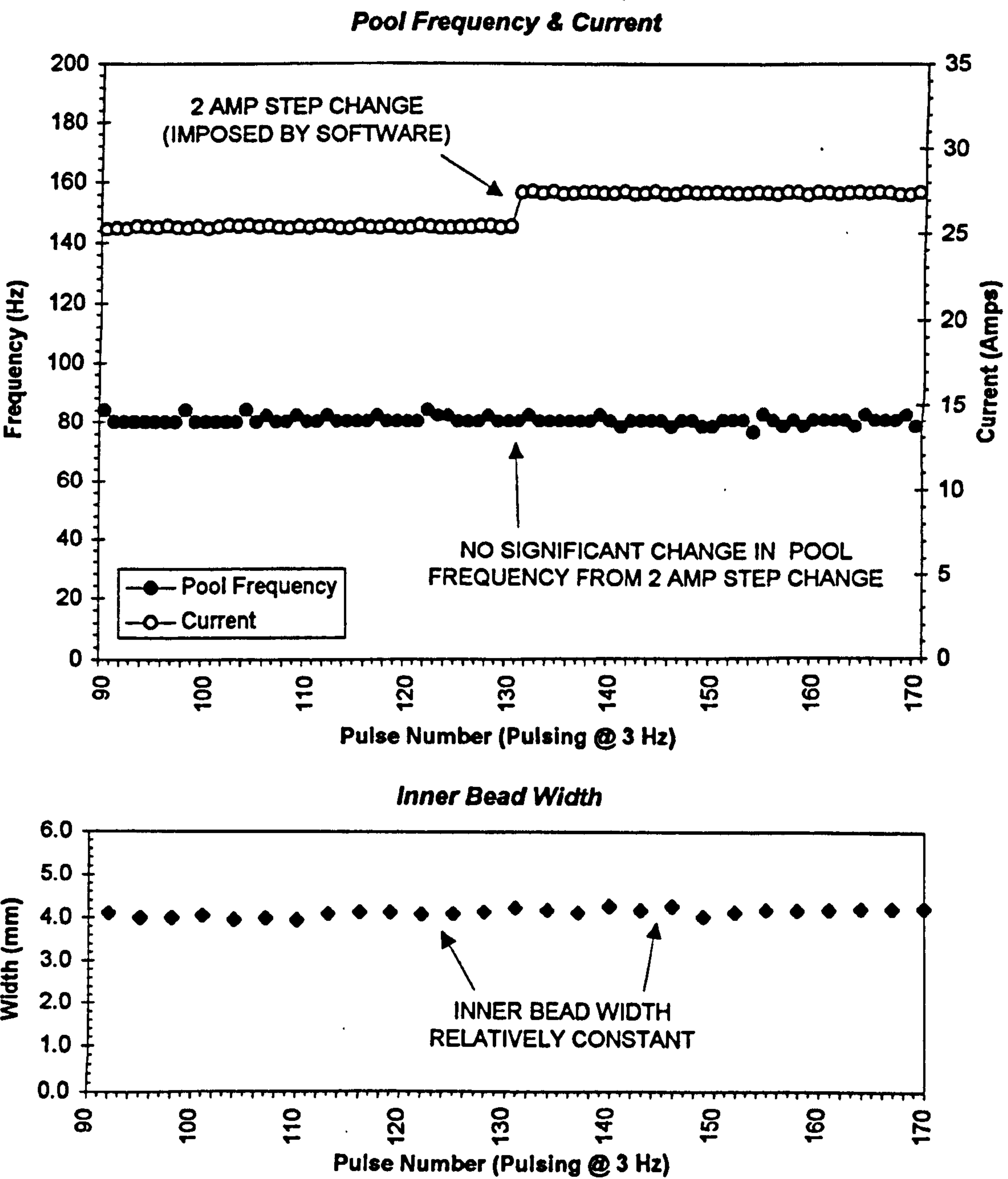


Figure 84

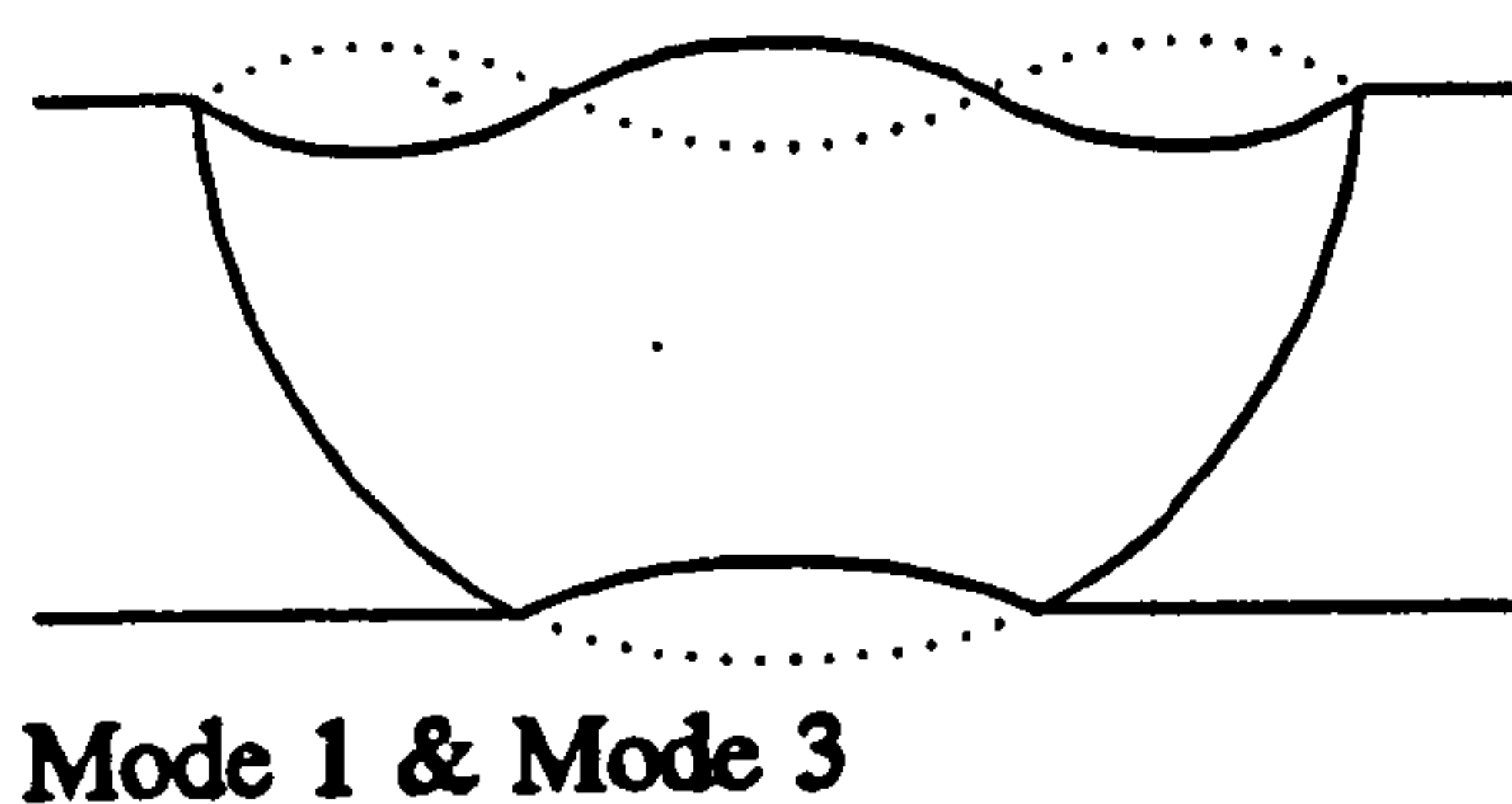


Figure 85 Proposed mixed-mode behaviour

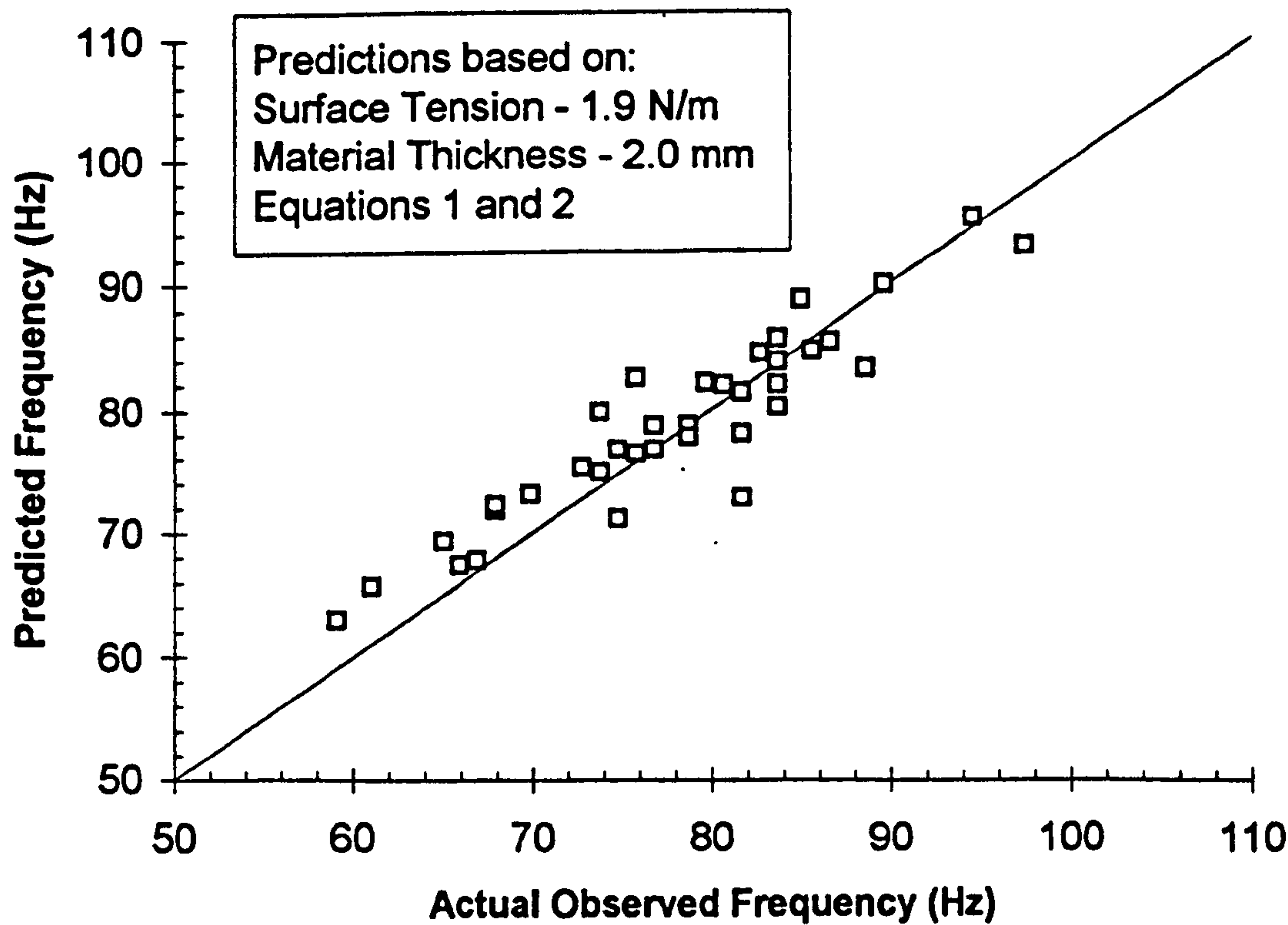


Figure 86 Stationary pools (basic work) - comparison between experimentally observed data and Xiao (1992) for Mode 3

'Time-to-penetrate' Behaviour
'Cast 1' (HS) and 'LS Kobe' (LS) Materials

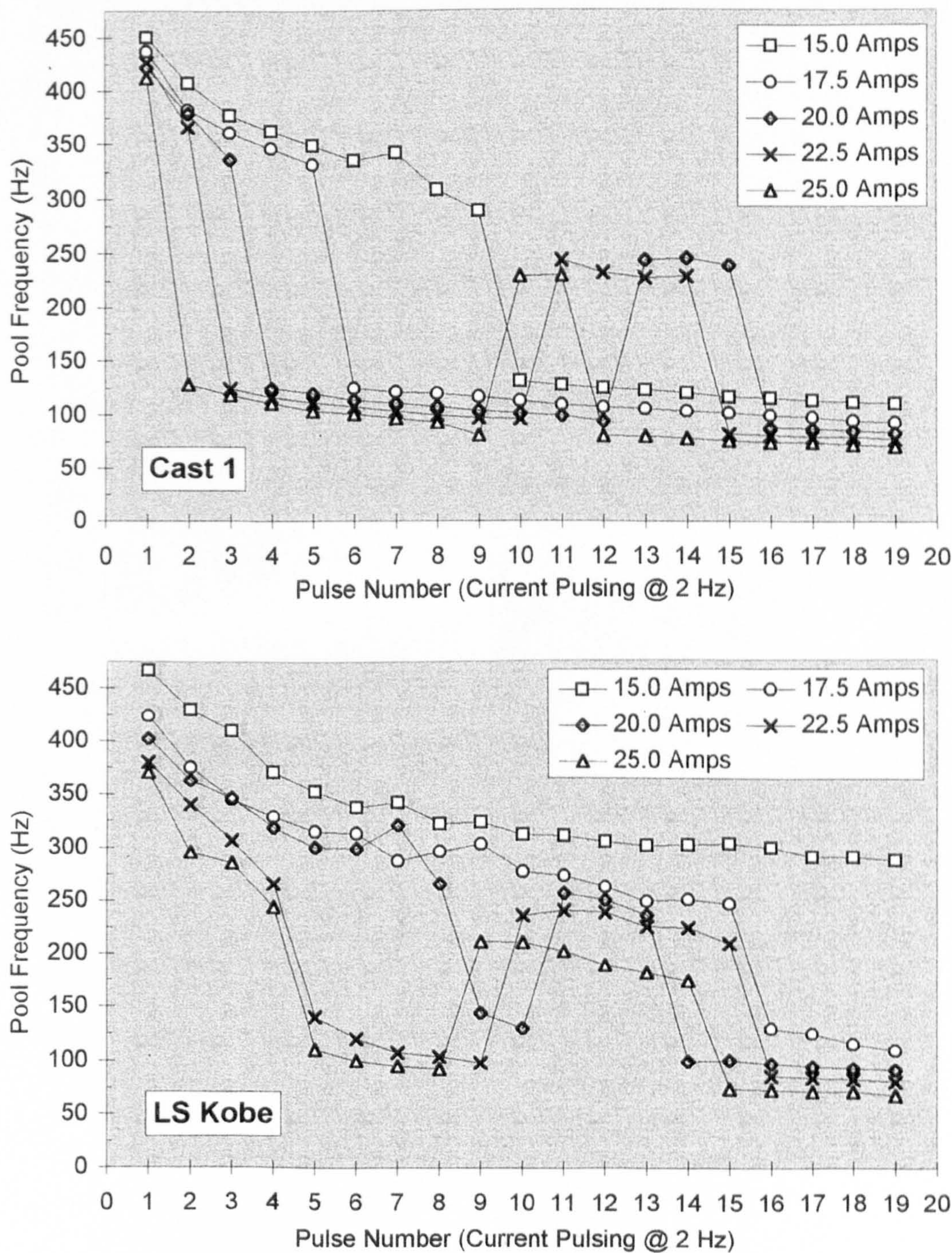


Figure 87